Synthesis, anion binding studies and applications of mono- and bimetallic lanthanide complexes

Laura Elizabeth Mason

Keble College

University of Oxford

A Thesis submitted in partial fulfilment of the requirements for the degree of *Doctor of Philosophy*

Trinity term 2017

Abstract

‘Synthesis, anion binding studies and applications of mono- and bimetallic lanthanide complexes’

Laura Mason, Keble College, University of Oxford.

DPhil Thesis, Trinity Term 2017.

This work describes the preparation and study of lanthanide complexes derived from heptadentate DO3A and DO3AM ligands. The work described encompasses a range of synthetic studies using conventional Click chemistry, novel gold catalysed couplings to prepare mono- and bi- metallic complexes and synthesis of DO3AM derivatives. These complexes have been used in a variety of studies to explore proton and anion binding events, and to develop catalysts for fluorination in protic solvents.

Chapter one describes the fundamental properties of the lanthanides with a focus on their luminescent behaviour, as well as a brief review of possible applications for lanthanide ions and complexes.

Chapter two explores the use of click reactions, firstly with propargylDO3A and 2-azidopyridne to explore any pH dependant behaviour of the complexes. The corresponding d-f hybrids of these complexes were also explored to investigate how the addition of a d block metal can affect the behaviour of d-f hybrids compared to the parent complex. This chapter also explores the novel synthesis of a strained dibenzocyclooctyne lanthanide complex, that has potential for efficient formation of bioconjugates using *in vivo* bio-orthogonal click reactions.

Chapter three describes the development of a novel synthetic method that uses lanthanide complexes in novel three component gold catalysed couplings to form new lanthanide

architectures, and study their binding affinity for anions. We also describe how this methodology can be extended to form bimetallic lanthanide complexes. These bimetallic systems form ternary complexes with aryl dicarboxylates, in which guest binding can be used to modulate the intramolecular energy transfer mechanisms giving rise to a ratiometric red/green response.

Chapter four defines the synthesis of rigid, chiral heptadentate DO3AM derivatives bearing aspartate derived pendant arms, and explores their fluoride binding by NMR and luminescence, revealing that binding of axial fluoride is less favourable than fluoride binding in the plane of the carbonyl donors. The use of these complexes as catalysts is also investigated for the fluorination of α-halocarboxylic acids.

Chapter five summarises the work done throughout the thesis, highlighting some overarching conclusions, as well as describing areas for further study.

Chapter six provides experimental procedures and characterisation data for the compounds studied.

Contents

Abstract ..... **i**

Contents ..... **iii**

Acknowledgements ..... **vi**

Abbreviations ..... **viii**

1 Introduction **1**

1.1 Introduction **1**

1.2 General Aspects of Lanthanide Chemistry **1**

1.3 Stability and the Macrocyclic Effect **2**

1.3.1 Thermodynamic Stability 3

1.3.2 Kinetic Stability 5

1.4 Lanthanide Photophysics **7**

1.4.1 Sensitised Emission 9

1.4.2 Energy transfer mechanisms 11

1.4.3 Quenching 12

1.5 NMR **15**

1.5.1 Paramagnetic NMR 15

1.5.2 Isomers in NMR 17

1.6 Applications of lanthanide complexes **20**

1.6.1 Sensing Anions 20

1.6.2 MRI 24

1.6.3 Positron Emission Tomography (PET) 26

1.6.4 Catalysis 29

1.7 Aims **31**

1.8 References **32**

2 Click Chemistry with DO3A complexes 36

2.1 Introduction 36

2.2 Synthesis and characterisation 38

2.3 pH studies 41

2.3.1 NMR studies 41

2.3.2 Photophysical studies 46

2.4 d-f hybrids 50

2.4.1 Introduction 50

2.4.2 Synthesis and photophysical studies 51

2.5 Bio-orthogonal Click Chemistry 57

2.5.1 Introduction 57

2.5.2 Synthesis and characterisation 59

2.5.3 Method A 61

2.5.4 Method B 67

2.6 Conclusions 70

2.7 References 71

3 Gold Catalysed Couplings with p-DO3A complexes 73

3.1 Introduction 73

3.2 Monometallic complexes 74

3.2.1 Synthesis and characterisation 74

3.2.2 Photophysical measurements and binding studies 83

3.3 Bimetallic complexes 85

3.3.1 Synthesis and characterisation 85

3.3.2 Photophysical and anion binding 89

3.4 Conclusion 103

3.5 References 104

4 Rigid DO3AM derivatives 105

4.1 Introduction 105

4.2 Synthesis and characterisation 106

4.3 Fluoride binding 108

4.3.1 NMR studies 108

4.3.2 Photophysical studies 116

4.4 Catalysis 124

4.4.1 Introduction 124

4.4.2 Hexaester studies 125

4.4.3 Hexaacid studies 132

4.4.4 Eu.p.DO3A studies 137

4.4.5 Regioselectivity and Catalysis 142

4.5 Conclusions 145

4.6 References: 147

5 Conclusions and future work 148

6 Experimental Methods 151

6.1 General Procedures 151

6.2 Titration methodology 153

6.3 Dynafit 154

6.4 Synthetic Methods 156

6.4.1 Click chemistry with DO3A complexes 156

6.4.2 Gold catalysed couplings with p.DO3A complexes 175

6.4.3 Rigid DO3AM derivatives 184

6.5 References 192

Acknowledgements

Firstly, I would like to thank Steve Faulkner for accepting me into his group. He has provided support from the outset and all throughout my time in Oxford, with his optimistic outlook he was always willing to supply faith and confidence even when mine waivered. My time in Oxford, though far from home, has benefited from your Cumbrian wisdom and compliment: ‘Thuz done alreet’ (see The illustrated Herdwick Shepard by James Rebanks for definition).

I would also like to extend my gratitude to all the staff at the Chemistry Research Laboratory for all support and analytical services provided. In particular, I would like to thank Dr Nick Rees and the NMR facilities and mass spectrometry services for recording accurate mass and MALDI spectra. Special thanks also to Dr Alan Kenwright of the University of Durham for measuring of some paramagnetic NMR spectra of lanthanide complexes.

During my time in Oxford I have met some wonderful people and would like to thank all of the Faulkner group members, both past and present for your help and encouragement along the way - including the cathartic tea breaks. To Dr Gearóid Ó’Mállie, Dr Octavia Blackburn and Dr Manuel Tropiano your support, advice and humour have made me a better chemist and my time here all the more enjoyable. Also to, Dr Louise Natrajan, thank you for all your guidance over the years.

I would like to thank Gearóid for your patience, putting up with all my questions and your never-ending willingness to help. I’m not sure how we ended up starting our time in Oxford together but I really lucked out to have someone who, in many ways, is probably too similar to me! From our first week with of updates over an Irish news story, your stories, phrases and humour has kept me fully entertained.

To Octavia and Manuel, I would like to thank you both for teaching me the Faulkner ways and passing on your expertise and knowledge. Octavia your northern spirit has been a breath of fresh air and you have been a great friend and our squash games can only keep improving (we'll watch the professionals one day). Manuel, you had the patience to teach two novices squash, supply amazing homemade pizza and always being great company both in and out of the lab.

I would also like to thank my family, who have always given me support and encouragement. In particular, I want to thank my mum who has always been there for me with love, support, wisdom and advice – we've dealt with elephants, mountain, mazes… (and cats), it's been a kerfuffle, at times felt like a flapdoodle but as always you were there to guide me though. Also to Dad, Grandma, Aunty Jayne, thank you for your belief and encouragement, to Claire and David who provide support and entertainment in your own unique ways, and to Jack you've put up with me since we were at school and kept me smiling along the way.

Abbreviations

a.u.	arbitrary units
amu	atomic mass units
Ln	lanthanide
EDTA	ethylenediaminetetraacetic acid
MRI	magnetic resonance imaging
CA	contrast agent
NSF	nephrogenic systemic fibrosis
UV	ultraviolet
UV-Vis	ultraviolet-visible
ATR	attenuated total reflectance
BET	back energy transfer
br	broad
CT	charge transfer
cyclen	1,4,7,10-tetraazacyclododecane
DO3A	1,4,7,10-tetraazacyclododecane-1,4,7-triacetic acid
p.DO3A	2,2',2''-(10-(prop-2-yn-1-yl)-1,4,7,10-tetraazacyclododecane-1,4,7-triyl) triacetic acid
DOTA	1,4,7,10-tetraazacyclododecane-1,4,7,10-tetraacetic acid
DTPA	diethylene triamine pentaacetic acid
DO3AM	2,2′,2” -(1,4,7,10-tetraazacyclododecane-1,4,7-triyl) triacetamide

ESMS	electrospray mass spectrometry
ET	energy transfer
HRMS	high resolution mass spectrometry
IC	internal conversion
IR	infrared
ISC	inter-system crossing
IC	internal conversion
LMCT	ligand to metal charge transfer
BET	back energy transfer
m	multiplet
MALDI	matrix-assisted laser desorption and ionisation
MLCT	metal to ligand charge transfer
MWCO	molecular weight cut-off
NIR	near infrared
PET	positron emission tomography
TLC	thin layer chromatography
SAP	square anti-prism
S	singlet state
T	triplet state
TBAF	Tetrabutylammonium fluoride

TFA	trifluoroacetic acid
THF	tetrahydrofuran
LIS	lanthanide induced shift
NMR	nuclear magnetic resonance
TSAP	twisted square anti-prism
PeT	photoelectron transfer
LIR	lanthanide induced relaxation
MMCT	metal-metal charge transfer

1 Introduction

1.1 Introduction

In recent years, the use of lanthanides has largely focused on their biomedical applications as imaging agents and luminescent sensors.[1–3] In this thesis, I will explore how lanthanide complexes interact with anions in ways that can be can be exploited in a variety of applications.

In this chapter, the key aspects of lanthanide chemistry will be discussed along with reviews of the current applications of lanthanides and their complexes.

1.2 General Aspects of Lanthanide Chemistry

Lanthanide ions predominately exist in the 3+ oxidation state, though samarium, europium and ytterbium are notable exceptions as they can also exist in the 2+ oxidation state, while cerium, praseodymium and terbium can form 4+ species.[4]

The characteristic chemical properties of the trivalent lanthanides arise from the nature of their electronic configurations. Their partially filled 4*f* orbitals are radially contracted and highly penetrating, (more so than the fully occupied 5*s* or 5*p* orbitals), this results in the 4f orbitals being highly shielded, and the resuling interactions with ligand orbitals to be considered negligible. Consequently the bonding in lanthanide complexes is dominated by electrostatic bonding interactions with a small crystal field effect (c.a. 10^2 cm^{-1}), with the crystal field splitting generally being considered small relative to spin orbit coupling.[5]

Due to the low degree of covalency, the coordination geometries of lanthanide complexes are therefore dictated almost entirely by the demands of ligand structure, steric constraints and electrostatic considerations. To achieve kinetically and

thermodynamically stable lanthanide complexes, multidentate ligands are necessary; these usually incorporate hard Lewis donors such as N or O which bind preferentially to the hard Lewis acid lanthanide ions. For biological and imaging applications, it is particularly important to ensure kinetic and thermodynamic stability as free lanthanide ions are known to be highly toxic to humans[6] as they have a similar ionic radius to Ca^{2+}, and can bind more strongly due to its higher charge, disrupting calcium-dependent pathways in the body. This can lead to a condition known as Nephrogenic Systemic Fibrosis (NSF).[7]

1.3 Stability and the Macrocyclic Effect

The stability of lanthanide containing complexes is crucial when assessing their potential use in biology and medicine. Thermodynamic and kinetic stabilities both need to be considered when designing lanthanide containing complexes, though kinetic factors tend to dominate as a consequence of the low solubility of lanthanide phosphates and colloids. Thermodynamic considerations are largely based on the number of interactions with hard donors which maximise electrostatic interactions, and on entropic and enthalpic advantages conferred by the chelate and macrocyclic effects. Kinetic stability is of greater importance due to the possibility of demetallation in the body leading to conditions such as NSF.[7] The risk of demetallation can be decreased by exploiting the macrocyclic effect, where rigid ligands with multiple chelating arms reduce the rate of the demetallation processes.[8,9] This discussion focuses on the thermodynamic and kinetic stability considerations for linear and macrocyclic polyaminocarboxylate complexes with Ln(III) ions.

1.3.1 Thermodynamic Stability

The thermodynamic stability of a lanthanide containing complex stems from the enthalpically favourable complexation of electropositive lanthanide ions with electron rich ligands. Polyaminocarboxylate based ligands show high thermodynamic stabilities for both linear and macrocyclic complexes due to the high number of interactions with hard donor atoms, as well as the favourable entropic driving force that comes from the desolvation of both the metal and ligand.[10–12] The thermodynamic stabilities of a series of lanthanide complexes with polyaminocarboxylate ligands are demonstrated in Table 1.1.

Table 1.1: Thermodynamic stability constants(log K) for linear and macrocyclic polyaminecarboxylate complexes with lanthanide ions (298 K, 0.1 M NaCl, H_2O)[13]

	EDTA	**DTPA**	**DOTA**
La^{3+}	15.5	19.5	22.9
Eu^{3+}	17.3	22.5	23.5
Gd^{3+}	17.4	22.5	24.7
Tb^{3+}	17.9	22.7	24.2
Lu^{3+}	19.9	22.4	25.4

Complexes with EDTA are less stable than their DTPA and DOTA counterparts due to the flexibility of the ligand being less enthalpically favourable and reduced denticity when compared to the $[Ln(DTPA)]^{2-}$ and $[Ln(DOTA)]^{-}$ complexes as shown in Figure 1.1.

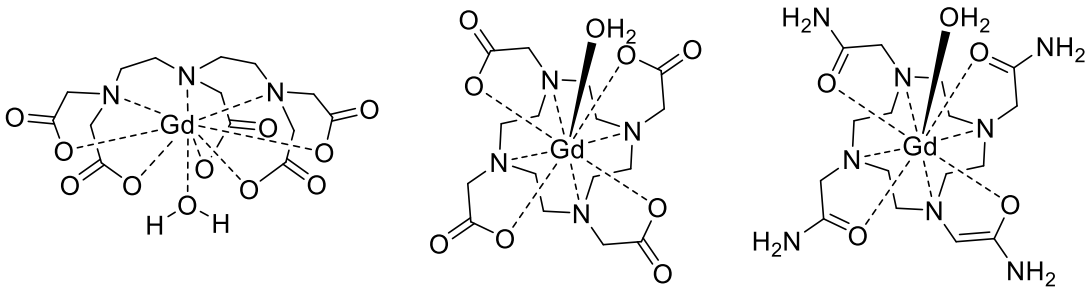

Figure 1.1: Structures of gadolinium complexes with DTPA, DOTA and DOTAM

While DTPA shows greater thermodynamic stability than EDTA, it is less thermodynamically stable than complexes with DOTA. This is largely due to entropic considerations, whereby the pre-organised DOTA ligand requires very little rearrangement upon complexation. Also, due to the rigid nature of macrocyclic ligands, they are less able to maximise their solvent interactions, resulting in the reduced solvation of the inner ligand cavity which can have an enthalpic contribution.[14] It can also be seen that the later lanthanides have generally increased stability constants. For EDTA and DOTA the increased charge density of the later lanthanides results in increased electrostatic interactions and a corresponding increase in thermodynamic stability. Whereas, for DTPA the maximum stability constants are reached around terbium, this is due to the reduced flexibility of the ligand making it less able to encapsulate the smaller lanthanide ions.

While polyaminocarboxylate ligands largely rely on the formal negative charge on the carboxylates to increase the electrostatic interactions, macrocyclic tetraamides such as DOTAM (Figure 1.1) rely on to the hard nature of the donors and entropic gain from the macrocyclic effect to give rise to thermodynamic stability.

1.3.2 Kinetic Stability

The kinetic stability of gadolinium based lanthanide complexes has been widely explored due to their extensive use as contrast agents for MRI imaging. The rate of complexation is dependent on many factors, such as: pH, concentration, temperature and the ligand used. Linear open chain ligands such as DTPA have a faster rate of complexation compared to macrocyclic ligands like DOTA, with DTPA having a rate of formation in the ms-s range whereas DOTA's rate of formation ranges from min-hour.[15] This is due to differences in the mechanism of complexations for the two ligands as well as the increased basicity of macrocyclic amines resulting in the need for a proton to dissociate before complexation can occur. DTPA forms complexes with Gd(III) through first maximising the electrostatic interactions between the electron deficient lanthanide ion and the electron rich carboxylate groups; this allows the conformationally flexible ligand to surround the lanthanide centre and displace all but one water molecule to form the $[Gd(DTPA)H_2O]^{2-}$ complex. This differs to the mechanism of formation for the $[Gd(DOTA)H_2O]^{-}$ complex which also uses the initial electrostatic interactions with the carboxylate group, but due to its increased rigidity cannot encapsulate the lanthanide ion in the same way as DTPA. In this case, once the gadolinium ion is transferred into the cavity it is first coordinated by two of nitrogen atoms in the macrocyclic ring then finally coordinated to the last two nitrogen donors to give the final complex.[16]

While linear open chain ligands have an increased rate of complexation compared to macrocyclic derivatives, it is the rate of dissociation of the metal that is of utmost importance, so although DTPA forms complexes faster than DOTA it will also dissociate faster. This is evident from the observed dissociation rates and half-lives of the gadolinium complexes as shown in Table 1.2, where k_{obs} is calculated from Equation 1.1, at pH 1 where the pH dependent term will dominate.[15,17,18]

$$k_{obs} = k_{ind} + k_{dep}[\mathrm{H}^+]$$

Equation 1.1:Observed rate of dissociation based on pH independent (k_{ind}) and dependent(k_{dep}) terms

Table 1.2: Dissociation kinetics for gadolinium complexes with DOTA and DTPA at pH 1

Complex	**k_{obs}**	**$T_{1/2}$**
[Gd(DOTA)]$^-$	>3x10^{-7}	> 1 month
[Gd(DTPA)]$^{2-}$	1.2x10^{-3}	10 min

The rate and mechanism for dissociation varies for different ligands, and for polyaminocarboxylates the two main mechanisms of metal dissociation are proton or acid catalysed dissociation and transmetallation. For example, complexes with EDTA typically undergo acid-catalysed dissociation leading to the loss of the metal centre, and complexes of DOTA dissociate via a proton-assisted mechanism which is a slow process even at pH 1 and negligible at physiological pH.[19,20] Gadolinium ions in DTPA complexes are generally displaced by transmetallation. This is the favoured mechanism of dissociation due to the increased charge on the complexes of DTPA with trivalent metal ion which make them better targets for electrophilic attack leading to dissociation of the lanthanide ion.

Transmetallation is an important factor to consider when looking at the kinetic stability of lanthanide complexes, this is especially true when considering the concentrations of Zn(II) (50 μM in serum) and Cu(II), both of which can displace gadolinium. For complexes with open chain ligands like DTPA the rate of transmetallation is directly proportional to the concentration of Zn(II) and Cu(II), suggesting direct attack on the encapsulated gadolinium ion.[17,20] While macrocyclic complexes have a rate of transmetallation that is independent of the concentration of Zn(II) or Cu(II) ions

concentration. This was demonstrated by Muller *et al*., who showed that for $[Gd(DOTA)]^-$ in 2.5 mM $ZnCl_2$ solution no dissociation was observed after 4 days.[21]

In recent years, the use of DO3A type ligands have been explored increasingly due to their potential for functionalisation of the pendant arm. However, unsurprisingly the pendant arms can have a significant effect on the overall kinetic stability of the complex. Caravan *et al*. investigated the kinetic inertness of DO3A complexes in the presence of Zn(II).[22] Although the complexes stability was not directly correlated with the ligand coordination number, having a third strongly coordinating arm (where the other two are carboxylates) is essential in terms of the complexes stability. Caravan also showed that the increased steric strain associated with the introduction a fourth arm, through N-alkylation of the fourth nitrogen on the macrocyclic ring, can serve to destabilise the system. They postulated that this instability resulted from steric strain causing the ligand to no longer be as effective in encapsulating the gadolinium ion and therefore produced a system that was destabilised.

1.4 Lanthanide Photophysics

Lanthanides display unique photophysical properties arising from several aspects of their structure and bonding. Their characteristic narrow emission bands, result from the minimal radial extension of the 4*f* orbital and small vibronic coupling.[23] As a consequence, the 4*f* orbitals do not interact significantly with the ligand orbitals, meaning that the emission is defined by quasi-atomic transitions between $^{2S+1}L_J$ states. In these ions, the spin-orbit coupling contributions effectively define the relative energies of the states, with minor effects from the crystal field giving rise to fine structure. As such, the form of lanthanide spectra tend to be very similar for a given lanthanide. The observed luminescence for the lanthanides ranges from the NIR (Nd^{3+}, Yb^{3+}) through the visible (Eu^{3+}, Tb^{3+}) to the UV (Gd^{3+}), but all show long luminescence lifetimes, ranging from

milliseconds to microsecond, due to the *f-f* transitions that give rise to the lanthanide centred luminescence being Laporte.[23] The long luminescent lifetimes of the lanthanides have been exploited in medical applications in order to remove the background auto-fluorescence of biological media, as demonstrated in Figure 1.2. This technique allows only the long-lived lanthanide luminescence to be collected even at very low concentrations of lanthanide probes (below femtomolar) and high signal-to-noise ratios to be achieved.[24–26]

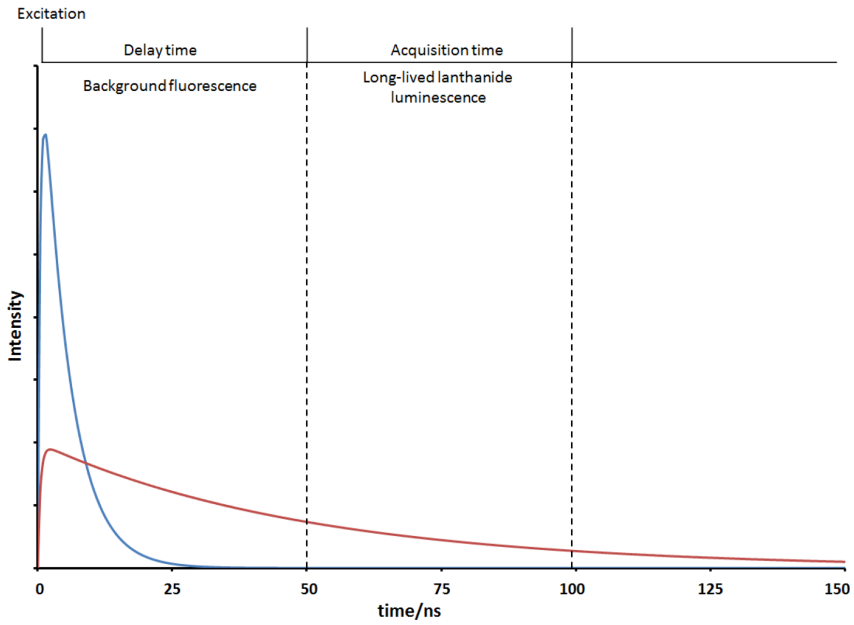

Figure 1.2: Schematic depicting the methodology for time gating, where the blue signal is the background fluorescence and the red signal is the lanthanides luminescence

While the lanthanides are known for having similar emission spectra for a given lanthanide, the intensity and form of hypersensitive transitions such as the $\Delta J=2$ transition for Eu^{3+} can vary substantially depending on the coordination environment. Hypersensitive transitions are electric dipole transitions which can show dramatic variations in intensity and splitting upon changes in local symmetry at the lanthanide ion. As such, these transitions can give important information about even small changes to the ligand field around the metal. It has been postulated that hypersensitive transitions

arise due to the non-zero electric dipole transitions arising from the electric dipole in the ligand being induced by the *f* orbitals of the lanthanide ion. Indeed, Judd and Ofelt published expressions for the intensities of induced electric dipole transitions for the lanthanide ions - resulting in the Judd-Ofelt theory which can be used to predict oscillator strengths in the absorption and emission spectra of lanthanides.[27–29]

1.4.1 Sensitised Emission

Due to the low *f-f* oscillator strengths, direct excitation of the lanthanide is inefficient.[30] This can be circumvented by exploiting the use of a sensitiser ("the antenna effect"), see Scheme 1.1. This was first reported by Weissman for the sensitisation of a europium complex.[31] This strategy allows energy to be absorbed by a chromophore (typically an aryl group or a d-block transition metal MLCT chromophore) to be transferred to a lanthanide centre, which then emits light.

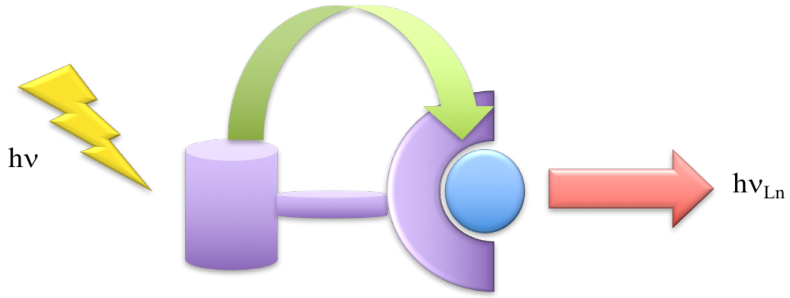

Scheme 1.1:Cartoon representation of the antenna effect

In order to attain efficient transfer of energy, the excited state manifold of the chromophore must have good orbital overlap with the lanthanide. The mechanisms for sensitised emission are outlined in Figure 1.3.[32]

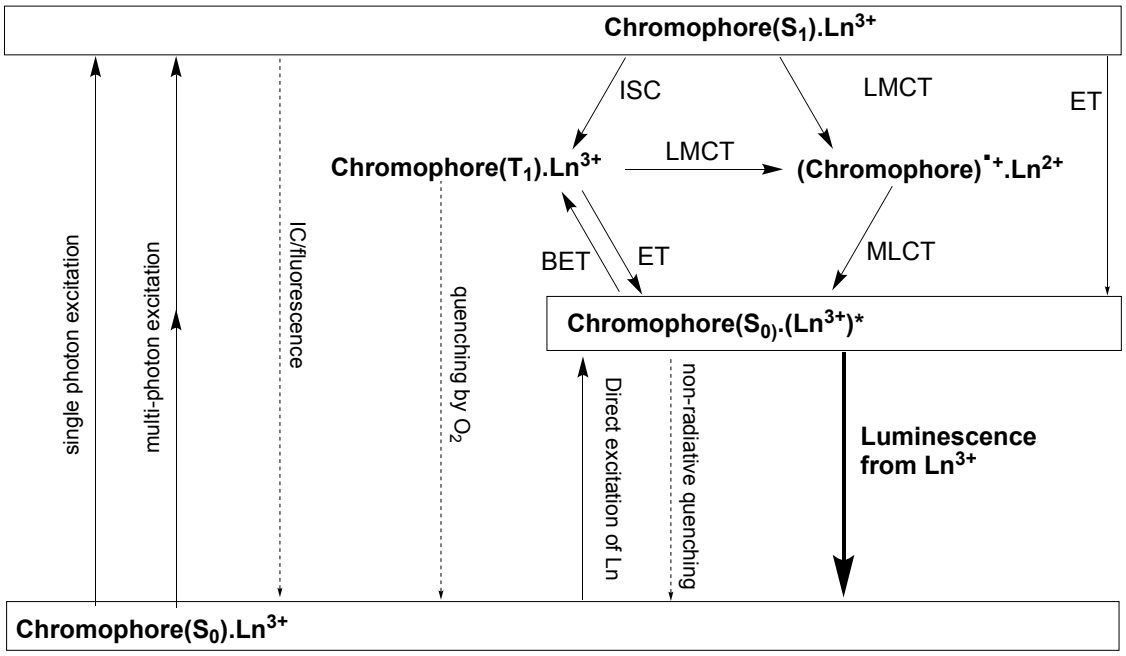

Figure 1.3: Energy diagram showing the sensitised emission of a lanthanide ion[33]

This process invariably begins *via* a photon absorbed by the chromophore, either single or multi-photon.[34,35] This excitation of the chromophore generates a singlet excited state, which can undergo radiative (fluorescence) to the ground state, non-radiative decay to the ground state or undergo intersystem crossing (ISC) to the chromophore triplet state. Energy transfer from the T_1 state can then populate the lanthanide excited states through Förster or Dexter exchange.[32,36] The lanthanide-centred excited state can then undergo radiative (luminescence) or non-radiative decay which leads to the deactivation of the triplet state. In order to minimise back-energy transfer (BET), the chromophore T_1 state needs to be around 2000 cm^{-1} above the lanthanide excited state to facilitate efficient lanthanide sensitisation.[37] Sensitisation directly from the chromophore S_1 state can also play a role, and is more common in systems where intraligand charge transfer states are present.[38,39]

Charge transfer mechanisms are increasingly important when considering lanthanides with an accessible stable +2 oxidation state, such as ytterbium and europium.[40] For

example, for ytterbium, this mechanism proceeds via a two sequential electron transfer steps, since (with electron rich ligands) the Yb(III) emissive $^7F_{5/2}$ state is generally lower in energy than the intermediate LMCT state, making the transfer more favourable. The accessed LMCT state can then populate the emissive $^7F_{5/2}$ state via MCLT.[32] This is also possible for europium but less common due to the LMCT state generally being lower in energy than europium's $^5D_0$ emissive state. This charge transfer mechanism allows for sensitisation when there is poor spectral overlap between the lanthanide and sensitiser.[41]

1.4.2 Energy transfer mechanisms

There are two main mechanisms for energy transfer in lanthanide luminescence: Förster energy transfer and Dexter exchange as outlined in Figure 1.4.

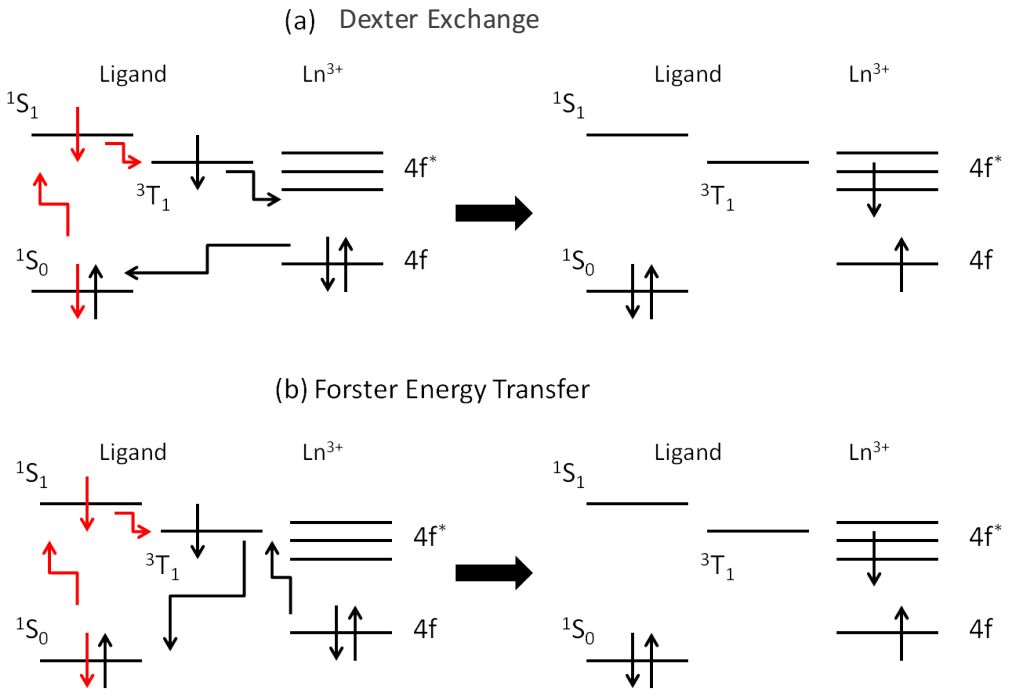

Figure 1.4: Mechanisms for energy transfer via Förster or Dexter exchange

The Dexter mechanism proceeds as a consequence of exchange and requires direct orbital overlap to be an efficient mechanism.[42] The efficiently of the exchange is therefore governed by the e^{-r} distance dependence and coupled with the requirement of orbital

overlap which results in the mechanism only being effective if there is a short inter-component distance between the donor and acceptor. This means it is likely to be the dominant mechanism if the donor is directly bound the lanthanide centre, however, energy transfer over longer distances can be obtained by this mechanism if there is extended conjugation between the donor and acceptor.[32,43] The Förster mechanism involves a through-space interaction and can occur over a longer range as it is a coulombic interaction and governed by a r^{-6} distance dependence in the case of dipole-dipole interactions, with the distance dependence becoming even greater in the case of interactions between multipoles.[44,45] The mechanism is also dependant on the donor-acceptor spectral overlap between the donor state and the narrow absorption bands associated with 4*f*-4*f* transitions, meaning Förster energy transfer is inefficient. Despite this being an inefficient mechanism (particularly in the case of lanthanides) it is often the only available mechanism due to the short distance dependence of the Dexter exchange mechanism.

1.4.3 Quenching

There are many possible mechanisms by which non-radiative quenching of the chromophore and lanthanide excited states can occur. As shown in Figure 1.3 for the chromophores excited states: the S_1 state can undergo collisional quenching by photoelectron transfer,[46] while the T_1 state can be quenched by singlet oxygen.[47] One of the most common mechanisms for quenching of the lanthanide excited states is through non-radiative pathways such as vibrational quenching by X-H oscillators e.g. OH, NH or CH due to the overlap of the vibrational harmonics of the *f-f* transition with the solvent oscillator.[48] If solvent XH oscillators are bound to the lanthanide centre, this can reduce the intensity of the lanthanide centred luminescence considerably, thereby reducing the quantum yield. The degree of quenching by water is inversely proportional to the energy

gap between the emissive and ground state of the lanthanide in question. This results in lanthanides with a large energy gap such as Eu(III) and Tb(III) to be less prone to quenching by vibrational deactivation than lanthanides with a smaller energy gap, such as Nd(III) or Er(III), which are efficiently quenched by solvent oscillators (Figure 1.5). This is reflected in the observed lifetime of the lanthanide emissive state, with Eu(III) and Tb(III) having lifetimes in the order of milliseconds and Nd(III) and Er(III) in the order of nanoseconds.[49–52] Using the corresponding XD oscillator can reduce the quenching efficiency of the solvent, as the lower stretching frequencies give an increased energy of the vibrational state resulting in less Franck-Condon overlap and less efficient quenching.[48,53] This also means that the lifetimes in deuterated solvents are longer than their protonated counterparts.

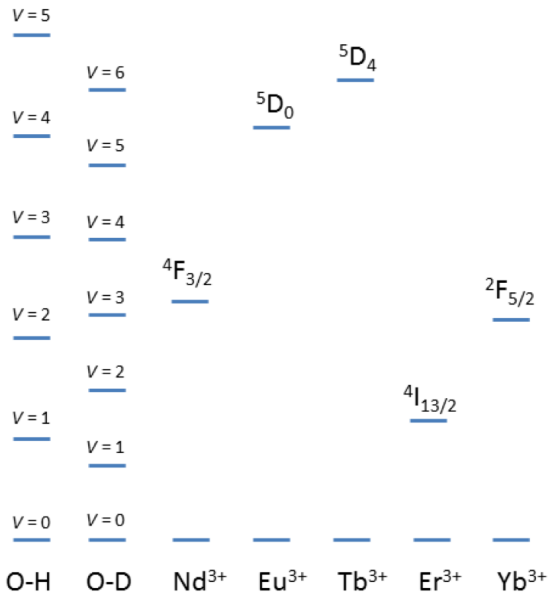

Figure 1.5:Schematic energy level diagram showing the energy levels of the ground and emissive states of selected lanthanide ions compared to the vibrational energy of OH/OD oscillators

The differences in lifetimes for deuterated and protonated media can be used to calculate the number of bound solvent molecules, q, using the modified Horrocks equation[48]

(Equation 1.2). This equation uses the rate of depopulation of the lanthanide excited state in H_2O and D_2O, and makes the assumption that the quenching via OH/OD oscillators is the dominant mechanism of depopulation.

$$q = A(k_{H2O} - k_{D2O}) - B$$

Equation 1.2: Modified Horrocks equation for the calculation of the number of bound solvent molecules for a lanthanide centre

Where q is the number of bound solvent molecules, k is the rate constant of decay (in H_2O and D_2O), A is a proportionality constant that is specific to the lanthanide in question and describes the affinity of the lanthanide to binding OH oscillators, and B is an empirical correlation factor that accounts for outer sphere quenching from solvent molecules and other donors e.g. oxygen from the ligand carboxylates. Some lanthanides are particularly sensitive to oscillators in the ligand scaffold, for europium an additional correlation factor taking the number of NH amines into account is applied to better calculate the value of q, as shown in Equation 1.3.

$$q = A(k_{H2O} - k_{D2O}) - B - 0.075x$$

Equation 1.3: Modified Horrocks equation including an amide NH contribution for europium systems; x is the number of exchanging amide NH oscillators in close proximity to the lanthanide centre in the ligand scaffold, defines the correlation factors A and B for Eu(III), Tb(III) and Yb(III) (in H_2O/D_2O as values for A double and B halve when measured in MeOH/MeOD).

Table 1.3: A and B values for the modified Horrocks equationin aqueous solution

	A	**B**
Eu	1.2 ms	0.25 ms^{-1}
Tb	5 ms	0.06 ms^{-1}
Yb	1 μs	0.2 μs^{-1}

While this can be a useful tool to assess the number of solvent molecules bound to a lanthanide centre, it is also worth noting that as systems become increasingly complicated and when other energy transfer mechanisms are present the assumptions are no longer wholly valid, and caution is needed when analysing these cases. These circumstances can arise in systems where more than one metal centre (or more than one species) need to be accounted for: the profound differences in quantum yield between systems with different values of q mean that calculations must, of necessity, be based on quantum yield weighted averages. Such issues arise in the subject matter of this thesis and will be discussed later.

1.5 NMR

1.5.1 Paramagnetic NMR

The NMR of lanthanide complexes is dominated by their paramagnetic nature. This dramatically changes the broadness of the resonances and the observed chemical shift. Equation 1.4 describes the components which contribute to the Lanthanide Induced Shift observed (LIS, Δ_{obs}) where Δ_d is the diamagnetic contribution, Δ_c is the contact shift – a through bond interaction and Δ_p is the pseudocontact shift – a through-space interaction.[54]

$$\Delta_{obs} = \Delta_d + \Delta_c + \Delta_p$$

Equation 1.4: Contributions to the overall observed lanthanide induced shift

The contact shift contribution is described by Equation 1.5, where A is the hyperfine coupling constant, γ is the gyromagnetic ratio of the nucleus in question, B_0 is the strength of the applied field and $\langle S \rangle$ is the total spin expectation value. The contact shift results from through-bond spin coupling between the unpaired electron spins on the metal and the orbitals on the nucleus under investigation (Equation 1.5).[54] As the unpaired electrons in the *f* orbitals are radially contracted there is negligible overlap between the

metal and nucleus of interest, meaning the contact shift is often considered to have a minor contribution.

$$\Delta_c = -\frac{A \cdot \langle S \rangle}{h \cdot \gamma \cdot B_0}$$

Equation 1.5:Contact shift contribution to the LIS for paramagnetic lanthanide species

The pseudocontact shift is a through space dipole-dipole interaction that arises from the coupling of the electronic and magnetic dipole moments and can be described by Equation 1.6 where $\langle r^2 \rangle B_2^0$ and $\langle r^2 \rangle B_2^2$ are crystal field coefficients, r, θ, ϕ are the spherical coordinates nucleus with reference to lanthanide position, C_J is a constant containing magnetic susceptibility factors and μ_B is the Bohr magneton.

$$\Delta_{pc} = \frac{2\mu_B{}^2 C_J}{60k^2T^2}\left(\frac{\langle r^2 \rangle B_2^0(3cos^2\theta - 1) + \langle r^2 \rangle B_2^2(sin^2\theta cos2\varphi)}{r^3}\right)$$

Equation 1.6: Pseudo-contact shift contribution to the LIS for paramagnetic lanthanide species

As the pseudo contact shift is a dipole-dipole interaction, the magnitude of which depends on the magnitude of these dipoles as well their orientation and separation and it is not affected by the limited overlap with the *f* orbitals. Pseudocontact shift is therefore the dominant contribution to the observed shift. The magnitude of the observed shift for a specific metal ion is related to the effective magnetic moment μ_{eff}, a term that is included in the C_J parameter in Equation 1.6. This can be seen by looking at the overall spectral width of the ^{1}H NMR for different lanthanides, for example Nd(III) with a μ_{eff} of 3.62 has a spectral width of 100 ppm whereas Tb(III) with a much higher μ_{eff} of 9.72, has a spectral width around 800 ppm.[55]

Bleaney used this to model the phenomenon, using Equation 1.7 for axially symmetric systems, as this results in the second term in Equation 1.6 to tend to zero allowing a simplified equation to be applied:

$$\Delta_p = \frac{2\mu_B{}^2 C_J}{60(kT)^2}\left(\frac{3(cos^2\theta - 1)}{r^3}\right)B_0^2$$

Equation 1.7:Simplified Bleaney equation for calculating the pseudocontact shift in axially symmetric systems

Where C_J and $\mu_B{}^2$ are constants, θ and r are polar coordinates relative to the principle axis and B_0^2 is the second order crystal field parameter.[54] It should be noted that, while the second order crystal field parameter dominates, other higher order parameters also play a role.[56] Furthermore, changes to the local crystal field can have profound consequences on the anisotropy of the lanthanide ground state - sometimes even reversing the order of the peaks in the NMR spectrum.[57]

While this equation makes several assumptions, it works well for systems with small contact shifts, such as ytterbium, and high symmetry complexes as shown by Blackburn *et al*.[56,57] The theory falters when modelling lanthanides such as europium, which show large contact shift contributions and when looking at low symmetry systems. To fit such systems, the equation becomes increasingly complex, with up to 27 possible parameters.[58]

1.5.2 Isomers in NMR

The degree of lanthanide induced shift undergone by nucleus depends on its location relative to the magnetic axis of the lanthanide. This can be illustrated by Figure 1.6 where the pseudo contact shift isosurface for an axially symmetric complex, like [Eu.DOTA]. The geometric term can be related to that of a $d_z{}^2$ orbital where the protons in the red zones will be deshielded and shifted downfield, while protons in the blue zone will be

shielded and shifted upfield, the degree of the shift experienced by the protons in these environments depends on r and θ.

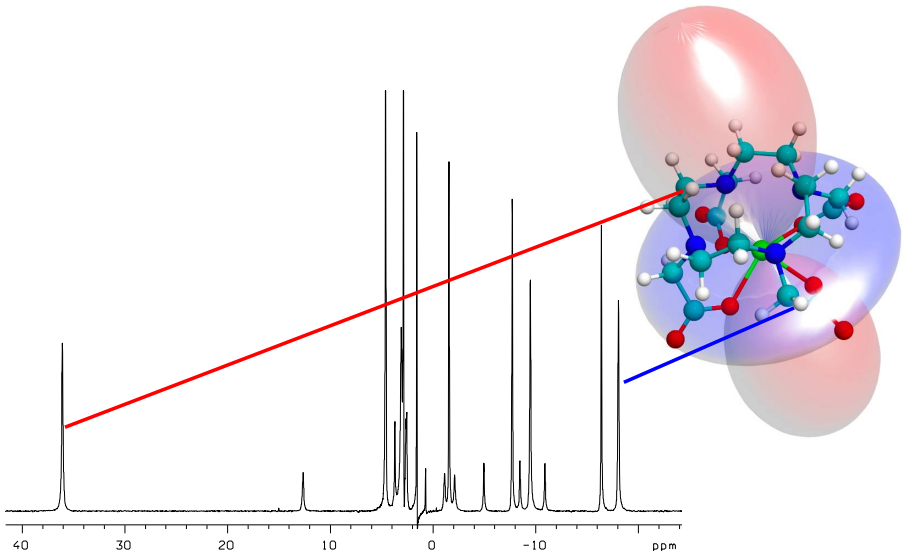

Figure 1.6: Cartoon relating the geometric positon of protons in an EuDOTA complex to their observed ^{1}H NMR shift

The distance and angles in C_4 complexes are largely determined by the isomers present in solution. Axially symmetric complexes can exist in four isomeric species (two diastereoisomeric pairs of enantiomers) in solution as shown in Figure 1.7. The square antiprism (SAP) isomers are defined by their larger twist angle of 40° compared to the twisted square antiprism (TSAP) which has a twist angle of 30°.[59,60] These isomers can undergo interconversion either through cooperative arm rotation or by ring inversion, although for systems like DOTA the barrier to interconversion means the exchange is slow on typical NMR timescales.[61]

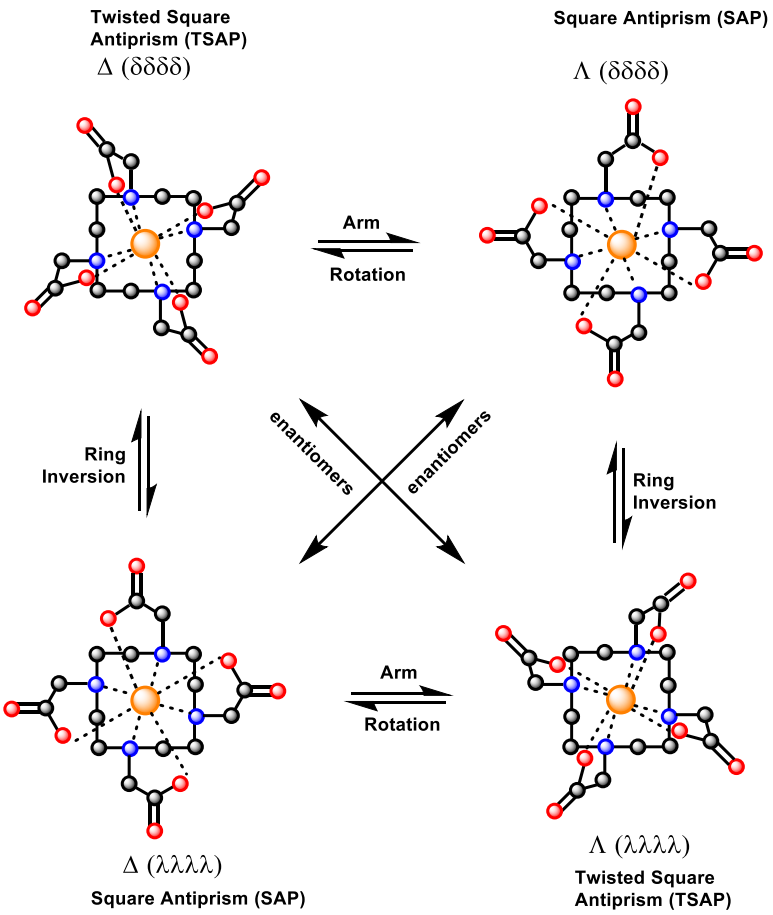

Figure 1.7:Schematic diagram for the possible isomers of [Ln(DOTA)]$^-$ complexes

However, for complexes like DO3A the interconversion can be much faster due to the reduced barrier to arm rotation; this fast exchange on the NMR timescale results in broader resonances than for C4 symmetric systems.[62] While the broken symmetry of DO3A complexes makes the interpretation and assignment non-trivial, it is sometimes possible to distinguish between isomers in solution by comparing back to and drawing analogies from the symmetric systems.

1.6 Applications of lanthanide complexes

1.6.1 Sensing Anions

The sensing of anions has become a widely-researched area, and has been applied to anions such as: carboxylates, phosphates, citrate, bicarbonate and fluoride.[63–67] The sensing of anions can be monitored by a change, such a monitoring changes in: q, luminescence spectra, NMR.

For example, Lowe *et al*. developed a MRI probe that modulated q as a function of pH.[68] This idea worked on the basis that tumours are known to be more acidic (pH 6.8) compared to healthy tissue (pH 7.4) therefore a probe that would have increased relaxivity in acidic conditions would be advantageous. To achieve this, they synthesised dpp based complexes, shown in Scheme 1.2, where Ln=Gd or Eu.

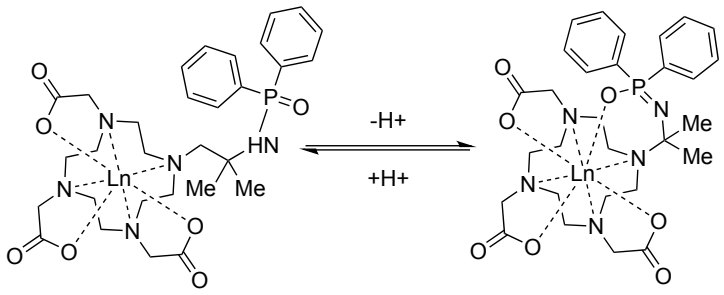

Scheme 1.2: [Ln(dpp)]complex and its pH dependant intramolecular coordination[68]

The relaxivity was first studied using the gadolinium analogue, at varying pH. The results showed increased relaxivity with decreasing pH - the change in relaxivity was significant (4.4 at pH 10 compared to 8.2 at pH 5), and it was reasoned that this was the result of increased hydration due to the reversible intramolecular coordination favouring the open form at low pH, shown in Scheme 1.2. This theory was explored using the europium analogue where the measured q values at high and low pH confirmed the presence of a q=1 complex at high pH and a q=2 complex at low pH. The europium complex also

showed an increase in emission intensity with increasing pH (Figure 1.8) which would correspond to the formation of a complex with decreased hydration.

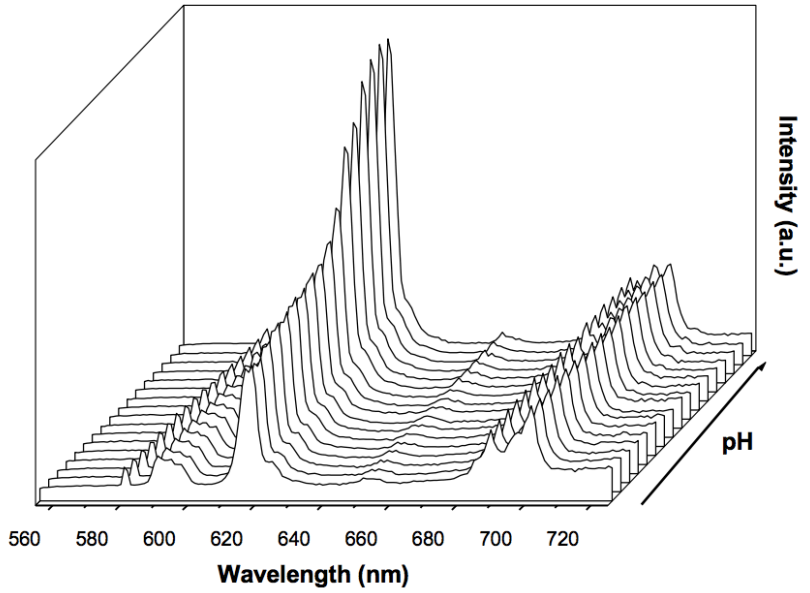

Figure 1.8: Observed change in the emission spectra of the [Eu(dpp)] analogue with varying pH. Taken from reference 68

While using lanthanide complexes as MRI agents is a vital part of biomedical imaging, they can also be used to sense biologically important species directly.[65,69] Phosphate species, for example, play an important role in physiological processes and the glycolysis pathway. The ability to sense the presence of phosphate can be biologically important due to the changing balance of phosphate species associated with hypoxic environments *in vivo*.

One example of phosphate binding uses a bridging ligand bound to two lanthanide complexes.[70] When an anion is introduced then bridging ligand dissociates and the anion becomes bound the metal centres as shown in Scheme 1.3.

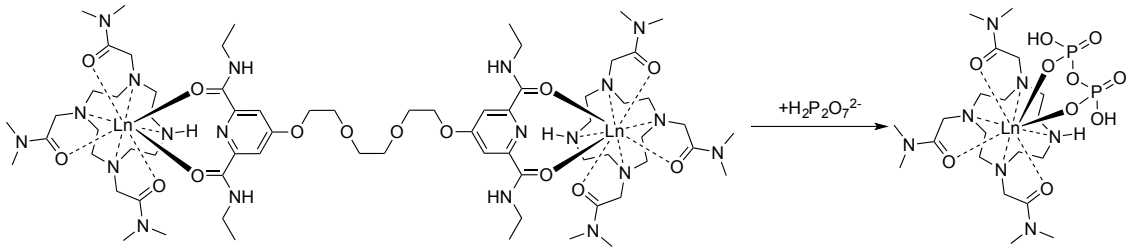

Scheme 1.3 Displacement of a bridging ligand by dihydrogen phosphate

This serves an "on-off" probe where the luminescence of the lanthanide is effectively switched off by the binding of phosphate, as illustrated in Figure 1.9.

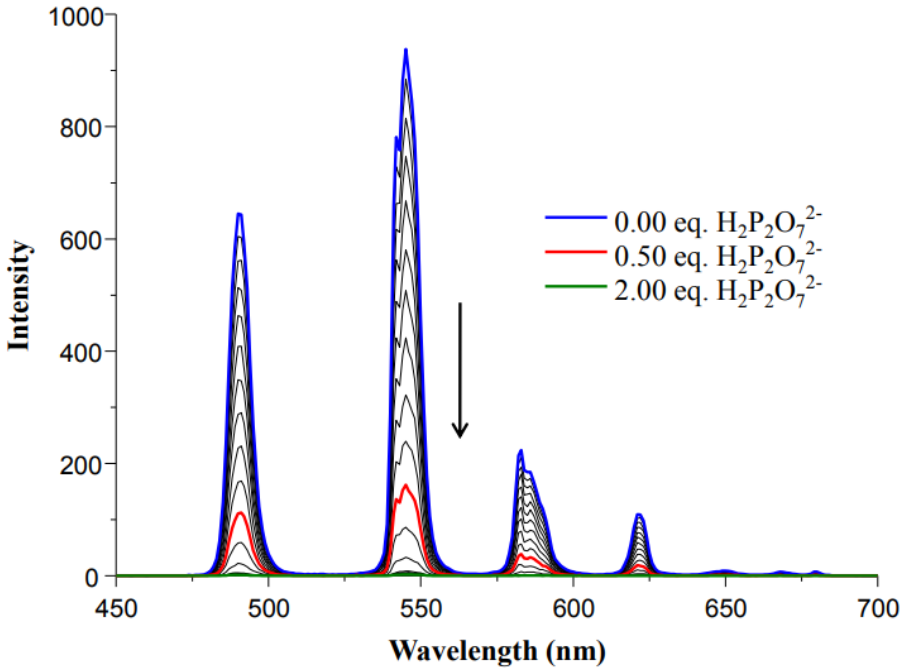

Figure 1.9:Emission spectra showing the decrease in emission intensity upon binding of dihydrogen phosphate[70]

Sensing of other anions such as fluoride can be important due to the potential military applications in sensing chemical agents such as sarin and sensing of fluoride levels in water.

Fluoride binding to lanthanide complexes has been widely researched, including a study by Blackburn *et al*. which showed that the binding of fluoride to C_4 symmetric complexes

based on picolyl-containing cyclen ligands display a significant change in the luminescence spectrum shown for the europium complex in Figure 1.10.[71]

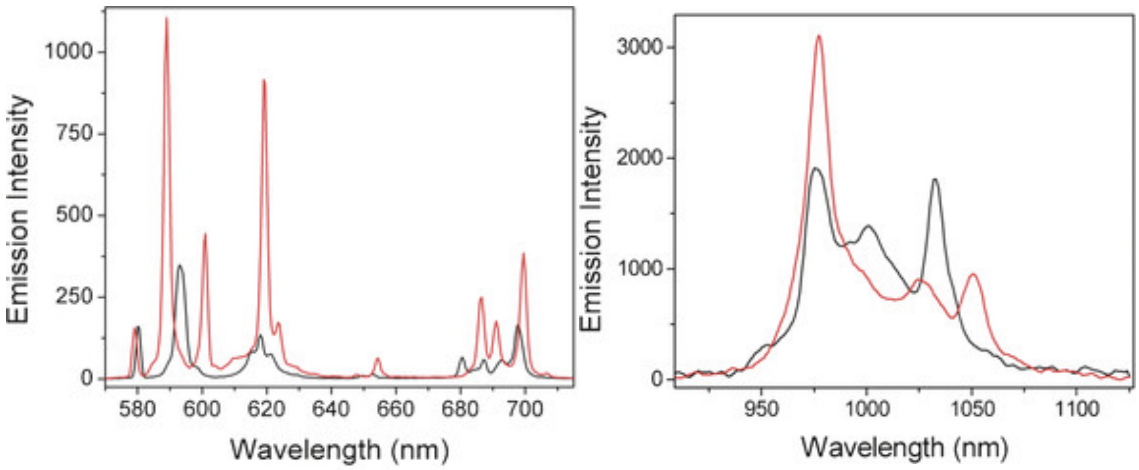

Figure 1.10:Examples of changes to spectral fine structure as a consequence of fluoride binding in a europium complex (L) and an ytterbium complex (R). (In each case, the red spectrum was recorded in the presence of fluoride) Taken from reference 71.

The changes in the luminescence is indicative of changes in the crystal field as a result of fluoride binding, as indicated by the increased Stark splitting in the Eu $^5D_0$-$^7F_1$ band. The study also showed changes in the ^{1}H NMR spectrum illustrated by the Yb and Eu analogues shown in Figure 1.11. The binding affinities were also assessed by a ^{1}H NMR titration giving values of logK of 5.0 and 5.2 for the europium and ytterbium complexes respectively, which are in good agreement with the binding constants obtained from the luminescence study.

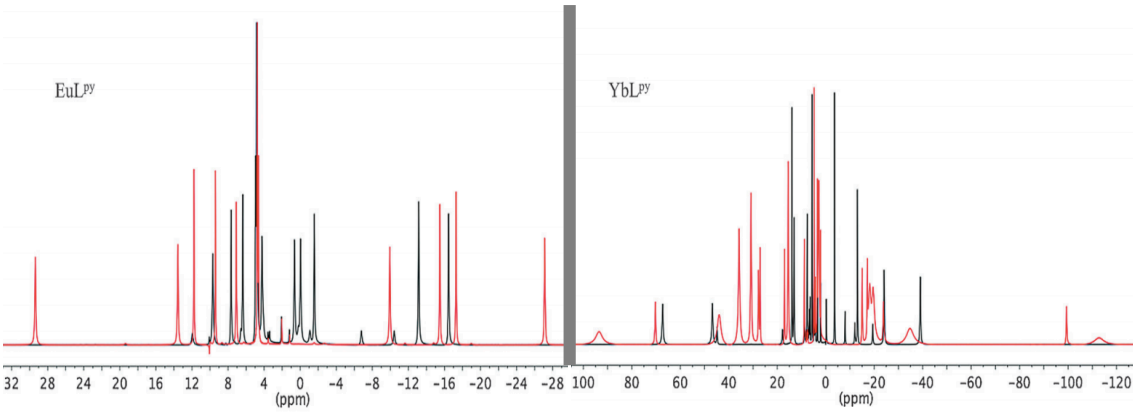

Figure 1.11:Changes to the NMR spectra of two complexes on binding fluoride.(In each case, the red spectrum was recorded in the presence of fluoride) Taken from reference 71.

The NMR spectra show the loss of peaks from the original complex and the appearance of new peaks associated with the fluoride bound analogue which is in slow exchange. While the analysis of the ytterbium complex is relatively straightforward, that of the europium complex, with its increased contact shift, broad linewidths and range of isomers (SAP and TSAP) is much less so.

While this study focuses on how fluoride binding and affect the spin and magnitude of the crystal field and magnetic anisotropy it also illustrates how these techniques could be exploited for applications to sense fluoride.

1.6.2 MRI

MRI responsive is a non-invasive technique widely used in medicine as a diagnostic tool. It has become increasingly common since first proposed in the 1970's[6] as it achieves high resolution capable of whole body images, without the use of ionising radiation. MRI works by the detecting the different relaxation rates of water in various healthy and damaged tissues in the body to give images such as Figure 1.12.[72]

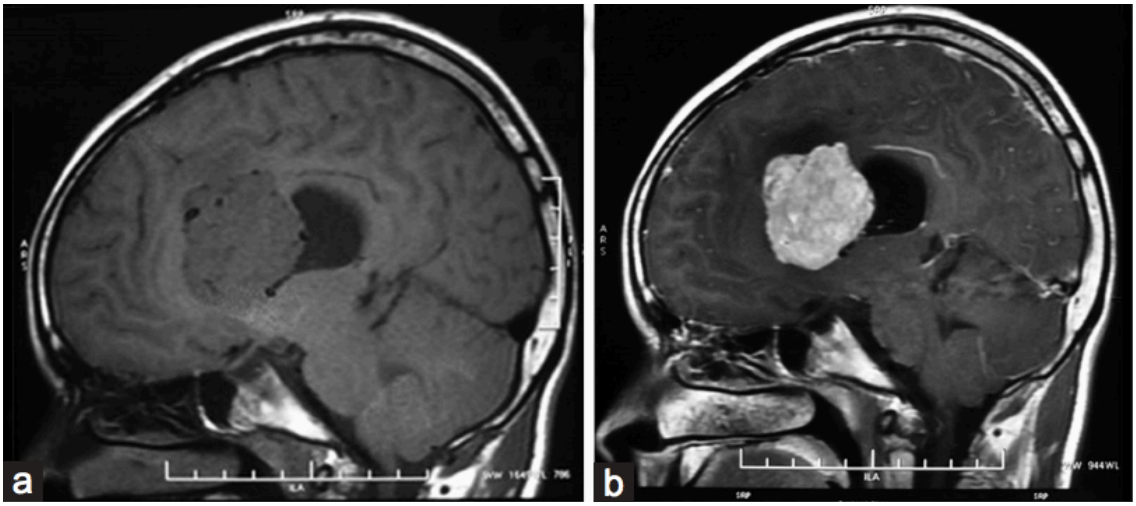

Figure 1.12: MRI without (image a: left)and with gadolinium contrast agent (image b: right) showing the presence of a glioblastoma[73]

These images can be improved by the use of contrast agents, first used clinically in 1988.[74] Examples such as DOTA and Omniscan,[15] shown in Figure 1.13, are commercially available, but a wide range of suitable compounds can also be found in the literature. [75–78]

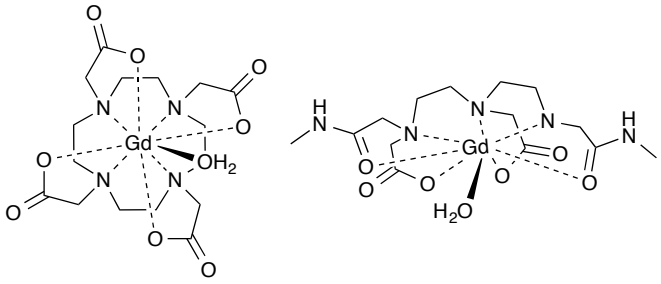

Figure 1.13: Typical clinical MRI contrast agents Gd[DOTA] and Omniscan

These complexes improve the image by accelerating the rate at which the surrounding water molecules relax, thorough lanthanide induced relaxation (LIR).[79] Inner sphere water molecules bound to the paramagnetic centre will undergo relaxation, these can then exchange with the bulk giving an overall increased relaxation rate.

Gadolinium complexes generally give the highest relaxivity, and so are used in most of the commercially available CAs, such as those shown in Figure 1.13. Gadolinium is used

because it has 7 unpaired electrons with isotropic distribution, which leads to slow relaxation rates and rapid exchange by shortening the longitudinal relaxation time (T_1).

It is necessary to ensure that gadolinium based contrast agents are highly kinetically and thermodynamically stable it is known to be highly toxic to humans.[6]

Kinetic and thermodynamic stability of these agents can be achieved through encapsulating gadolinium in a polydentate macrocyclic compound as discussed earlier. Kinetic stability can also be improved using bulky and rigid arms or by introducing lipophilic groups which can increase the overall kinetic stability of the complex. Therefore, when designing contrast agents macrocyclic based complexes e.g. Gd[DOTA], are favoured over contrast agents such as Omniscan as they are less stable and therefore more likely to result in complications due to the presence of unbound gadolinium - as reflected by the FDA issued warning for the use of this contrast agent in patients with compromised kidney function.

1.6.3 Positron Emission Tomography (PET)

PET is a sensitive method that allows for the quantitative measurement of metabolic and physiological process *in vivo* by exploiting the physiological differences for healthy verses cancerous tissue. PET is a nuclear imaging technique that employs radionuclides that decay by positron emission, these positrons produce high energy gamma photons though annihilation with electrons, and these gamma signals can then be detected by gamma cameras. This can be coupled with other imaging techniques to create multimodal images as shown in Figure 1.14.[80]

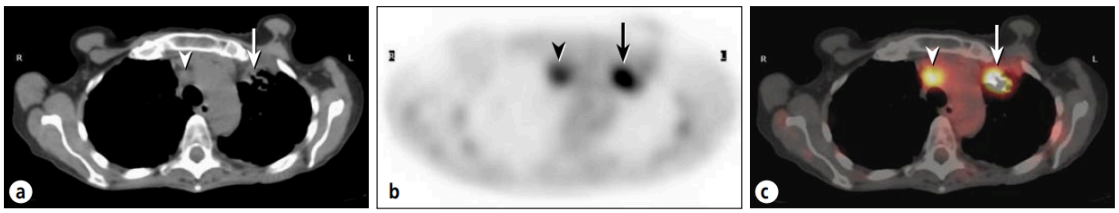

Figure 1.14:Multimodal images of lung tumours, where A: CT scan, B: PET scan and C: PET-CT image[80]

While positron emitting nuclides such as ^{15}O, ^{13}N and ^{11}C can be used, ^{18}F is typically favoured.[81] There are several reasons for this, firstly ^{18}F has a half-life of 110 minutes (ca. 2, 10 and 20 minutes for ^{15}O, ^{13}N and ^{11}C respectively) which allows for more elaborate labelling syntheses and for the tracer to become well distributed *in vivo*, while being short enough to ensure the dose of radiation received by the patient is not too high.[81] ^{18}F also has a high positron decay pathway probability (97 %) and low positron energy (max= 0.6 MeV), resulting in a short diffusion range allowing for increased resolution limits.[81]

Due to these favourable properties for PET imaging synthesis and radiolabelling for ^{18}F has become a widely-researched area.[82–84] Nucleophilic aliphatic and aromatic substitution reactions for this purpose are typically considered to be the most robust and reliable, examples of these reactions are shown in Scheme 1.4.[81,85]

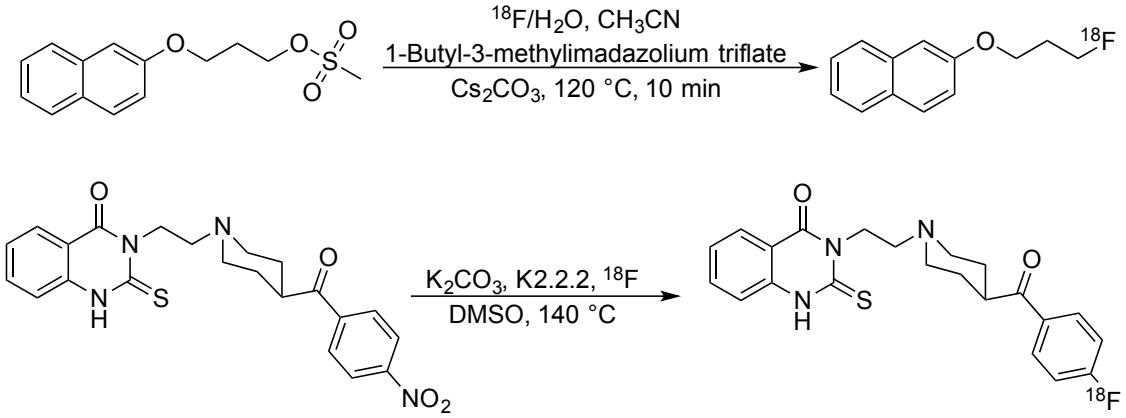

Scheme 1.4:Examples of Nucleophilic aliphatic and Nucleophilic aromatic substitution for ^{18}F fluorination[81,85]

However, there is scope for the use of other labelling techniques such as: transition metal mediation or by strain promoted azide-alkyne cycloadditions are also being increasingly explored (Scheme 1.5).[86,87]

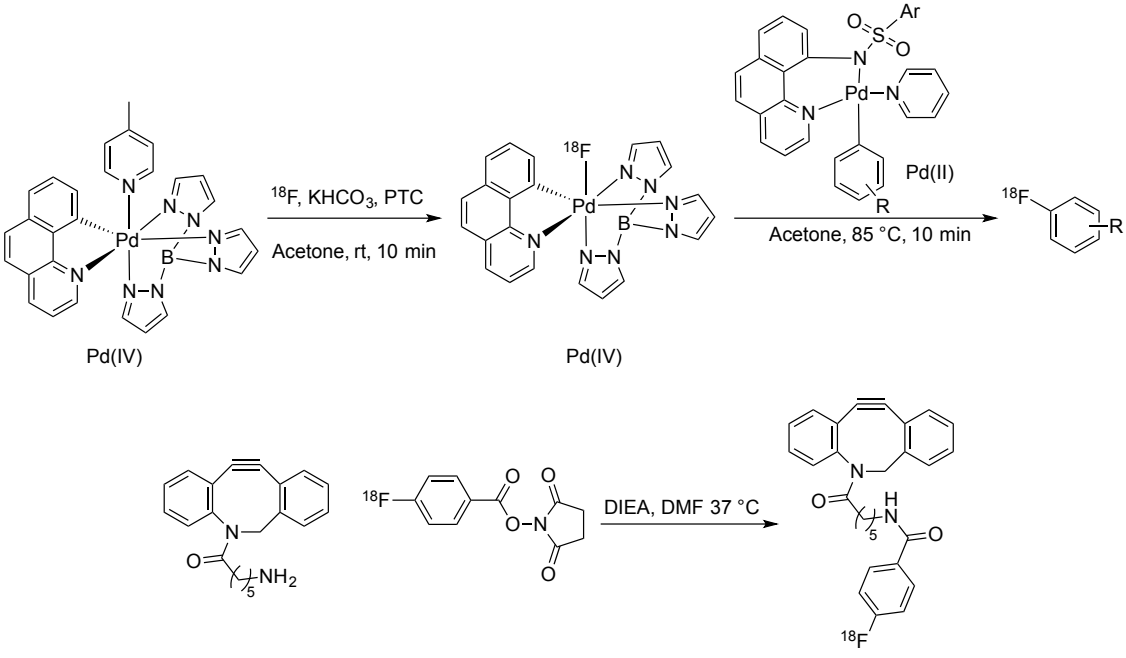

Scheme 1.5:Examples of the use of a palladium complex and cyclooctyne for ^{18}F fluorination[86,87]

The versatility of these methods of labelling means the development and improvement of these labelling techniques is expanding rapidly becoming an important in the development of new probes for PET imaging.[84]

1.6.4 Catalysis

Lanthanides, although most commonly known for their uses in sensing and imaging, have used as catalysts for a wide variety of reactions. They are commonly associated with their uses a doped components in zeolites for catalytic cracking (to reduce emissions of hydrocarbons, carbon monoxide and nitrous oxides),[88] but they have also been applied to a wide variety of organometallic reaction including: hetero-Diels Alder, hydroamination, acetalisation, hydrogenation, reductions of esters and α-substituted ketones (selected examples shown in Scheme 1.6).[89–94]

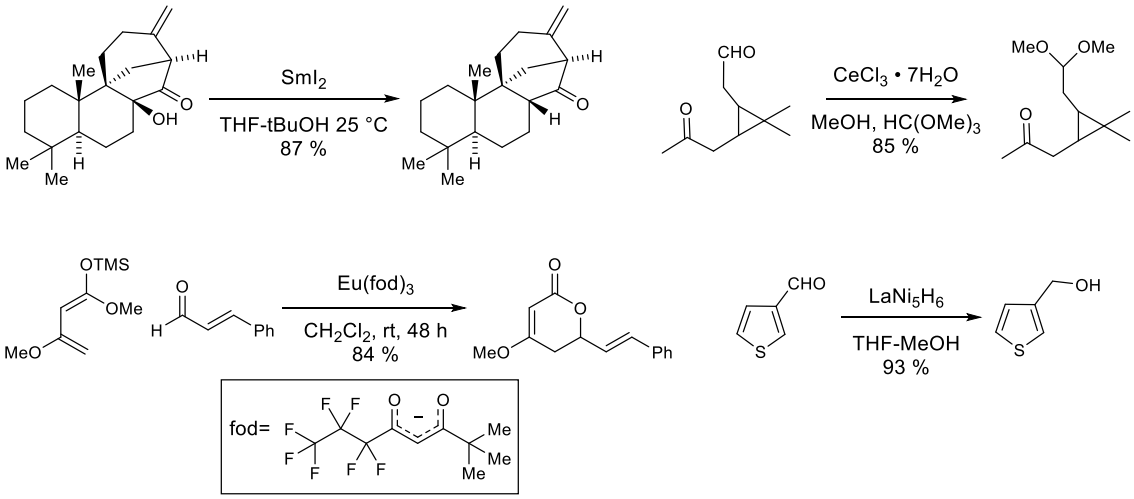

Scheme 1.6: Clockwise left to right: reduction of an α- substituted ketone, acetalization, hetero-Diels-Alder and hydrogenation[89–94]

Lanthanides are attractive candidates to be employed as catalysts for several reasons. One major advantage for lanthanide based catalysts is their water solubility, this means they can be utilised when more traditional Lewis acid catalysts such as aluminium chloride or ferric chloride would require organic solvents. The ability to catalyse reactions in aqueous media means they are considered to be green catalysts as they remove/limit the need for organic solvents.[95] Lanthanides are known to be hard Lewis acids and with high oxophilicity they lend themselves to catalytic transformations such as Luche reductions or hetero-Diels-Alder reactions that have transitions states involving substrates bound via

oxygen atoms to the catalyst.[89,96] While many of the advantages of using lanthanides as catalysts stem from their inherent chemical properties, there is also extensive literature precedent for functionalising the lanthanide centre in order to achieve selectivity, meaning they can be applied to a wide range of reactions.

Lanthanides have been used in many forms as catalysts and while most use the lanthanide triflates or oxides, due to the ease of use and availability, more complex architectures have also been explored. For example, asymmetric lanthanide catalysts have been used to achieve high enantioselectivity, as with the asymmetric nitroaldol reaction. This has been achieved using chiral based ligands give enantiomerically enhanced products as shown in Scheme 1.7.[97]

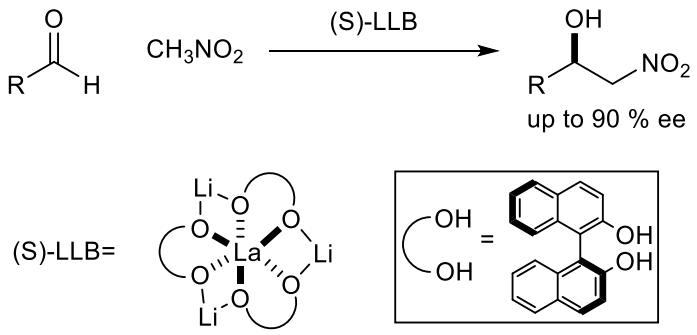

Scheme 1.7: Asymmetric nitroaldol reaction with asymmetric lanthanide catalyst[97]

The large number of available lanthanide complexes and the wide range of different functionalities that can be introduced means that their use as catalysts is evolving to cover a multitude of reactions. However, there have been very few reports of using lanthanide complexes with cyclen derivatives in catalytic applications. The only notable example is the work of Dickins *et al.*, who showed that the chirality of such systems can be exploited to deliver moderate enantioselectivity with the catalysis of Henry reactions.[5,98]

1.7 Aims

This thesis aims to develop new methods that can be used to elaborate the structures of kinetically stable lanthanide complexes - ultimately with a view to preparing responsive complexes and bioconjugates that can be used for a range of applications.

This will be achieved through exploring the use of heptadentate DO3A ligand systems as substrates for Click reaction, gold catalysed couplings and synthesising heptadentate rigid DO3AM derivatives. These systems will then be used to study anion binding and potential for use in applications such imaging, anion sensing and catalysis.

1.8 References

1. D. Jones, M. B. Andrews, A. N. Swinburne, S. W. Botchway, A. D. Ward, J. Lloyd, and L. Natrajan, *Chem. Sci.*, 2015.
2. S. P. Fricker, *Chem. Soc. Rev.*, 2006, **35**, 524–33.
3. I. Hemmilä and V. Laitala, *J. Fluoresc.*, 2005, **15**, 529–42.
4. S. P. Sinha, *Systematics and the Properties of the Lanthanides*, Springer Netherlands, 1983.
5. R. S. Dickins, S. Gaillard, S. P. Hughes, and A. Badari, *Chirality*, 2005, **17**, 357–363.
6. K. M. Hasebroock and N. J. Serkova, *Expert Opin. Drug Metab. Toxicol.*, 2009, **5**, 403–16.
7. B. Y. C. Cheong and R. Muthupillai, *Tex. Heart Inst. J.*, 2010, **37**, 508–15.
8. F. P. Hinz and D. W. Margerum, *J. Am. Chem. Soc.*, 1974, **96**, 4993–4994.
9. D. K. Cabbiness and D. W. Margerum, *J. Am. Chem. Soc.*, 1969, **91**, 6540–6541.
10. W. P. Cacheris, S. K. Nickle, and A. D. Sherry, *Inorg. Chem.*, 1987, **26**, 958–960.
11. R. M. Smith and A. E. Martell, *Sci. Total Environ.*, 1987, **64**, 125–147.
12. K. Kumar, C. A. Chang, and M. F. Tweedle, *Inorg. Chem.*, 1993, **32**, 587–593.
13. J.C. G. Bünzli and V. K. Pecharsky, *Handbook on the physics and chemistry of rare earths including actinides. Volume 51*.
14. E. C. Constable, *Coordination chemistry of macrocyclic compounds*, Oxford University Press, 1999.
15. A. D. Sherry, P. Caravan, and R. E. Lenkinski, *J. Magn. Reson. Imaging*, 2009, **30**, 1240–8.
16. J. Moreau, E. Guillon, J.-C. Pierrard, J. Rimbault, M. Port, and M. Aplincourt, *Chem. - A Eur. J.*, 2004, **10**, 5218–5232.
17. L. Sarka, L. Burai, and E. Brücher, *Chem. - A Eur. J.*, 2000, **6**, 719–724.
18. É. Tóth, R. Király, J. Platzek, B. Radüchel, and E. Brücher, *Inorganica Chim. Acta*, 1996, **249**, 191–199.
19. Z. Baranyai, Z. Pálinkás, F. Uggeri, A. Maiocchi, S. Aime, and E. Brücher, *Chem. - A Eur. J.*, 2012, **18**, 16426–16435.
20. E. Toth, E. Brucher, I. Lazar, and I. Toth, *Inorg. Chem.*, 1994, **33**, 4070–4076.
21. S. Laurent, L. Vander Elst, and R. N. Muller, *Contrast Media Mol. Imaging*, 2006, **1**, 128–137.
22. M. Polasek and P. Caravan, *Inorg. Chem.*, 2013, **52**, 4084–4096.
23. J.-C. G. Bünzli and C. Piguet, *Chem. Soc. Rev.*, 2005, **34**, 1048–77.
24. S. Faulkner, S. J. A. Pope, and B. P. Burton-Pye, *Appl. Spectrosc. Rev.*, 2005, **40**, 1–31.
25. A. Beeby, S. W. Botchway, I. M. Clarkson, S. Faulkner, A. W. Parker, D. Parker, and J. A. G. Williams, *J. Photochem. Photobiol. B Biol.*, 2000, **57**, 83–89.
26. H. L. Handl and R. J. Gillies, *Life Sci.*, 2005, **77**, 361–371.
27. B. R. Judd, *J. Chem. Phys.*, 1966, **44**, 839–840.
28. B. R. Judd, *Phys. Rev.*, 1962, **127**, 750–761.

29. G. S. Ofelt, *J. Chem. Phys.*, 1962, **37**, 511–520.

30. D. Parker, *Coord. Chem. Rev.*, 2000, **205**, 109–130.

31. S. I. Weissman, *J. Chem. Phys.*, 1942, **10**, 214–217.

32. S. Faulkner, L. S. Natrajan, W. S. Perry, and D. Sykes, *Dalton Trans.*, 2009, 3890–9.

33. P. Hänninen and H. Härmä, Eds., *Lanthanide Luminescence*, Springer Berlin Heidelberg, Berlin, Heidelberg, 2011, vol. 7.

34. T. J. Sørensen, O. A. Blackburn, M. Tropiano, and S. Faulkner, *Chem. Phys. Lett.*, 2012, **541**, 16–20.

35. L.-O. Pålsson, R. Pal, B. S. Murray, D. Parker, A. Beeby, R. A. Poole, H. Puschmann, P. A. Stenson, A. L. Thompson, J. Yu, and J. H. Yu, *Dalt. Trans.*, 2007, **4**, 5726.

36. G. D. Scholes, *Annu. Rev. Phys. Chem.*, 2003, **54**, 57–87.

37. A. Beeby, L. M. Bushby, D. Maffeo, J. A. Gareth Williams, A. M. Kenwright, D. Parker, A. S. de Sousa, J. A. G. Williams, and M. Woods, *J. Chem. Soc. Dalt. Trans.*, 2002, **30**, 48–54.

38. A. D'Aléo, F. Pointillart, L. Ouahab, C. Andraud, and O. Maury, *Coord. Chem. Rev.*, 2012, **256**, 1604–1620.

39. M. Kleinerman, *J. Chem. Phys.*, 1969, **51**, 2370–2381.

40. A. Beeby, S. Faulkner, J. A. G. Williams, L. E. L. Reynolds, W. deW. Horrocks, F. A. J. Geurts, J. W. Hofstraat, G. Siligardi, and J. A. G. Williams, *J. Chem. Soc. Dalt. Trans.*, 2002, **10**, 1918–1922.

41. W. D. Horrocks, J. P. Bolender, W.D. Smith, and R. M. Supkowski, *J. Chem. Soc.,* 1997, **119**, 5972-5973.

42. D. L. Dexter, *J. Chem. Phys.*, 1953, **21**, 836–850.

43. T. Lazarides, D. Sykes, S. Faulkner, A. Barbieri, and M. D. Ward, *Chem. - A Eur. J.*, 2008, **14**, 9389–9399.

44. T. Főrster, *Discuss. Faraday Soc.*, 1959, **27**, 7–17.

45. S. Faulkner, L. S. Natrajan, W. S. Perry, D. Sykes, J. Feng, J. Narvainen, R. Shaw, E. Scales, R. Kauppinen, A. M. Kenwright, and S. Faulkner, *Dalt. Trans.*, 2009, **130**, 3890.

46. C. Allain and S. Faulkner, *Future Med. Chem.*, 2010, **2**, 339–350.

47. T. J. Sørensen, A. M. Kenwright, and S. Faulkner, *Chem. Sci.*, 2015.

48. A. Beeby, I. M. Clarkson, R. S. Dickins, S. Faulkner, D. Parker, L. Royle, A. S. de Sousa, J. A. G. Williams, and M. Woods, *J. Chem. Soc. Perkin Trans. 2*, 1999, 493–504.

49. D. G. Smith, G. Law, B. S. Murray, R. Pal, D. Parker, K.-L. Wong, J. Pastorek, and W. S. Sly, *Chem. Commun.*, 2011, **47**, 7347.

50. M. P. Placidi, A. J. L. Villaraza, L. S. Natrajan, D. Sykes, A. M. Kenwright, and S. Faulkner, *J. Am. Chem. Soc.*, 2009, **131**, 9916–9917.

51. T. J. Sørensen, M. Tropiano, O. A. Blackburn, J. A. Tilney, A. M. Kenwright, and S. Faulkner, *Chem. Commun.*, 2013, **49**, 783–785.

52. C. Song, Z. Ye, G. Wang, J. Yuan, and Y. Guan, *Chem. - A Eur. J.*, 2010, **16**, 6464–6472.

53. C. M. Andolina, R. A. Mathews, and J. R. Morrow, *Helv. Chim. Acta*, 2009, **92**, 2330–2348.

54. J. A. Peters, J. Huskens, and D. J. Raber, *Prog. Nucl. Magn. Reson. Spectrosc.*, 1996, **28**, 283–350.

55. A. F. Cockerill, G. L. O. Davies, R. C. Harden, and D. M. Rackham, *Chem. Rev.*, 1973, **73**, 553–588.

56. O. A. Blackburn, A. M. Kenwright, P. D. Beer, and S. Faulkner, *Dalton Trans.*, 2015.

57. O. A. Blackburn, N. F. Chilton, K. Keller, C. E. Tait, W. K. Myers, E. J. L. McInnes, A. M. Kenwright, P. D. Beer, C. R. Timmel, and S. Faulkner, *Angew. Chem. Int. Ed. Engl.*, 2015.

58. T. A. Babushkina, V. F. Zolin, and L. G. Koreneva, *J. Struct. Chem.*, 1984, **25**, 194–199.

59. S. Aime, M. Botta, M. Fasano, M. M. Marques, C. F. G. C. Geraldes, D. Pubanz, and A. E. Merbach, *Inorg. Chem*., 1997, **36**, 2059-2068.

60. M. Purgel, Z. Baranyai, A. de Blas, T. Rodríguez-Blas, I. Bányai, C. Platas-Iglesias, and I. Tóth, *Inorg. Chem.*, 2010, **49**, 4370–4382.

61. M. Polášek, J. Kotek, P. Hermann, I. Císařová, K. Binnemans, and I. Lukeš, *Inorg. Chem.*, 2009, **48**, 466–475.

62. M. Placidi, L. Natrajan, D. Sykes, A. Kenwright, and S. Faulkner, *Helv. Chim. Acta*, 2009, **92**, 2427–2438.

63. T. Gunnlaugsson, A. J. Harte, J. P. Leonard, and M. Nieuwenhuyzen, *Chem. Commun.*, 2002, 2134–2135.

64. Z. F. Kanyo and D. W. Christianson, *J. Biol. Chem.*, 1991, **266**, 4264–4268.

65. R. S. Dickins, S. Aime, A. S. Batsanov, A. Beeby, M. Botta, J. I. Bruce, J. A. K. Howard, C. S. Love, D. Parker, R. D. Peacock, and H. Puschmann, *J. Am. Chem. Soc.*, 2002, **124**, 12697–12705.

66. T. Liu, A. Nonat, M. Beyler, M. Regueiro-Figueroa, K. Nchimi Nono, O. Jeannin, F. Camerel, F. Debaene, S. Cianférani-Sanglier, R. Tripier, C. Platas-Iglesias, and L. J. Charbonnière, *Angew. Chemie Int. Ed.*, 2014, **53**, 7259–7263.

67. S. J. Butler and D. Parker, *Chem. Soc. Rev.*, 2012, **42**, 1652–1666.

68. M. Giardiello, M. Botta, and M. P. Lowe, *Inorg. Chem.*, 2013, **52**, 14264–14269.

69. J. I. Bruce, R. S. Dickins, L. J. Govenlock, T. Gunnlaugsson, S. Lopinski, M. P. Lowe, D. Parker, R. D. Peacock, J. J. B. Perry, S. Aime, and M. Botta, *J. Am. Chem. Soc.*, 2000, **122**, 9674–9684.

70. D. F. Caffrey and T. Gunnlaugsson, *Dalton Trans.*, 2014, **43**, 17964–70.

71. O. A. Blackburn, A. M. Kenwright, A. R. Jupp, J. M. Goicoechea, P. D. Beer, and S. Faulkner, *Chem. - A Eur. J.*, 2016, **22**, 8929–8936.

72. D. H. Carr, J. Brown, G. M. Bydder, R. E. Steiner, H. J. Weinmann, U. Speck, A. S. Hall, and I. R. Young, *AJR. Am. J. Roentgenol.*, 1984, **143**, 215–24.

73. A. Patnaik, S. S. Mishra, and S. B. Senapati, *Asian J. Neurosurg.*, 2017, **12**, 75–77.

74. E. Debroye and T. N. Parac-Vogt, *Chem. Soc. Rev.*, 2014, **43**, 8178–8192.

75. S. Aime, D. Delli Castelli, and E. Terreno, *Angew. Chem. Int. Ed. Engl.*, 2002, **41**, 4334–6.

76. N. Cakić, S. Gündüz, R. Rengarasu, and G. Angelovski, *Tetrahedron Lett.*, 2015, **56**, 759–765.

77. P. Caravan, J. J. Ellison, T. J. McMurry, and R. B. Lauffer, *Chem. Rev.*, 1999, **99**, 2293–2352.

78. N. Sim and D. Parker, *Chem. Soc. Rev.*, 2015, **44**, 2122–34.

79. M. D. Kemple, B. D. Ray, K. B. Lipkowitz, F. G. Prendergast, and B. D. N. Rao, *J. Am. Chem. Soc.*, 1988, **110**, 8275–8287.

80. L. K. Griffeth, *Proc. (Bayl. Univ. Med. Cent).*, 2005, **18**, 321–30.

81. O. Jacobson, D. O. Kiesewetter, and X. Chen, *Bioconjug. Chem.*, 2015, **26**, 1–18.

82. I. Ojima and 1945-, *Fluorine in medicinal chemistry and chemical biology*, Wiley-Blackwell, 2009.

83. A. Zhu, D. Lee, and H. Shim, *Semin. Oncol.*, 2011, **38**, 55–69.

84. N. J. Long and W.-T. Wong, *The chemistry of molecular imaging*, .

85. K. Hamacher and H. H. Coenen, *Appl. Radiat. Isot.*, 2006, **64**, 989–994.

86. R. D. Carpenter, S. H. Hausner, and J. L. Sutcliffe, *ACS Med. Chem. Lett.*, 2011, **2**, 885–889.

87. E. Lee, A. S. Kamlet, D. C. Powers, C. N. Neumann, G. B. Boursalian, T. Furuya, D. C. Choi, J. M. Hooker, and T. Ritter, *Science, 80*, 2011, **334**.

88. J. H. Walrod, D. A. Atwood, J. H. Walrod II, and D. A. Atwood, in *Encyclopedia of Inorganic and Bioinorganic Chemistry*, John Wiley & Sons, Ltd, Chichester, UK, 2012.

89. S. Castellino and J. J. Sims, *Tetrahedron Lett.*, 1984, **25**, 4059–4062.

90. M. A. Giardello, V. P. Conticello, L. Brard, M. R. Gagne, and T. J. Marks, *J. Am. Chem. Soc.*, 1994, **116**, 10241–10254.

91. L. Sanzhong, Z. Baolian, X. Ming, A. JaÑczuk, X. Wenhua, C. Jinpei, and P. G. Wang, *Chinese Sci. Bull.*, 2001, **46**, 1673–1681.

92. T. Imamoto, T. Mita, and M. Yokoyama, *J. Org. Chem.*, 1987, **52**, 5695–5699.

93. J.-T. Hwang and C.-C. Liao, *Tetrahedron Lett.*, 1991, **32**, 6583–6586.

94. J. D. White and T. C. Somers, *J. Am. Chem. Soc.*, 1987, **109**, 4424–4426.

95. S. Kobayashi and K. Manabe, *Pure Appl. Chem.*, 2000, **72**.

96. A. L. Gemal and J. L. Luche, *J. Am. Chem. Soc.*, 1981, **103**, 5454–5459.

97. M. S. Shibasaki and N. Yoshikawa, *Chem. Revs.*, 2002, 102, 2182-2210.

98. S. U. Pandya, R. S. Dickins, D. Parker, D. J. Tozer, S. Salamano, J. A. K. Howard, C. S. Love, R. D. Peacock, and H. Puschmann, *Org. Biomol. Chem.*, 2007, **5**, 3842.

2 Click Chemistry with DO3A complexes

2.1 Introduction

The use of copper-catalysed alkyne/azide cycloadditions (CuAAC) 'click' reactions has been widely reported.[1–5] The immense versatility of these reactions stems from their propensity to produce high yields, that they allow for the use of mild conditions and that they have a large tolerance for different functional groups, including a wide range of alkyne and azide substituents[6–8] – even those incorporating lanthanide complexes[2,8]

These click reactions have been used for an extensive range of applications such as: in dye sensitised solar cells, as phosphors for electronic displays, in bioconjugation, molecular electronics, in the preparation of dendrimers, and for radiolabelling.[9–12]

Another advantage of these click reactions is the resulting 1,2,3-triazoles, which not only support many ligand designs due to high tolerances for functionality, they can also be used to coordinate to metal centres.[9] This can be achieved through monodentate binding or through functionalisation to give bidentate moieties, as illustrated in Figure 2.1.[13–15] The types of bidentate moieties shown are typically favoured due to their similarity to known chelates such as 2,2'-bipyridyl: they also offer the potential for enhanced affinity for a metal ion as a consequence of the chelate effect, while the availability of an extra nitrogen donor atom means that they can act as bridging and as chelating ligands.

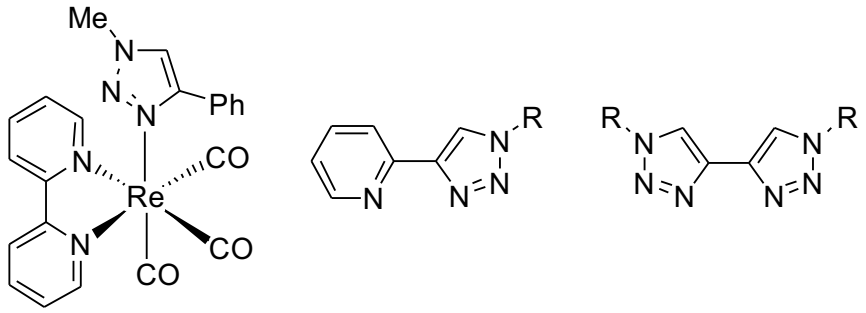

Figure 2.1: Examples of a rhenium complex with monodenate triazole binding and two bidentate triazole based moieties[13–15]

The ability to coordinate metals to nitrogen based moieties, (including 2,2'-bipyridine and triazoles) has also led to their investigation in d-f hybrids,[16–19] as they can be used to mediate energy transfer to the lanthanide *via* a ^{3}MLCT state. With this arrangement, the d-block metal can act as a sensitiser e.g. for NIR emission,[20] giving the possibility of dual imaging probes.

Due to the growing interest in using click reaction for biological applications, the use of copper-free click reactions is currently increasing, due to the cytotoxicity of copper ions.[21–24] These copper free reactions can be used for radiolabelling, or for conjugation to DNA, proteins and other biologically relevant molecules.[25–27] They generally exploit the strain-promoted click reaction to achieve copper free reactions as the strained geometry resembles the transition state required for the click reaction.[27]

In this chapter I will describe the synthesis of lanthanide complexes by click reactions and show the pH dependence of across the lanthanide series and then use these complexes to synthesise the corresponding d-f hybrids to study the effect on energy transfer. The synthesis of lanthanide complexes appended to strained cyclooctynes for use in biorthogonal copper-free click reactions will also be discussed.

2.2 Synthesis and characterisation

This work is based on clicking of 2-azidopyridine with lanthanide p.DO3A complexes. 2-Azidopyridine was chosen as the coordination chemistry of the resulting triazolopyridines is largely unexplored, despite offering a range of potential coordination modes to three different nitrogen atoms. The azide was synthesised according to an adapted literature procedure as shown in Scheme 2.1.[28]

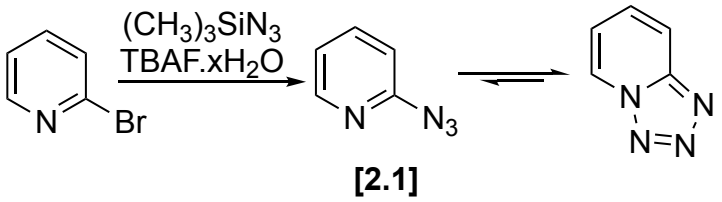

[2.1]

Scheme 2.1: Synthesis and cyclisation of 2-azidopyridine 2.1

It was observed by Huisgen *et al.* in 1969 that 2-azidopyridine exists in equilibrium with the major tautomer tetrazido[1,5-a]pyridine, as depicted in Scheme 2.1.[29] This observation is also confirmed by the IR spectrum, which does not show the characteristic azide stretch between 2160-2120 cm^{-1}. Despite the reactive species being the minor tautomer present, its reactivity is not affected in dipolar cycloaddition with alkynes.

The lanthanide complexes Ln.2.5 (where Ln = Eu, Tb. Gd, Yb and Lu) were synthesised according to literature procedures as shown in Scheme 2.2.[2,30,31]

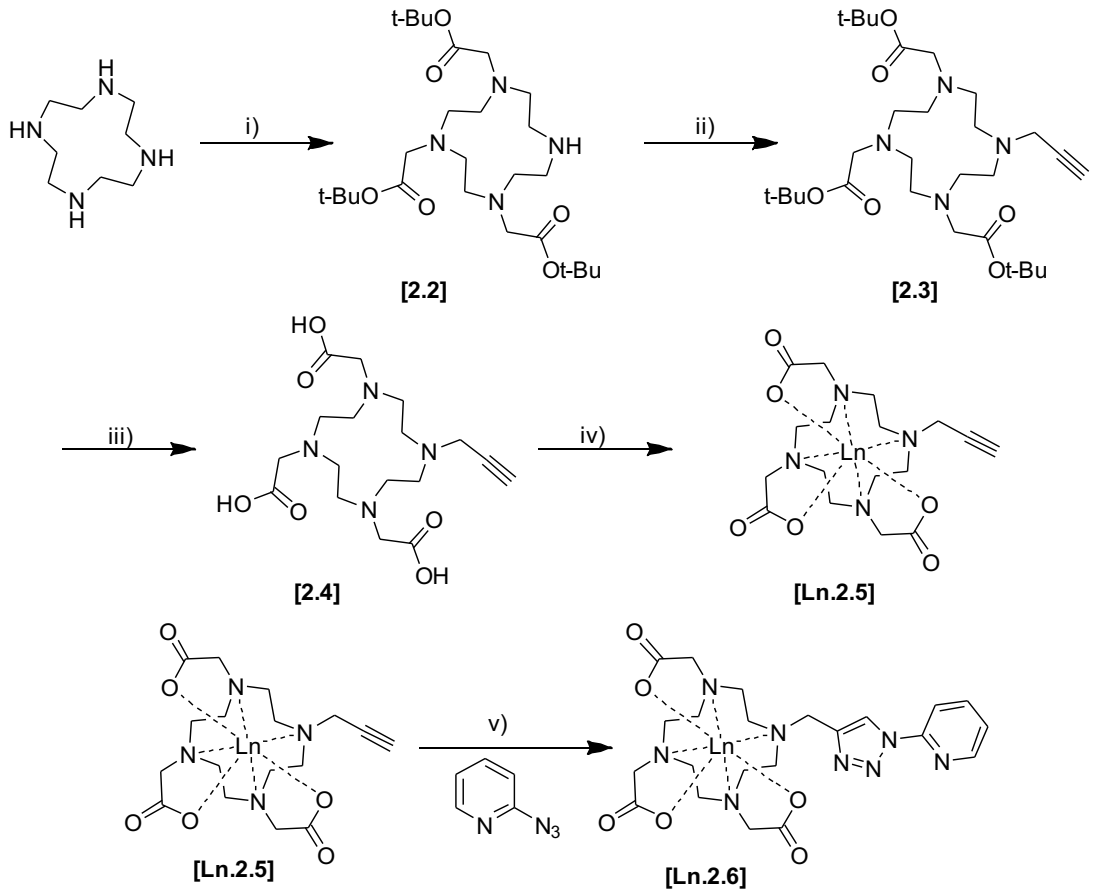

i) $BrCH_2COOC(CH_3)_3$, $HNaCO_3$ ii) $HCCH_2Br$, K_2CO_3 iii) TFA iv) $Ln(OTf)_3$
v) $(CuOTf)_2{\bullet}C_6H_6$, MeOH, N_2, 75 °C,24 h

Scheme 2.2: Synthesis of compound 2.2-4 to give Ln.p-DO3A complexes Ln.2.5 and click reaction between Ln.2.5 and 2.1 to give complex Ln.2.6

The click reactions were all performed by adapted literature procedures shown in Figure 2.2. [1,32] The products were confirmed firstly by ^{1}H NMR, initially by comparison to the diamagnetic complex Lu.2.6, synthesised to aid characterisation. As shown in Figure 2.2, there is a clear change in the ^{1}H NMR spectrum before and after the click reaction, with the appearance of aromatic peaks showing the formation of the click product.

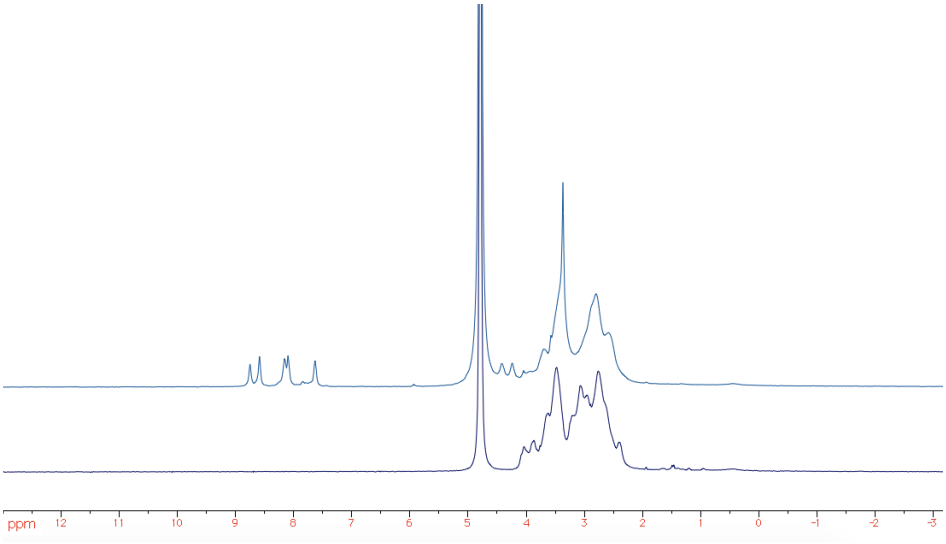

Figure 2.2: ^{1}H NMRs before and after click reaction. Bottom: Lu.p-DO3A Lu.2.5 Top: Lu.2.6 (298 K, D_2O, 400 MHz).

The paramagnetic complexes also show clear changes in the ^{1}H NMR from the starting complex as illustrated by Yb.2.6 in Figure 2.3 confirming the click reaction to have occurred. All products were also confirmed by HRMS.

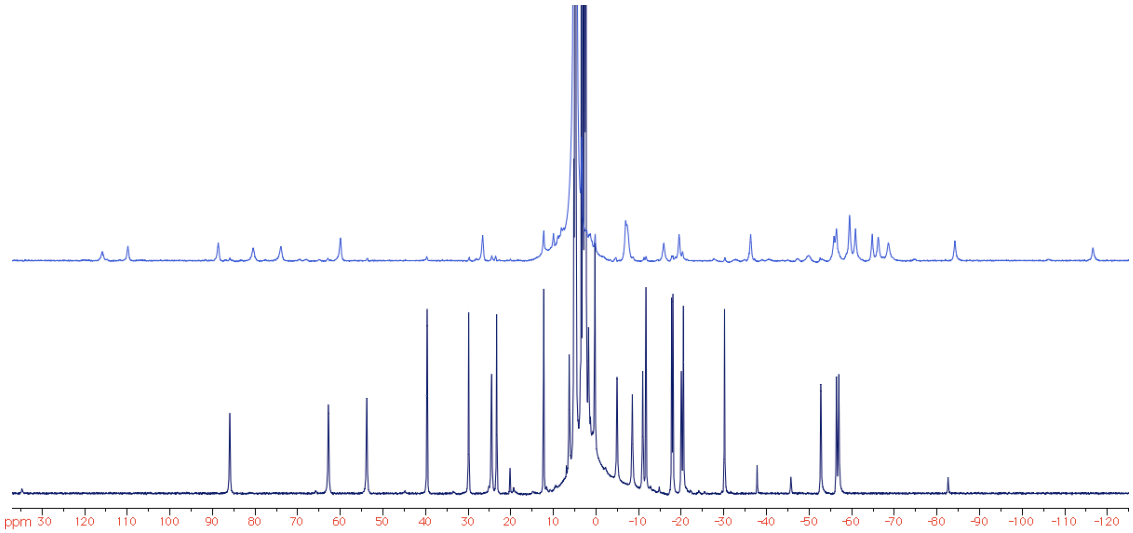

Figure 2.3: ^{1}H NMRs before and after click reaction. Bottom: Yb.2.5 Top: Yb.2.6 (298 K, D_2O, 400 MHz).

As previously discussed, the presence of copper after click reaction can be undesirable, especially for *in vivo* applications.[21,24] In this case, the presence of copper may also be an issue, not only because of the toxic effect of free copper, but because there is the

possibility of copper being bound by the complex due to number of potential coordination sites available in the resulting complexes. If the copper were coordinated this could potentially affect the resulting observed ^{1}H NMR spectra.

To explore this possibility, several methods of copper removal were attempted. Methodologies using dialysis and amberlite ion exchange resin, proved unsuccessful, as while they did remove some free copper, they were not successful in the complete removal of copper from the samples with the complexes remaining a visibly green in colour. The final method used Cuprisorb®, an ion exchange resin which removes free and bound copper.[33,34] This method proved effective, and could be observed visually as the samples after treatment were white solids (compared to the green starting complexes) and upon removal no changes in the ^{1}H NMR were observed.

2.3 pH studies

2.3.1 NMR studies

For these systems, there are a range of potential coordination and protonation sites of the complexes Ln.2.6 as detailed in Figure 2.4. Where it is possible for the triazole N3 and pyridine nitrogen to be protonated at low pH (Ln.2.6 a), then with increasing pH it is possible for the pyridine position (pKa 5.2) to be deprotonated (Ln.2.6 b), then triazole N3 nitrogen (pKa 9.3) when deprotonated can either be coordinated or uncoordinated to the lanthanide centre (Ln.2.6 c/d). It also possible at high pH to deprotonate the lanthanide bound water (Ln.2.6 e).

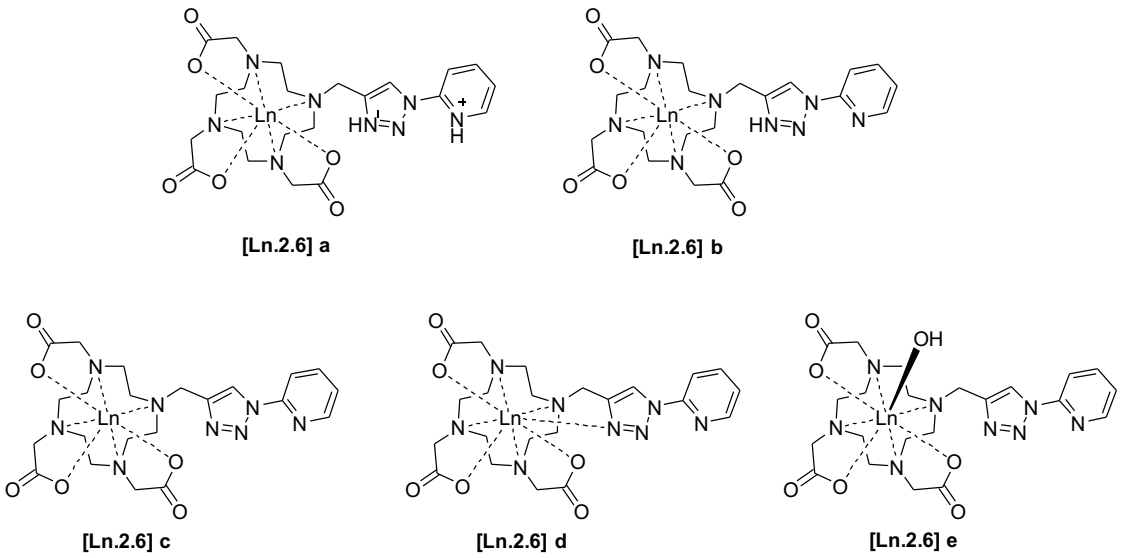

Figure 2.4:Possible coordination and protonation modes for complexes Ln.2.6

There is also the possibility of aggregation or dimerization for these complexes. This could occur though the binding of anions in solution such as carbonate or hydroxide, which has been observed for other lanthanide spiecies[35] or bridging by the triazolopyridine unit.

Due to the range of potential coordination and protonation sites of the complexes Ln.2.6, shown in Figure 2.4, a series of ^{1}H NMR experiments were undertaken to explore the effect of varying pH on these systems. ^{1}H NMR studies using the europium (Eu.2.6) and terbium (Tb.2.6) analogues revealed there was no significant dependence of the spectra on pH in the ^{1}H NMR shown in Figure 2.5.

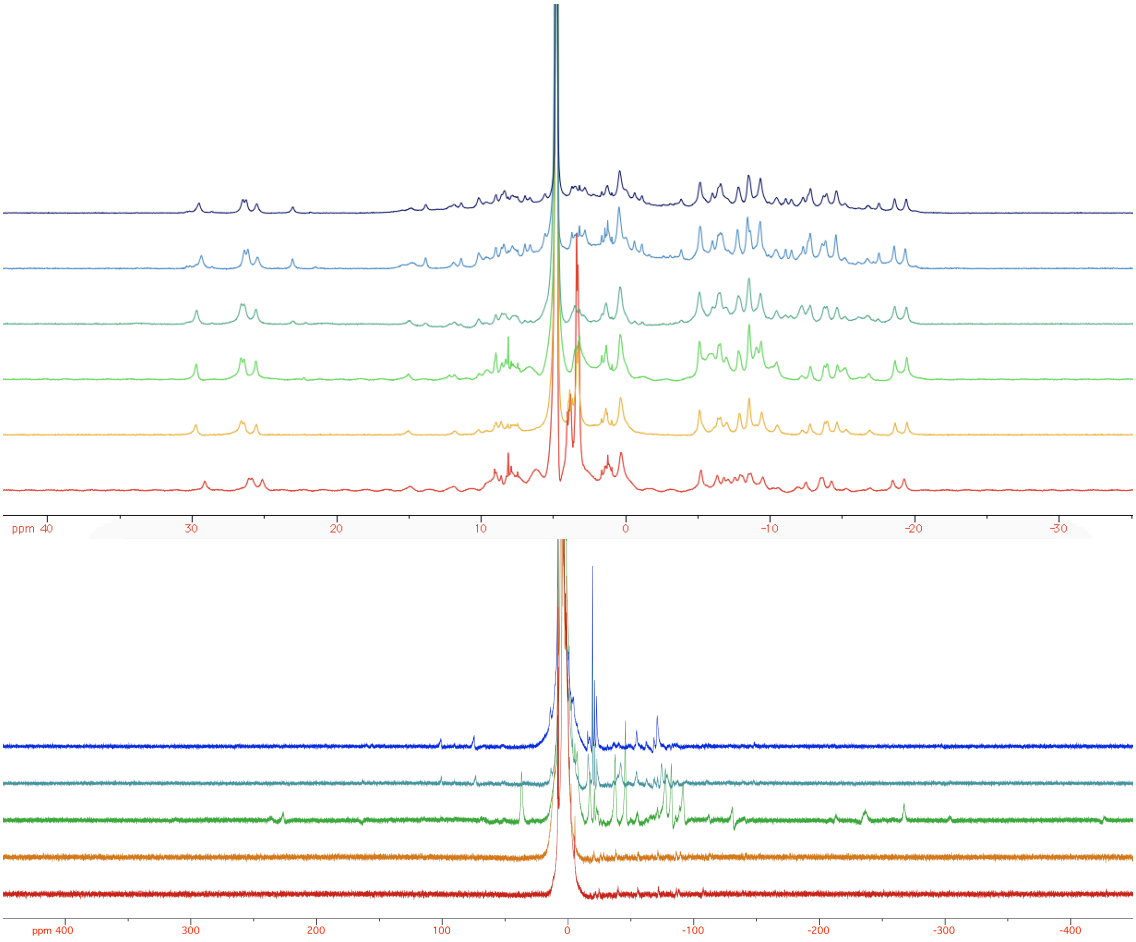

Figure 2.5: Top ^{1}H NMR of Eu.2.6 at pD's 2(red), 4(orange), 6(light green), 8(dark green), 10(light blue) and 12(dark blue). Bottom ^{1}H NMR of Tb.2.6 at pD's 1 (red), 3 (orange), 6 (green), 9 (light blue), 12 (dark blue) (298 K, D_2O, 400 MHz).

While the intensity of the peaks may change over the range of pHs, the overall positions do not alter. For both complexes (although more clearly seen for the Eu.2.6 complex, which displays relatively sharp spectral lines) the lack of observed change in the NMR spectra suggests that the triazole group is coordinated to the lanthanide centres at all pHs as shown in Figure 2.6, creating an eight-coordinate lanthanide centre. This contrasts with a similar system studied by Lowe *et al.* which showed the pH dependent behaviour of an Eu.p.DO3A complex clicked to give an unsubstituted triazole, which showed large shifts in the ^{1}H NMR due to protonation.[8]

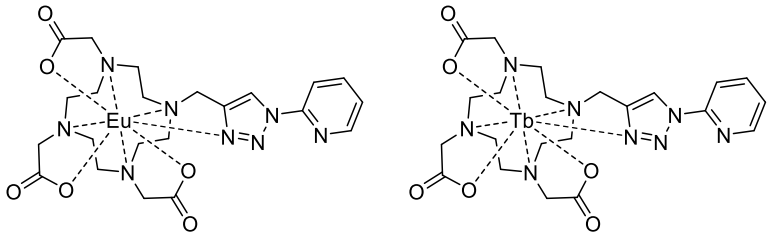

Figure 2.6: Structures of Eu.2.6 and Tb.2.6 showing the coordination of the triazole group to the lanthanide centre

However, both the ytterbium (Yb.2.6) and lutetium (Lu.2.6) complexes showed marked changes in the ^{1}H NMR spectra with varying pH, as can be seen from Figure 2.7.

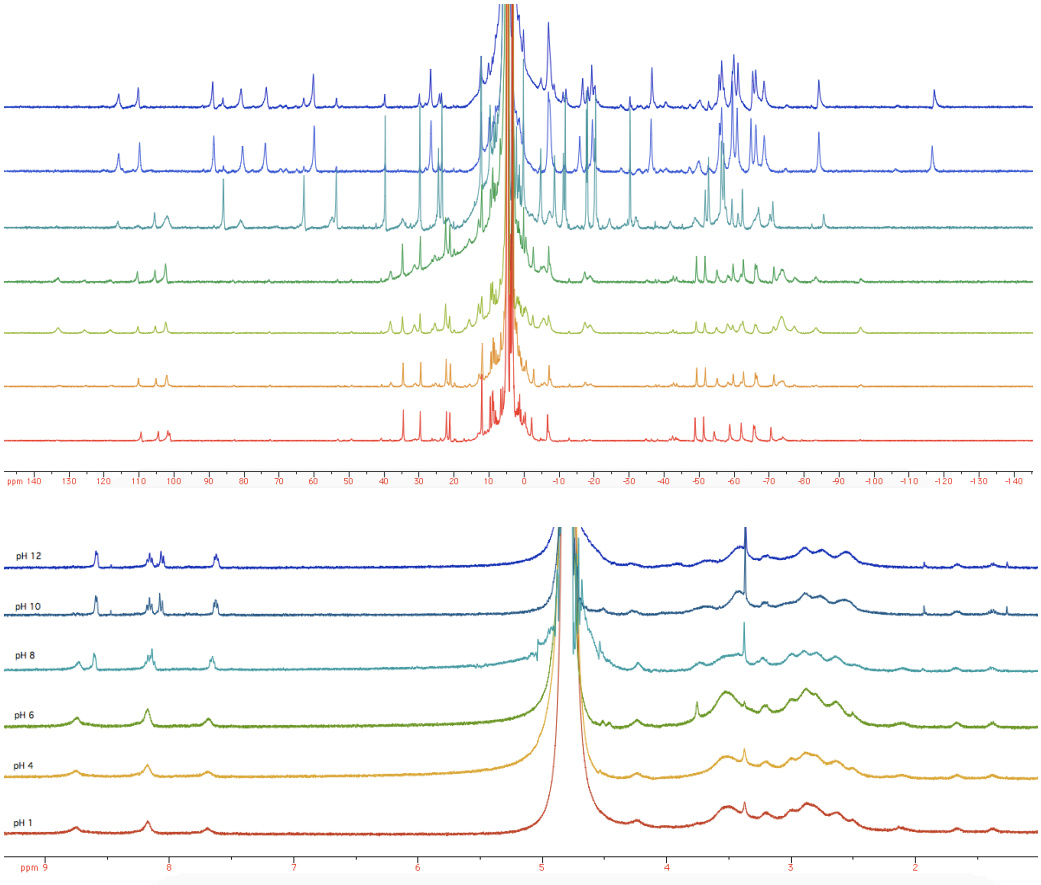

Figure 2.7: Top: NMR of Yb.2.6 at pD's 1(red), 3(orange), 5(light green), 7(dark green), 9(turquoise), 10(light blue) and 12 (dark blue). Bottom: NMR of Lu.2.6 at pD's 1(red), 4(orange), 6(light green), 8(turquoise), 10(light blue) and 12(dark blue) (298 K, D_2O, 400 MHz)

These studies were repeated, and the spectral changes were found to be reproducible and reversible over a large pH range - ruling out the possibility of the complexes' decomposing at very high or low pH values

To investigate if any aggregation or dimerisation processes contributes to the observed ^{1}H NMR spectrum, the complex Lu.2.6 was studied by DOSY at pH 12, 9 and 2. These showed essentially identical diffusion coefficients at all pHs, suggesting that aggregation does not play a significant role observed ^{1}H NMR spectra.

Instead, it is postulated that the major observed change is due to the protonation/deprotonation of the triazole, which has a pKa of 9.3, causing the triazole to no longer be coordinated to the lanthanide centre as shown in Scheme 2.3. This is most clearly seen with the Lu.2.6 complex which shows the appearance of a new species at pH 9, which then dominates the spectrum at pD 10 (Figure 2.7 bottom).

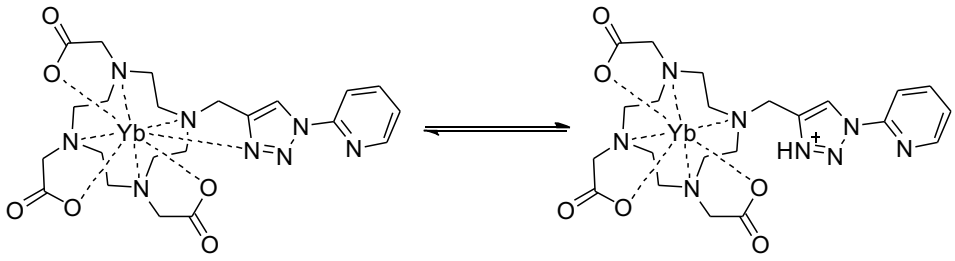

Scheme 2.3: Equilibrium at pD 9 leading to the deprotonation of the triazole and then possible coordination to the lanthanide centre

While the further changes observed in the Yb.2.6 ^{1}H NMR at pD 5 and 10 are most likely due to the deprotonation of the pyridine (species [Ln.2.6 b], shown in Figure 2.4) and deprotonation of bound water (species [Ln.2.6 e] – shown in Figure 2.4) respectively.

We can speculate that the changes in the ^{1}H NMR observed for Yb.2.6 and Lu.2.6 are due to protonation events and are observed for the later lanthanides only because of their reduced ionic radii and higher charge density results in the complexes favouring hydration over the coordination of the triazole. These results are in line with the study by Lowe *et al.* that attributes changes in ^{1}H NMR to be due to protonation and deprotonation events of both the triazole and the bound water.[8]

2.3.2 Photophysical studies

To further understand the nature of the pH dependences observed in the ^{1}H NMR studies, complexes Eu.2.6, Tb.2.6 and Yb.2.6 were analysed using photophysical techniques.

The europium (Eu.2.6) and terbium (Tb.2.6) complexes were excited at λ = 270 nm though the chromophore and the resulting lanthanide centred emission was measured over a range of pHs, as shown in Figure 2.8.

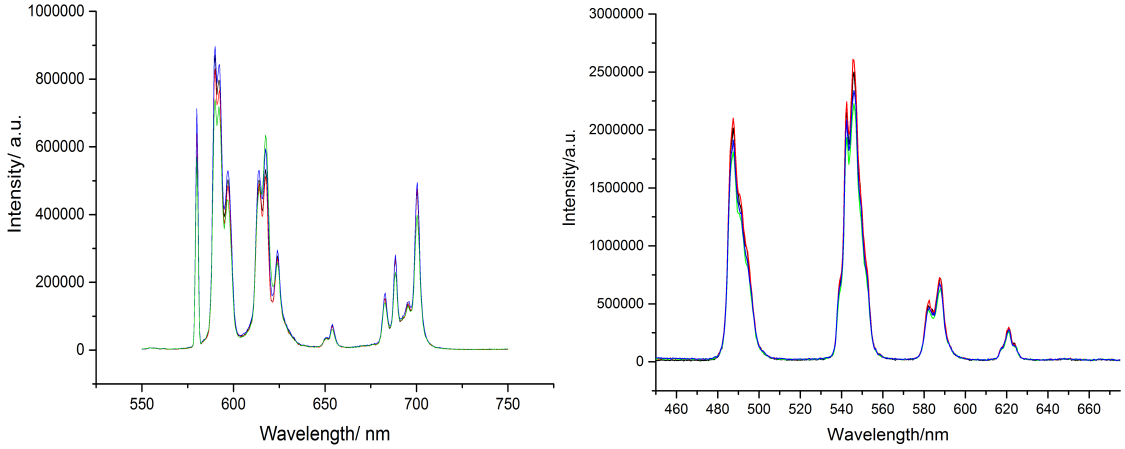

Figure 2.8: Left: Observed emission spectra of Eu.2.6 at pH 3 (black), 6(red), 11(blue) and 12(green). Right: Observed emission for Tb.2.6 at pH 2(red), 6(black), 10(blue) and 12(green).(λex= 270 nm)

For both Eu.2.6 and Tb.2.6 there is no significant change in the observed emission spectra of a wide pH range, some small variations can be seen but these most likely arise from small dilution effects during gradual pH adjustments.

The lifetimes of complexes Eu.2.6 and Tb.2.6 were measured at pHs 5.5 and 12 as shown in Table 2.1.

Table 2.1:Measured lifetime values in H_2O and D_2O for complexes Eu.2.6 and Tb.2.6 at different pH values

	τ_{H2O}/ms [a]	τ_{D2O}/ms [a]	q
Eu.2.6 pH 5.5	$\tau_1 = 0.37$	$\tau_1 = 1.02$	1.7
Eu.2.6 pH 12	$\tau_1 = 0.50$	$\tau_1 = 2.05$	1.5
Tb.2.6 pH 5.5	$\tau_1 = 1.31$	$\tau_1 = 2.20$	1.3
Tb.2.6 pH 12	$\tau_1 = 1.47$	$\tau_1 = 2.51$	1.1

[a] *where the typical errors on measured values are around 10 %*

The measured lifetimes for both Eu.2.6 and Tb.2.6 show an increase in lifetime at high pH. This can be rationalised by the deprotonation of water leading to reduced quenching of hydroxide compared to water. It is also conceivable that hydrogen bonding between solvent and the other available nitrogen atoms could give rise to enhanced quenching, even in the case of full coordination of the N3 nitrogen on the triazole, which could also contribute to a shorter observed lifetime. The observed change in lifetime with pH in D_2O for both the europium and terbium suggests the removal of a non-radiative quenching pathways at high pH.

For europium complexes, an NH correction factor can be applied as shown by Equation 2.1 where x is the number of NH oscillators.[36] The use of an NH correction factor would be consistent with established practice (as it is already normal to correct for exchangeable N-H oscillators in ligand structures).

$$q = A(k_{H2O} - k_{D2O}) - B - 0.075x$$

Equation 2.1: Modified Horrocks equation: where q is the number of bound solvent molecules, k is the rate constant of decay and A and B are proportionality constants to correct for inner and outer sphere quenching respectively and x is the number of NH oscillators

However, the x value in Equation 2.1 refers to amide NH oscillators, whereas it is amine NH oscillators that are present in complexes Ln.2.6. Due to their faster exchange rate, their contribution is more comparable to half a water molecule per NH oscillator. When

taking this into account, the higher q values at low pH (1.77 and 1.3 for Eu.2.6 and Tb.2.6 respectively) are unsurprising due to the close proximity of an amine oscillator. This indicates that while we observe a change in the lifetimes for these complexes there is no real change in the overall q values, which is consistent with the NMR and luminescence data for the complexes retaining the same geometry at all pH values.

The ytterbium complex Yb.2.6 was firstly studied by UV/vis absorption as shown in Figure 2.9 (left). An increase in the band at 270 nm is observed with increasing pH, this was shown to be reversible with a corresponding decrease in absorbance with decreasing pH (Figure 2.9 right). This supports NMR evidence that the complexes are stable over a large range of pH values and through multiple cycles of pH variation.

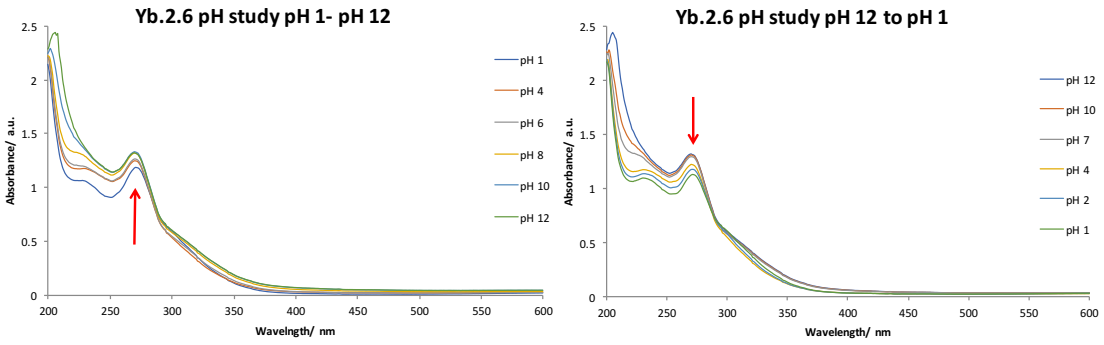

Figure 2.9: UV/Vis absorption of Yb.2.6 showing reversibility over pH's 1-12

The emission spectra of Yb.2.6 at high (pH 11) and low pH (pH 3) were also measured (Figure 2.10), where a change in the ratios of the bands at 980 and 1050 nm can be observed. This is suggestive of a change in the local coordination environment of the lanthanide centre that would be consistent with the proposed theory of protonation and de-coordination of the triazole.

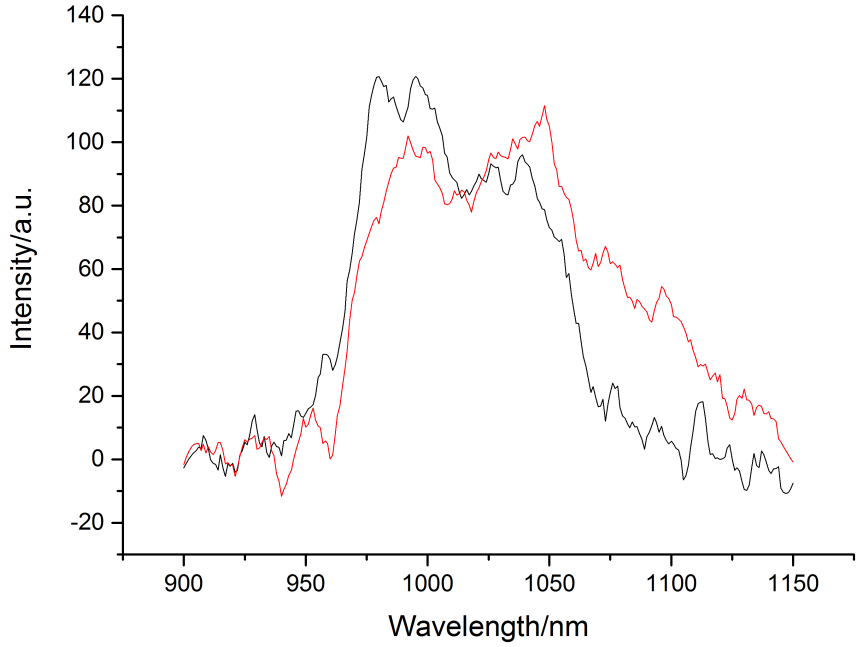

Figure 2.10: Observed emission spectrum of Yb.2.6 at pH 3 (red) and pH 11 (black), (λ_{ex}= 270 nm)

The lifetimes of complex Yb.2.6 were measured at pH 2 and 10 and the corresponding q values calculated according to Equation 2.2 (where A = 1 μs and B = 0.2 μs are for ytterbium) as shown in Table 2.2.[36]

$$q = A(k_{H2O} - k_{D2O}) - B$$

Equation 2.2: Modified Horrocks equation where q is the number of bound solvent molecules, k is the rate constant of decay and A and B are proportionality constants to correct for inner and outer sphere quenching respectively

Table 2.2:Measured lifetime values and calculated q values for complex Yb.2.6 at high and low pH's

	τ_{H2O}/μs[a]	τ_{D2O}/μs[a]	q
Yb.1 pH 2	τ_1 = 1.47	τ_1 =4.06	0.23
Yb.1 pH 10	τ_1 = 1.74	τ_1 = 4.74	0.16

[a] *where the typical errors on measured values are around 10 %*

As with the Eu.2.6 and Tb.2.6 analogues, there is an increase in the lifetimes in H_2O and D_2O, which can also be explained by the same removal of non-radiative quenching pathways at high pH.

The q values indicate that less than one solvent molecule is bound at both high and low pH, which is not consistent with the NMR and luminescence data, which suggests a change in triazole coordination with varying pH. However, when analysing q values, we need to consider that this is an average measurement for a system that is fluctuating and where a weighted average favours the more emissive species in solution. Figure 2.10 shows that at 980 nm the deprotonated species is more emissive and so may be expected to dominate in the lifetime measurements even at low pH. This may account for the lower q value as it would be expected that the triazole would be coordinated to the lanthanide centre therefore reducing the number of bound solvent molecules.

2.4 d-f hybrids

2.4.1 Introduction

d-f hybrids have become a widely researched area due to the ease of modification allowing for a large variety of ligand structures and metals to be incorporated into complexes.[16–18]

The use of d-block chromophores for sensitisation of the near infra-red lanthanides such as Nd(III), Er(III) and Yb(III) has dominated research in the field to date.[37,38] This is due to their possible applications in biological imaging (where longer wavelengths giving deeper tissue penetration) and with uses in telecommunications of Er(III) in particular, as its emission wavelength of 1550 nm closely corresponds to the "window of transparency" of silica - making it an ideal candidate for use in fibre optic data transmission. [20,39]

The use of low spin d^6 or d^8 metal ions is advantageous for sensitising lanthanide luminescence due to their comparatively lower lying ^{3}MLCT states (ca. organic chromophores) being good matches for accessing *f-f* levels, particularly for the near infra-red emissive Ln(III) ions.[40] Although the later lanthanides are of particular interest in this area, due to the wide range of applications and lower sensitisation energies, a variety of both lanthanide centres and d-block metals have been incorporated into complexes as illustrated in Figure 2.11. [20,37,41]

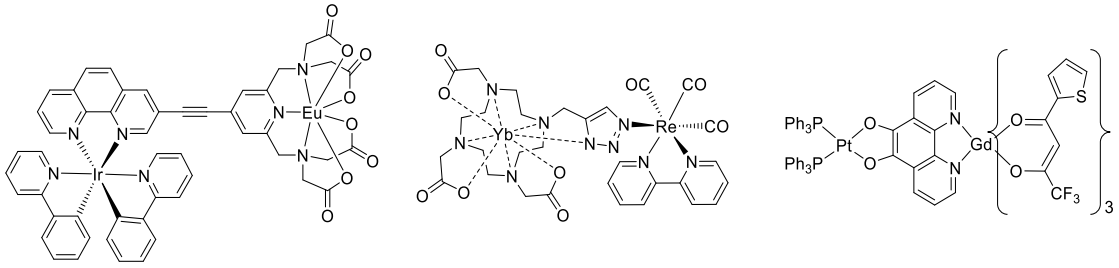

Figure 2.11: Examples of d-f hybrids

This work focuses on how the addition of a rhenium metal centre to complexes Eu.2.6, Tb.2.6 and Yb.2.6 can affect energy transfer processes when compared to the parent complexes.

2.4.2 Synthesis and photophysical studies

The d-f hybrids were synthesised from the parent click products Ln.2.6, as shown in Scheme 2.4 by adapting the literature methods used for the synthesis of d-f hybrid complexes of bipyridyl-DO3A.[17,42]

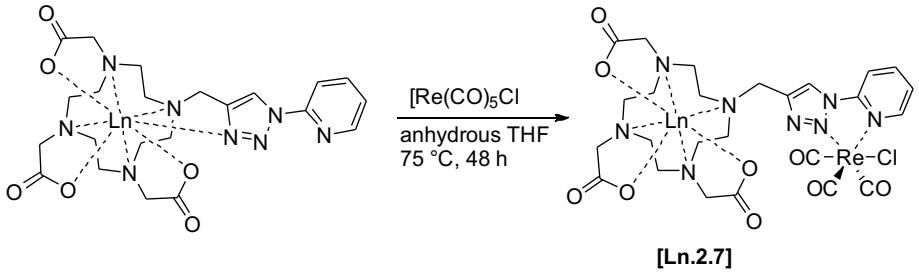

[Ln.2.7]

Scheme 2.4: Synthesis of d-f hybrids LnRe.2.7 where Ln = Eu, Tb, Gd, Yb, Lu

The products were analysed by ^{1}H NMR spectroscopy, but the resulting spectra showed no significant changes from the corresponding Ln.2.6 complex as demonstrated in Figure 2.12 for the ytterbium analogues. This lack of change relative to the parent complex Ln.2.6 in the ^{1}H NMR was not wholly unexpected, as the rhenium centre is far removed from the lanthanide centre and contributes no additional proton signals.

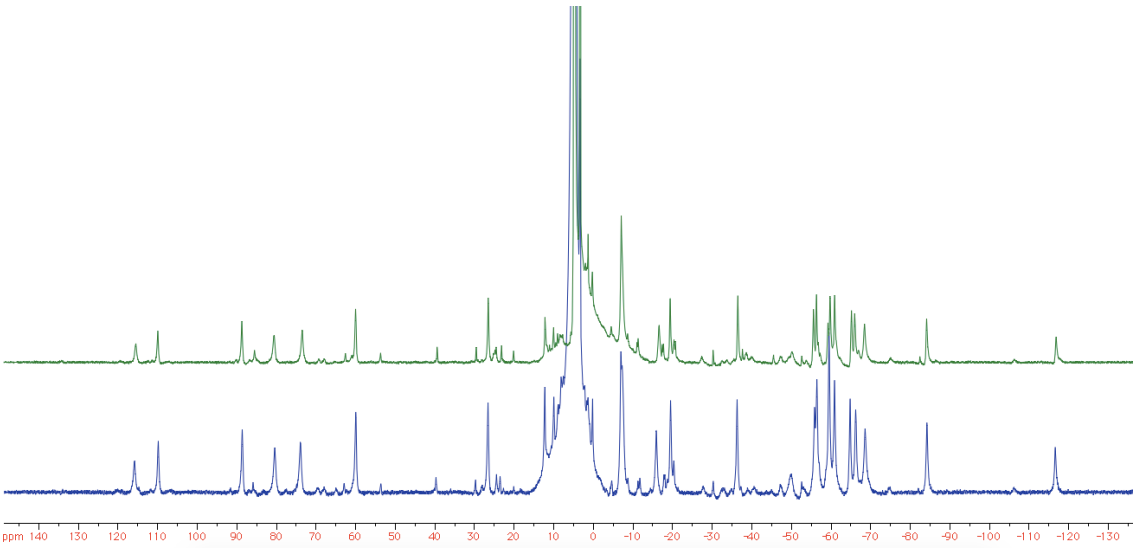

Figure 2.12: Comparison of NMR spectra for Yb.2.6 (blue) and YbRe.2.7 (green) at pD 10 (298 K, D_2O, 400 MHz).

IR spectroscopy of the complexes LnRe.2.7 clearly shows the characteristic carbonyl stretches that would be expected for the rhenium bound species, as illustrated in Figure 2.13 for LuRe.2.7 and TbRe.2.7 The carbonyl frequencies tabulated for all LnRe.2.7 complexes (Table 2.3), when compared to the starting $Re(CO)_5Cl$ complex changes in stretching frequencies confirm that despite the lack of change to the ^{1}H NMR the complexation to form the d-f hybrids proceeds as shown in Scheme 2.4.

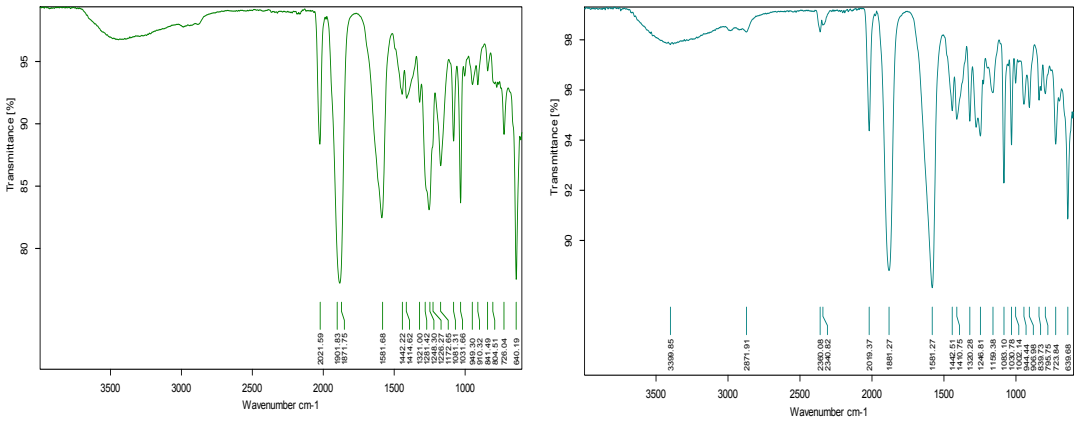

Figure 2.13: IR of LuRe.2.7 (left) and TbRe.2.7(right)

Table 2.3: IR carbonyl stretches for rhenium pentacarbonyl chloride and complexes Ln.2.7

Species	**IR $\nu_{C=O}$ /cm^{-1}**
$Re(CO)_5Cl$	1988, 2047, 2160
EuRe.2.7	2020, 1898
TbRe.2.7	2019, 1881
GdRe.2.7	2021, 1864
YbRe.2.7	2018, 1899
LuRe.2.7	2021, 1901

Although these complexes could not be observed by mass spectrometry (due to easy fragmentation), luminescence data for the complexes also indicates the presence of rhenium. The excitation spectra for these LnRe.2.7 are consistent with the binding of rhenium to a trizolopyridine moiety, rather than the simple MLCT for the parent carbonyl species (Figure 2.14).

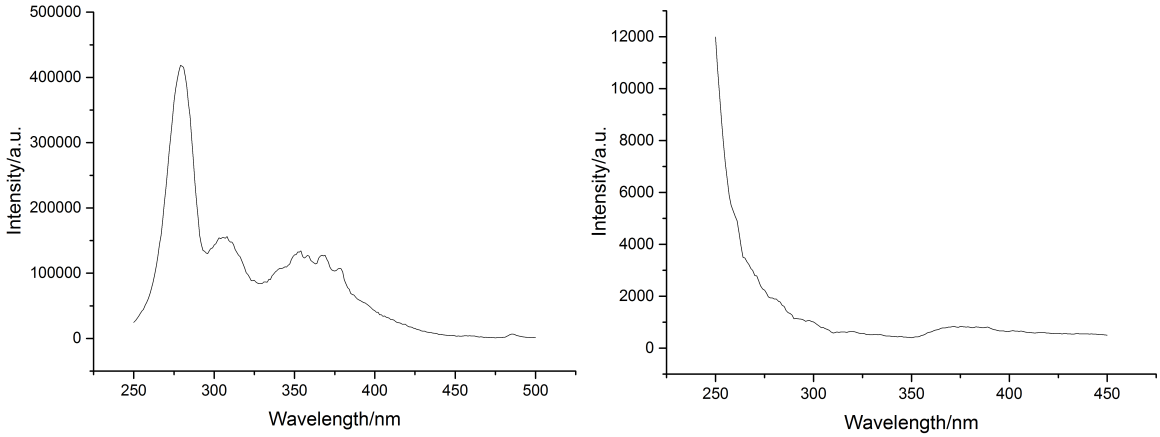

Figure 2.14: Excitation spectrum comparing TbRe2.7 (left) and $Re(CO)_5Cl$

Following excitation of YbRe.2.7 at 375 nm we can see rhenium MLCT emission, as shown in Figure 2.15.

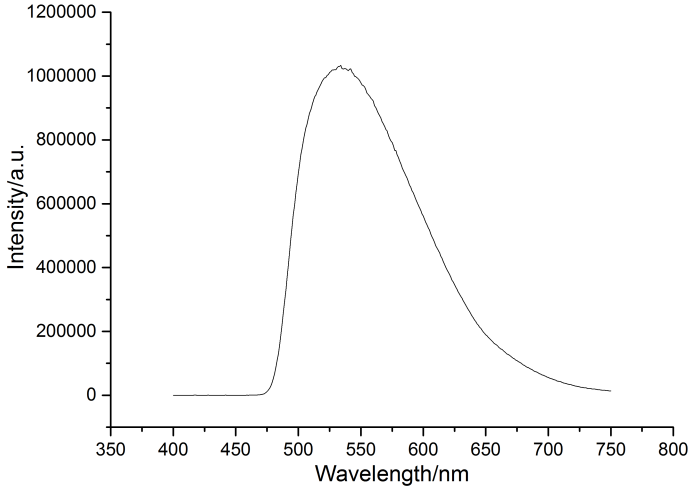

Figure 2.15: ^{3}MLCT Emission from YbRe.2.7 (λex= 375 nm)

This is also possible for the europium and terbium dyads but the rhenium emission overlaps with the lanthanide centred emission as shown in Figure 2.16. The short-lived rhenium emission can be removed by employing time-gating techniques to collect the lanthanide centred emission only. However, by analysing the ytterbium dyad whose emission is in the near infra-red region we can clearly see rhenium centred emission around λ = 550 nm.

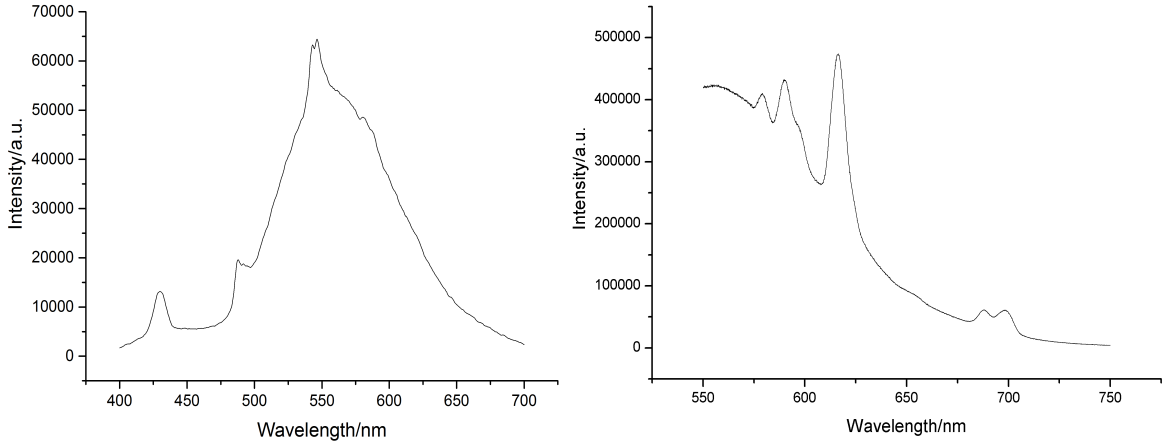

Figure 2.16:Observed emission of TbRe.2.7(left) and EuRe.2.7 (right). (λex= 375 nm)

The TbRe.2.7 and EuRe.2.7 complexes were initially studied via luminescence to see if it was possible to sensitise the lanthanide centre via the rhenium centre. The complexes were excited at 375 nm and the emission spectra collected with the application of a time delay to allow observation of the lanthanide centred emission only. As shown in Figure 2.17, both complexes clearly exhibit sensitised emission of the lanthanide when exciting into the d-block chromophore.

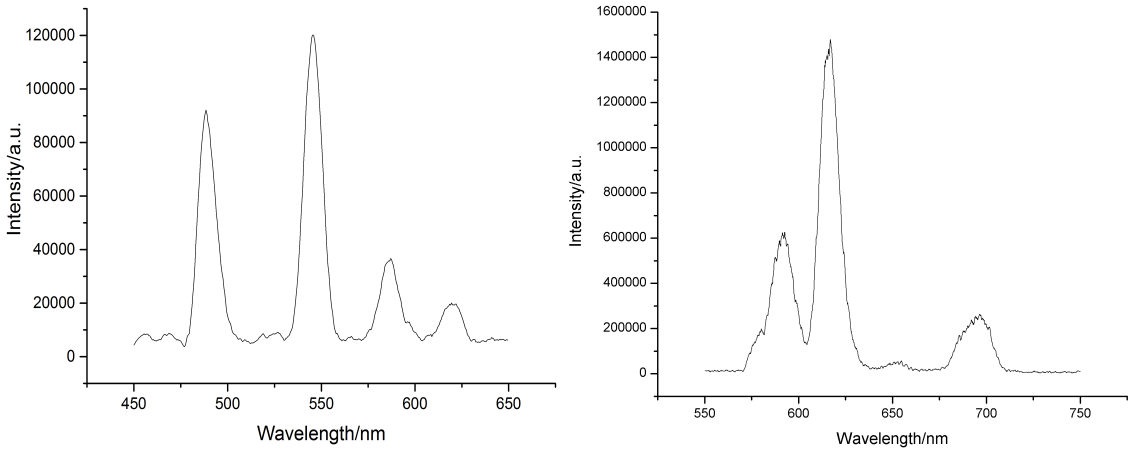

Figure 2.17: TbRe.2.7 (left) and EuRe.2.7 (right) (λex =375 nm and time delay of 50 ms)

Although YbRe.2.7 showed the same ^{1}H NMR behaviour as its parent complex Yb.2.6 (at specified pH), it displayed very different luminescent behaviour. Figure 2.18 shows how the luminescence is almost completely quenched in the d-f dyad.

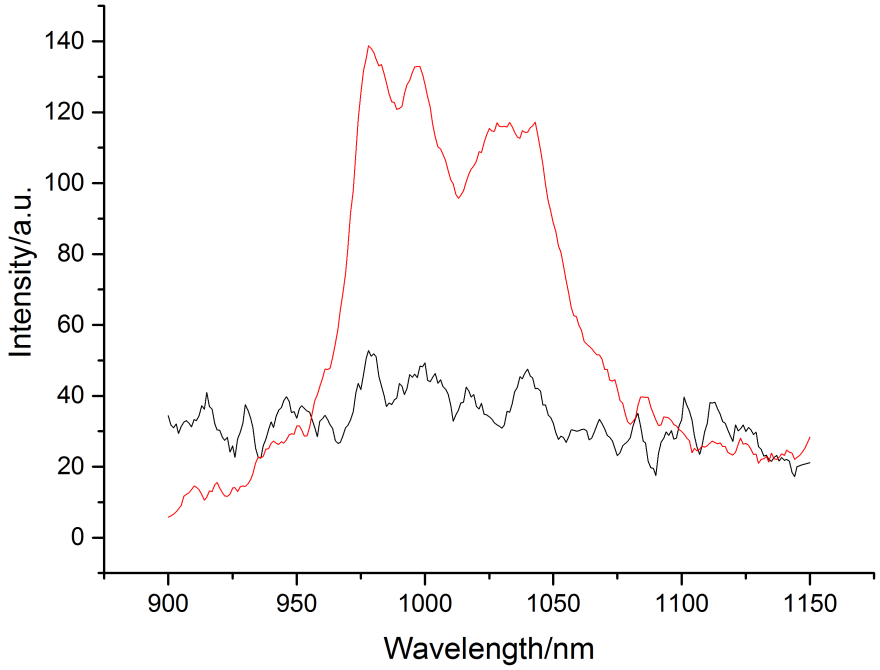

Figure 2.18: Emission spectrum on Yb.2.6 (red) and YbRe.2.7 (black) (λex= 260 nm)

Having ruled out the possibility of oxygen quenching pathways being responsible for the observed emission, we propose two possible mechanisms for quenched luminescence in the YbRe.2.7 complex. One possibility is the introduction of a fast non-radiative deactivation pathway involving the triplet MLCT state as depicted in Figure 2.19 (left). This differs to the behaviour seen for the terbium and europium analogues due to the lower energy of the ytterbium excited state, meaning that overlap and quenching with the low energy ^{3}MCLT is much more likely to occur. Another possibility is quenching occurring through metal-metal charge transfer - where it may be possible to oxidise the rhenium centre and in turn form Yb(II). This requires the combined energetic cost of oxidising the rhenium centre and reducing the ytterbium centre to be less than the energy available from the Yb(III) excited state. If the energy of the rhenium intervalence metallic

charge transfer band, relative to the $^2F_{5/2}$, is lower in energy this would lead to quenching lanthanide centred emission as depicted in Figure 2.19 (right). The energy of this MMCT state is likely to be in the NIR range around 8000 cm^{-1},[43,44] and therefore lower than the $^2F_{5/2}$ ytterbium excited state which is around 10,000 cm^{-1} resulting in the lanthanide emission being quenched.

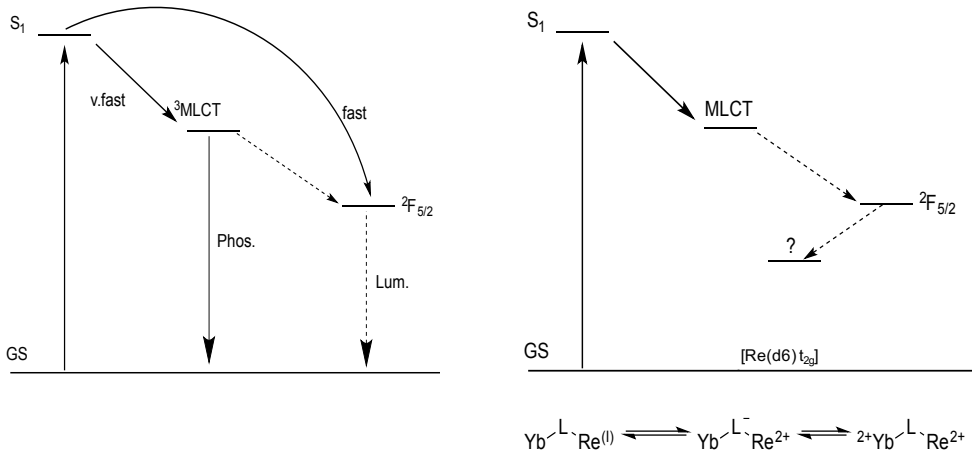

Figure 2.19: Two proposed energy transfer pathways for YbRe.2.7 leading to the quenching of lanthanide centred luminescence

As the pH is below 9 the triazole will be coordinated to the lanthanide centre allowing for the MMCT to occur. Although, the terbium and europium analogues also have coordinated triazole there is no MMCT, despite europium also being able to access the stable 2+ state. This difference in behaviour is likely to be due to the difference is energy of the lanthanides excited states relative to the MMCT state; it is to be expected that the very poor energy match in europium complexes will slow quenching of the lanthanide emissive state.

2.5 Bio-orthogonal Click Chemistry

2.5.1 Introduction

The use of strain promoted azide/alkyne cycloaddition (SPAAC) reactions eliminates the need for cytotoxic copper catalysts in a biological context, and offers

biorthogonality.[25,45,46] The term bio-orthogonal was first introduced by Bertozzi *et al.* in 2003 and was used to describe reactions that can occur *in vivo* without interfering with the natural biological processes.[47] Since that time, bio-orthogonal click chemistry has become increasingly important.

It has been widely conjectured that bio-orthogonal chemical methods may offer a facile way to label and visualize biomolecules *in vivo*. SPAAC bio-orthogonal reactions typically involve the labeling of a biomolecule e.g. lipids, proteins and carbohydrates, with an azide and in conjunction with a strained cyclo-octyne probe.[48,49] For example, this technique was used in 2008 to image glycans in developing zebra fish by using the difluorinated cyclooctyne derived probe shown in Figure 2.20.[50]

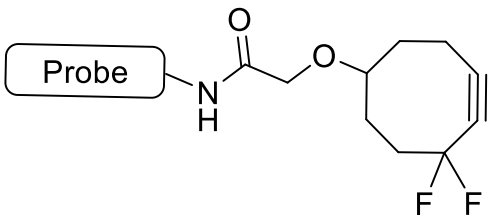

Figure 2.20: Strained difluorinated cyclootyne probed used to image glycans in zebra fish

It has also been reported that the use of dibenzocyclooctyne derivatives results in an increased rate of reaction for these bioorthogonal click reactions.[51] However, these strained cyclooctyne probes generally use organic fluorophores to provide an addressable component; these can have issues with high background signals due to auto-fluorescence of biological materials. To our knowledge no system has incorporated lanthanide complexes which can be used to overcome the problem of auto-fluorescence by employing time gating techniques (or which could alternatively be visualised using MR imaging methodologies).

In the final part of this chapter, we explore the synthesis of a strained dibenzocyclooctyne lanthanide complex that will allow for efficient imaging of *in vivo* bioorthogonal reactions.

2.5.2 Synthesis and characterisation

Our synthetic strategy envisaged forming a ligand system incorporating a dibenzocyclooctyne moiety as part of a DOTA-monoamide. In order to access such compounds, we needed to prepare the chloracetamide 2.11. This was prepared as shown in Scheme 2.5, using literature procedures to synthesise compounds 2.8-2.11.[27]

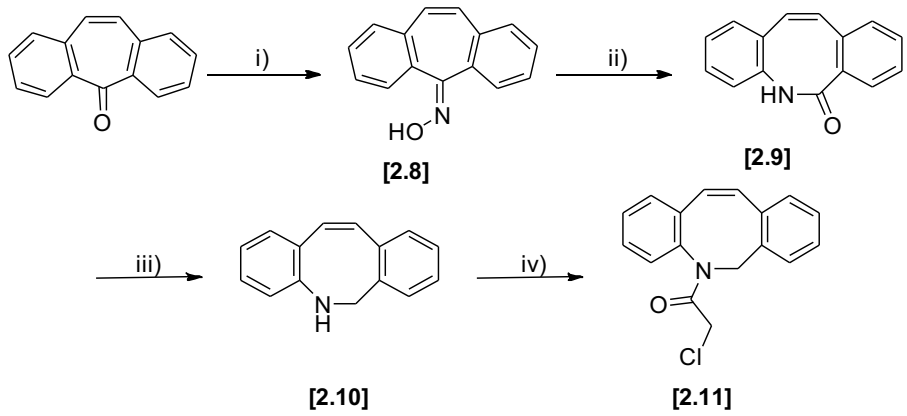

i) $NH_2OH \cdot HCl$, C_5H_5N ii) polyphosphoric acid iii) $LiAlH_4$ iv) $ClCOCH_2Cl$, Cs_2CO_3

Scheme 2.5: Synthesis of compounds 2.8-2.11

The final step to form the chloroacetamide 2.11 which was formed in good yield and purity as shown by the ^1H NMR in Figure 2.21.

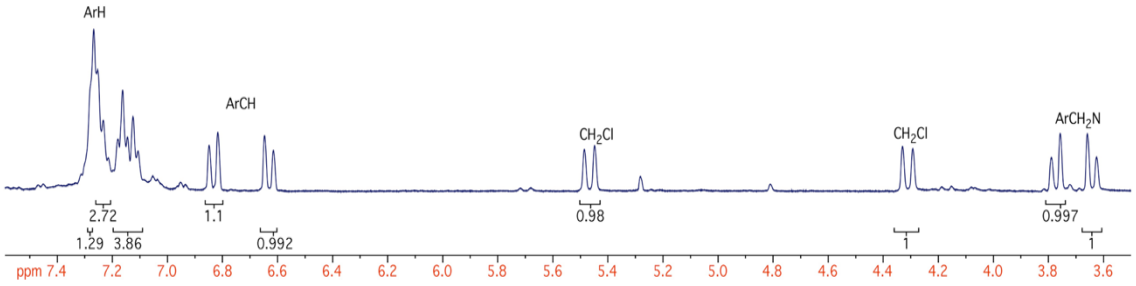

Figure 2.21: ^1H NMR of 2.11 (298 K, $CDCl_3$, 400 MHz).

Two synthetic methods to obtain a strained cyclooctadiene appended to a cyclen moiety were then explored.

The first method (Method A) proposed reacting compound 2.11 directly with $^{t}Bu_3$DO3AH (2.2) to yield compound 2.12 as shown in Scheme 2.6, followed by in in situ formation of the triple bond, deprotection and complexation to yield complex Ln.2.16.

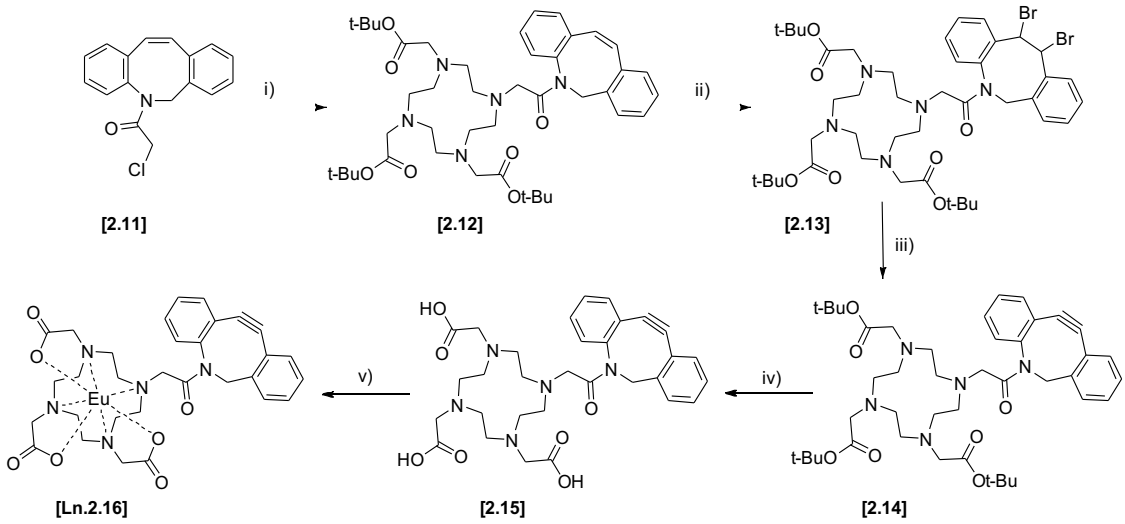

i) $^{t}Bu_3$DO3AH, Cs_2CO_3 ii) pyridinium tribromide iii) 1M ^{t}BuOK in THF iv) TFA v) $Ln(OTf)_3$

Scheme 2.6: Synthetic method A for the formation of an lanthanide linked strained cyclooctyne Ln.2.16

A second methodology looked to form the strained cyclooctyne appended chloroacetamide (compound 2.18) directly and then appended to $^{t}Bu_3$DO3AH (2.2) as outlined in Scheme 2.7, followed by deprotection and complexation to form complex Ln.2.16.

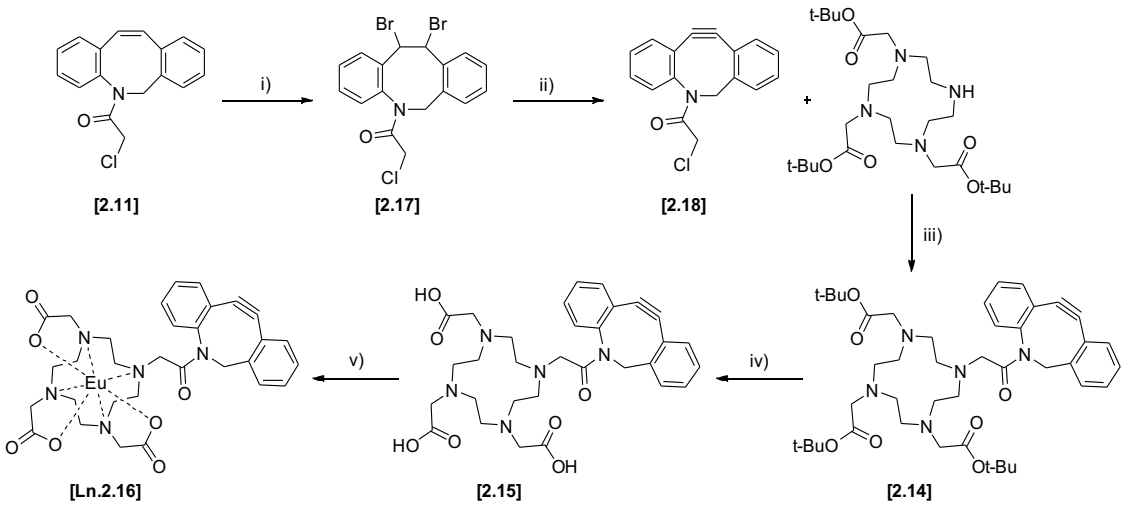

i) pyridinium tribromide ii) 1M ^{t}BuOK in THF iii) Cs_2CO_3 iv) TFA v) $Ln(OTf)_3$

Scheme 2.7: Synthetic method B for the alternative synthesis of lanthanide linked stained cyclooctyne Ln.2.16

2.5.3 Method A

Following the synthetic scheme set out in Scheme 2.6 the compound 2.12 was successfully synthesised as shown by the ^{1}H NMR in Figure 2.22.

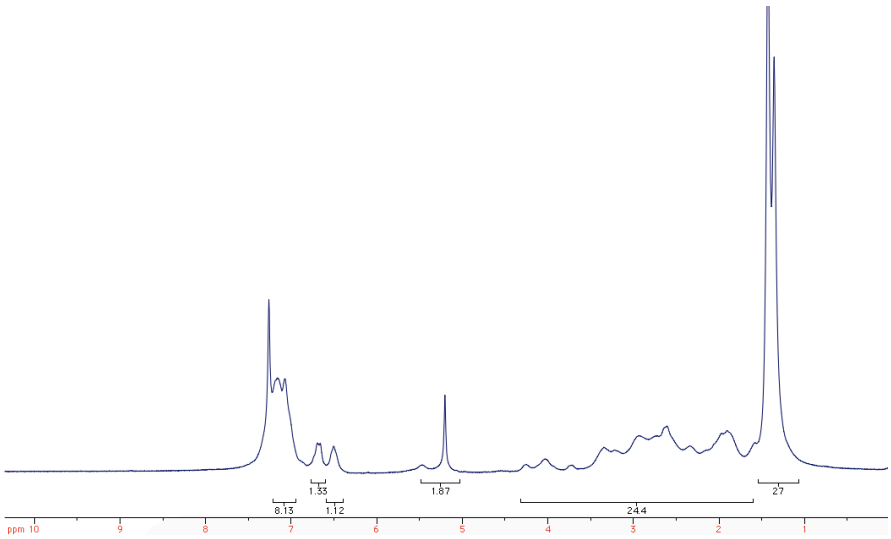

Figure 2.22: ^{1}H NMR of 2.12 (298 K, $CDCl_3$, 400 MHz).

This was then brominated to yield 2.13 before accessing the cyclooctyne by eliminating two molecules of HBr in the presence of base to form the triple bond 2.14 as shown in Scheme 2.6. The ^{1}H NMR showed the formation of product with a slight excess of 2.11,

due to similar solubilities of product and starting material it was determined that purification would be more facile after the deprotection step when the organic compound 2.11 could be separated from the more water soluble product. Once fully deprotected, the ligand 2.15 was complexed with europium to produce complex Eu.2.16, shown by the ^{1}H NMR (Figure 2.23).

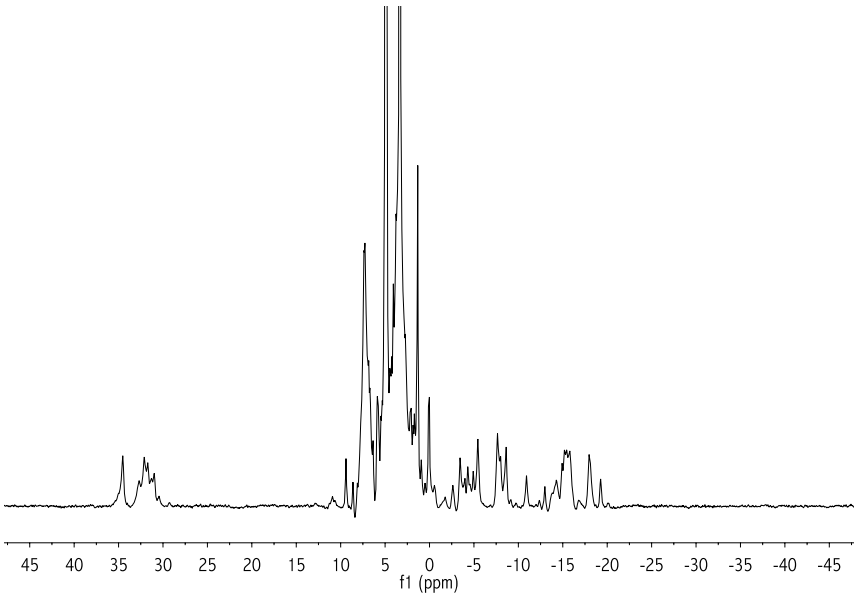

Figure 2.23: ^{1}H NMR Eu.2.16 (298 K, d_4-methanol, 400 MHz)

The ^{1}H NMR of Eu.2.16 cyclootcyne shows that, while the possibility of isomerism is inherent to the system, it exists almost entirely in the SAP conformation which may in part be due to the bulky nature of the pendant strained cyclooctyne arm and restricted rotation about the C-N bond.

Complex Eu.2.16 was also studied by luminescence spectroscopy, and the dibenzocyclooctyne group was found to be an effective sensitising chromophore. Excitation and emission spectra are shown in Figure 2.24.

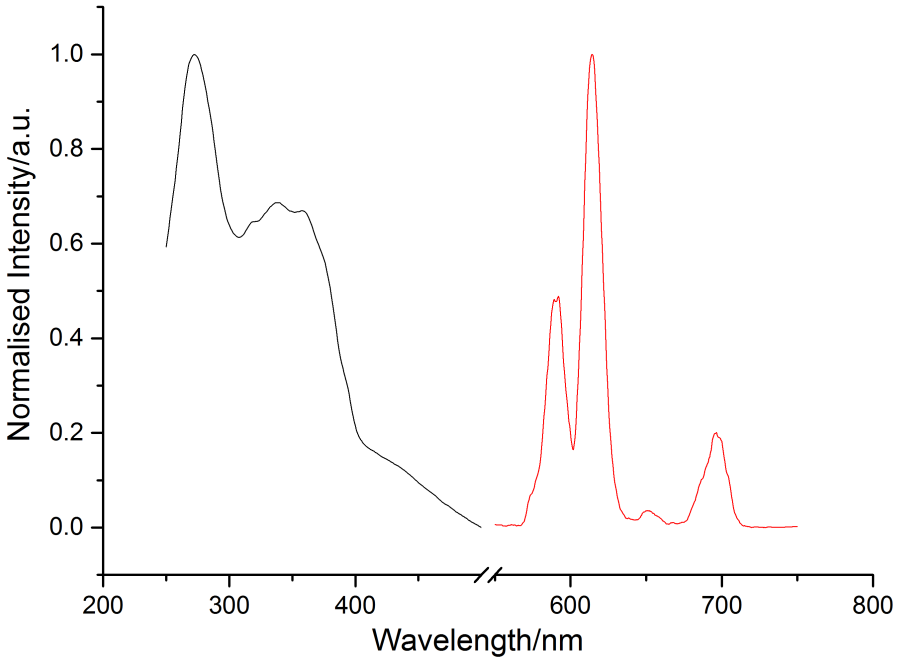

Figure 2.24: Excitation and emission spectra of Eu.2.16 (λem=616nm λex=275nm)

The excitation spectra show two main bands at 275 nm and 360 nm. The band around 275 nm can be attributed to the benzene rings on the pendant arm, while the large broad band centred around 360 nm we attribute to increased conjugation arising from the presence of the triple bond.

To test if this system could be used in a copper-free click reaction, benzyl azide was reacted at room temperature with complex Eu.2.16 as outlined in Scheme 2.8.

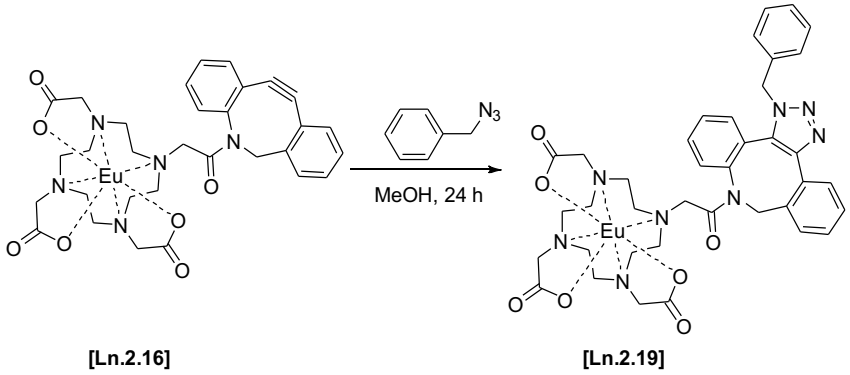

Scheme 2.8: Click reaction of Eu.2.16 with benzyl azide to form complex Eu2.19

The product of the reaction, Eu.2.19, shown in Scheme 2.8 was analysed by ^{1}H NMR as shown in Figure 2.25. Where there are changes not only in the spectral width, which has been increased post-click reaction, but also changes in the shifts and presence of peaks, suggesting the reaction has been successful. It also demonstrates that the restricted rotation of the CN bond persists after the click reaction, with the SAP isomer still dominating.

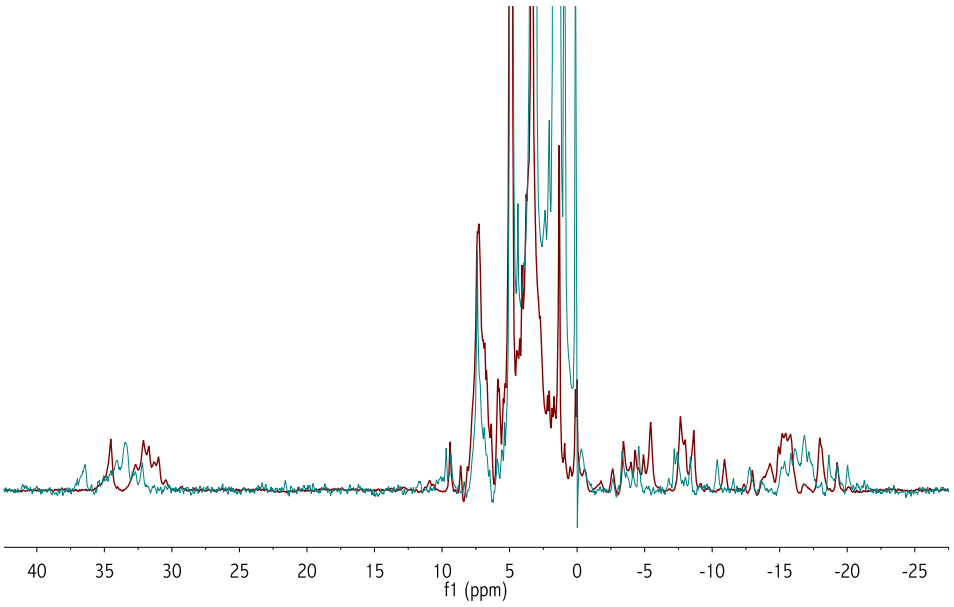

Figure 2.25: Comparison of ^{1}H NMR for Eu.2.16 (red) and resulting click product Eu.2.19 (blue) (298 K, d_4-methanol, 400 MHz)

The product was also investigated by luminescence, with the measured excitation and emission spectra shown in Figure 2.26.

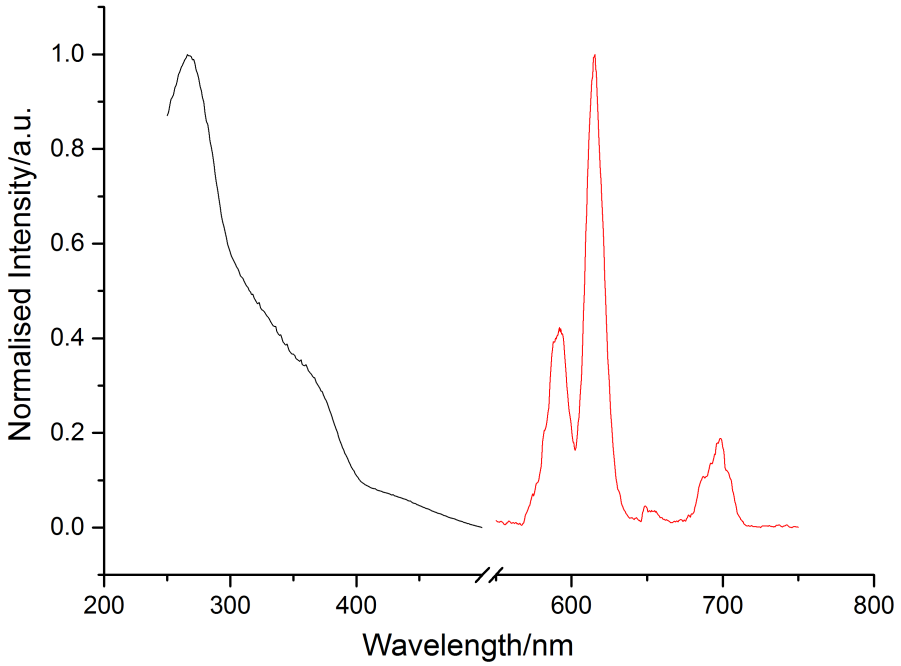

Figure 2.26: Excitation and emission spectra for Eu.2.19. (λex=616 λem=265 nm)

The most noticeable difference is when comparing the excitation spectra of the two complexes (Figure 2.27 left). We can see a small shift of the 275 nm band in complex Eu.2.16 to 265 nm for complex Eu.2.19 which may be due to the presence of the triazole ring in complex Eu.2.19. There is also a significant decrease in the band centred around 360 nm which is significantly decreased after the click reaction due to the loss of the triple bond. Figure 2.27 (right) also shows that the intensity ratio of the ΔJ=1 to ΔJ=2 bands are altered before and after the click reaction. This change in the hypersensitive band maybe indicative of changes in the system due to the formation of Eu.2.19, possibly due to the reduced strain now experienced by the system.

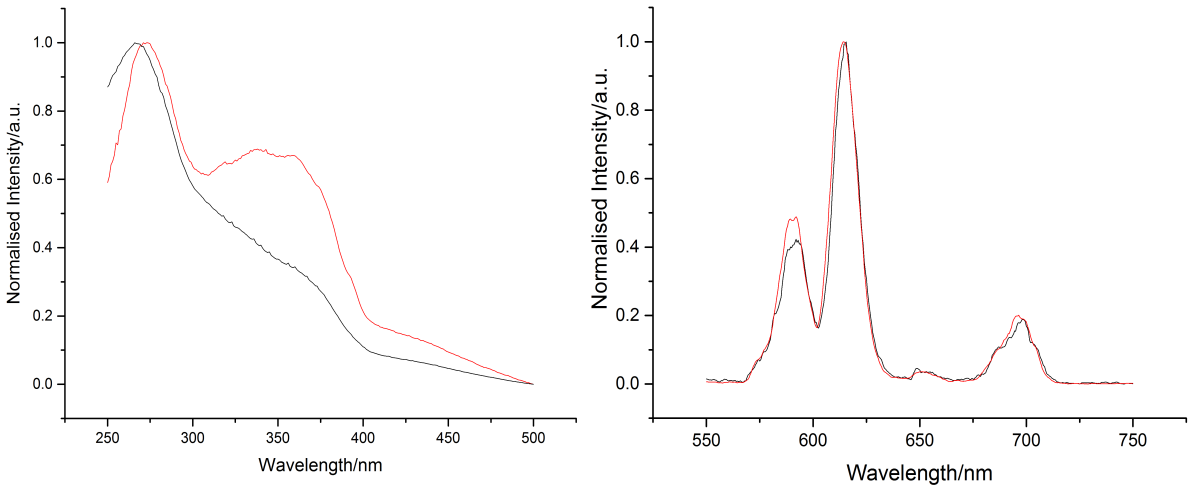

Figure 2.27: Comparison of: left- excitation spectra for Eu.2.16 (red) and Eu.2.19 (black) and right- normalised emission spectra of Eu.2.16 (red) and Eu.2.19 (black)

The lifetimes of both complexes, Eu.2.16 and Eu.2.19, were also measured in methanol and d_4-methanol and their calculated q values as shown in Table 2.4.

Table 2.4: Measured lifetime values and calculated q values for complex Eu.2.16 and Eu.2.19 (q is calculated according to Equation 2.2: where A=2.4 ms and B=0.125 ms)

	τ_{MeOH}/ms[a]	τ_{MeOD}/ms[a]	q
Eu.2.16	$\tau_1 = 0.89$	$\tau_1 = 1.71$	0.97
Eu.2.19	$\tau_1 = 0.85$	$\tau_1 = 1.76$	1.1

[a] *where the typical errors on measured values are around 10 %*

The calculated q values indicate that there is no overall change in q before and after the copper-free click reaction. The q values also show there is one bound solvent molecule for both systems indicating that the carbonyl on the cyclooctyne arm may be coordinated to the lanthanide centre as shown in Figure 2.28. This isn't particularly surprising as the ^{1}H NMR shows the restricted rotation of the CN bond persists in both cases.

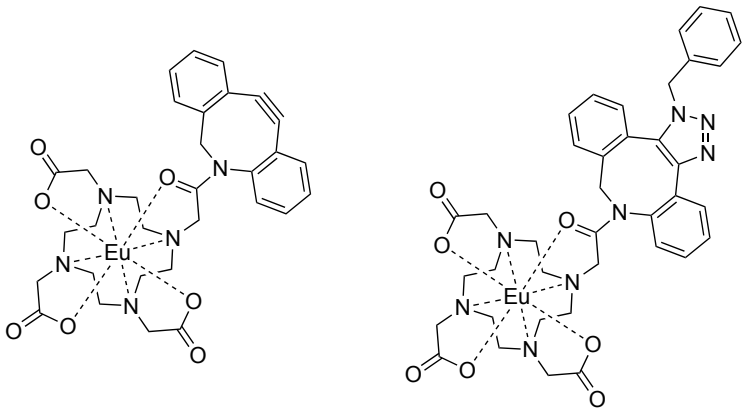

Figure 2.28:Proposed coordination geometries of complexes Eu2.16 and Eu.2.19

This interaction would not only give a q=1 complexes as calculated from the measured lifetimes, but may help impose the favourable geometry. The favourable interaction may also contribute to the similarities observed in the ^{1}H NMR and the persistence of restricted rotation post click reaction.

2.5.4 Method B

The second synthetic methodology set out in Scheme 2.7 looks to form the strained cyclooctyne pendant arm independently rather than forming the triple bond *in situ*.

To achieve this, the bromination method's purification was modified to allow the trituration of the crude product (in ethyl acetate/ dichloromethane 1:1 v/v) to successfully yield compound 2.17 as a white solid, which was confirmed by ^{1}H NMR (Figure 2.29).

27

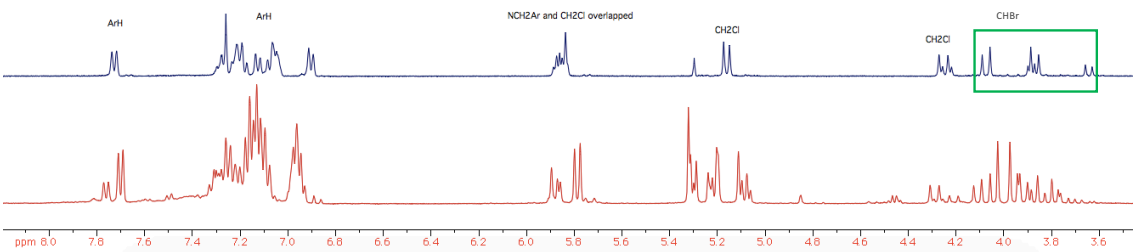

Figure 2.29: ^{1}H NMR comparing 2.17 before (red) and after (blue) purification (298 K, $CDCl_3$, 400 MHz)

An enlargement of the region boxed in Figure 2.29 is shown in Figure 2.30 and depicts the CHBr protons.

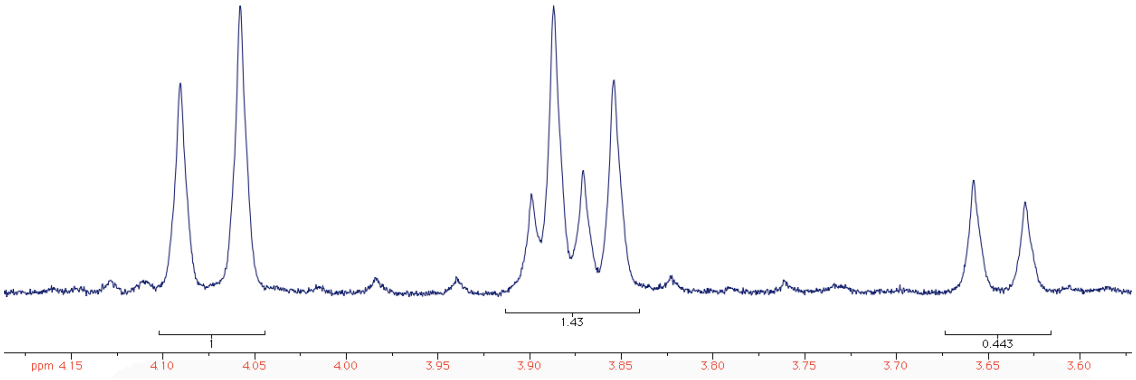

Figure 2.30: enlarged region of the ^{1}H NMR for the purified 2.17

This show the presence of 2 stereoisomers created by opening the intermediate bromonium ion (Scheme 2.9), as was also confirmed by 2D COSY NMR. Analysis of the integrations of these peaks also indicates an approximate 2:1 ratio of the stereoisomers.

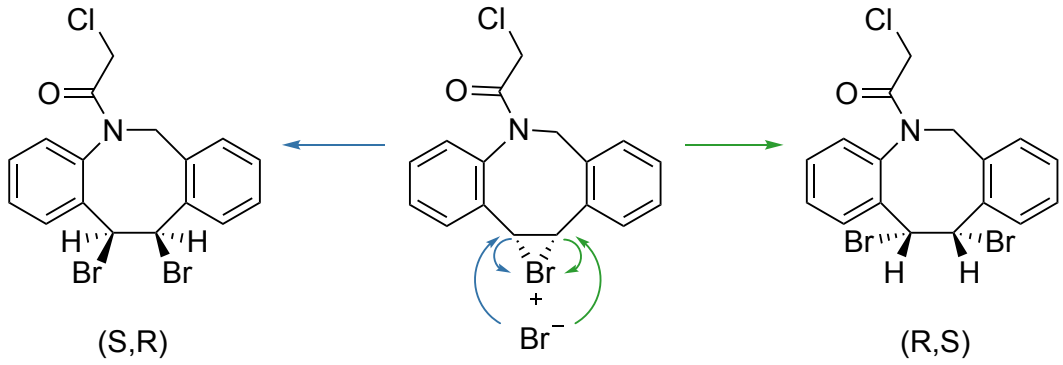

Scheme 2.9: Ring opening of bromonium ion for 2.17 leading to the formation of two disterioisomers (S,R) or (R,S)

Having successfully synthesised and purified compound 2.17 the compound was used to form the triple bond by adapting the literature methodology to give compound 2.18 as illustrated in Figure 2.31. [27]

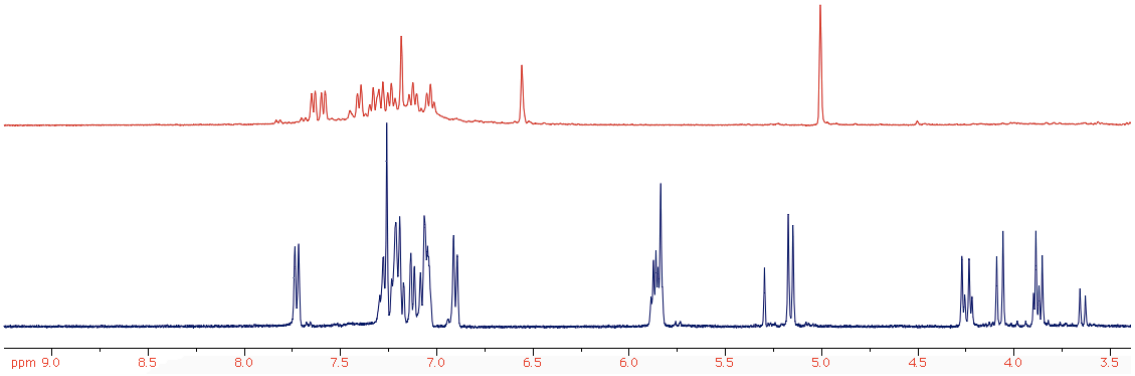

Figure 2.31: ^{1}H NMR comparison of 2.17 (bottom) 2.18 (top (298 K, $CDCl_3$, 400 MHz))

The coupling between 2.18 and $^{t}Bu_3$DO3AH (2.2) proved to be unsuccessful, with little evidence of the desired product being formed by ^{1}H NMR. While the synthetic method of heating under reflux in acetonitrile for 48 hours proved unsuccessful, the coupling may still be possible with further exploration and adaptation of the methodology.

2.6 Conclusions

In this chapter, it has been shown for a series of click reactions between Ln.p.DO3A and 2-azidopyridine that we can synthesise complexes with a range of possible protonation and coordination modes based on pH. We have demonstrated that complexes can be pH dependant or independent based on their position in the lanthanide series, with the later lanthanides (having reduced ionic radii and higher charge density) favouring hydration over coordination of the triazole, thus experiencing a change in coordination and geometry.

We have also shown how these complexes can be used to make the corresponding d-f hybrids with rhenium, and explored the effect of the on the ^{1}H NMR and luminescence. While the NMR behaviour does not differ from that of the parent complexes, the luminescent behaviour of the ytterbium-rhenium dyad showed quenching of the ytterbium luminescence. We propose this may be due to fast deactivation pathways involving the MLCT or by quenching occurring through metal-metal charge transfer.

We have also demonstrated how copper-free click chemistry can be explored by appending a strained cyclooctyne to a lanthanide complex for use in bio-orthogonal click reactions. We have shown two possible synthetic methods, one of which was successfully used to synthesise a strained cyclooctyne europium complex and demonstrate a copper free click reaction. The second proposed method was not able to successfully append the strained cyclooctyne pendant arm but we assert that with further exploration and adaptation of the methodology for this step could yield positive results in the future.

2.7 References

1. B. Chattopadhyay, C. I. R. Vera, S. Chuprakov, and V. Gevorgyan, *Org. Lett.*, 2010, **12**, 2166–9.
2. M. Jauregui, W. S. Perry, C. Allain, L. R. Vidler, M. C. Willis, A. M. Kenwright, J. S. Snaith, G. J. Stasiuk, M. P. Lowe, and S. Faulkner, *Dalton Trans.*, 2009, 6283–5.
3. M. Tropiano, A. M. Kenwright, and S. Faulkner, *Chemistry*, 2015, **21**.
4. H. Akiba, J. Sumaoka, K. Tsumoto, and M. Komiyama, *Anal. Chem.*, 2015, **87**, 3834–3840.
5. I. Stengel, A. Mishra, N. Pootrakulchote, S.-J. Moon, S. M. Zakeeruddin, M. Grätzel, and P. Bäuerle, *J. Mater. Chem.*, 2011, **21**, 3726.
6. W. K. C. Lo, G. S. Huff, J. R. Cubanski, A. D. W. Kennedy, C. J. McAdam, D. A. McMorran, K. C. Gordon, and J. D. Crowley, *Inorg. Chem.*, 2015, **54**, 1572–1587.
7. K. Jobe, C. H. Brennan, M. Motevalli, S. M. Goldup, and M. Watkinson, *Chem. Commun. (Camb).*, 2011, **47**, 6036–8.
8. G. J. Stasiuk and M. P. Lowe, *Dalton Trans.*, 2009, 9725–7.
9. P. I. P. Elliott, *Organometallic Chemistry*, Royal Society of Chemistry, Cambridge, 2014, vol. 39.
10. J. E. Moses, A. D. Moorhouse, V. P. Mocharla, R. J. Lin, M. E. Phelps, H. C. Kolb, H.-R. Tseng, M. G. Finn, K. B. Sharpless, J. H. Elder, and V. V. Fokin, *Chem. Soc. Rev.*, 2007, **36**, 1249–1262.
11. M. Gil, M. Arévalo, and Ó. López, *Synthesis (Stuttg).*, 2007, **2007**, 1589–1620.
12. L. Frullano, C. Catana, T. Benner, A. D. Sherry, and P. Caravan, *Angew. Chemie Int. Ed.*, 2010, **49**, 2382–2384.
13. B. S. Uppal, R. K. Booth, N. Ali, C. Lockwood, C. R. Rice, P. I. P. Elliott, I. Kinoshita, T. Kusumoto, H. Hashimoto, M. Harada, Y. Mikata, T. Funabiki, and S. Yano, *Dalt. Trans.*, 2011, **40**, 7610.
14. U. Monkowius, S. Ritter, B. König, M. Zabel, and H. Yersin, *Eur. J. Inorg. Chem.*, 2007, **2007**, 4597–4606.
15. J. T. Fletcher, B. J. Bumgarner, N. D. Engels, and D. A. Skoglund, *Organometallics*, 2008, **27**, 5430–5433.
16. S. J. A. Pope, B. J. Coe, and S. Faulkner, *Chem. Commun. (Camb).*, 2004, 1550–1.
17. S. J. A. Pope, B. J. Coe, S. Faulkner, and R. H. Laye, *Dalton Trans.*, 2005, 1482–90.
18. F. Kennedy, N. M. Shavaleev, T. Koullourou, Z. R. Bell, J. C. Jeffery, S. Faulkner, and M. D. Ward, *Dalton Trans.*, 2007, 1492–9.
19. M. Tropiano, C. J. Record, E. Morris, H. S. Rai, C. Allain, and S. Faulkner, *Organometallics*, 2012, **31**, 5673–5676.
20. N. M. Shavaleev, L. P. Moorcraft, S. J. A. Pope, Z. R. Bell, S. Faulkner, and M. D. Ward, *Chem. Commun.*, 2003, 1134–1135.
21. L. Gaetke, *Toxicology*, 2003, **189**, 147–163.
22. Astdr, *U.S Public Heal. Serv. Agency Toxic Subst. Dis. Regist.*, 2004, 121–189.
23. W. S. Perry, S. J. A. Pope, C. Allain, B. J. Coe, A. M. Kenwright, and S. Faulkner, *Dalton Trans.*, 2010, **39**, 10974–83.
24. C. L. Dupont, G. Grass, C. Rensing, P. E. Bourne, Y. Zen, K. Tomita, N. L. Brown, R. Shillam, P. Christian, T. S. J. Elliott, and T. F. Stocker, *Metallomics*, 2011, **3**, 1109.
25. J. M. Baskin, J. A. Prescher, S. T. Laughlin, N. J. Agard, P. V Chang, I. A. Miller, A. Lo, J. A. Codelli, and C. R. Bertozzi, *Proc. Natl. Acad. Sci. U. S. A.*, 2007, **104**, 16793–7.
26. A. Bernardin, A. Cazet, L. Guyon, P. Delannoy, F. Vinet, D. Bonnaffé, and I. Texier, *Bioconjug. Chem.*, 2010, **21**, 583–588.

27. A. Kuzmin, A. Poloukhtine, M. A. Wolfert, and V. V Popik, *Bioconjug. Chem.*, 2010, **21**, 2076–85.

28. J. Laha and G. Cuny, *Synthesis (Stuttg).*, 2008, 4002–4006.

29. R. Huisgen, K. Fraunberg, and H. J. Sturm, *Tetrahedron Lett.*, 1969, **10**, 2589.

30. M. Tropiano, N. L. Kilah, M. Morten, H. Rahman, J. J. Davis, P. D. Beer, and S. Faulkner, *J. Am. Chem. Soc.*, 2011, **133**, 11847–9.

31. A. Dadabhoy, S. Faulkner, and P. G. Sammes, *J. Chem. Soc. Perkin Trans. 2*, 2002, 348–357.

32. V. V Rostovtsev, L. G. Green, V. V Fokin, and K. B. Sharpless, *Angew. Chem. Int. Ed. Engl.*, 2002, **41**, 2596–9.

33. D. Rösner, T. Schneider, D. Schneider, M. Scheffner, and A. Marx, *Nat. Protoc.*, 2015, **10**, 1594–1611.

34. S. I. Presolski, V. P. Hong, and M. G. Finn, *Curr. Protoc. Chem. Biol.*, 2011, **3**, 153–162.

35. J. Hall, R. Häner, S. Aime, M. Botta, S. Faulkner, D. Parker, A. S. de Sousa, M. Grandi, and P. Paoli, *New J. Chem.*, 1998, **22**, 627–631.

36. A. Beeby, I. M. Clarkson, R. S. Dickins, S. Faulkner, D. Parker, L. Royle, A. S. de Sousa, J. A. G. Williams, and M. Woods, *J. Chem. Soc. Perkin Trans. 2*, 1999, 493–504.

37. A. Jana, S. J. A. Pope, and M. D. Ward, *Polyhedron*, 2017, **127**, 390–395.

38. N. M. Shavaleev, L. P. Moorcraft, S. J. A. Pope, Z. R. Bell, S. Faulkner, and M. D. Ward, *Chem. - A Eur. J.*, 2003, **9**, 5283–5291.

39. M. H. V. Werts, J. W. Verhoeven, J. W. Hofstraat, F. J. Steemers, E. G. Kerver, W. Verboom, D. N. Reinhoudt, and S. Yanagida, *J. Chem. Soc. Perkin Trans. 2*, 2000, **4**, 433–439.

40. T. Lazarides, D. Sykes, S. Faulkner, A. Barbieri, and M. D. Ward, *Chem. - A Eur. J.*, 2008, **14**, 9389–9399.

41. M. Tropiano, C. J. Record, E. Morris, H. S. Rai, C. Allain, and S. Faulkner, *Organometallics*, 2012, **31**, 5673–5676.

42. A. Boulay, A. Seridi, C. Zedde, S. Ladeira, C. Picard, L. Maron, and E. Benoist, *Eur. J. Inorg. Chem.*, 2010, **2010**, 5058–5062.

43. G. Canzi, J. C. Goeltz, J. S. Henderson, R. E. Park, C. Maruggi, and C. P. Kubiak, *J. Am. Chem. Soc.*, 2014, **136**, 1710–1713.

44. P. H. Dinolfo, M. E. Williams, A. C. L. Stern, and J. T. Hupp, *J. Am. Chem. Soc.*, 2004, 126, 12989-13001.

45. J. Dommerholt, S. Schmidt, R. Temming, L. J. A. Hendriks, F. P. J. T. Rutjes, J. C. M. Van Hest, D. J. Lefeber, P. Friedl, and F. L. Van Delft, *Angew. Chemie - Int. Ed.*, 2010, **49**, 9422–9425.

46. R. K. Iha, K. L. Wooley, A. M. Nyström, D. J. Burke, M. J. Kade, and C. J. Hawker, *Chem. Rev.*, 2009, **109**, 5620–5686.

47. H. C. Hang, C. Yu, D. L. Kato, and C. R. Bertozzi, *Proc. Natl. Acad. Sci. U. S. A.*, 2003, **100**, 14846–51.

48. G. Wittig and A. Krebs, *Chem. Ber.*, 1961, **94**, 3260–3275.

49. A. A. Poloukhtine, N. E. Mbua, M. A. Wolfert, G.-J. Boons, and V. V. Popik, *J. Am. Chem. Soc.*, 2009, **131**, 15769–15776.

50. S. T. Laughlin, J. M. Baskin, S. L. Amacher, and C. R. Bertozzi, *Science , 80.*, 2008, **320**, 664–667.

51. N. E. Mbua, J. Guo, M. A. Wolfert, R. Steet, and G.-J. Boons, *ChemBioChem*, 2011, **12**, 1912–1921.

3 Gold Catalysed Couplings with p-DO3A complexes

3.1 Introduction

While a variety of methods for synthesising lanthanide architectures from stable building blocks, including Huisgen cyclisations ("click" chemistry)[1–3] and Ugi reactions,[4–6] have recently been established, the development of new synthetic procedures is still a vital area of research in order to access novel lanthanide containing moieites. This is particularly true for accessing coordinatively unsaturated systems. This chapter deals with the development of methods that can be used to elaborate complexes of propargyl DO3A into more complicated architectures that retain a heptadentate donor ligand.

Transition metal-catalysed three component couplings between aldehydes, alkynes and amines have been investigated for the C-H activation of propargylamines.[7,8] These couplings have been used successfully with a variety of organic substituents and with a range of catalysts including copper, zinc, silver and gold,[9–11] showing considerable scope for expansion and development. However, this methodology has never been used with metal complexes, still less with kinetically stable lanthanide containing complexes.

This Chapter explores the development of a new synthetic procedure using Ln.p.DO3A as a component in gold catalysed three-component couplings also demonstrates how this methodology can be extended to synthesise heterometallic lanthanide complexes. These studies have resulted in the preparation of a number of complexes that interact with anions and can be used to explore energy transfer mechanisms and anion binding.

3.2 Monometallic complexes

3.2.1 Synthesis and characterisation

To utilise lanthanide complexes as a reagent for three component coupling Ln.p.DO3A was synthesised, as previously described in Chapter 2. A synthetic procedure based on work by Kung. *et al.* was used in the first instance to see if the methodology could be directly applied to work with a lanthanide complex.[12] However, this procedure was not successful and modification was therefore needed to work with a lanthanide component. This may be due to differences in solubility of the products and in the reactivity of lanthanide complexes compared to simpler organic based reagents.

To find the right conditions, test reactions using Ln.p.DO3A, piperidine and benzaldehyde were carried out. Experimental factors such as time, temperature and catalyst were iteratively changed to optimise the reaction conditions, as shown in Table 3.1 and the same tests where the aldehyde was changed to 2-naphthaldehyde produced the same outcome.

Table 3.1:Table showing various reaction conditions and their outcomes (where Ln=Lu- or Eu-p.DO3A, amine=piperidine, aldehyde= benzaldehyde or 2-naphthaldehyde)

Equivalents: (Ln:pipeidine:aldehyde:catalyst)	**Catalyst**	**Temperature**	**Time**	**Outcome**
1:1:1.0.1	$AuCl_4 \cdot 3H_2O$	40 °C	2 h	X
1:1:1.0.1	$AuCl_4 \cdot 3H_2O$	60 °C	4 h	X
5:10:10:1	$AuCl_4 \cdot 3H_2O$	40 °C	20 h	X
2:10:10:1	$AuCl_4 \cdot 3H_2O$	40 °C	20 h	✓
1:1:1:0.1	$CuSO_4 \cdot 5H_2O$	40 °C	20 h	X
1:1:1:0.1	CuCl	40 °C	20 h	X

The most successful of these tests revealed the best conditions were using a gold chloride tri-hydrate catalyst in water at 40 °C for 20 hours using an excess of amine and aldehyde components. These conditions proved to be versatile with respect to varying the starting materials - working successfully with benzaldehyde and 2-naphthaldehyde substrates and a variety of lanthanide ions, as shown in Scheme 3.1

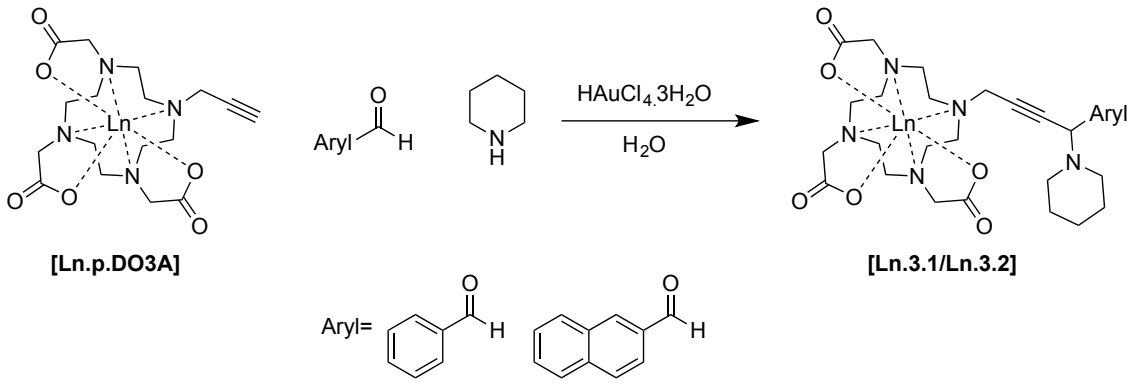

Scheme 3.1:Synthesis of Ln.3.1 and Ln.3.2 showing variation of the lanthanide centre and aldehyde component where Ln.3.1 has aryl=benzene and Ln.3.2 has aryl=2-naphthaldehyde

During these couplings, gold nanoparticle formation was observed; this has not been reported in similar couplings to our knowledge, and may be indicative of instability in the gold containing intermediates in these reactions. These gold nanoparticles proved challenging to remove from solution as they showed stability over an extended period without aggregating further. This stability may suggest that they are capped – most likely through interactions of piperidine with the nanoparticle surface.

Several methods were tried in an attempt to remove the colloidal nanoparticles from solution including: centrifugation, micropore syringe filter and celite filtration, but all these methods proved ineffective. It was found that using a column of amberlite beads successfully removed the nanoparticles and salt from the complex after multiple water washes, allowing the pure complex to be obtained using a 20 % solution of acetonitrile in water.

Having found a suitable procedure, the complexes were characterised. For the europium complex, paramagnetic ^{1}H NMR was used to compare the europium complex Eu.3.2 to the starting Eu.p.DO3A complex. Figure 3.1 shows a clear change between the starting material and the coupling product Eu.3.2.

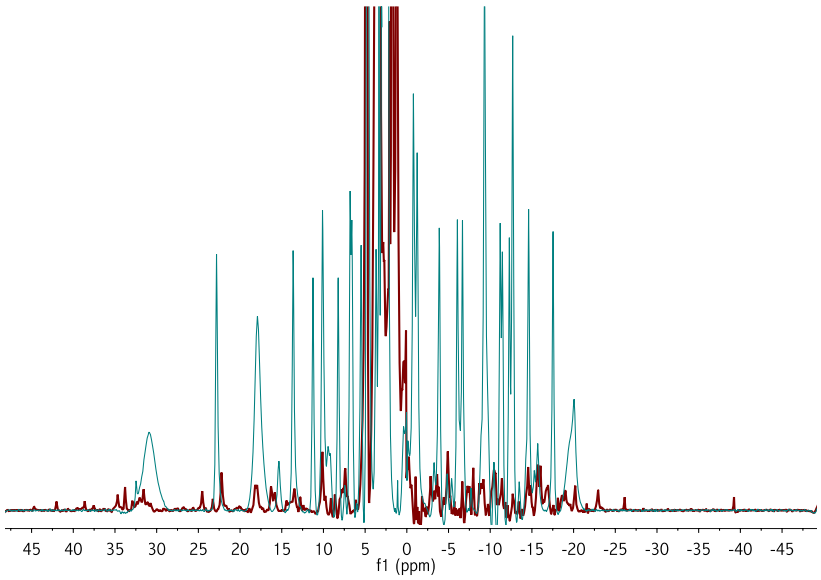

Figure 3.1:^{1}H NMR comparing Eu.p.DO3A (blue) and gold coupling product Eu.3.2 (red). (298 K, D2O, 400 MHz)

From Figure 3.1 it can be seen that there is a significant increase not only in the number of peaks but in their breadth and overall spectral width. This is due to the increased conformational flexibility of the coupling product compared to Eu.p.DO3A, partly due to the additional chiral centre greatly increasing the number of diastereoisomers present in solution. This chiral centre is clearly too remote from the macrocycle to act as a chiral auxiliary for the orientation of the cyclen ring and pendant arms, but still enhances the number of available isomers so that the product mixture might be expected to contain four pairs of enantiomers. This increase of the number of species in solution corresponds to the increase in the number of peaks and fast exchange between isomers causes broadening of the observed signals.

In order to explore the structure further, the diamagnetic lutetium containing complexes provided the opportunity for a more thorough analysis, though the relatively narrow spectral range was likely to complicate the picture regarding identification of diastereoisomers. The ^{1}H NMR shown in Figure 3.2 was first analysed.

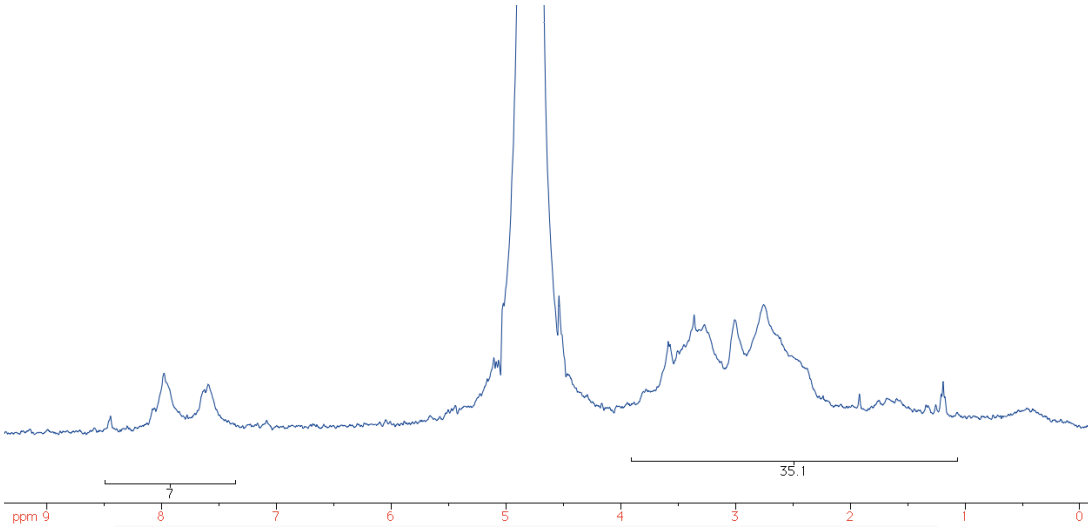

Figure 3.2: ^{1}H NMR for complex Lu.3.2 (298 K, D_2O, 400 MHz)

Although the presence of aromatic signals in the ^{1}H NMR after the reaction suggests that coupling has occurred, the broadness of the peaks around 1.00-4.00 ppm means that analysis of the integrations is complicated and may not be relied upon to definitively prove the presence of piperidine in the coupling product, or show the connectivity present for the coupling product. DOSY NMR experiments were carried out to establish that the aromatic and aliphatic peaks were due to the presence of the desired complex and not free starting materials. This showed the coupling product Lu.3.2 to have a significantly different diffusion coefficient (around 9 x 10^{-8} cm^2s^{-1}) compared to the free aldehyde and p.DO3A starting material (which have a diffusion coefficients of the order of 4 x 10^{-7} cm^2s^{-1} and 2 x 10^{-7} cm^2s^{-1} respectively), suggesting that no aldehyde starting material was present. Furthermore, the slow diffusion expected with the greater molecular diameter of the product would appear in line with the enhanced molecular size expected of the

coupling product. Though, as with the ^{1}H NMR, the broadness of the aliphatic resonances does not allow the presence or absence of piperidine in the complex to be determined.

The proposed mechanism[10] (Scheme 3.2) shows that for the coupling to take place both the piperidine and aldehyde are required. The proposed mechanism also requires that the triple bond be intact in the final structure, though tests to prove the existence of the alkyne bond (e.g. Raman spectroscopy) were unable to verify the presence of the alkyne bond. However, the data presented (such as DOSY and changing ^{1}H NMR) are consistent with successful coupling, and with the proposed structure, although no mass spectrometry data was obtained for these complexes there is also no evidence of other products such as a coupling product with a loss of piperidine.

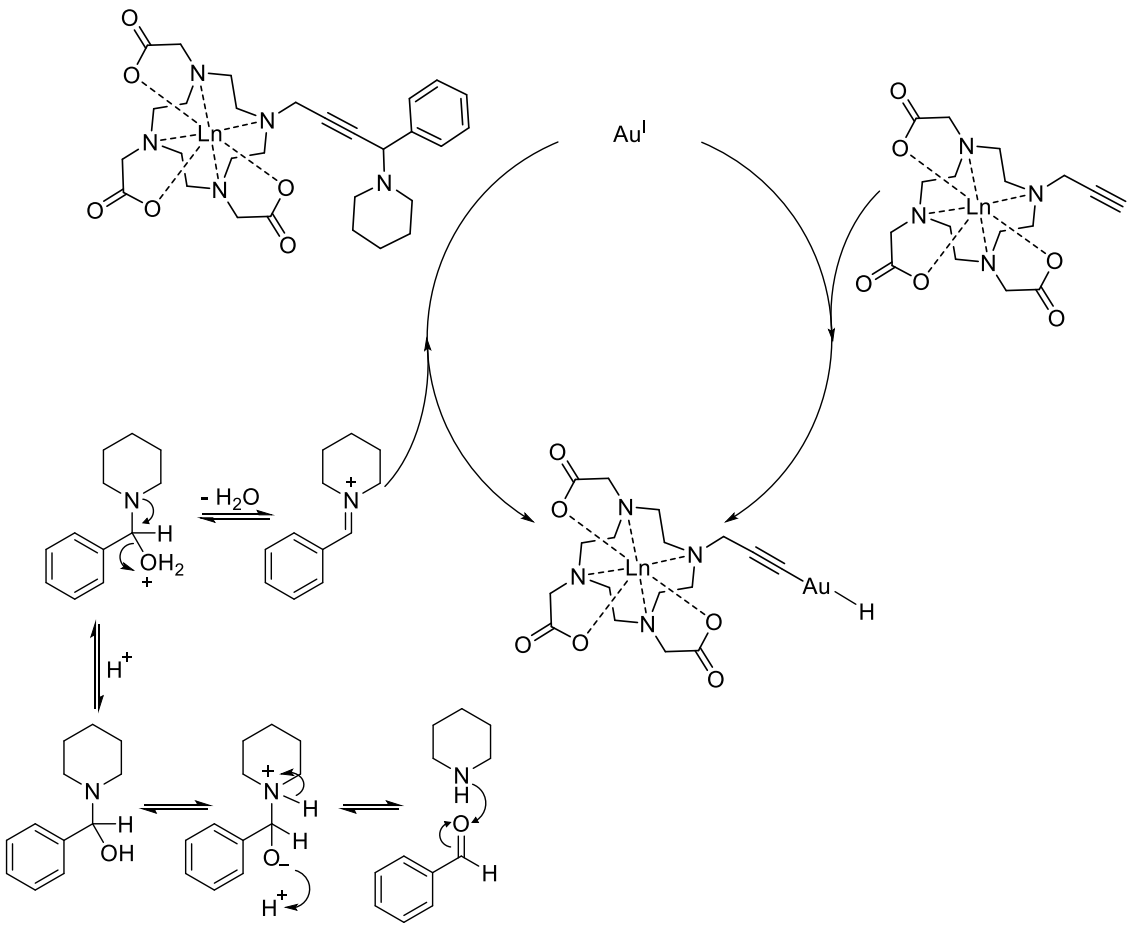

Scheme 3.2: Proposed mechanism (adapted from reference 10) for gold catalysed three component couplings with Ln.p.DO3A to form Ln.3.1

One reason for some uncertainty in the structure of the coupling product arises from the possible hydrolysis pathway of the coupled product which could lead to the loss of piperidine (as shown in Scheme 3.3).

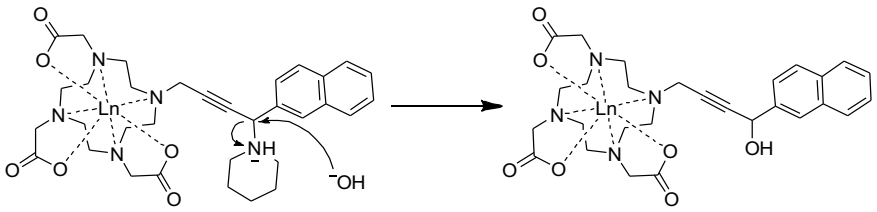

Scheme 3.3: Possible mechanism for the loss of piperidine

This mechanism of hydrolysis has not been reported for any of the organic-based three component couplings. Furthermore, while a Lewis acidic lanthanide ion is present in the compound, the rigidity of the propargyl pendant arm means that this centre is unlikely to be significantly favoured in the reactivity of the complex compared to that of 'normal' coupling products.

To aid interpretation of these compounds, a rigid analogue using a pendant arm derived from N-propargyl acetamide, which incorporates an amide domain that can chelate to the metal ion and rigidify the complex, was synthesised (Scheme 3.4).[13,14] The aim of using this complex in the coupling was to form a system with fewer diasterisomers (since DOTA monoamide derivatives exist predominantly as SAP isomers) and with greater conformational rigidity; the greater control of chemical structure resulting from these effects would also be expected to slow exchange between species and help to elucidate the structure.

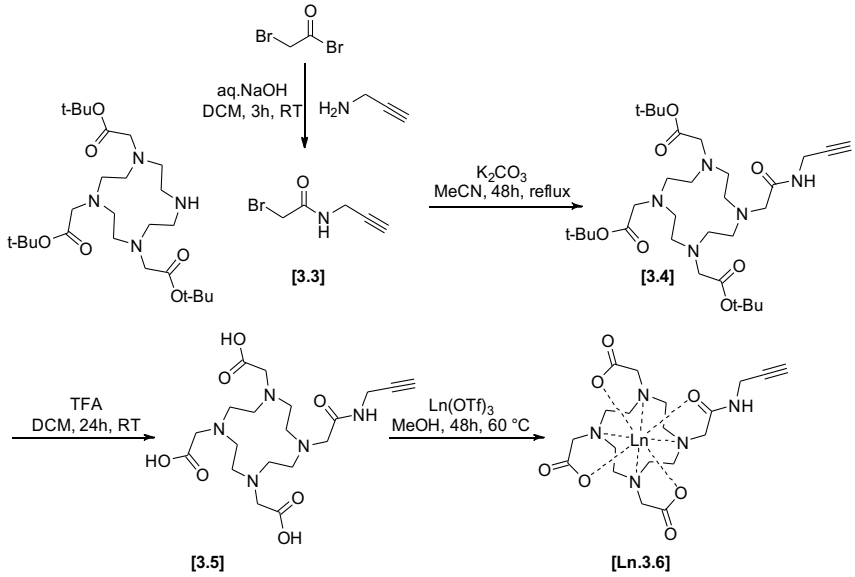

Scheme 3.4: Synthesis of rigid p.DO3A analogues Ln.3.6

Indeed, as can be seen in in Figure 3.3, the rigid analogue shows fewer and sharper peaks when compared to the p.DO3A complex. Furthermore, these are completely consistent with the formation of just the SAP isomer (as a pair of enantiomers).

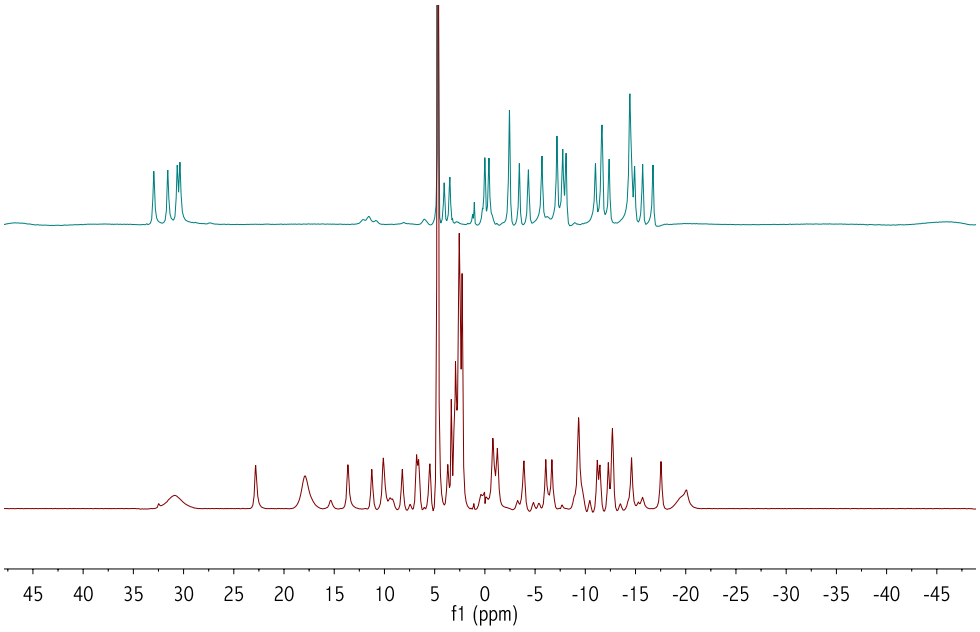

Figure 3.3: ^{1}H NMR comparing Eu.p.DO3A (red) to the rigid analogue Eu.3.6 (blue) (298 K, D_2O, 400 MHz)

The rigid analogue of p.DO3A, Ln 3.6 was used in the coupling using the same reaction conditions previously described (Scheme 3.5).

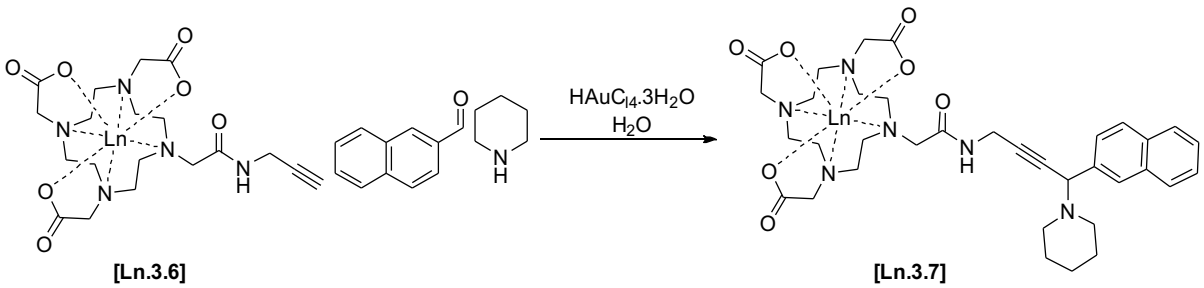

Scheme 3.5: Gold catalysed three component coupling of Ln.3.6 to give coupling product Ln.3.7

The product of this reaction was analysed by ^{1}H NMR (Figure 3.4) but showed no evidence of coupling to yield Lu.3.7, evident when compared to the ^{1}H NMR of the successful coupling product Lu.3.2.

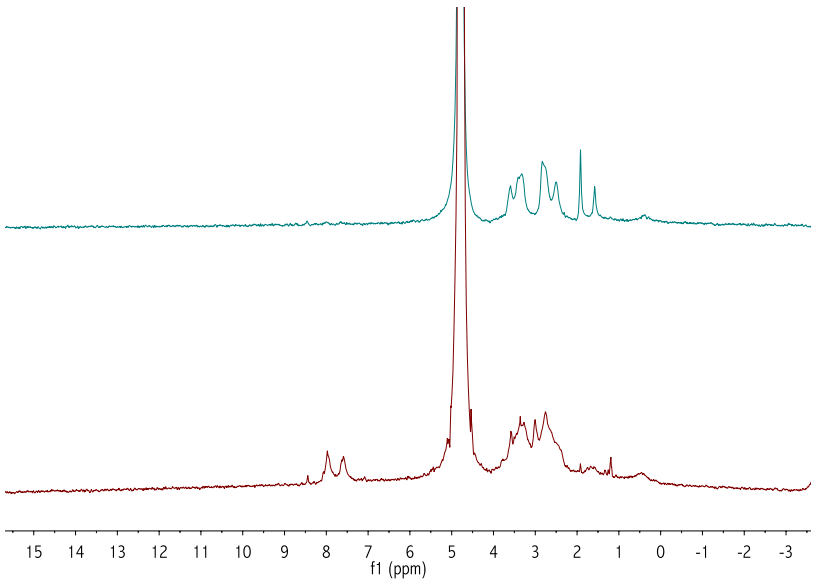

Figure 3.4: ^{1}H NMR showing the failed coupling of Lu.3.7(blue) compared with successful coupling product Lu.3.2 (red) (298 K, D_2O, 400 MHz)

The europium complex Eu.3.7 was also synthesised and analysed by ^{1}H NMR. While it showed a clear change from the starting complex (Figure 3.5) it is also apparent that the DOTA complex was now present in solution, as indicated by peaks at 33.8, -1.1, -6.6, -8.0, -14.6 and -16.1 ppm.[15]

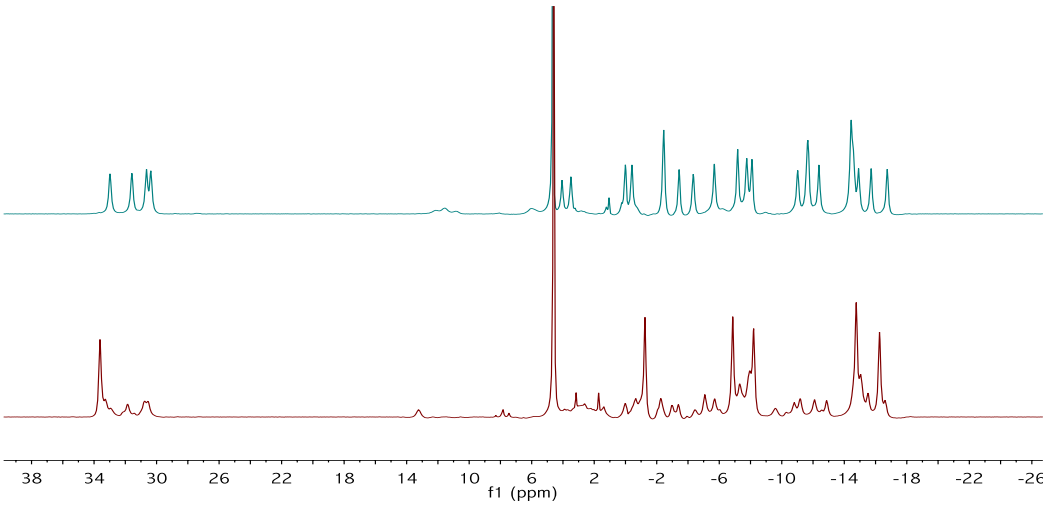

Figure 3.5: ^{1}H NMR comparison of the starting complex Eu.3.6 (blue) with the coupling product Eu.3.7 (red) (298 K, D_2O, 400 MHz)

As DOTA is not present in the starting complex, we surmised that the basic work up caused *in-situ* hydrolysis of the propargyl acetamide arm, resulting in DOTA formation as shown in Scheme 3.6.

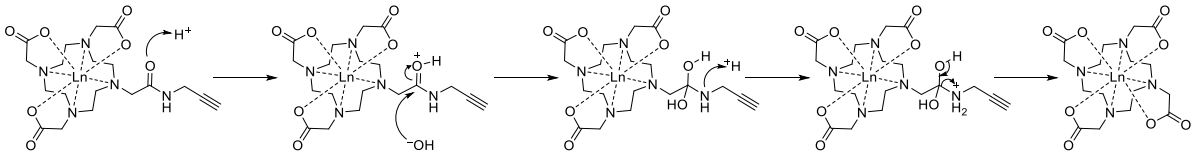

Scheme 3.6: Hydrolysis of Ln.3.6 leading to the formation of DOTA

The formation of DOTA as a hydrolysis product (mediated by the Lewis acidity of the lanthanide centre) of similar compounds has previously been described[16] for related structures in the presence of aqueous base. To try and prevent hydrolysis occurring, basic work up was avoided. The product resulting from this gave the ^{1}H NMR shown in Figure 3.6. By changing the work up procedure there is significantly less DOTA formation, however it is still present in solution. We propose this is due to piperidine acting as a weak base causing small amounts of hydrolysis.

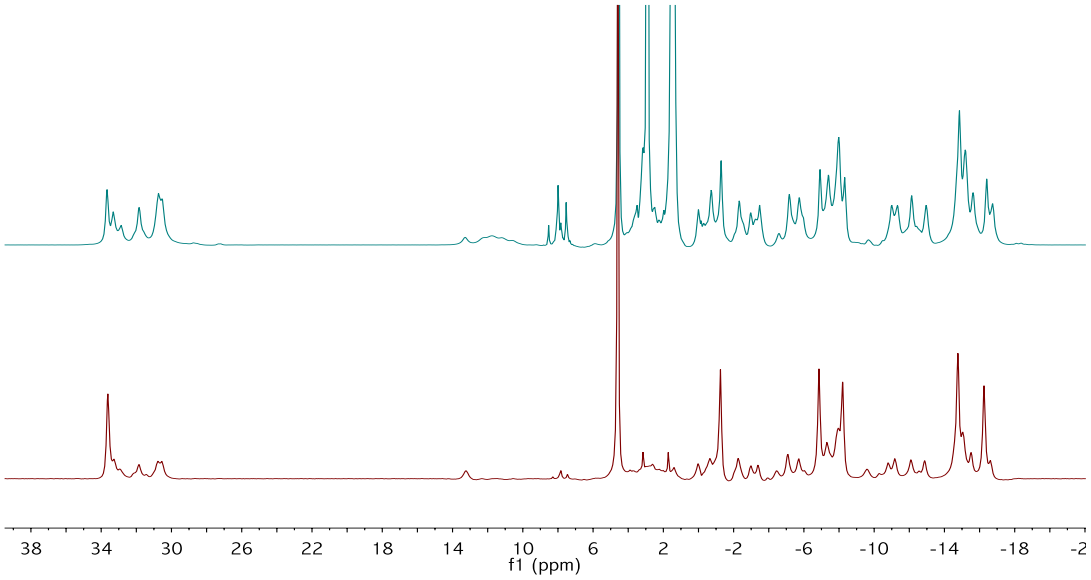

Figure 3.6: ^{1}H NMR comparison of Eu.3.7 with basic work up (red) and #Eu.3.7 without basic work up (blue) (298 K, D_2O, 400 MHz)

While we have demonstrated that using gold catalysed three component couplings affords a potential synthetic route to new lanthanide based architectures the reaction is capricious and unreliable, especially when taking into account issues surrounding the elucidation of the final structures. However, considering all the evidence and the proposed mechanism, it is most likely that the complexes are being formed as proposed. Although there is the possibility of the loss of piperidine, the lack of literature precedent and experimental data suggest this to be unlikely.

3.2.2 Photophysical measurements and binding studies

The europium complex Eu.3.2 was used to explore the nature of the interaction with carboxylic acids (Scheme 3.7). Acridone-N-acetic acid was used initially to investigate the binding by luminescence titrations.

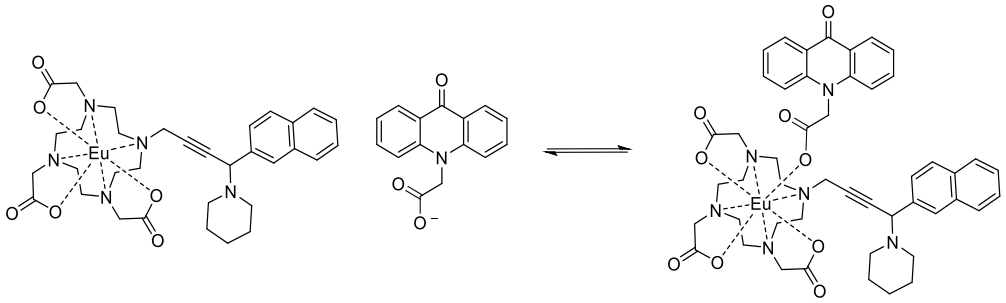

Scheme 3.7: Binding of acridone-N-acetic acid to complex Eu.3.2

Following excitation through the acridone chromophore at 415 nm and monitoring the changes in emission upon addition of acridone-N-acetic acid, we observed a substantial change in the emission, as shown in Figure 3.7. This change in luminescence intensity indicated binding was occurring, causing an increase in intensity due to sensitisation of lanthanide emission through the acridone excited state. The changes in the band corresponding to the hypersensitive $^5D_0$-$^7F_2$ transition (Figure 3.7) also shows there has been a change in the local coordination of the lanthanide centre as a result of binding.

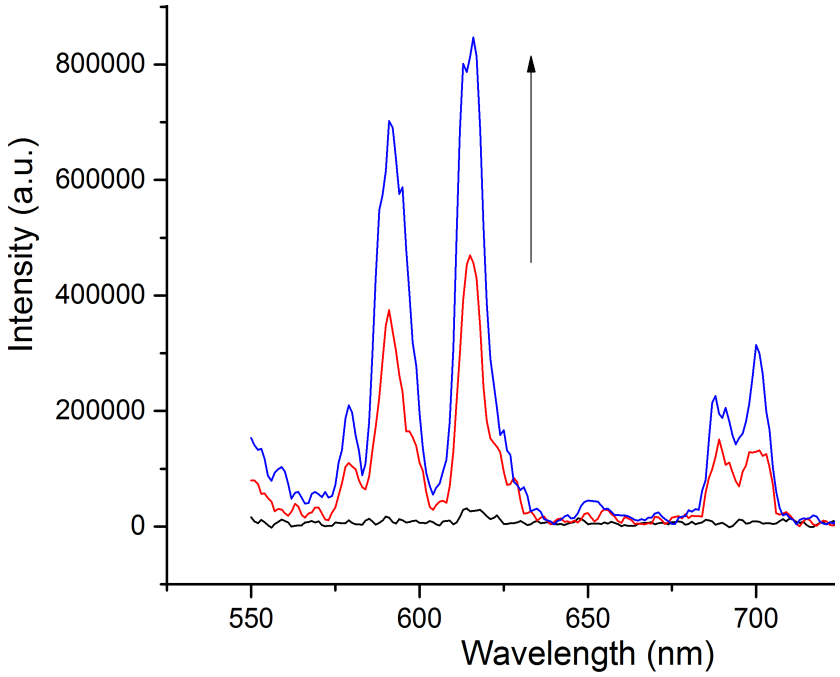

Figure 3.7: Qualitative study of the changing emission spectrum of Eu.3.2 with increasing concentration of acridone-N-acetic acid λ_{ex} =415 nm

To obtain a binding constant, a reverse titration was carried out, in which aliquots of Eu.3.2 were added to a solution of acridone-N-acetic acid while maintaining constant concentration of acridone-N-acetic acid. The data was fitted using DYNAFIT®,[17] an iterative fitting programme, to produce the binding curves shown in Figure 3.8, (green: ΔJ=1, yellow: ΔJ=2, blue: ΔJ=4) with a calculated binding constant of log K_1[95% confidence interval] being 5.12 [4.92-5.38] in methanol. This indicates that there is very strong binding to the Eu.3.2 complex in methanol.

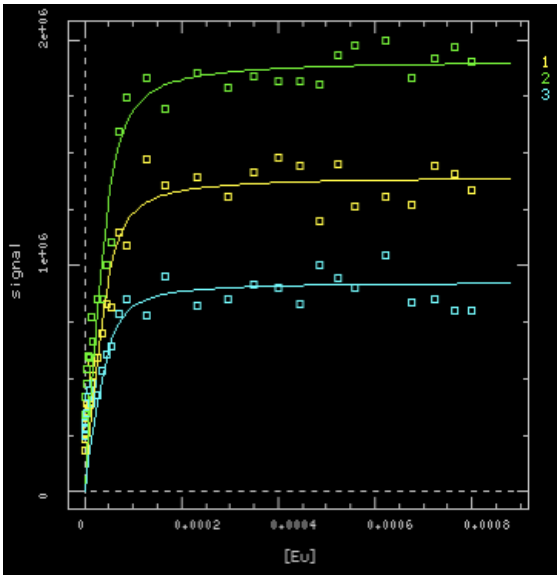

Figure 3.8: Binding curves calculated for the titration of Eu.3.2 with acridone-N-acetic aicd

3.3 Bimetallic complexes

3.3.1 Synthesis and characterisation

Having previously demonstrated the ability to vary the aldehyde component with ease it was predicted that the use of terephthaldehyde could lead to the formation of bimetallic systems. Initially, it was thought the reaction would proceed to give a bimacrocyclic product; however, we observed the formation of the monomacrocyclic complex with an unsubstituted aldehyde, as shown in Scheme 3.8.

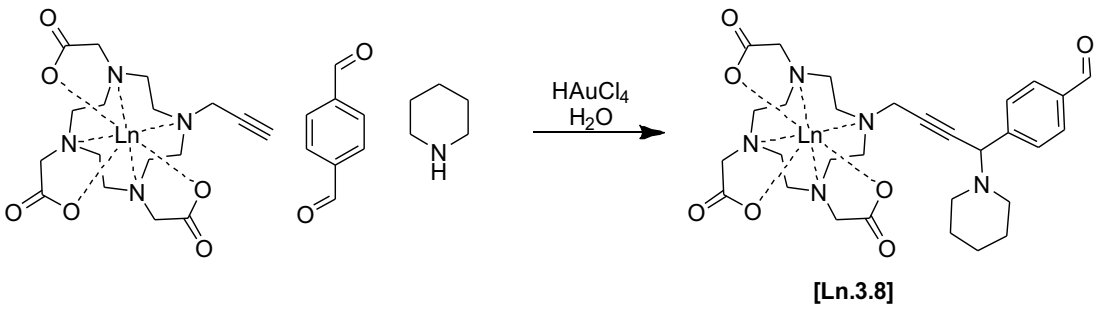

Scheme 3.8: Synthesis of Ln.3.8

Successful synthesis of the lutetium complex Lu.3.8 was confirmed by ^{1}H NMR, which clearly shows the presence of a broad aldehyde peak at 10 ppm (Figure 3.9).

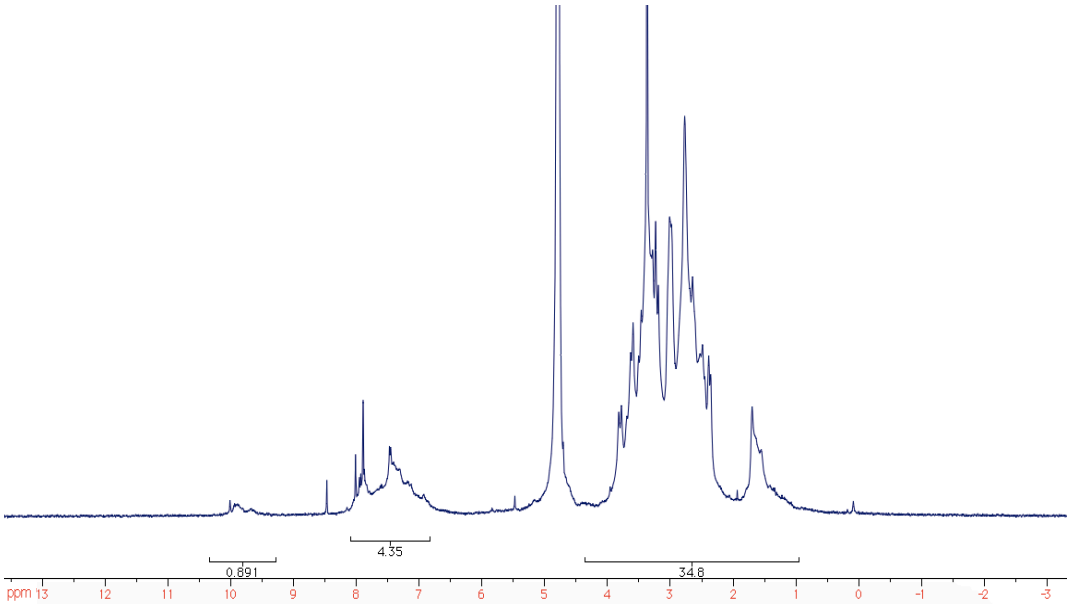

Figure 3.9: ^{1}H NMR of Lu.3.8 (298 K, D_2O, 400 MHz)

The formation of the mono-coupled product permits the sequential addition of lanthanide complexes, allowing the preparation of bimetallic complexes with two different lanthanide centres as shown in Scheme 3.9. This approach is unusual in effectively offering a new pathway to heterometallic lanthanide complexes in which kinetic resolution is used to control product speciation.

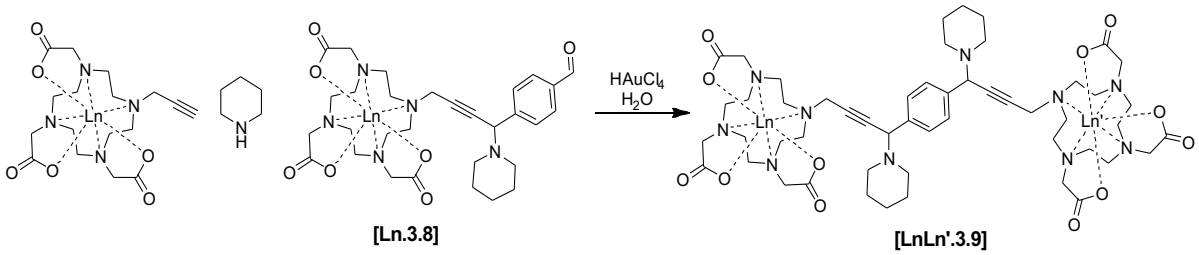

Scheme 3.9: Three component coupling using Ln.3.8 to form bimetallic lanthanide complexes LnLn'.3.9

To explore if the coupling shown in Scheme 3.9 was possible, Lu.p.DO3A was coupled with Lu.3.8. The diamagnetic ^{1}H NMR (Figure 3.10) shows the integrations now correspond to the presence of double the aliphatic protons compared to aromatic suggesting the second coupling has occurred. The DOSY NMR experiments also confirmed that all the protons in the coupling product LuLu'.3.9 diffuse with the same diffusion coefficient of around 4 x 10^{-8} cm^2s^{-1}. This is notably slower than the aldehyde complex Lu.3.8, which has diffusion coefficient of around 8 x 10^{-8} cm^2s^{-1}, suggesting that the addition of an additional macrocycle has slowed diffusion significantly.

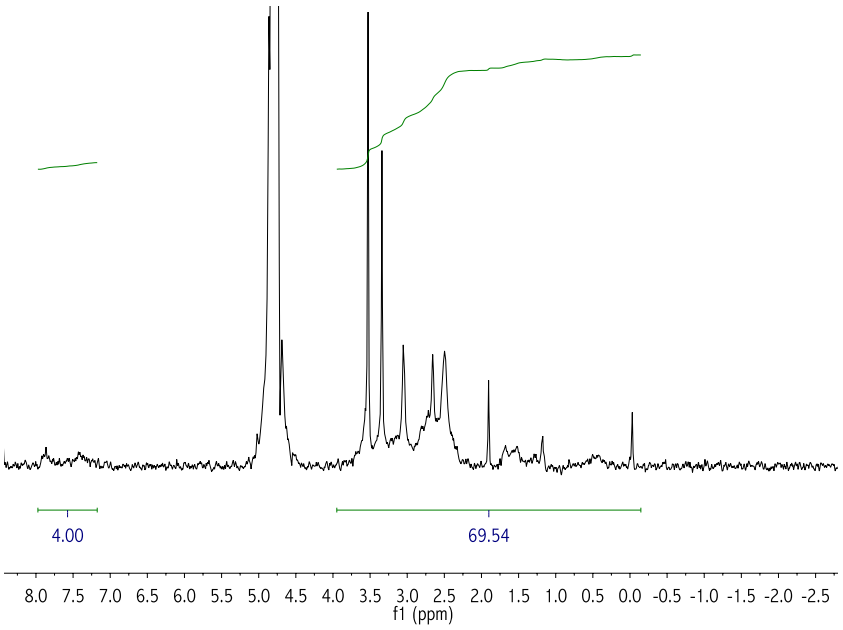

Figure 3.10: ^{1}H NMR of LuLu'.3.9 (298 K, D_2O, 400 MHz)

Following this result, Lu.3.8 was used to couple Eu.p.DO3A to form the complex LuEu.3.9, according to the procedure outlined in Scheme 3.9. Excitation of the LuEu.3.9 complex through the chromophore at 275 nm revealed europium centred emission as shown in Figure 3.11, this confirms the coupling has occurred, thereby allowing sensitised emission to the europium centre.

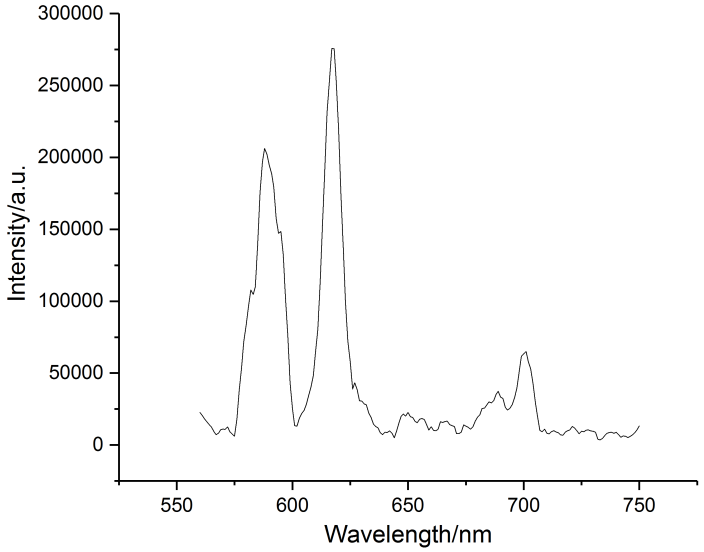

Figure 3.11: Observed emission spectrum of LuEu.3.9 in water λ_{ex} = 275 nm, slit width ex: 5 nm, em: 2 nm

Having established that two independent lanthanide centres could be coupled, the complex EuTb.3.9 (Figure 3.12) was synthesised by first synthesising the europium aldehyde complex (Eu.3.8) according to Scheme 3.8 and coupling this to Tb.p.DO3A, using the methodology described in Scheme 3.9.

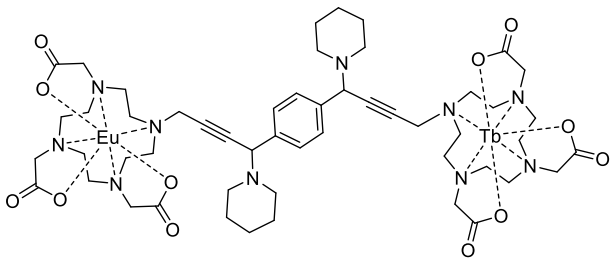

Figure 3.12: Structure of complex EuTb.3.9

From the ^{1}H NMR spectrum (Figure 3.13) it is clear that the dramatic increase in spectral width is due to the presence of terbium in the complex, indicating that the coupling was been successful. Peaks associated with both the europium and terbium bound ligand domains are observed in the spectrum.

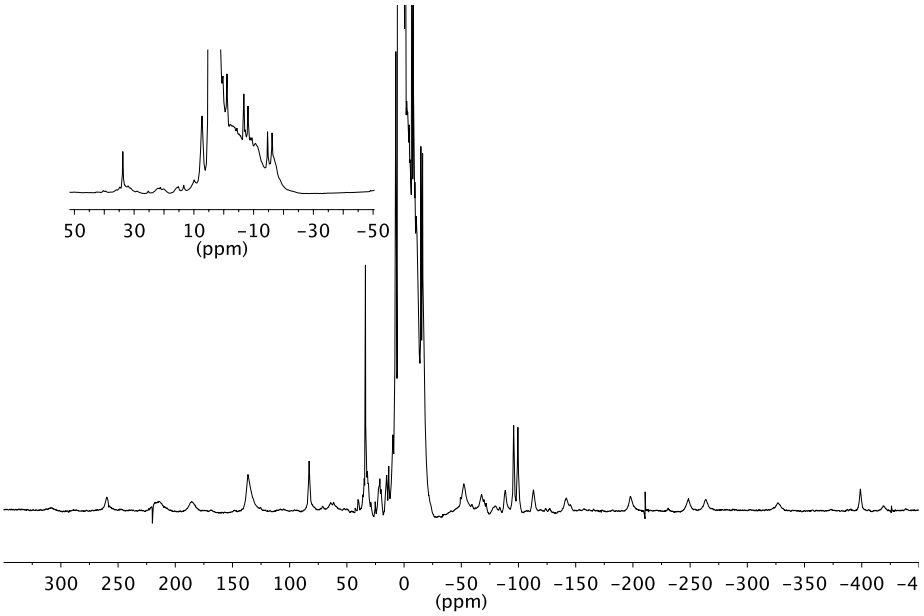

Figure 3.13: ^{1}H NMR of EuTb.3.9 (298 K, D_2O, 500 MHz)

3.3.2 Photophysical and anion binding

The complex EuTb.3.9 was chosen for in-depth photophysical study because it offers possibilities for exploring the energy transfer between the two lanthanide centres and using these to establish additional detail about guest binding. It is possible to investigate these processes using EuTb.3.9 because the configurations of each component's excited states are such that they are close enough in energy to be able to communicate (Figure 3.14). In the absence of a bridging ligand that favours energy transfer by Dexter exchange, energy transfer from terbium to europium would be expected to be limited by the space between the centres through a dominant Forster energy transfer pathway. There is a small but significant energy gap between the $^{5}D_4$ state of terbium (III) and the $^{5}D_1$ state of europium (III) which (when combined with the sharp absorption and emission

transitions associated with lanthanide ions) mitigates against effective through space energy transfer, even when surplus energy can be dissipated by phonon assistance.

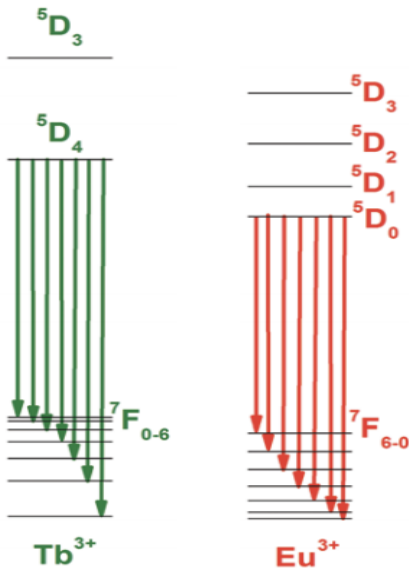

Figure 3.14: Schematic energy level diagram for Eu and Tb adapted from reference [18] N.B.: the $^5D_4$ state of Tb(III) has an energy of 20,500 cm^{-1}, while the $^5D_2$ state of Eu(III) has an energy of 21,500 cm^{-1} and the energy of $^5D_1$ is 19,030 cm^{-1}.

To see if this kind of energy transfer was possible in our system, the complex was excited at 488 nm: directly exciting the terbium $^7F_6$-$^5D_4$ transition where there is no possibility of europium excitation (the two europium (III) absorption bands either side of this wavelength occur at 465 nm and 525 nm). Therefore, any observed europium emission is solely due to energy transfer from the terbium.

Figure 3.15 shows that as well as a terbium only emission band (545 nm) there are bands with contributions from both centres (585 and 616 nm) and two small bands around 655 and 695 nm corresponding only to europium emission.

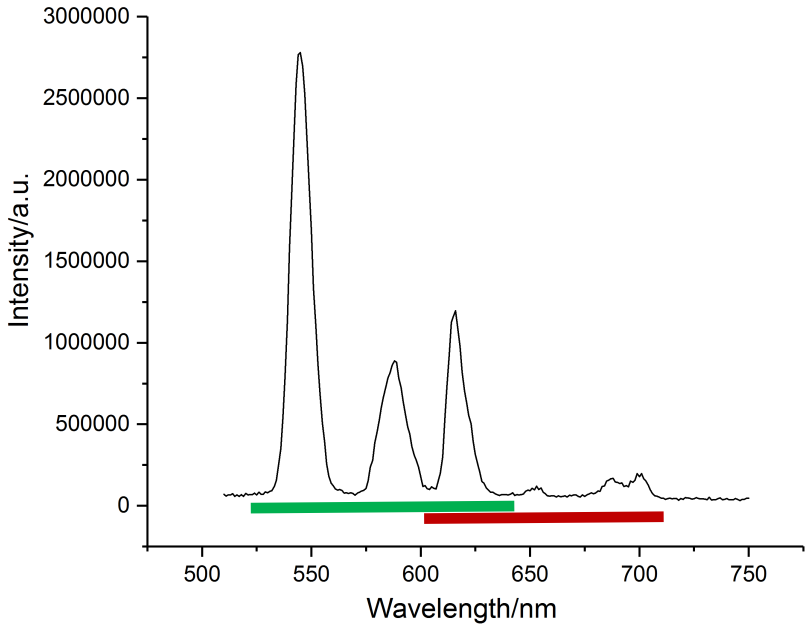

Figure 3.15: Observed emission spectrum of EuTb.3.9 in water λ_{ex} =488 nm, slit widths λex: 10 nm, λem: 14 nm

Figure 3.15 confirms that we can set up an energy pathway as depicted in Figure 3.16 where the direct excitation of terbium leads to direct energy transfer to the europium excited state, and result in europium centred emission as well as terbium centred emission.

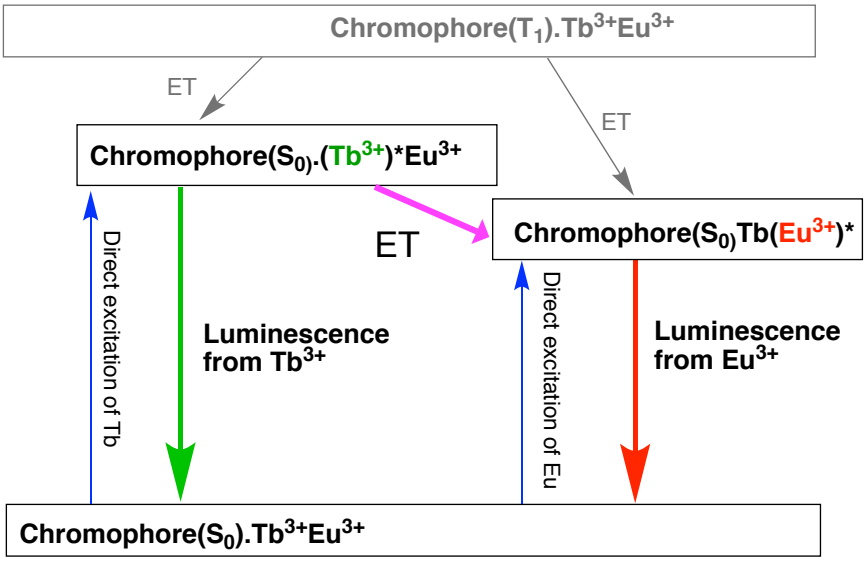

Figure 3.16: Schematic energy diagram for the energy transfer to europium from direct excitation of terbium

Having shown the possibility of phonon assisted through-space communication between lanthanide centres, we explored how introducing a bridging analyte anion would affect the system both in terms of binding and exploring any modulation of the energy pathways when compared to the unbound complex.

For this purpose, two dicarboxylic acids were chosen: 2,6-naphthalene dicarboxylic acid and biphenyl-4,4'-dicarboxylic acid shown in Figure 3.17. Both these dicarboxylates have the potential to act as bridging ligands between metal centres, and incorporate sensitising chromophores. Furthermore, their structures permit the possibility of through bond energy transfer by Dexter exchange, in the case of the naphthyl derivative, or superexchange, in the case of the biphenyl derivative.

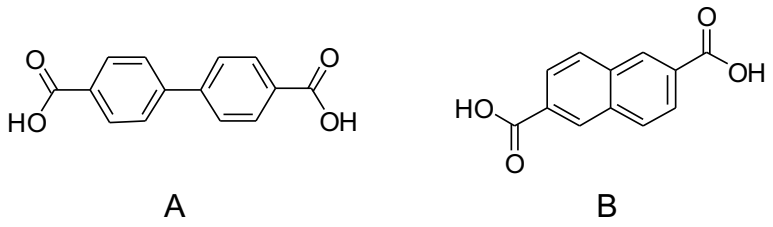

Figure 3.17: Biphenyl-4,4-dicarboxylic acid (A) and 2,6-naphthalene dicarboxylic acid (B)

The binding of the analytes was first examined by indirect excitation at $\lambda = 280$ nm which populates the chromophore triplet state and both terbium and europium excited states as shown above in Figure 3.16. The binding of EuTb.3.9 with 2,6-naphthalene dicarboxylic acid was studied as shown in Scheme 3.10.

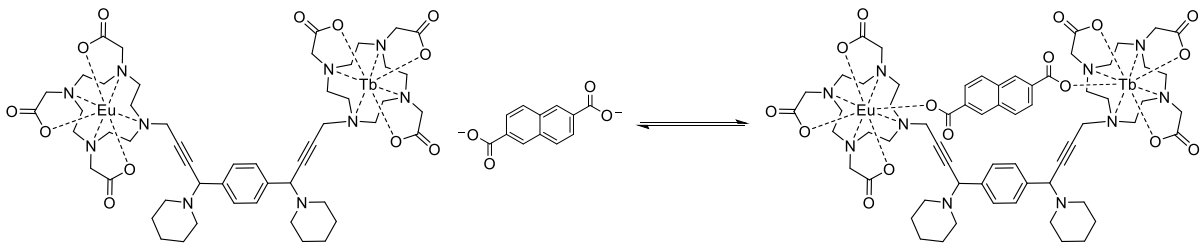

Scheme 3.10: Binding of 2,6-naphthalene dicarboxylic acid (B) to EuTb.3.9

The observed emission spectrum Figure 3.18, shows a significant increase in the lanthanide centred emission upon addition of 2,6-naphthalene dicarboxylic acid.

The increase in emission intensity can be partly rationalised by the binding of the carboxylic acid replacing bound solvent molecules that give rise to vibration quenching, as well as the addition of an extra chromophore.

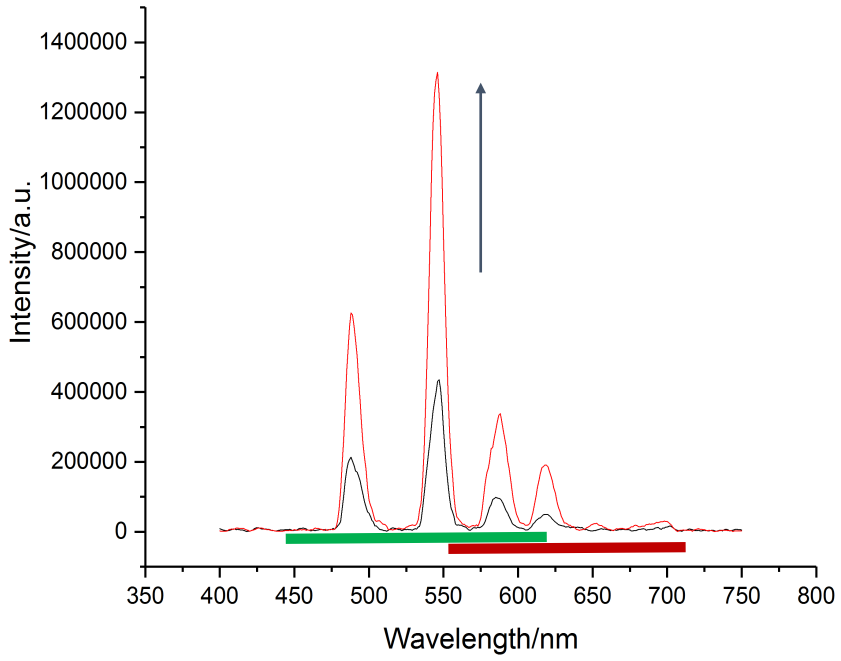

Figure 3.18: Changing emission spectrum of EuTb.3.9 in methanol with the addition of 2,6-naphthalene dicarboxylic acid (A) λ_{ex} =280 nm, slit widths λex: 5 nm, λem: 5 nm

Due to the low solubility of the 2,6-naphthalene dicarboxylic acid in water and methanol, a luminescence titration could not be performed. However, the relatively weak europium centred emission suggests that it is difficult to accommodate both lanthanide ions on opposite ends of the dicarboxylate anion in this case. This is likely to be a general effect, given that the quantum yields observed for terbium complexes tend to be much greater than those of europium analogues, owing to the longer observed luminescence lifetimes for terbium complexes and the similarity between radiative lifetimes of europium and terbium. The lifetimes in methanol and d_4-methanol were measured for the complex before and after addition of 2,6-naphthalene dicarboxylic acid, separately monitoring

emission from the terbium and europium centres, allowing for the calculation of the corresponding q values, as detailed in Table 3.2.

Table 3.2:Measured lifetime value for EuTb.3.9 and calculated q values before and after binding of 2,6-naphthalene dicarboxylic acid (B) for both lanthanide centres in methanol. λex= 280 nm and λem as stated.

	τ_{MeOH}/ms [a]	τ_{MeOD}/ms [a]	q
EuTb.3.9 λ_{em} 545 nm	1.79	2.27	0.9
EuTb.3.9 +B λ_{em} 545	1.25	0.96	-2[b]
EuTb.3.9 λ_{em} 690 nm	0.93	1.84	1
EuTb.3.9 +B λ_{em} 545	0.69	1.15	1.1

[a] *where the typical errors on measured values are around 10 %*

[b] *calculated value can be discounted as described in the text*

The calculated q values for the EuTb.3.9 complex indicate one solvent molecule for both the terbium and europium centres. With the addition of 2,6-naphthalene dicarboxylic acid the apparent q values does not change as a result of binding for the europium centre. This phenomenon is not unknown and has previously been reported for other bimetallic lanthanide systems.[19] The calculated q value for the terbium centre upon binding gives a negative value of q, this is due to the inability of the Horrocks equation to account for other energy transfer pathways if they are more effective than X-H oscillator quenching. In this case, where the observed lifetimes are essentially within error of one another, and energy transfer to the europium centre and back energy transfer to the chromophores triplet state are possible (Figure 3.19), the Horrocks equation fails to accurately describe q. However, while the calculated value of q may not be an accurate description, the measured lifetimes for both lanthanide centres in both protic and deuterated solvent

decreases upon binding. This indicates other quenching pathways have been introduced because of anion binding.

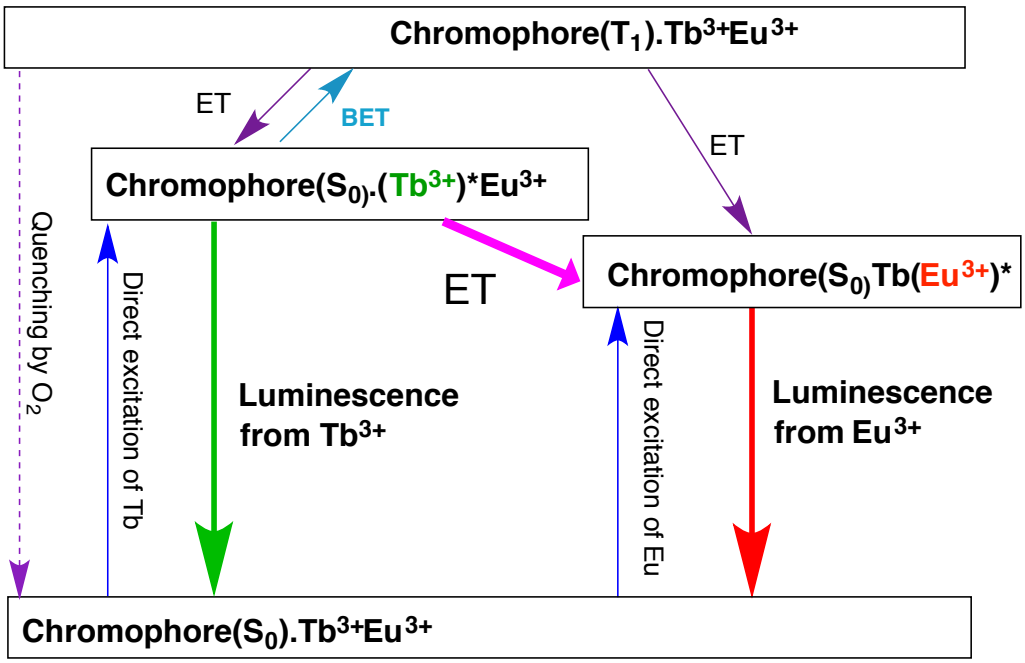

Figure 3.19: Energy diagram showing the processes that populate or depopulate lanthanide emissive states

To investigate if there was any back-energy transfer from the terbium excited state to the chromophore triplet state, the oxygen dependence of the terbium emission was explored. If there is fast depopulation of terbium's $^5D_4$ excited state though back-energy transfer to the chromophore T_1 can lead to quenched by oxygen, resulting in a decrease in emission intensity with increasing oxygen concentration as illustrated in Figure 3.19. Whereas, if this process is slow or not thermally accessible the emission intensity of terbium is independent of oxygen concentration.

Figure 3.20 shows the emission spectra of EuTb.3.9 while degassed and aerated. While there is a small decrease in terbium-centred emission intensity when aerated there is not a significant oxygen dependence. This suggests that any back-energy transfer processes are not a fast for this system.

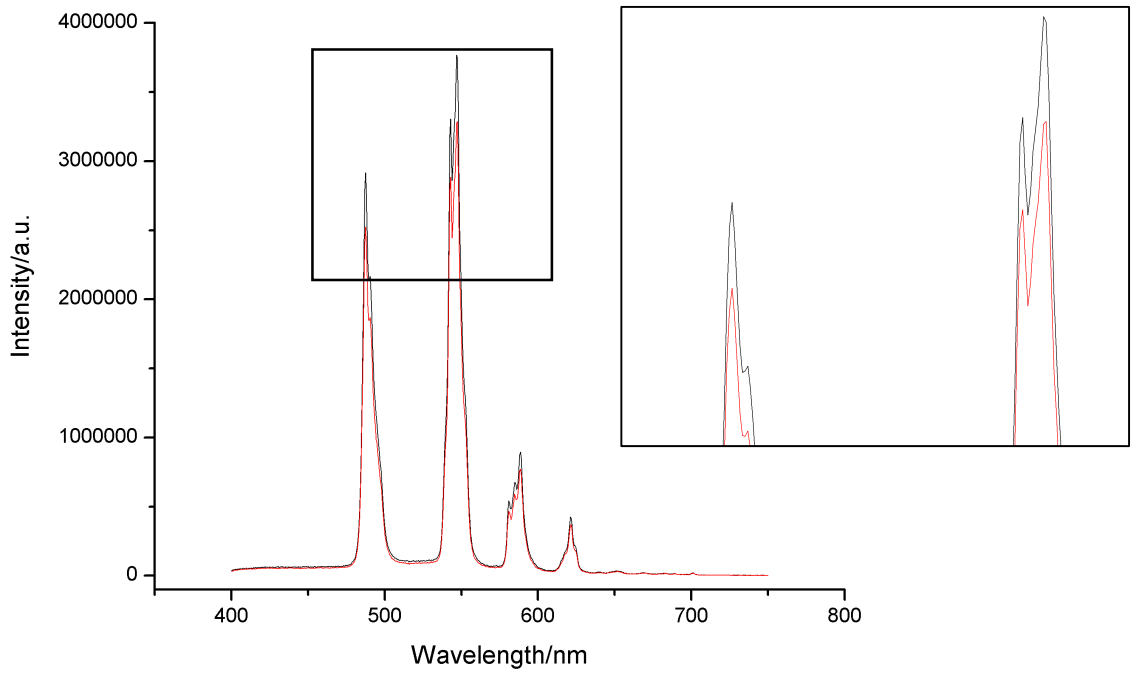

Figure 3.20:Emission of complex EuTb.3.9 when degassed (black) and aerated (red) λex =280 nm

While there is no oxygen dependence for the EuTb.3.9 complex, when in the presence of 2,6-naphthalenedicarboxyic acid there may be a change in the oxygen dependence as naphthalene chromophores have been known to have a significantly lower emission intensity in the presence of oxygen.[20] EuTb.3.9 in the presence of 2,6-naphthalenedicarboxyic acid was measured while degassed and aerated as shown in Figure 3.21.

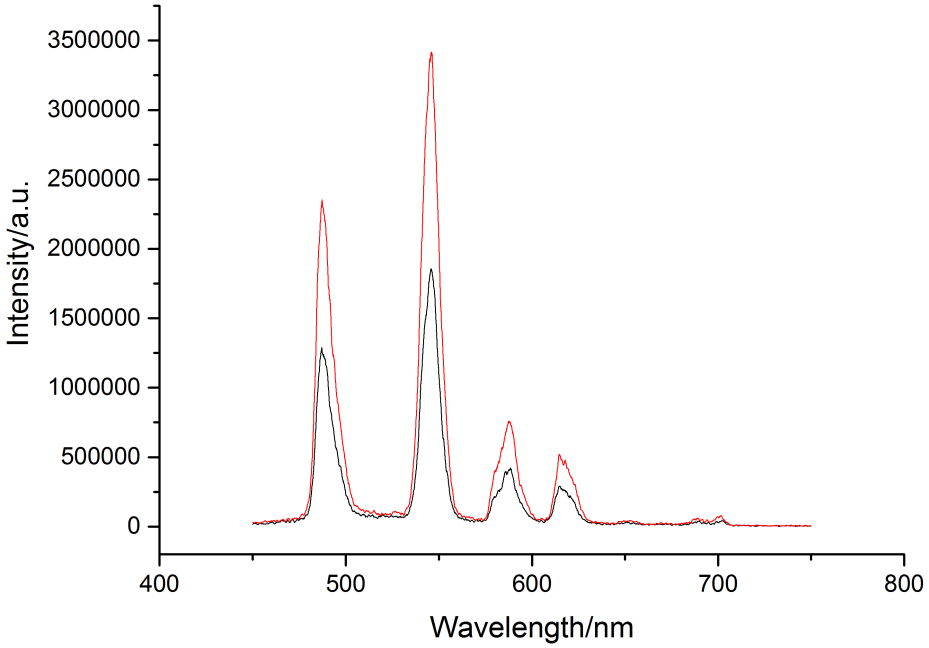

Figure 3.21: Emission of complex EuTb.3.9 + 2,6-naphthalene dicarboxylic acid (B) when degassed (black) and aerated (red) time gated λex 280 nm and time delay of 50 ms

This shows that rather than the emission being quenched by oxygen the emission intensity increases with increased oxygen concentration. It is proposed that, as for the complex alone, there is little back energy transfer and quenching due to oxygen and the increase in emission may be due to an enhanced rate of intersystem crossing in the presence of oxygen populating the triplet state resulting in an increased emission intensity. Intersystem crossing can be mediated by collisions between $^{3}O_2$ molecules and the S_1 state of the chromophore adding to the mediation of intersystem crossing by heavy atom effects. As such, collisional intersystem crossing will accelerate and enhance the generation of the triplet state T_1. Unlike the other literature examples the 2,6-naphthalenedicarboxylic acid is directly bound to the lanthanide centre and while the triplet state energy of 2,6-naphthalene dicarboxylic acid could not be measured, the results suggest the direct binding to the lanthanide centre has a significant effect on the oxygen dependant behaviour observed. It should be noted that collision with molecular oxygen will promote formation of triplet states from excited singlet states as well as

promoting the non-radiative decay of the triplet. Indeed, the rate of formation of the triplet could be described effectively by the sum of two terms as $k_{obs} = k_{isc} + k'[O_2]$, while the rate of oxygen mediated triplet state quenching will be described by $k_q[O_2]$. As such, if k' >> kq, an increase in oxygen concentration ought to enhance the lanthanide centred luminescence. The difficulty in measuring the triplet energy of the dicaboxylate lends credence to this hypothesis, since it may result from an inherently low triplet yield in the absence of oxygen. However, this must remain a hypothesis- at least until a definitive study can be carried out.

The study of interactions between EuTb.3.9 and biphenyl-4, 4-dicarboxylic acid, Scheme 3.11, was also performed.

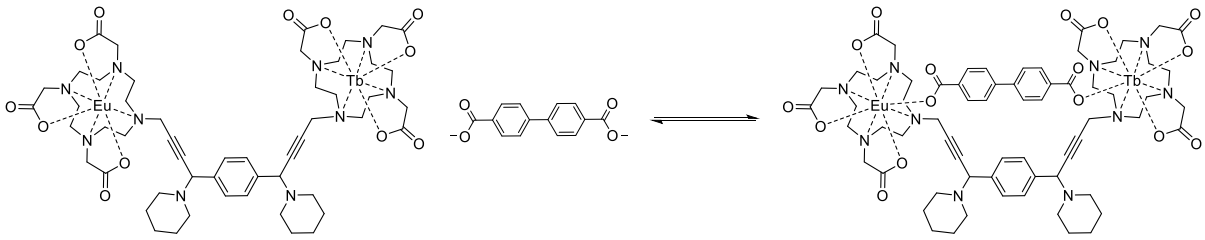

Scheme 3.11: Binding of biphenyl-4, 4-dicarboxylic acid (A) to EuTb.3.9

The observed emission spectra Figure 3.22 show that there is a relatively larger increase in the lanthanide centred emission upon addition of biphenyl-4,4-dicarboxylic acid than observed for the 2,6-naphthalene dicarboxylic acid. The larger increase in emission intensity is hypothesised to be due to a better size match between the analyte and the cavity size.

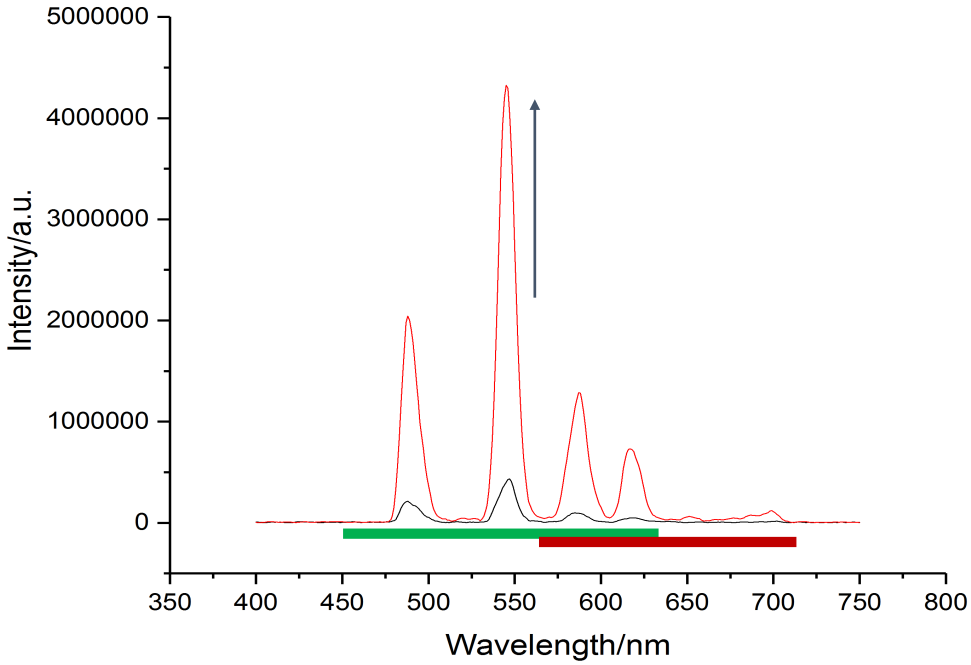

Figure 3.22: Changing emission spectrum of EuTb.3.9 with addition of biphenyl-4, 4-dicarboxylic acid (A) in methanol λ_{ex} =280 nm, slit widths λex: 5 nm, λem: 5 nm

Due to the low solubility of the biphenyl-4,4-dicarboxylic acid in water and methanol a luminescence titration could not be performed. The lifetimes in methanol and d_4-methanol were measured for the complex before and after addition of biphenyl-4,4-dicarboxylic acid, monitoring the separate emissions for the terbium and europium centres, allowing the calculation of the corresponding q values (Table 3.3).

Table 3.3: Measured lifetime values for EuTb.3.9 and calculated q values before and after binding of biphenyl-4,4-dicarboxylic acid (A) for both lanthanide centres in methanol. λex= 280 nm and λem as stated.

	τ_{MeOH}/ms [a]	τ_{MeOD}/ms [a]	q
EuTb.3.9 em 545 nm	1.79	2.27	0.9
EuTb.3.9 +A em 545	0.99	1.08	0.5
EuTb.3.9 em 690 nm	0.69	1.15	1
EuTb.3.9 +A em 545	0.73	1.24	1

[a] *where the typical errors on measured values are around 10 %*

As for the binding of 2,6-naphthalene dicarboxylic acid, the calculated q values for the europium centre do not change upon binding. While the q value for the terbium centre decreases upon binding it does not give a negative value as calculated for binding with 2,6-naphthalene dicarboxylic acid, the reduced luminescence terbium-centred lifetimes are clearly indicative of an additional quenching pathway for the terbium centred excited state. Furthermore, the measured lifetimes in MeOH and MeOD are within error of one another, indicating that q value calculations have very limited meaning for terbium centres in these systems.

Having demonstrated the binding of these two analytes, their effect on energy transfer processes was explored by directly exciting the terbium centre at 488 nm and observing the changes in the lanthanide centred emission. Figure 3.23 shows emission spectra before and after the addition the biphenyl-4, 4-dicarboxylic acid. There is a clear increase in the emission intensity of both lanthanide centre due to the binding of the biphenyl-4,4'-dicarboxylic acid, the increase of the europium signal shows that the bridging analyte is modulating the energy transfer mechanism, making the process more efficient than in the unbound complex EuTb.3.9. If we consider that the quenching of terbium by solvent molecules is more effective than quenching of europium by solvent[*], the relative enhancement of the europium signal over the terbium signal cannot be attributed to solvent displacement effects, suggesting that the signal enhancement is the result of the through bond [†]of the guest molecule. Notably, the ratio of the europium $^5D_0$-$^7F_2$ transition has changed significantly upon binding to the biphenyl-4,4'-dicarboxylic acid, signifying that there has been a change in the local coordination environment upon binding.

[*]The A factors in the modified Horrocks equation reflects the efficiency of quenching by OH oscillators. Where: A_{Tb}=5 ms and A_{Eu}=1.2 ms.

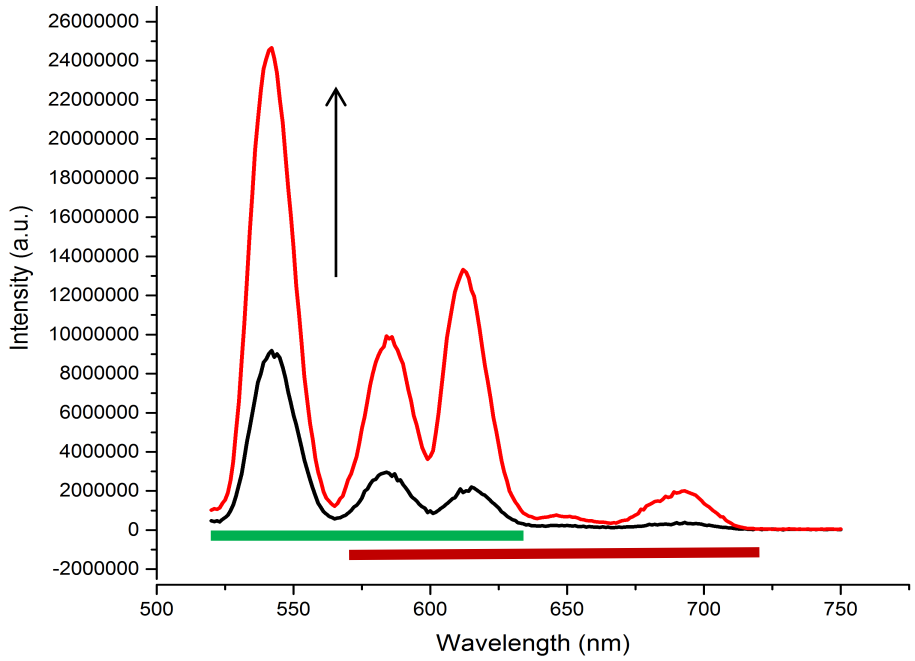

Figure 3.23: Observed emission spectrum of EuTb.3.9 before and after addition of biphenyl-4, 4-dicarboxylic acid (A) in methanol λ_{ex} =488 nm, slit widths ex: 14 nm, em: 14 nm and time delay of 50 ms

The same study was performed using 2,6-naphthalene dicarboxylic acid, Figure 3.24 shows the emission spectra before and after binding.

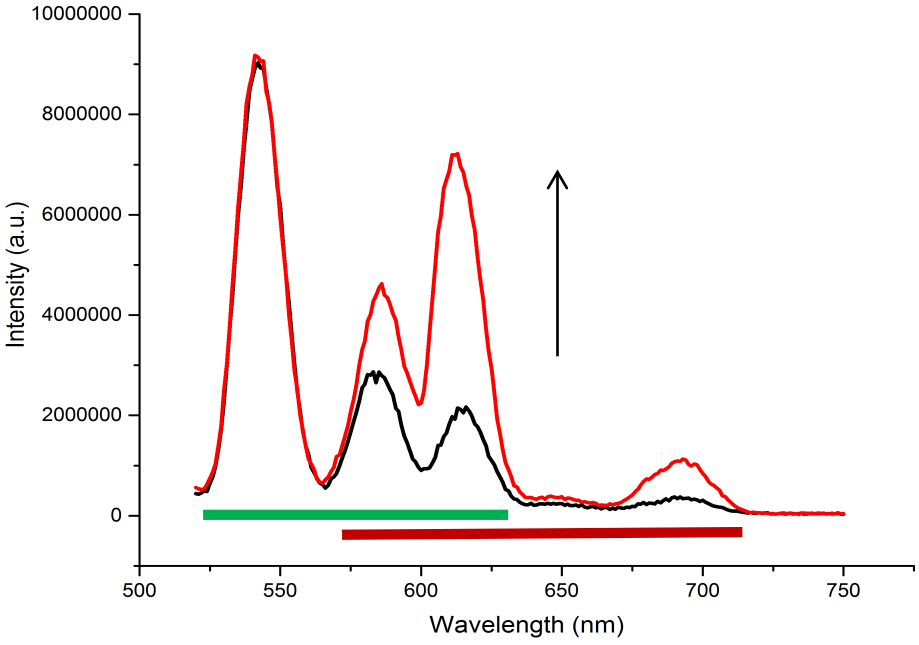

Figure 3.24 :Observed emission spectrum of EuTb.3.9 before and after addition of 2,6-naphthalene dicarboxylic acid (B) in methanol. λex =488 n slit widths ex: 14 nm, λem: 14 nm and time delay of 50 ms

When compared to biphenyl-4,4-dicarboxylic acid test there are some interesting similarities and differences between the results. Figure 3.24 shows the same change in the $^5D_0$-$^7F_2$ transition, suggesting the same local coordination environment is present after binding in both systems. The binding of 2,6-naphthalene dicarboxylic acid also results in an increase in the europium centred emission, but interestingly, the terbium centred emission intensity is independent of the analyte added. This may be due to energy transfer to the europium becoming more efficient and the terbium excited state has become depopulated to the extent that no change in emission is observed. It is also possible for the terbium excited state to be depopulated through back energy transfer to the chromophore triplet state which in turn can populate the europium excited state as shown in Figure 3.19.

Having a system with two lanthanide centres where the signal of one remains constant means that for this analyte EuTb.3.9 can be used as a ratiometric probe. Ratiometic probes have been increasingly explored[20–22] to exploit a signal that is independent of the analyte concentration as a reference to quantify the concentration of probe and analyte by comparing the ratios of the relative intensities of the two emission bands, in this case Tb and Eu.

The difference in the way the two analytes modulate the energy transfer pathways can be rationalised by examining their structures. The 2,6-naphthalene dicarboxylic acid shows the most efficient energy transfer to the europium centre, this is due to the conjugated nature of the bridging analyte, which allows for a very efficient through-bond mechanism of energy transfer. Thus, although the biphenyl-4,4-dicarboxylic acid has a better size match for the cavity, the broken conjugation results in a through-space mechanism for energy transfer, which while more efficient than the unbridged complex is not the most efficient mechanism.

3.4 Conclusion

In this chapter, we have demonstrated a possible new synthetic method to incorporate lanthanide complexes into novel architectures via three component gold catalysed couplings. These methods have also been applied to the synthesis of bimacrocyclic complexes where the two lanthanide centres can be incorporated to give homo- or heterometallic complexes.

While these syntheses are possible they do not currently provide a reliable method for use with lanthanide complexes. Although there is some uncertainty in the final structures we have shown that the structures proposed in this chapter are they most likely products of the coupling reactions.

We have also shown the interesting anion binding properties both with monomacrocyclic product which show very strong binding to acridone-N-acetic acid, and bimacrocyclic which while the strength of binding could not be quantified we have used to demonstrate energy transfer processes both with the complex alone and they effect of introducing bridging anions which can affect the energy transfer processes.

This work forms the basis of developing gold catalysed three component couplings to be able to reliably synthesise a wide range of novel lanthanide architectures in the future.

3.5 References

1. G. J. Stasiuk and M. P. Lowe, *Dalton Trans.*, 2009, 9725–7.
2. J. M. Baskin, J. A. Prescher, S. T. Laughlin, N. J. Agard, P. V Chang, I. A. Miller, A. Lo, J. A. Codelli, and C. R. Bertozzi, *Proc. Natl. Acad. Sci. U. S. A.*, 2007, **104**, 16793–7.
3. I. Stengel, A. Mishra, N. Pootrakulchote, S.-J. Moon, S. M. Zakeeruddin, M. Grätzel, and P. Bäuerle, *J. Mater. Chem.*, 2011, **21**, 3726.
4. G. Piersanti, F. Remi, V. Fusi, M. Formica, L. Giorgi, and G. Zappia, *Org. Lett.*, 2009, **11**, 417–420.
5. M. Main, J. S. Snaith, M. M. Meloni, M. Jauregui, D. Sykes, S. Faulkner, A. M. Kenwright, E. Scales, R. Kauppinen, A. M. Kenwright, and S. Faulkner, *Chem. Commun.*, 2008, **39**, 5212.
6. T. J. Sørensen, M. Tropiano, O. A. Blackburn, J. A. Tilney, A. M. Kenwright, and S. Faulkner, *Chem. Commun.*, 2013, **49**, 783–785.
7. V. A. Peshkov, O. P. Pereshivko, and E. V Van der Eycken, *Chem. Soc. Rev.*, 2012, **41**, 3790–807.
8. C. Wei and C.-J. Li, *J. Am. Chem. Soc.*, 2003, **125**, 9584–5.
9. W. Fan, W. Yuan, and S. Ma, *Nat. Commun.*, 2014, **5**, 3884.
10. G. Abbiati and E. Rossi, *Beilstein J. Org. Chem.*, 2014, **10**, 481–513.
11. G. A. Price, A. K. Brisdon, K. R. Flower, R. G. Pritchard, and P. Quayle, *Tetrahedron Lett.*, 2014, **55**, 151–154.
12. K. K.-Y. Kung, G.-L. Li, L. Zou, H.-C. Chong, Y.-C. Leung, K.-H. Wong, V. K.-Y. Lo, C.-M. Che, and M.-K. Wong, *Org. Biomol. Chem.*, 2012, **10**, 925–30.
13. D. E. Prasuhn, Jr., R. M. Yeh, A. Obenaus, M. Manchester, M. G. Finn, V. Ose, P. Pumpens, V. Ose, I. Gusars, and P. Pumpens, *Chem. Commun.*, 2007, **249**, 1269–1271.
14. R. F. H. Viguier and A. N. Hulme, *J. Am. Chem. Soc.*, 2006, **128**, 11370–1.
15. S. Aime, M. Botta, and G. Ermondi, *Inorg. Chem.*, 1992, **31**, 4291–4299.
16. L. S. Natrajan, A. J. L. Villaraza, A. M. Kenwright, S. Faulkner, D. Parker, A. S. de Sousa, J. A. G. Williams, E. Scales, R. Kauppinen, A. M. Kenwright, and S. Faulkner, *Chem. Commun.*, 2009, **36**, 6020.
17. P. Kuzmič, *Anal. Biochem.*, 1996, **237**, 260–273.
18. Z. Xia, Q. Wei, Q. Yang, C. Qiao, S. Chen, G. Xie, G. Zhang, C. Zhou, S. Gao, C. H. Huang, C. H. Hung, and K. L. Lu, *CrystEngComm*, 2013, **15**, 86–99.
19. T. J. Sørensen, L. R. Hill, J. A. Tilney, O. A. Blackburn, M. W. Jones, M. Tropiano, and S. Faulkner, *Eur. J. Inorg. Chem.*, 2014, **2014**, 2520–2528.
20. T. J. Sørensen, A. M. Kenwright, and S. Faulkner, *Chem. Sci.*, 2015, 6, 2054-2059.
21. J.-L. Tang, C.-Y. Li, Y.-F. Li, and C.-X. Zou, *Chem. Commun. (Camb).*, 2014, **50**, 15411–15414.
22. D. G. Smith, B. K. McMahon, R. Pal, D. Parker, J. B. Mitchell, D. Parker, R. D. Peacock, J. J. B. Perry, S. Aime, and M. Botta, *Chem. Commun.*, 2012, **48**, 8520.

4 Rigid DO3AM derivatives

4.1 Introduction

DO3AM and its derivatives have been widely reported for a number of applications, such as in MRI contrast agents and in sensing (e.g. pH and pO_2 sensors).[1–3] The use of pendant amide arms offers several advantages over their DO3A analogues; in particular the amide arms offer a wide scope for modification as well as the ability to add functionality through the unsubstituted nitrogen position on the cyclen ring. The reduced charge on the DO3AM based amide arms also means there is opportunity to explore the effect of changing the localisation of charge in the complexes.

Fluoride sensing is of interest due to the potential military applications in sensing chemical warfare agents such as sarin and sensing of fluoride levels in water. The binding of fluoride to DTMA complexes and some of its derivatives have been explored by Blackburn *et al*., who observed changes in the luminescence and NMR spectra as a consequence of fluoride binding modulating the magnetic anisotropy at the lanthanide.[4–6]

In this chapter, I will show the multi-step synthesis of rigid chiral triamides with pendant arms derived from N-acetylaspartate. I will explore how the changes in steric bulk and introduction of water solubility between two triamide DO3AM analogues can affect their behaviour with regards to fluoride binding, and compare these triamides to an analogous DO3A complex. In addition to exploring the nature of fluoride binding, I will investigate the use of these complexes for their unprecedented use as potential catalysts in the fluorination of α-halocarboxylic acids.

4.2 Synthesis and characterisation

To synthesise chiral triamides, a multi-step synthetic approach was used. Established protecting group chemistry was employed to selectively protect one position as depicted in Scheme 4.1.[1]

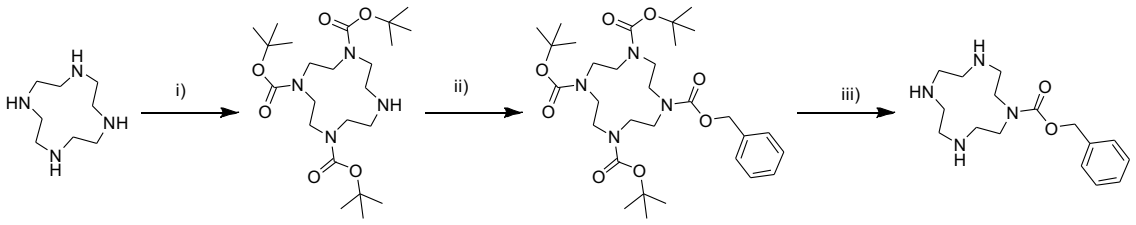

i) $[(CH_3)_3COCO]_2O$, Et_3N ii) $ClCO_2CH_2C_6H_5$ iii) HCl

Scheme 4.1:Synthesis of 4.3

Compound 4.3 was then used to synthesise the final triamide complexes, as shown in Scheme 4.2.

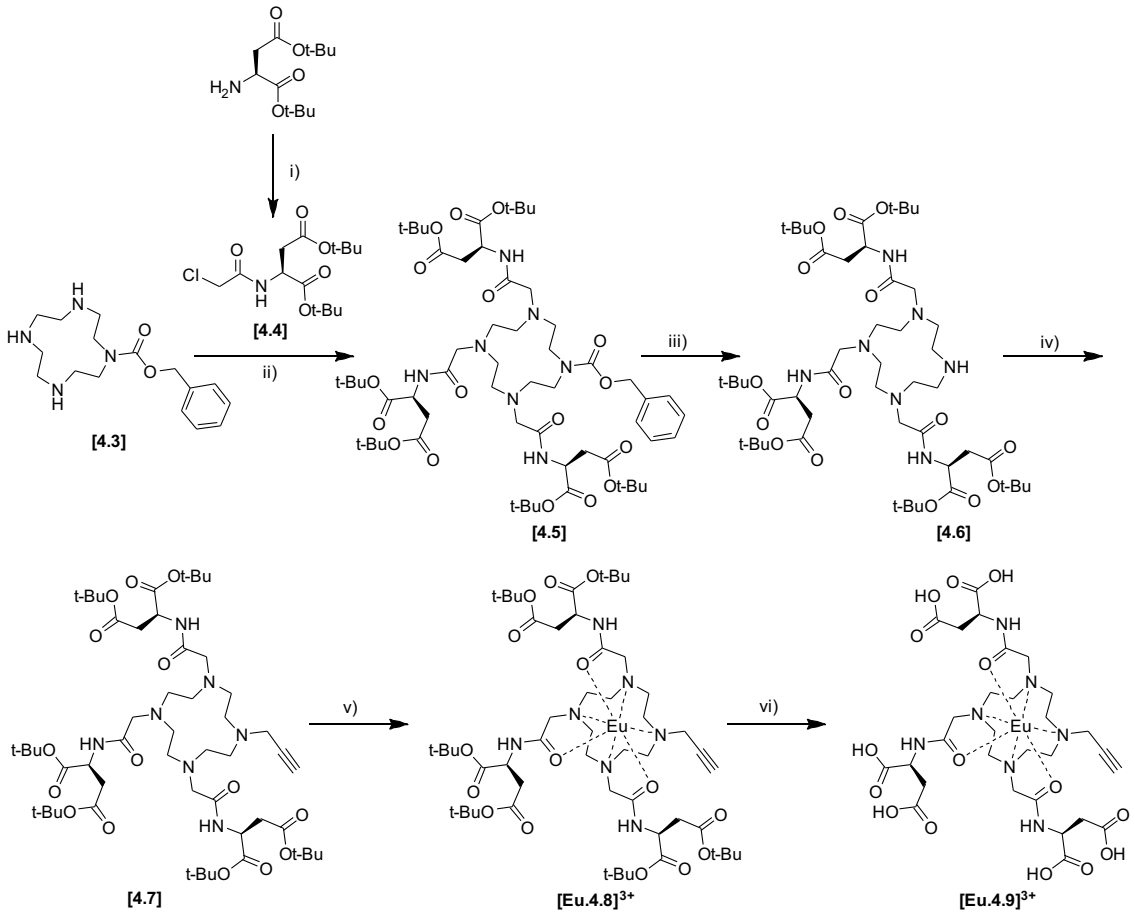

i) $ClCOCH_2Cl$, Et_3N ii) K_2CO_3, **[4.4]** iii) 10 % Pd/C, H_2 vi) $CHCCH_2Br$, K_2CO_3 v) $Ln(OTf)_3$ vi) TFA

Scheme 4.2:Multi-step synthesis of Eu.4.8 and Eu.4.9

This synthetic route allows for variation of the complexes to be easily accessed - where the final ligand position can be reacted to give a pendant propargyl arm. The propargyl derivative Eu.4.8 can also be deprotected to give the hexa-acid analogue: this allows for exploration of the effects of the changing charge, steric bulk and water solubility.

The triamides Eu.4.8 and Eu.4.9 were analysed by mass spectrometry, which showed complex ions with masses 2 amu less than the calculated values. This can be attributed to deprotonation of two of the pendant arms which results in an overall +1 charge for the complexes, as shown in Figure 4.1.

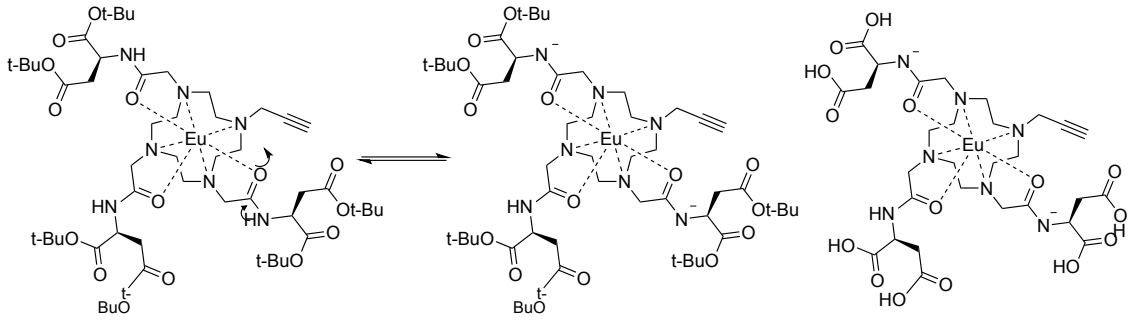

Figure 4.1:Deprotonation of complexes Eu4.8 and Eu.4.9

The chirality of the complexes was determined by polarimetry measurements and the values calculated according to Equation 4.1, where [α] is the specific optical rotation, α_{obs} is the observed optical rotation, *c* is the concentration in gml^{-1} and *l* is the path length in dm.[7]

$$[\alpha]_D^{25} = \frac{\alpha_{obs}}{c\ x\ l}$$

Equation 4.1: Calculation for the specific optical rotation

These measurements gave a value of -0.4 at two different concentrations. This value, while small, is suggestive of the presence of the L isomer, which is consistent with the enantiomerically pure L isomer starting material, N-acetylaspartate amide.

4.3 Fluoride binding

4.3.1 NMR studies

To study the effects of fluoride binding the complex Eu.4.8 was first studied by ^{1}H NMR. Figure 4.2 shows the dramatic change upon addition of fluoride (using TBAF.3H_2O as fluoride source).

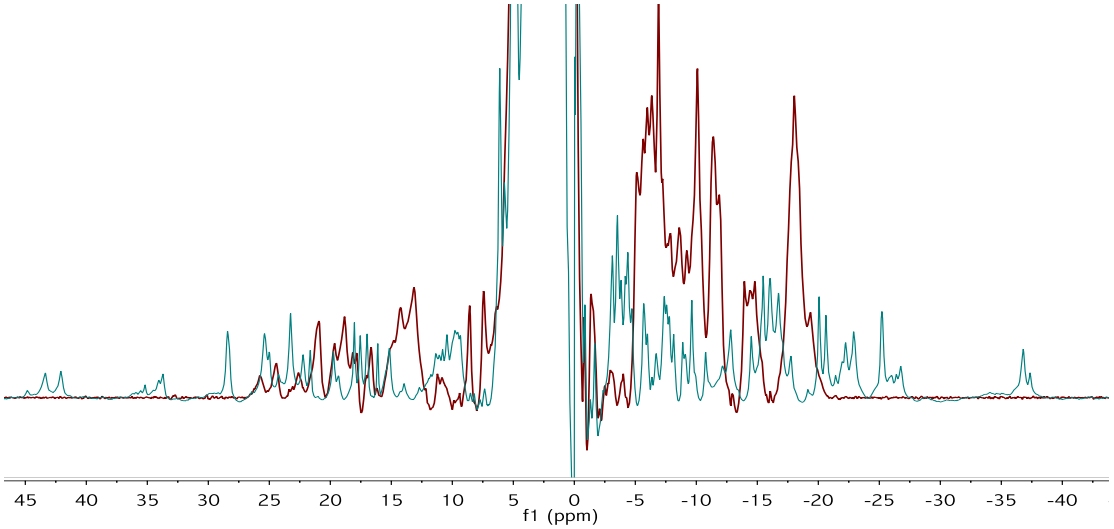

Figure 4.2: Comparison of ^{1}H NMRs for Eu.4.8 before (red) and after fluoride binding (blue) (298 K, d_4-methanol, 400 MHz)

The increased spectral width is indicative of a change to the crystal field. The corresponding ^{19}F NMR was explored and showed four distinct peaks - the shift of these peaks is indicative of fluoride bound to a lanthanide centre[8,9] shown in Figure 4.3.

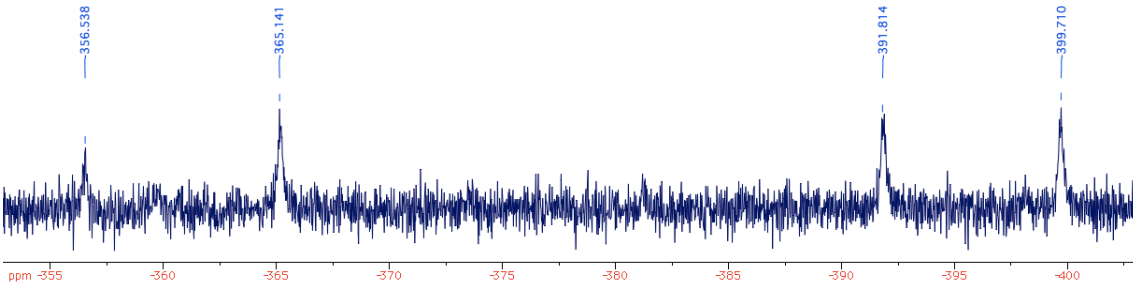

Figure 4.3:^{19}F NMR for Eu.4.8 in the presence of fluoride (298 K, d_4-methanol, 500 MHz)

It is proposed that the appearance of four fluoride bound peaks is due two bound fluorides: one in an equatorial position and one in the axial position, where two peaks are observed for both SAP and TSAP isomers of the complex.

To explore the proposed binding of multiple fluoride species a ^{1}H NMR study was performed. The results are shown in Figure 4.4.

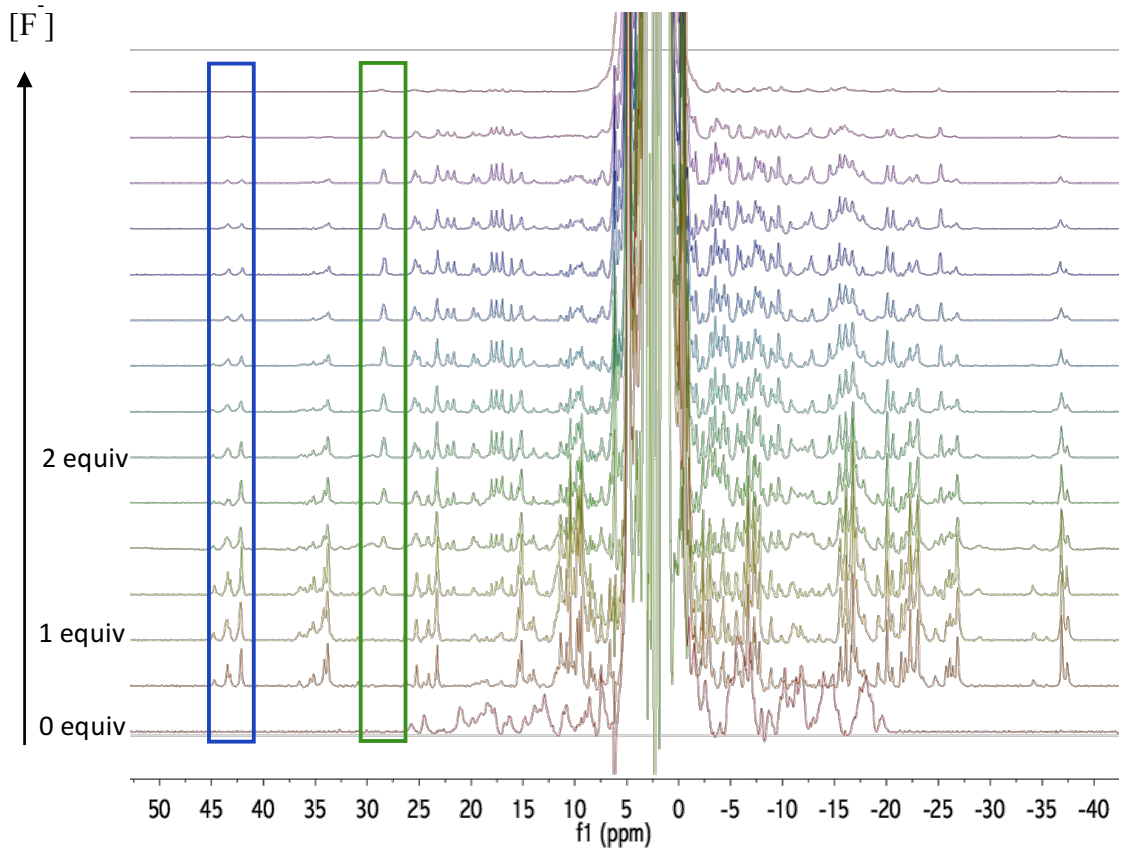

Figure 4.4:^{1}H NMR titration for Eu.4.8 with increasing TBAF.3H_2O highlighting changes in the spectra and where the spectra corresponding to 0,1 and 2 equivalents of added fluoride are indicated (298 K, d_4-methanol, 400 MHz)

This study shows an immediate initial increase in spectral width upon addition of fluoride. As the fluoride concentration is increased it was observed that the peaks at higher shift decreased (Figure 4.4 blue box) in intensity and peaks at a lower shift started to appear and grow in intensity (Figure 4.4 green box) until the solubility limit was reached.

This suggests that we are observing two distinct binding events. There are two possible modes of binding for Eu.4.8: equatorial (effectively in the plane of the pendant arm carbonyl donor atoms) and axial.

The Bleaney equation, (Equation 4.2), describes the pseudocontact shift contribution to the lanthanide induced shift, where the C_J term is a constant containing magnetic susceptibility factors.

$$\Delta_{pc} = \frac{2\mu_B{}^2 C_J}{60k^2T^2}\left(\frac{\langle r^2\rangle B_2^0(3cos^2\theta - 1) + \langle r^2\rangle B_2^2(sin^2\theta cos2\varphi)}{r^3}\right)$$

Equation 4.2: Simplified Bleaney equation for calculating the pseudocontact shift

The possible binding modes of fluoride ions are illustrated pictorially in Figure 4.5. Although europium has a significant contact shift contribution, an equatorial bound fluoride would be expected to increase the magnetic anisotropy of the complex, thereby increasing the observed spectral width. It is therefore reasonable that this is the first binding event observed in Figure 4.4. For an axially bound fluoride we would expect a decrease magnetic anisotropy resulting in a narrower spectral width, which for our system can be attributed to the growth of peaks highlighted in green in Figure 4.4. While the binding of an axial fluoride results in a smaller spectral width than for the equatorially bound species, the spectral width for the di-fluoride species is still greater than for the unbound complex.

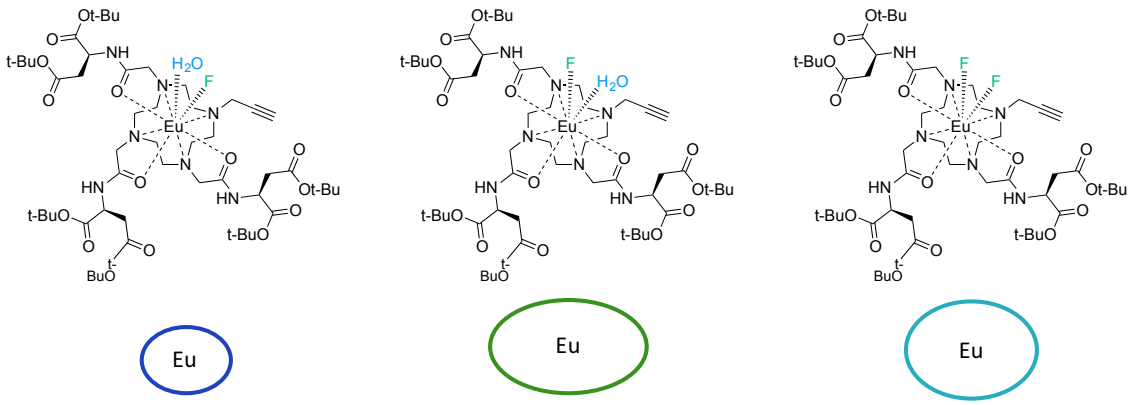

Figure 4.5:Fluoride binding to Eu.4.8 with schematic representation on the resulting magnetic anisotropy

To explore whether the hexa-acid analogue Eu.4.9 displayed similar behaviour, the complex was studied in the presence and absence of fluoride by ^{1}H NMR, as shown in Figure 4.6.

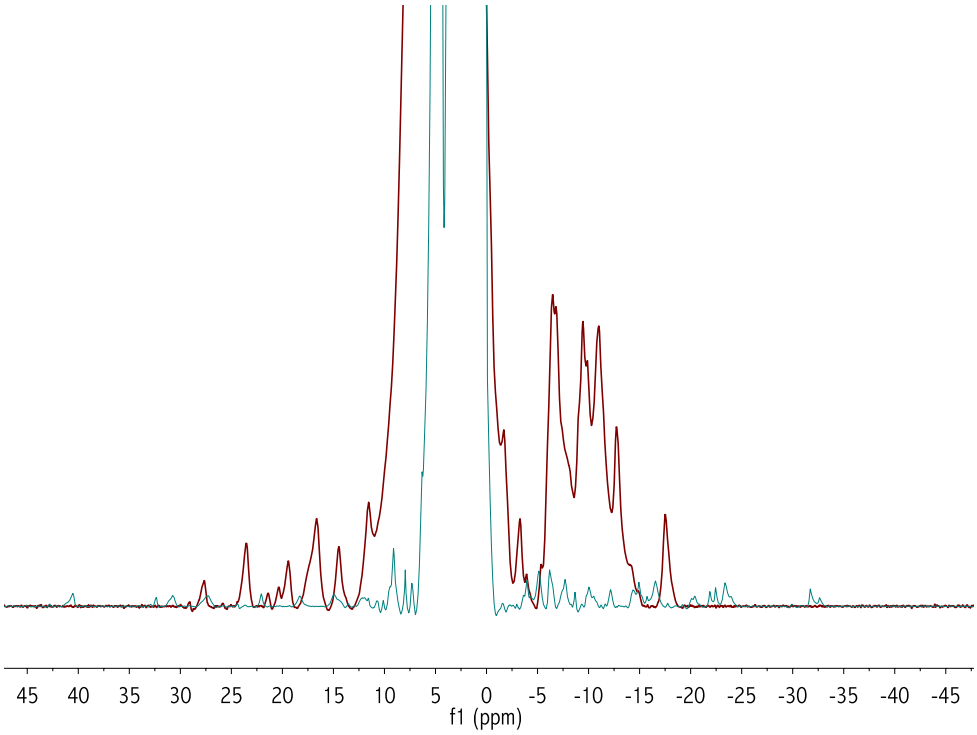

Figure 4.6: Comparison of ^{1}H NMRs for Eu.4.9 before (red) and after fluoride binding (blue) (298 K, D_2O, 400 MHz)

As for the complex Eu.4.8, complex Eu.4.9 also shows a large increase in the overall spectral width of the ^{1}H NMR as a consequence of fluoride binding, indicative of a change in the magnetic anisotropy of the complex due to binding. The ^{19}F NMR after fluoride addition (Figure 4.7) however, differs from that of complex Eu.4.8 by showing only a single signal, corresponding to a fluoride bound to the complex.

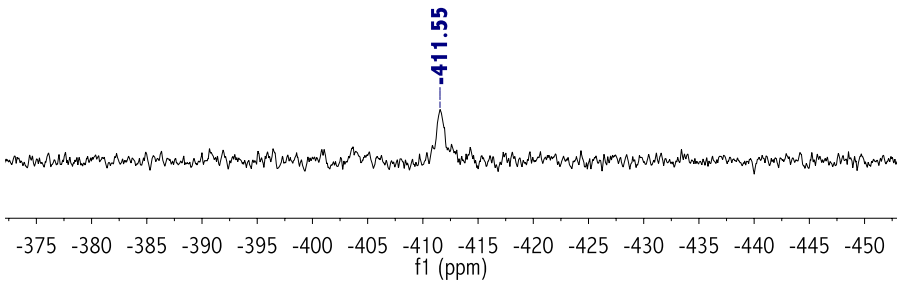

Figure 4.7: ^{19}F NMR for Eu.4.9 in the presence of fluoride (298 K, D_2O, 500 MHz)

Unlike complex Eu.4.8, the ^{19}F NMR of Eu.4.9 does not show peaks corresponding to two bound fluorides for the SAP and TSAP isomers. This could be interpreted as meaning that there is only one fluoride binding event for this complex. Due to the structure of Eu.4.9, we also have to consider the possibility of self-assembly, where the carboxylic acids on the N-acetylaspartate pendant arms can bind to other nearby lanthanide centres, creating restricted rotation and taking up a binding site on the lanthanide centre.

Also, due to its structure, there is the possibility of Eu.4.9 displaying pH dependency. The ^{1}H NMR was measured at pH 8 and pH 12, as shown in Figure 4.8.

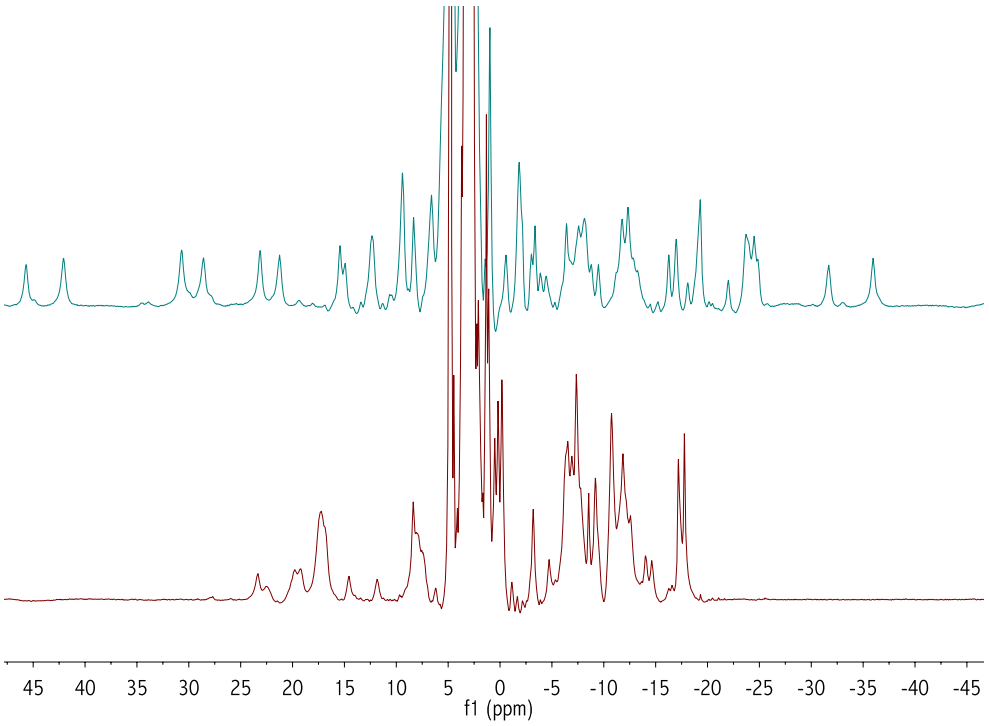

Figure 4.8: Comparison of ^1H NMRs for Eu.4.9 at pH 8 (red) and pH 12 (blue) (298 K, D_2O, 400 MHz)

At basic pH there is a dramatic increase in the spectral width, comparable to that seen with fluoride binding. It is likely that this change is not simply due the deprotonation of the N-acetylaspartate pendant carboxylic acids (pKa ≈ 4) but is suggestive of anion binding, which may be the result of hydroxide binding from bound water being deprotonated at high pH. It is also possible that a the aggregation previously proposed can lead to a carboxylate being displaced by hydroxide breaking the aggregates and leading to a change in spectral width and an increase in the number of peaks when the rotation is no longer restricted by the large scale self-assembly.

As a comparison to the two triamide complexes Eu.4.8 and Eu.4.9, Eu.p.DO3A (Figure 4.9) was also studied in order to explore if similar fluoride binding behaviour is observed.

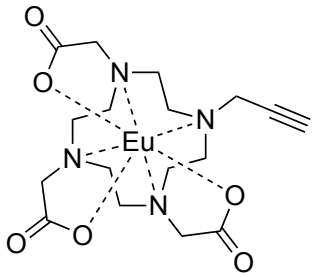

[Eu.p.DO3A]

Figure 4.9: Structure of Eu.p.DO3A

The increased spectral width upon binding is also observed for Eu.p.DO3A, as shown in Figure 4.10.

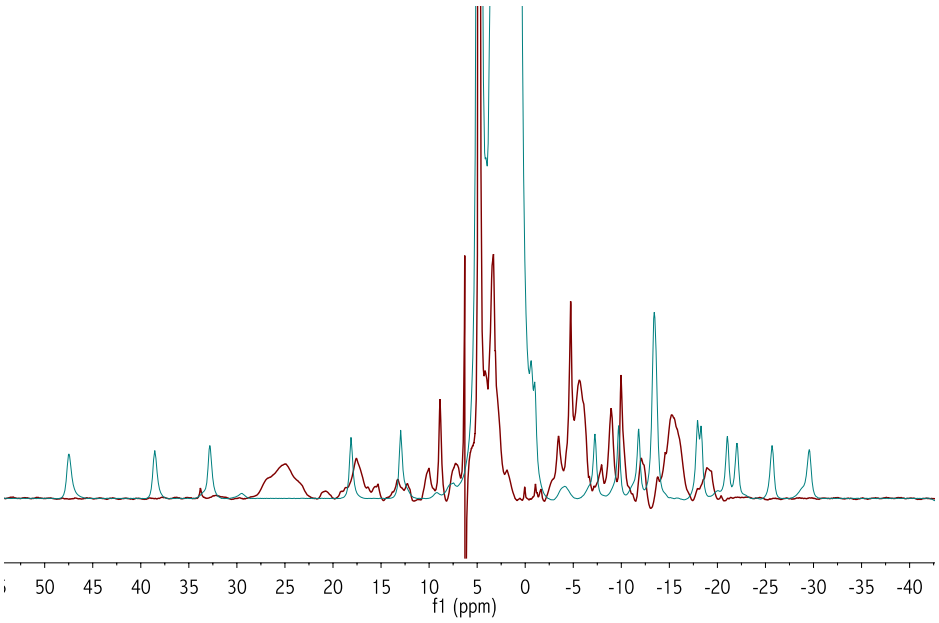

Figure 4.10: Comparison of ^{1}H NMRs for Eu.p.DO3A before (red) and after fluoride binding (blue) (298 K, D_2O, 400 MHz)

The ^{19}F NMR of the fluoride bound Eu.p.DO3A complex shows multiple peaks (Figure 4.11). This is comparable to the ^{19}F NMR for Eu.4.8, which displays four peaks corresponding to the two bound fluorides for SAP and TSAP isomers.

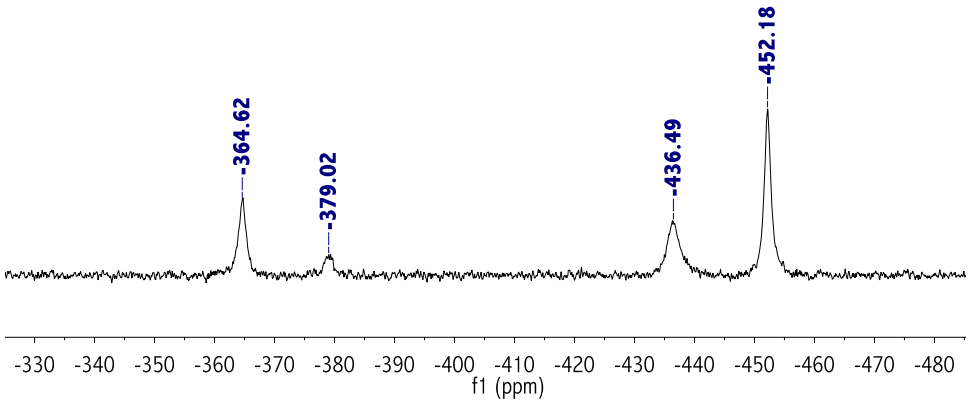

Figure 4.11: ^{19}F NMR for Eu.p.DO3A in the presence of fluoride (298 K, D_2O, 500 MHz)

When analysing these three complexes it can be seen that they all show similar behaviour in the ^{1}H NMR before and after binding to fluoride. The differences can be seen in the behaviour of the Eu.4.9 complex which not only displays pH-dependent behaviour but also has differences in the ^{19}F NMR which may be due to the possibility of self-assembly.

4.3.2 Photophysical studies

To confirm and explore the results observed in the NMR studies, luminescence studies were performed with the complexes Eu.4.8, Eu.4.9 and Eu.p.DO3A.

Complex Eu.4.8 was first investigated in methanol, where Figure 4.12 shows the emission spectra before and after the addition of fluoride.

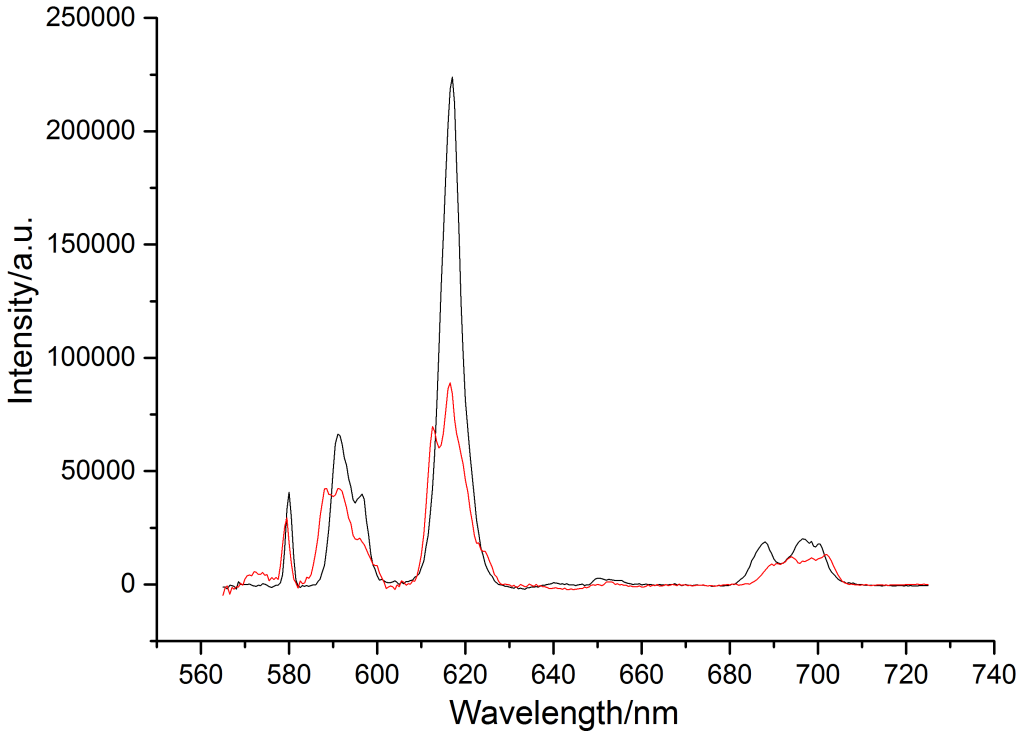

Figure 4.12: Emission spectra of Eu.4.8 in methanol before (black) and after fluoride binding (red) (λex= 395 nm)

It can be clearly seen that there is a significant decrease in emission intensity following the addition of fluoride. Figure 4.12 also shows a change in the crystal flied splitting due to the presence of fluoride.

To assess the strength of binding for each of the two events observed in the NMR and luminescence studies a luminescence titration was performed, where TBAF.$3H_2O$ was used as a source of fluoride and was iteratively added to a solution of Eu.4.8 in methanol and measuring the resulting emission spectra (Figure 4.13).

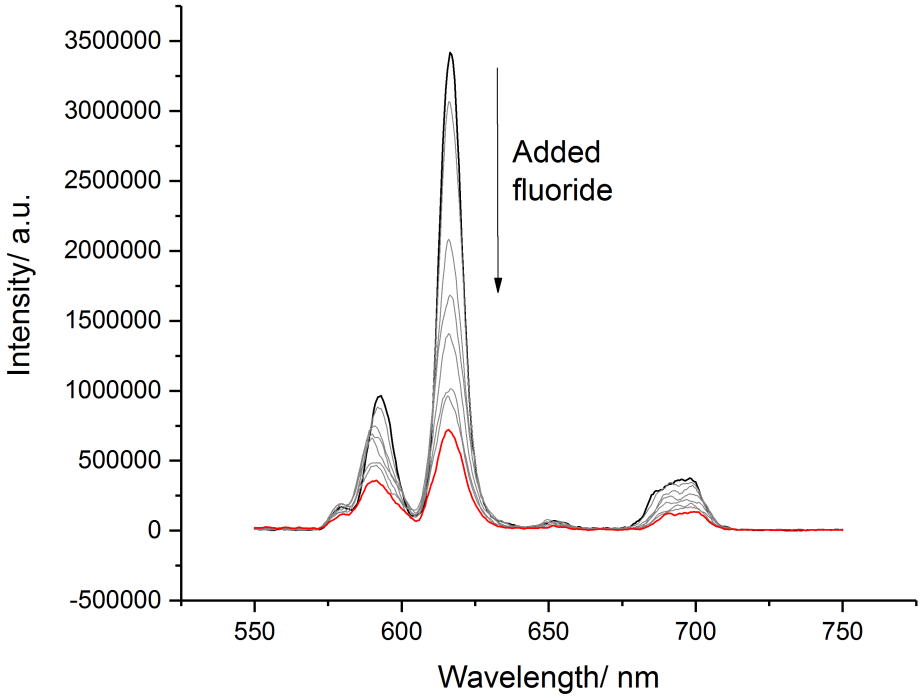

Figure 4.13: Observed emission spectra for the titration Eu.4.8 with increasing fluoride concentration in methanol (λex= 395 nm)

The data for the titration was then processed using DYNAFIT® and the resulting binding curves (green: Δ*J*=1, yellow: Δ*J*=2, blue: Δ*J*=4) were obtained are shown in Figure 4.14.

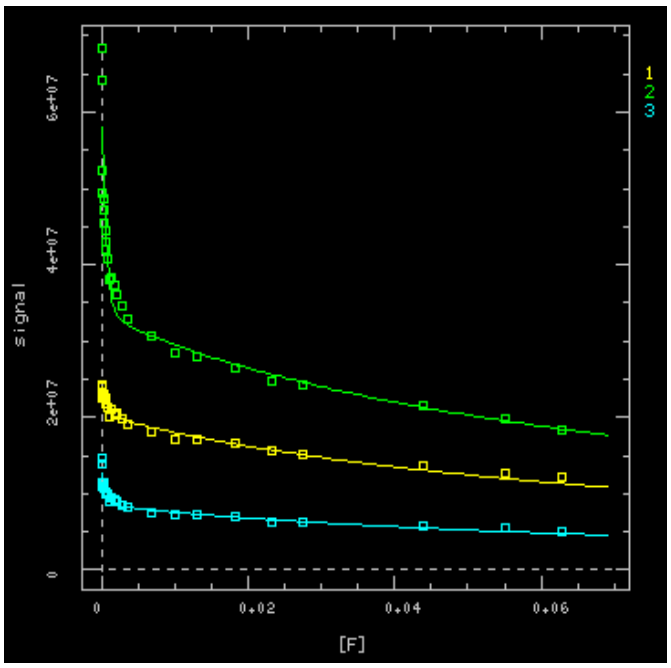

Figure 4.14: Binding curves calculated for the titration of Eu.4.8 with TBAF.3H_2O

The binding curves produced clearly show two binding events. The first binding is very strong, with log K_1 [95 % confidence interval] being 4.29 [2.74-8.64]. This is attributed to the equatorial bound fluoride, as the NMR studies showed this to be the first binding event to occur. The second binding event due to the axial binding of a second fluoride is considerably weaker, with log K_2 [95 % confidence interval] being 1.08 [0.93-1.22].

The lifetimes of the unbound complex and difluoride bound species were also measured and the resulting q values calculated (according to the Horrocks equation[10]) as detailed in Table 4.1.

Table 4.1:Measured lifetimes for Eu.4.8 before and after fluoride binding and corresponding calculated q values

	τ_{MeOH}/ms[a]	τ_{MeOD}/ms[a]	q
Eu.4.8	0.56	1.19	1.7
Eu.4.8 +excess F^-	0.89	1.48	0.7

[a] *where the typical errors on measured values are around 10 %*

The calculated q values show the unbound complex to have two bound solvent molecules, while with excess fluoride the q values fall to one. While this initially appears to be in contradiction to the NMR and luminescence titration data, when considering the binding constants of the two events, the second event shows weak binding and is likely to be in exchange with solvent molecules- leading to an overall averaged q value of one. It is also likely that calculations overestimate q in these circumstances- since quantum yields will reflect photoelectron transfer quenching of the lanthanide excited states in systems where fluoride is bound to europium (such quenching can clearly be seen from the data in Figure 4.14).

The same study was carried out with complex Eu.4.9, to assess and compare the strength of binding in aqueous solution. As shown in Figure 4.15, we observe an initial increase in the emission intensity then a large decrease.

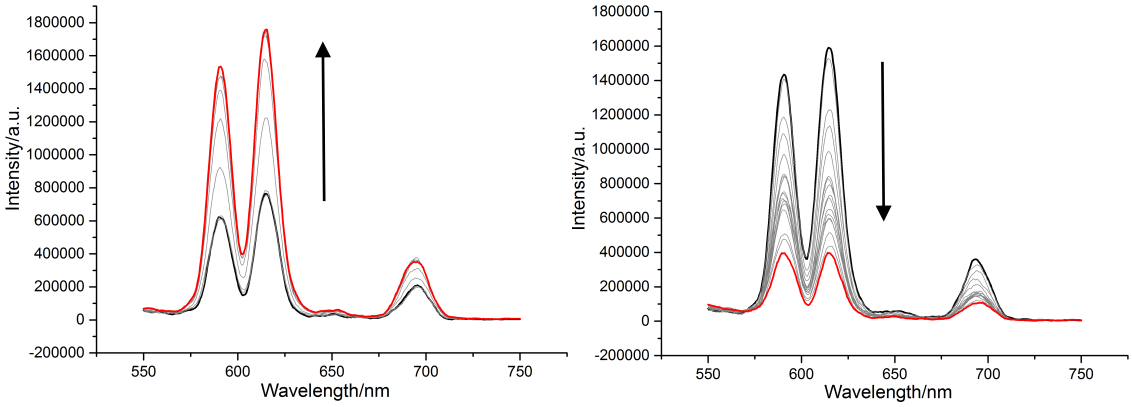

Figure 4.15: Observed emission spectra for the titration Eu.4.9 with increasing fluoride concentration in water, showing the initial increase in intensity (left) then decrease in emission intensity (right) (λex= 395 nm)

When analysing this data with DYNAFIT®, the curves produced show three events (Figure 4.16). We propose the initial increase to be due the breakdown of large scale aggregation caused by the carboxylic acids on the amide arms binding to other lanthanide centres. This is then followed by two fluoride binding events. Due to the limitations of the software, these processes cannot be accurately fit - as can be clearly seen in Figure 4.16. However, even a cursory inspection of the data reveals that there are three events in this titration- implying that fluoride binding is not the whole story.

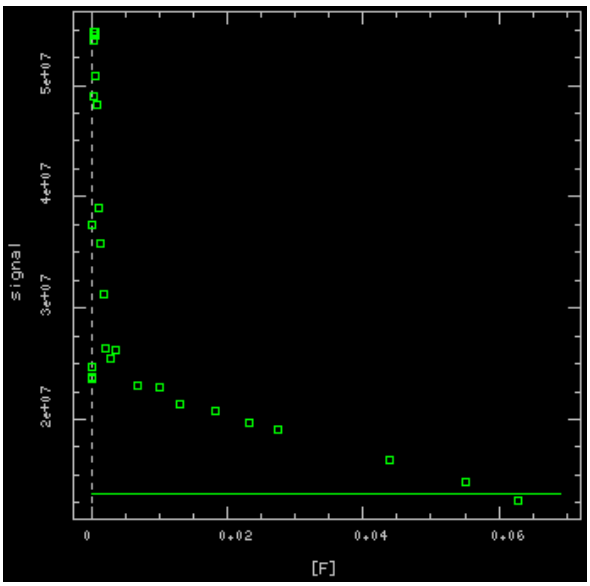

Figure 4.16: Binding curve calculated for the titration of Eu.4.9 with TBAF.3H_2O

The lifetimes for the free complex Eu.4.9 and with increasing fluoride concentration and the corresponding q values are shown in Table 4.2. The free complex Eu.4.9 shows short lifetimes and an implausibly high q value of 3 - this is attributed to the aggregation introducing quenching pathways leading to shortened measured lifetimes. The complicated nature of the system due to aggregation means that the Horrocks equation can no longer accurately describe the system, the complicated nature of the system and the resulting binding is also reflected by the multiexponential values for the fitted lifetimes. With increasing fluoride concentration, there is a steady decrease in the corresponding q values from q=2 to q=0. This can be can be rationalised by looking at the luminescent titration results, where with the addition of fluoride we see the breakdown of the aggregation followed by the two sequential fluoride binding events.

Table 4.2: Measured lifetimes for Eu.4.9 with increasing fluoride concentration and corresponding calculated q values

	τ_{H2O}/ms [a]	τ_{D2O}/ms [a]	q
Complex only	$\tau_1 = 0.02$	$\tau_1 = 0.93$	3[b]
	$\tau_2 = 0.23$	$\tau_2 = 0.25$	
+ TBAF	$\tau_1 = 0.11$	$\tau_1 = 0.21$	1.5
	$\tau_2 = 0.36$	$\tau_2 = 0.96$	
+ more TBAF	$\tau_1 = 0.07$	$\tau_1 = 0.21$	1.2
	$\tau_2 = 0.34$	$\tau_2 = 0.71$	
+excess TBAF	$\tau_1 = 0.15$	$\tau_1 = 0.24$	0.2
	$\tau_2 = 0.60$	$\tau_2 = 1.12$	

[a] *where the typical errors on measured values are around 10 %*

[b] calculated value can be discounted as described in the text

The fluoride binding of Eu.p.DO3A complex was also studied by a luminescence titration as shown in Figure 4.17.

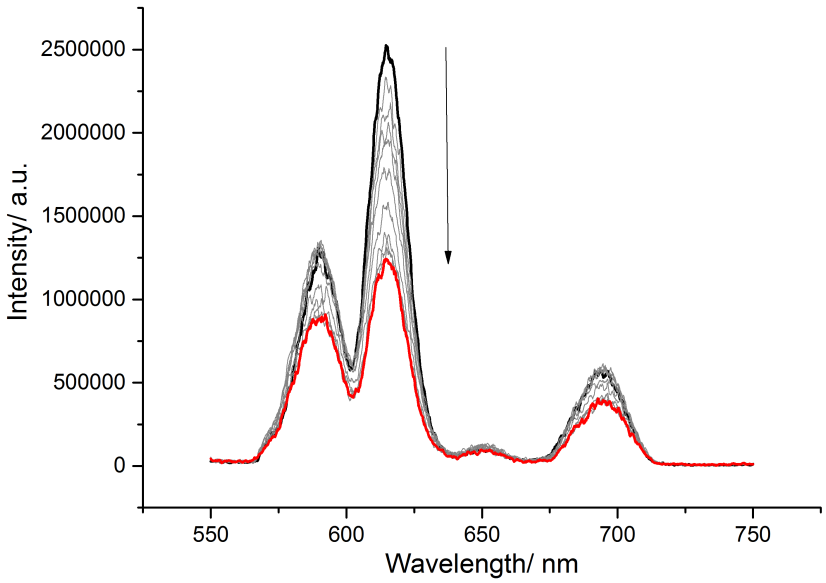

Figure 4.17: Observed emission spectra for the titration Eu.p.DO3A with increasing fluoride concentration in water (λex= 395 nm)

The strength of binding was assessed using DYNAFIT®, where Figure 4.18 shows the binding curves for left: bi-exponential corresponding to two binding events for ΔJ=1, ΔJ=2 and ΔJ=4, and right: mono-exponential binding for ΔJ=1. Of the two models the mono-exponential binding model gives better fit for the data with a binding constant of K_1[95 % confidence interval] being 212 [193-262]. While the binding model may suggestive of a single fluoride binding event, when we look at the binding data for Eu.4.8 the second binding event is very weak and so for a system with overall weaker binding the second fluoride binding will be in faster exchange and so the data we see corresponds to an averaged view where there is one strongly bound fluoride.

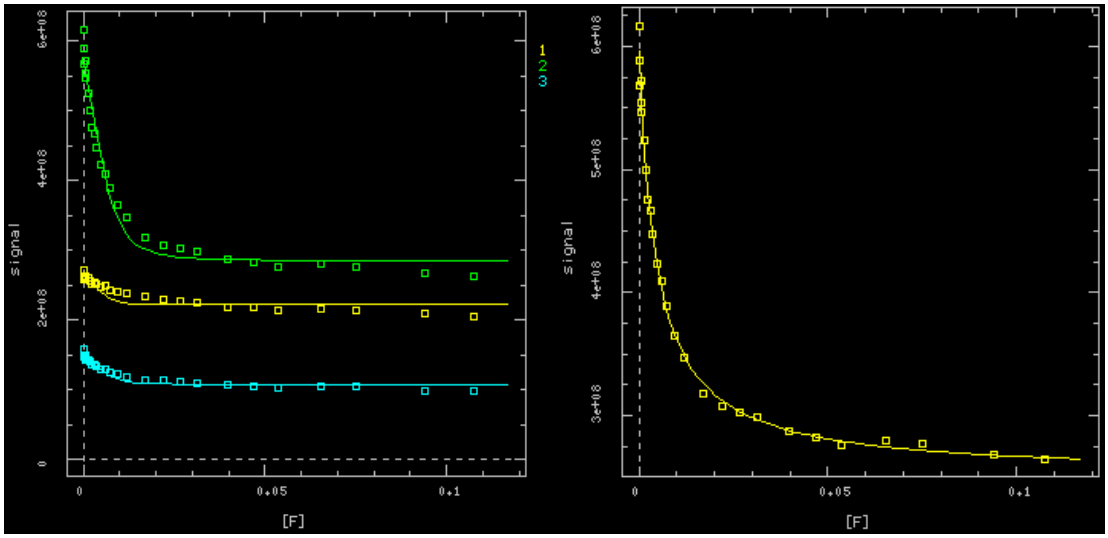

Figure 4.18: Binding curve calculated for the titration of Eu.4.9 with TBAF.3H_2O fitted for two binding events (left) and single binding event (right)

The observed lifetimes for the free complex Eu.p.DO3A in the presence and absence of fluoride concentration and the corresponding q values are shown in Table 4.3.

Table 4.3: Measured lifetimes for Eu.p.DO3A before and after the addition of fluoride and corresponding calculated q values

	τ_{H2O}/ms [a]	τ_{D2O}/ms [a]	q
Eu.p.DO3A	0.49	1.77	1.5
Eu.p.DO3A +excess F^-	0.59	1.94	1.1

[a] *where the typical errors on measured values are around 10 %*

The calculated q values also reflect results from the luminescence titration, showing a system where q value decreases upon addition of fluoride but indicates that there is still one water molecule bound to the lanthanide centre. As for the luminescence studies, this reflects a system where one fluoride and water are in exchange, leading to an averaged value of one bound solvent molecule for the system.

4.4 Catalysis

4.4.1 Introduction

Having explored the fluoride binding for complexes Eu.4.8, Eu.4.9 and Eu.p.DO3A, and established that two fluoride binding events can be explained by strong binding at an equatorial site, and weaker binding at an axial one, we reasoned that it might be possible to displace the weakly bound axial fluoride with a substrate of higher binding affinity. This would lead to the formation of a ternary complex which might play a role as a key intermediate to achieve catalysis through the pre-organisation of substrates. In order to explore this, the fluorination of α-halocarboxylic acids was chosen as a candidate reaction: the carboxylic acid should bind to the lanthanide centre and allow the halogen to be held in close proximity to the equatorially bound fluoride in order to achieve fluorination of the substrate, as shown in Figure 4.19.

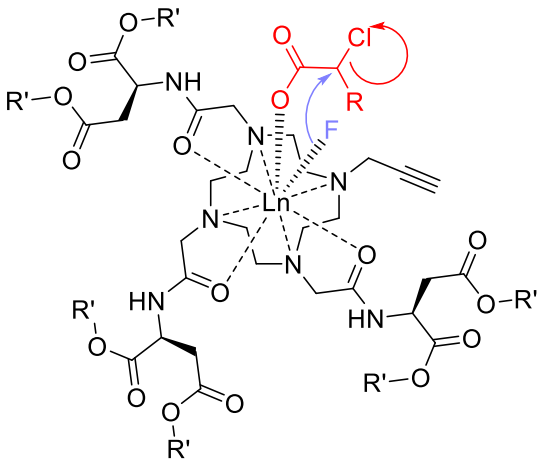

Figure 4.19: Formation of a quaternary complex for the fluorination of α-halocarboxylic acids

The fluorination of α-halocarboxylic acids is of particular interest due to its importance in radiopharmaceutical and medical chemistry of ^{18}F labelling.[11,12] Any increase in the rate of reaction would pose a significant advantage for labelling reactions, as the half-life of ^{18}F is 110 minutes.[11]

The three complexes Eu.4.8, Eu.4.9 and Eu.p.DO3A were studied with a series of α-halocarboxylic acids, where the rate of fluorination was followed by ^{19}F NMR, monitoring the appearance of product peaks in a catalysed system and a control. The substrates were chosen to cover different halogens, chain length and steric bulk as well as exploring the possibility of regioselectivity. While the use of lanthanides as catalysts is known,[13–19] the use of lanthanide macrocycles, including rigid chiral triamides to catalyse fluorination reactions is unprecedented.

4.4.2 Hexaester studies

The complex Eu.4.8 was studied first due to the fluoride binding studies clearly showing two fluoride binding events, where the axially bound fluoride has a binding constant over a 1000 times less than for the fluoride in the equatorial position.

The fluorination of chloroacetic acid (Scheme 4.3) in the presence and absence of Eu.4.8 was first studied

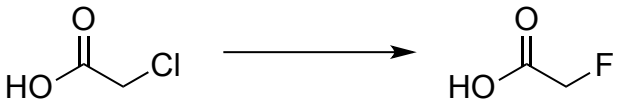

Scheme 4.3: Fluorination of chloroacetic acid

The control test consisted of 1:1 TBAF.$3H_2O$ and chloroacetic acid measured every 10 minutes after 5 minutes equilibration time. The catalysed test (referring to the test carried out in the presence of the potential lanthanide complex catalyst) was performed under the same conditions with the addition of 10 % Eu.4.8. The two tests are compared (control test: left and catalysed test: right) in Figure 4.20.

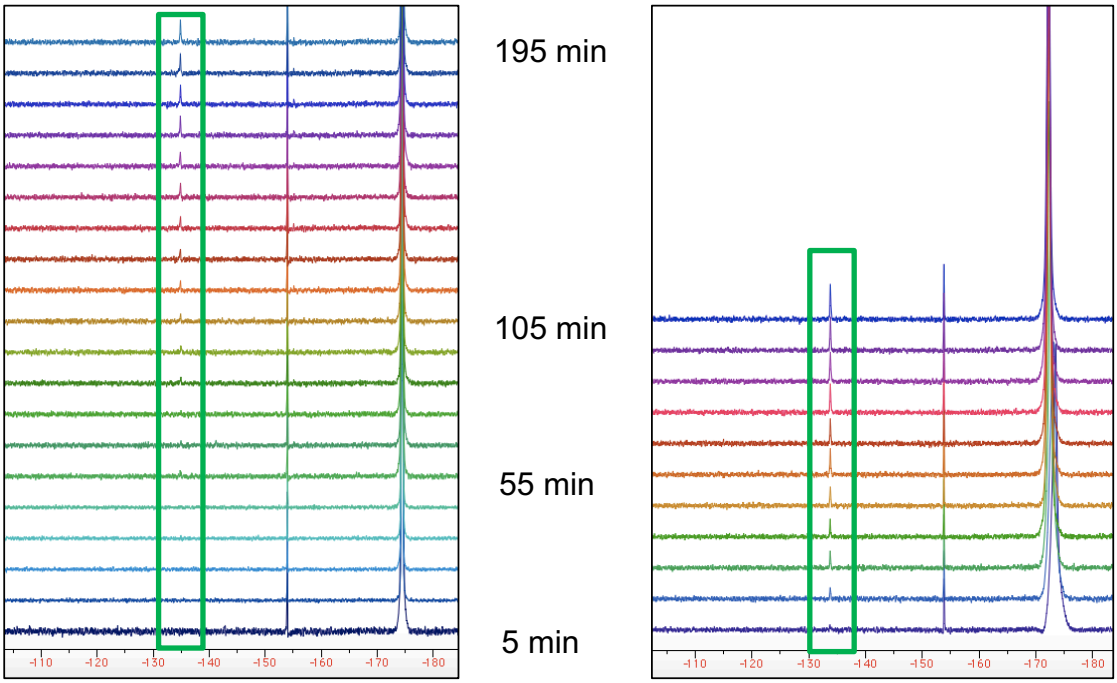

Figure 4.20: Comparison of ^{19}F NMR (298 K, d_4-methanol, 500 MHz) for Left: Control - 0.1 mol dm^{-3} chloroacetic acid and 0.1 mol dm^{-3} TBAF.3H_2O. Right: Catalysed - 0.1 mol dm^{-3} chloroacetic acid, 0.1 mol dm^{-3} and 10% loading of Eu.4.8 over time

It is clear from this study that the product peak (highlighted in the green boxes) appears much earlier for the catalysed test than for the control, showing that the rate fluorination of chloroacetic acid has been enhanced by the presence of Eu.4.8.

While Figure 4.20 shows evidence of an increased rate of reaction, this is only the initial rate of reaction, to further explore the kinetics of the reaction the catalysis and control tests were repeated over 13 hours, as shown in Figure 4.21 (left).

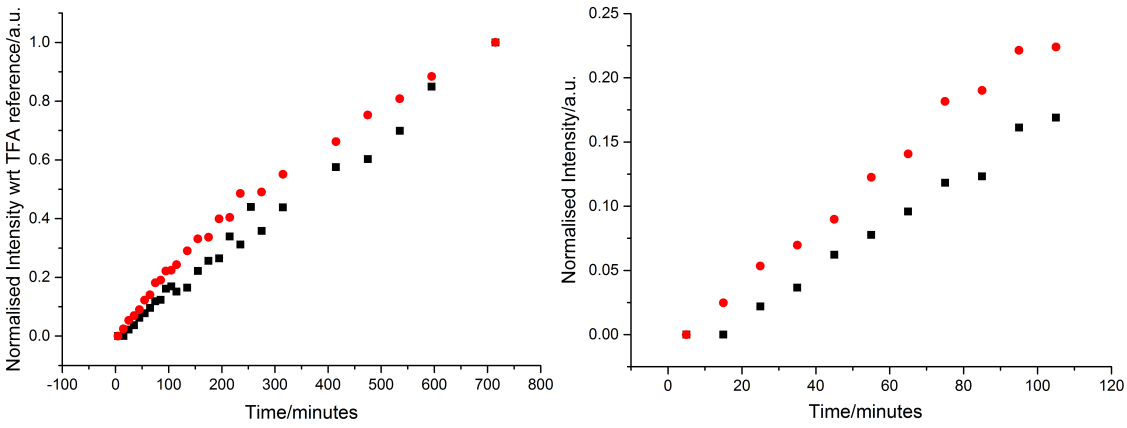

Figure 4.21:Changing integration of the ^{19}F NMR (298 K, d_4-methanol, 500 MHz) monitoring the formation of fluoroacetic acid for control (black) and catalysed test with Eu.4.8 (red) measured over 13 h (right) and initial rate (left)

As in the first study, Figure 4.21 (right) shows the initial rate of reaction is increased for the catalysed test compared to the control. After the initial increase in the rate of reaction Figure 4.21 (left) shows there is still an increased rate of reaction over the course of the reaction but after 13 hours the reaction shows no sign of being complete, indicating that, while there is evidence of the rate of reaction being enhanced by the presence of the lanthanide complex, the overall reaction is still relatively slow.

Having demonstrated that it is possible for Eu.4.8 to be used to enhance the rate of reaction in the fluorination of chloroacetic acid, we wanted to explore if this catalytic behaviour could be extended to other α-halocarboxylic acids. To do this, 2-bromopropionic acid and 3-bromopropionic acid were also studied.

Similarly, to the tests with chloroacetic acid, the fluorination of 2-bromopropionoic acid (Scheme 4.4) was explored by ^{19}F NMR in the presence and absence of Eu.4.8.

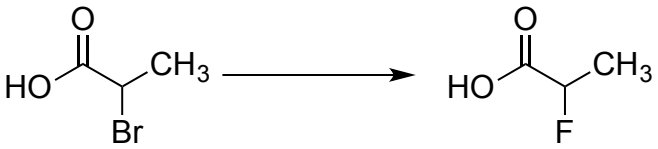

Scheme 4.4:Fluorination of 2-bromopropionic acid

Initial tests comparing the un-catalysed and catalysed fluorination of 2-bromopropionoic acid showed Eu.4.8 to enhance the reaction rate, where no fluorination is observed after over an hour in the control whereas a product peak was observed after around 25 minutes in the catalysed reaction, as shown in Figure 4.22.

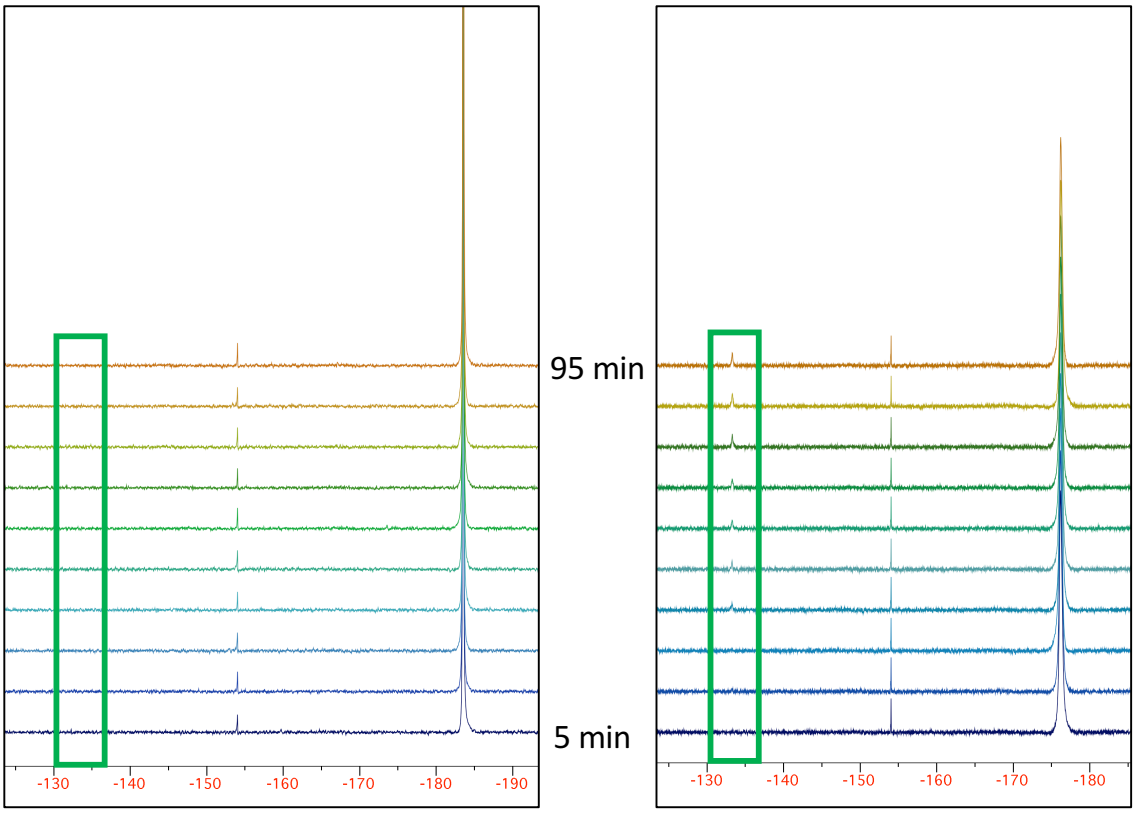

Figure 4.22: Comparison of ^{19}F NMR (298 K, d_4-methanol, 500 MHz) for Left: Control - 0.1 mol dm^{-3} 2-bromopropionic acid and 0.05 mol dm^{-3} TBAF.3H_2O. Right: Catalysed - 0.1 mol dm^{-3} 2-bromopropionic acid and 0.05 mol dm^{-3} TBAF.3H_2O and 10% loading of Eu.4.8 over time

The kinetics of the reaction was also monitored over 13 hours (Figure 4.23: right) to explore how the reaction proceed after the initial rate of reaction. Figure 4.23 (left) shows the same delay in reaction for the control test as observed in Figure 4.22, it can also be seen that there is an increased rate of reaction for the catalysed versus control test after this initial delay.

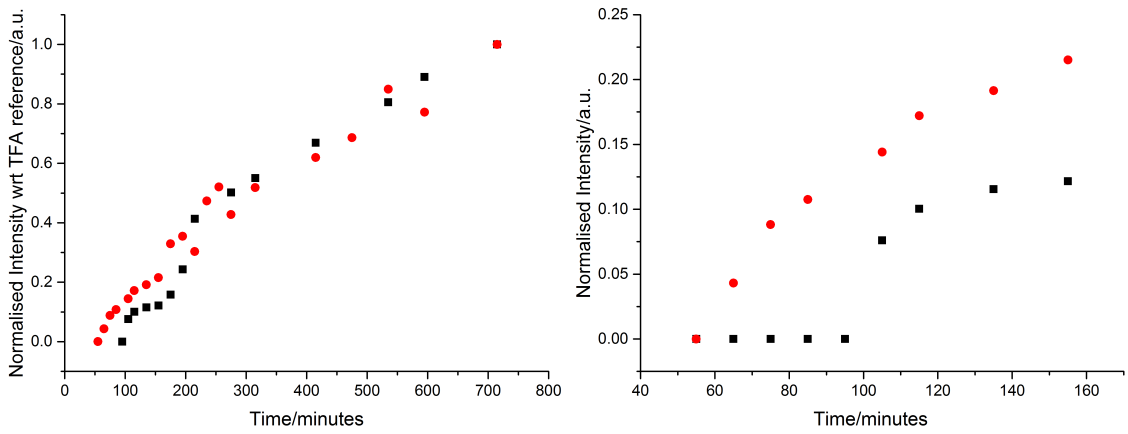

Figure 4.23: Changing integration of the ^{19}F NMR (298 K, d_4-methanol, 500 MHz) monitoring the formation of 2-fluoropropionic acid for control (black) and catalysed test with Eu.4.8 (red) measured over 13 h (right) and initial rate (left)

After the initial increase in the rate of reaction the rates of the control and catalysed tests coalesce and the overall rate is not increased by the presence of the catalyst. This difference compared to the fluorination of chloroacetic acid may be due to increased steric demands associated with the methyl group close to the centre of fluorination, which could either stabilise binding (and hence reduce turnover) or restrict available conformations that can react further. However, as in the case of the chloroacetic acid study, there is no evidence of a completed fluorination after 13 hours, also showing that the rate of the fluorination is slow.

To consider regioselectivity of the halogen exchange, the fluorination of 3-bromopropionoic acid (Scheme 4.5) was explored.

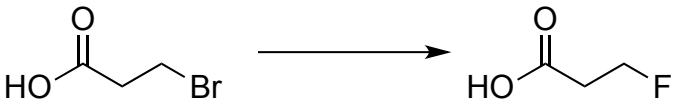

Scheme 4.5: Fluorination of 3-bromopropionic acid

The fluorination was followed by ^{19}F NMR in the presence and absence of Eu.4.8, as shown in Figure 4.24.

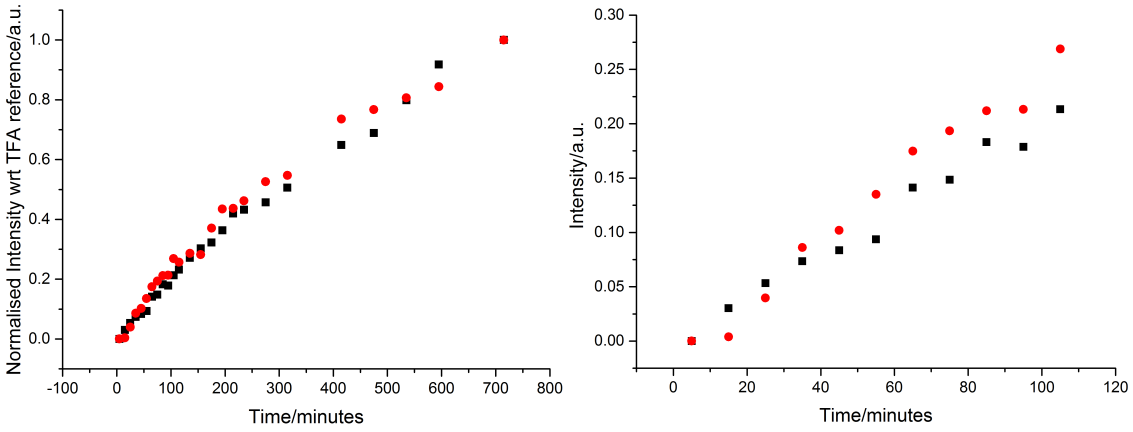

Figure 4.24: Changing integration of the ^{19}F NMR (298 K, d_4-methanol, 500 MHz) monitoring the formation of 3-fluoropropionic acid for control (black) and catalysed test with Eu.4.8 (red) measured over 13 h (right) and initial rate (left)

For the fluorination of 3-bromopropionoic acid there is little evidence that Eu.4.8 acts as an effective catalyst with only a small increase in the initial rate of reaction (Figure 4.24 right) and little evidence of catalysis over 13 hours (Figure 4.24 left). This decrease in catalytic activity compared to chloroacetic acid and 2-bromopropionoic acid may be attributed to the difference in the ring size formed between the substrate and lanthanide centre as shown in Figure 4.25, where the smaller ring size is favoured making the catalysis of 3-bromopropionoic acid less effective.

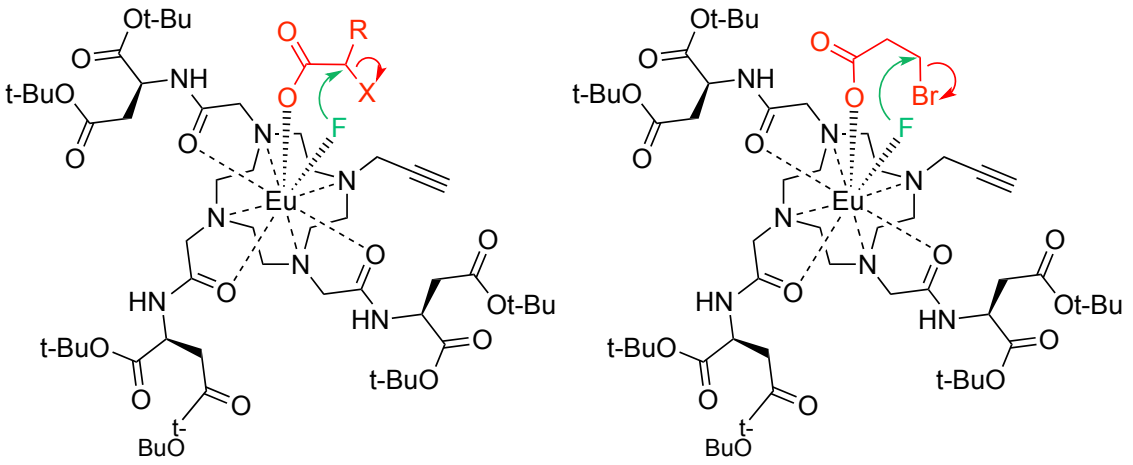

Figure 4.25:Catalysed fluorination of α-halocarboxylic acids with differing chain lengths by Eu.4.8 where R=H or CH_3 and X= Cl or Br

To assess the affect the effect of increased steric bulk the fluorination of α-bromophenylacetic acid was explored (Scheme 4.6).

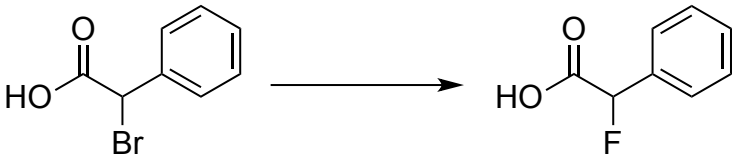

Scheme 4.6:Fluorination of α-bromophenylacetic acid

The rate was assessed by the monitoring the appearance of product peaks appeared in the ^{19}F NMR for catalysed and un-catalysed tests as shown in Figure 4.26.

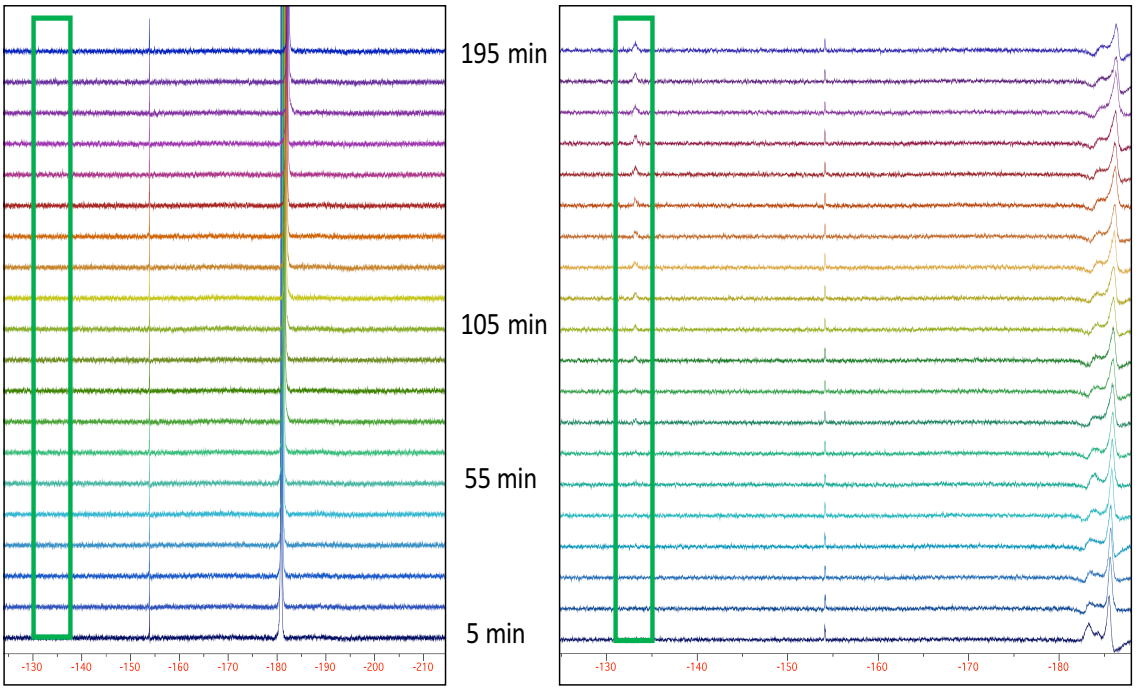

Figure 4.26: Comparison of ^{19}F NMR (298 K, d_4-methanol, 500 MHz) for Left: Control - 0.1 mol dm^{-3} α-bromophenylacetic acid and 0.05 mol dm^{-3} TBAF.3H_2O. Right: Catalysed - 0.1 mol dm^{-3} α-bromophenylacetic acid and 0.05 mol dm^{-3} TBAF.3H_2O and 10% loading of Eu.4.8 over time

As for the tests with 2-bromopropionic acid there is a delayed onset of reaction with the control showing no product conversion after over 3 hours. For the fluorination of α-bromophenylacetic acid there is also a delay in the appearance of a product peak for the catalysed test with no conversion for around an hour (c.a. 20 minutes for 2-

bromopropionic acid), this can be attributed to the increased steric bulk making the pre-organisation of the substrate harder for a sterically demanding system.

4.4.3 Hexaacid studies

While we have shown there is an increase rate of reaction of α-halocarboxylic acids in the presence of Eu.4.8 in methanol the ability to catalyse these fluorinations in water would be advantageous. Complex Eu.4.9 would therefore seem to be an ideal candidate for use as a water-soluble catalysis, however, from the fluoride binding tests we know that there is evidence of self-assembly and large scale aggregation for complex Eu.4.9. As such, we need to investigate to how/if this aggregation could affect the ability of Eu.4.9's to act as a catalyst for the fluorination of α-halocarboxylic acids. The three substrates (chloroacetic acid, 2-bromopropionic acid and 3-bromopropionic acid) studied with Eu.4.8 will be used to assess the potential use of Eu.4.9 as a potential catalyst.

The fluorination of chloroacetic acid was first explored (using the same methodology as described for Eu.4.8) monitoring the formation of products by ^{19}F, the rates of the control and catalysed reactions are shown in Figure 4.27.

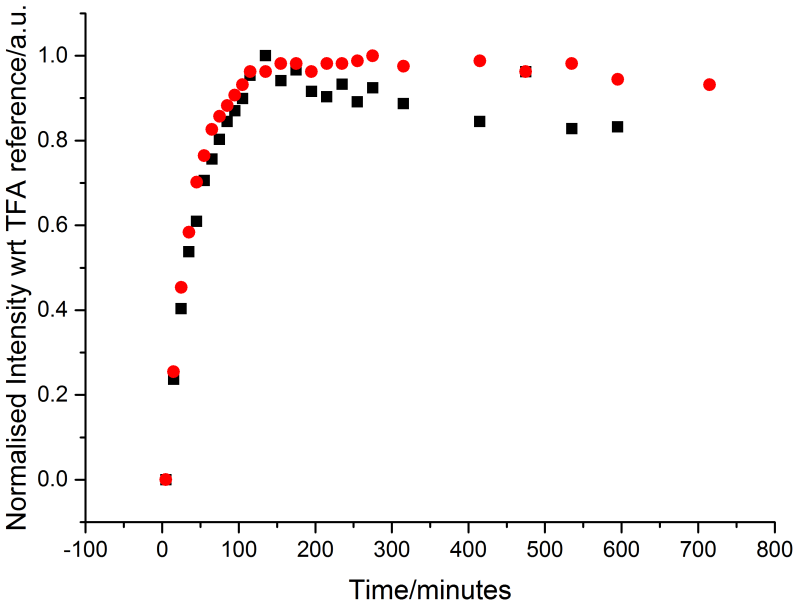

Figure 4.27: Changing integration of the ^{19}F NMR (298 K, D_2O, 500 MHz) monitoring the formation of fluoroacetic acid for control (black) and catalysed test Eu.4.9 (red) measured over 13 h

Figure 4.27 shows there is no catalysis or increase in the rate of reaction in the presence of Eu.4.9. As speculated, it is possible that the lack of catalytic activity is linked to the aggregation of Eu.4.9 hindering the formation of the quaternary complex needed to catalyse this reaction.

To see if this result is indicative of how Eu.4.9 will behave with other carboxylic acids, tests with 2-bromopropionic acid and 3-bromopropionic acid were carried out.

The tests with 2-bromopropionic acid showed there to be no catalytic effect for the fluorination reaction as shown in Figure 4.28.

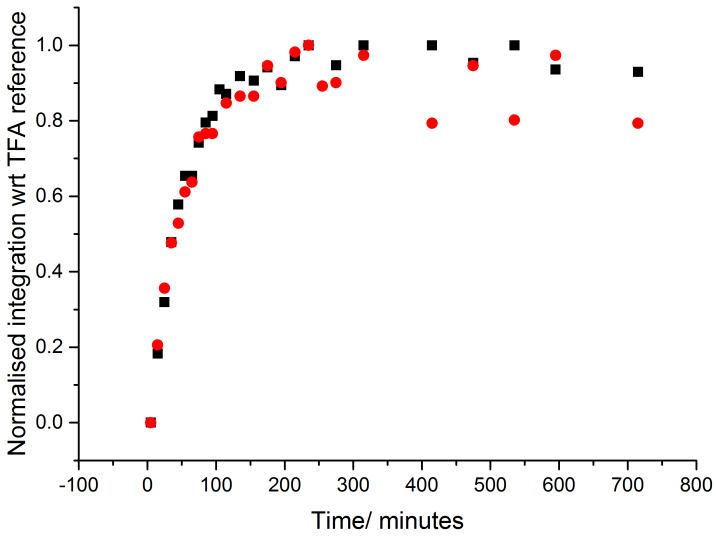

Figure 4.28: Changing integration of the ^{19}F NMR (298 K, D_2O, 500 MHz) monitoring the formation of 2-fluoropropionic acid for control (black) and catalysed test Eu.4.9 (red) measured over 13 h

Interestingly however, the ^{19}F NMRs for both the control and catalysed tests over 13 hours show the appearance of a second fluoride peak at 1.5 hours as shown in Figure 4.29.

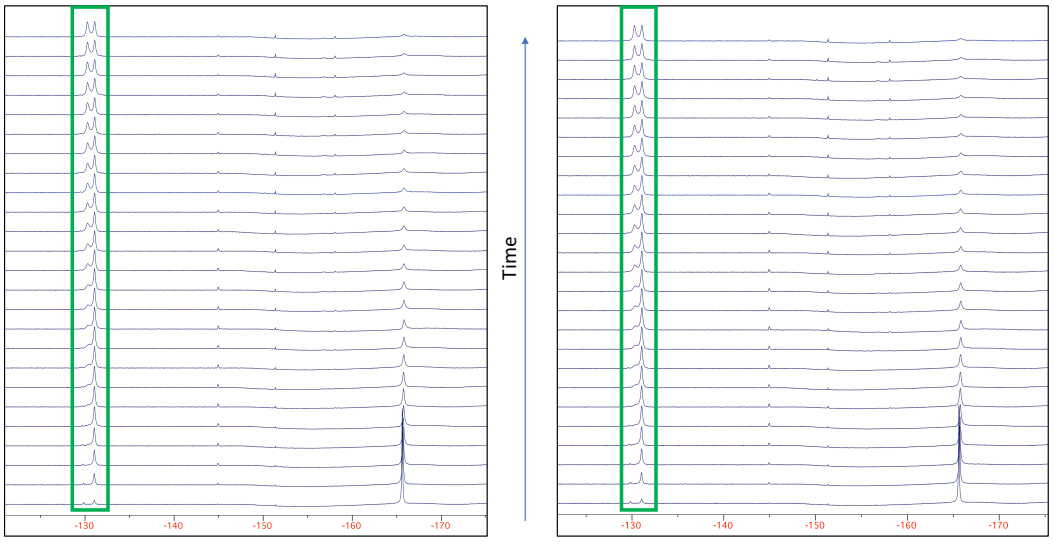

Figure 4.29: Comparison of ^{19}F NMR (298 K, D_2O, 500 MHz) for Left: Control - 0.1 mol dm^{-3} 2-bromopropionic acid and 0.05 mol dm^{-3} TBAF.$3H_2O$. Right: Catalysed - 0.1 mol dm^{-3} 2-bromopropionic acid and 0.05 mol dm^{-3} TBAF.$3H_2O$ and 10% loading of Eu.4.9 over time

The appearance of a second fluoride species in both catalysed and control tests rule out the possibility of Eu.4.9 acting as a chiral shift reagent to give peaks for *R* and *S* isomers. It likely that fluoride acts as a base causing the elimination of HBr and formation of acrylic acid, this can then result in the Michael addition of fluoride to give either the 2-fluropropionoic acid or 3-fluoropropionic acid[20] as shown in Scheme 4.7 which gives rise to two the two fluoride peaks in the ^{19}F NMR.

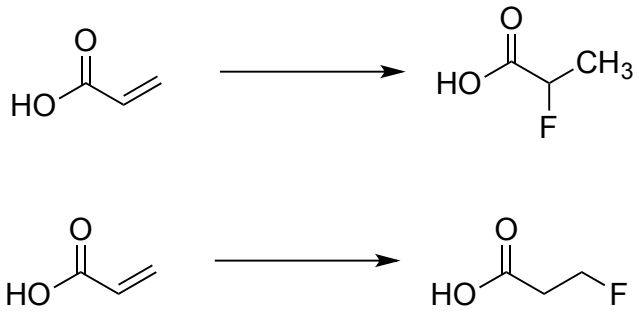

Scheme 4.7: Reaction of acrylic acid to give products 2-fluoropropionic acid or 3-fluoropropionic acid

Catalyst test for the fluorination of 3-bromopropionic acid with Eu.4.9 were also performed as shown in Figure 4.30.

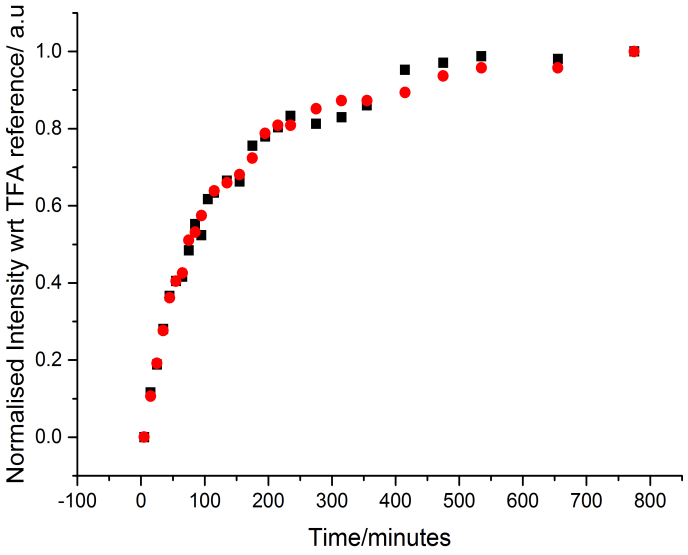

Figure 4.30: Changing integration of the ^{19}F NMR (298 K, D_2O, 500 MHz) monitoring the formation of 3-fluoropropionic acid for control (black) and catalysed test with Eu.4.9 (red) measured over 13 h

As for the other substrates, there is no evidence of catalysis after the addition of Eu.4.9, confirming that the previous observed results are seemingly representative for the fluorination of α-halocarboxylic acids with Eu.4.9. As discussed for the fluorination of chloroacetic acid the reason for the lack of catalytic activity is most likely linked to the self-assembly of the complex Eu.4.9.

However, there is a difference in the rates of reaction for 2-bromopropionic acid verses 3-bromopropionic acid as illustrated in Figure 4.31.

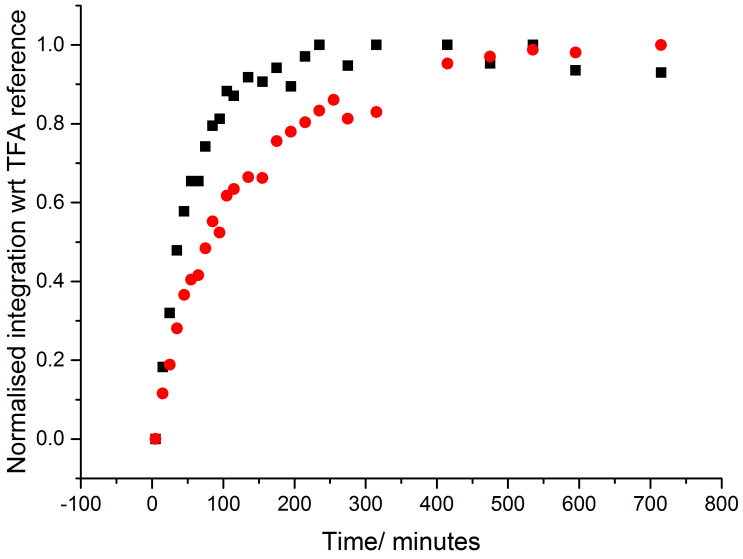

Figure 4.31:Comparison of the un-catalysed rates for the fluorination of 2-bromopropionic acid (black), and 3-bromopropionic acid (red)

The differences in the rate of reaction for 2-bromopropionic acid and 3-bromopropionic acid are most likely due to the differences in ring size between the substrate and fluoride lanthanide centre as depicted in Figure 4.25.

It is also of note that, while the reaction of all three substrates is not catalysed by Eu.4.9, the reactions go to completion - unlike the same reactions in methanol. This increased rate of reaction in water verses methanol is illustrated in Figure 4.32 by the control reactions for fluorination of 3-bromopropinoic acid in deuterium oxide verses d_4-

methanol. This indicates that while Eu.4.9 may not be a suitable catalyst, a water-soluble catalyst would offer a significant advantage in the catalysis of α-halocarboxylic acids.

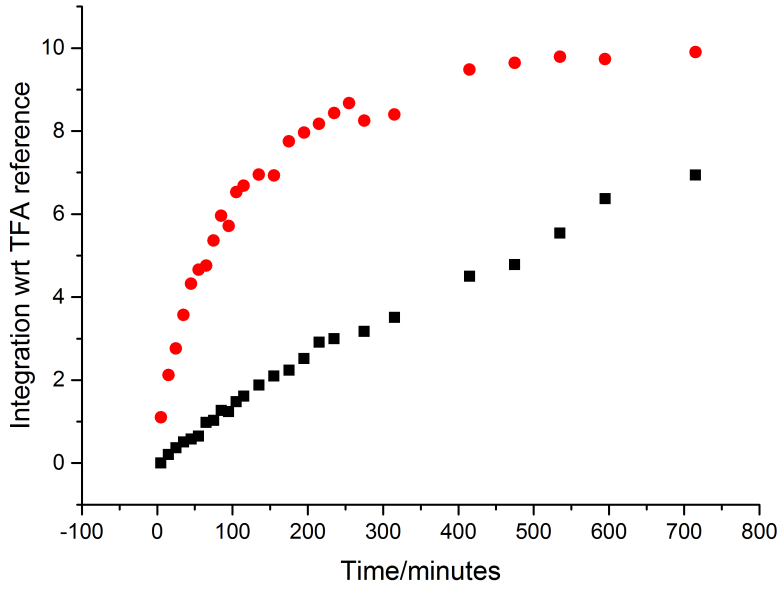

Figure 4.32: Comparison of the un-catalysed rates for the fluorination of 3- bromopropionic acid in d_4-methanol (black), and deuterium oxide (red)

4.4.4 Eu.p.DO3A studies

While Eu.4.8 has been shown to have an effect on the rate of reaction for the fluorination of α-halocarboxylic acids, the ability to catalyse the fluorination of α-halocarboxylic acids in water would give a signification advantage, as previously discussed. Eu.p.DO3A was investigated as a potential catalyst for the fluorination of chloroacetic acid, 2-bromopropionic acid and 3-bromopropionic acid.

The fluorination of chloroacetic acid was first explored in deuterium oxide as shown in Figure 4.33.

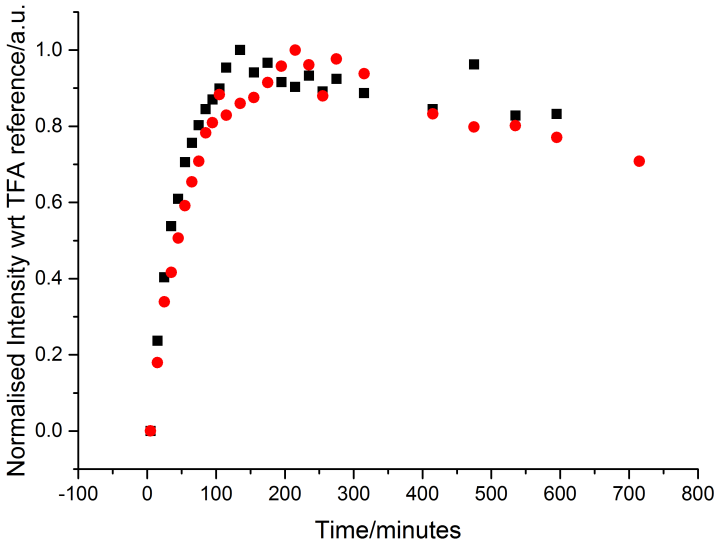

Figure 4.33: Changing integration of the ^{19}F NMR (298 K, D_2O, 500 MHz) monitoring the formation of fluoroacetic acid for control (black) and catalysed test with Eu.p.DO3A (red) measured over 13 h

While there appears to be no catalysis for this reaction in water, the same reaction in d_4-methanol shows strong evidence of Eu.p.DO3A's ability to act as a catalysis - as shown in Figure 4.34.

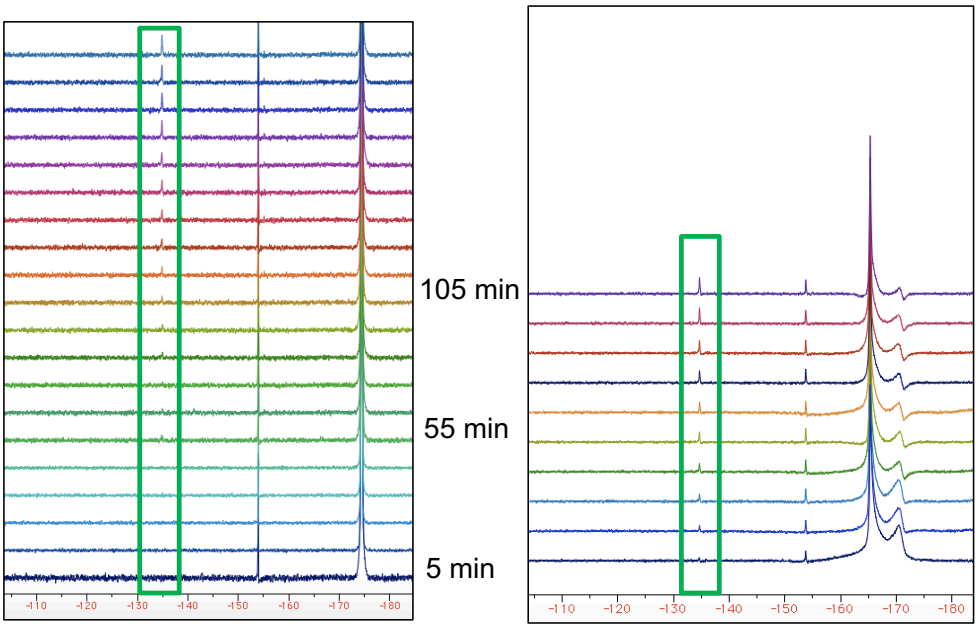

Figure 4.34: Comparison of ^{19}F NMR (298 K, d_4-methanol, 500 MHz) for Left: Control - 0.1 mol dm^{-3} chloroacetic acid and 0.1 mol dm^{-3} TBAF.$3H_2O$. Right: Catalysed - 0.1 mol dm^{-3} chloroacetic acid and 0.05 mol dm^{-3} TBAF.$3H_2O$ and 10% loading of Eu.p.DO3A in d_4-methanol over time

This shows the Eu.p.DO3A can act to increase the rate of reaction and the lack of catalytic activity in water may be due to the reaction occurring at its diffusion controlled rate in water and only when the rate of reaction is decreased (as is seen for the rates in d_4-methanol verses deuterium oxide) that any catalytic effect can be observed.

It is also worth noting that when comparing the catalysis of the fluorination of chloroacetic acid by Eu.4.8 and Eu.p.DO3A very similar rates are observed, as seen in Figure 4.35. Showing that both complexes enhance the rate of reaction and therefore are viable as potential catalysts for the fluorination chloroacetic acid in methanol, and the use of a simpler (and less synthetically challenging) Eu.p.DO3A complexes offers significant advantages.

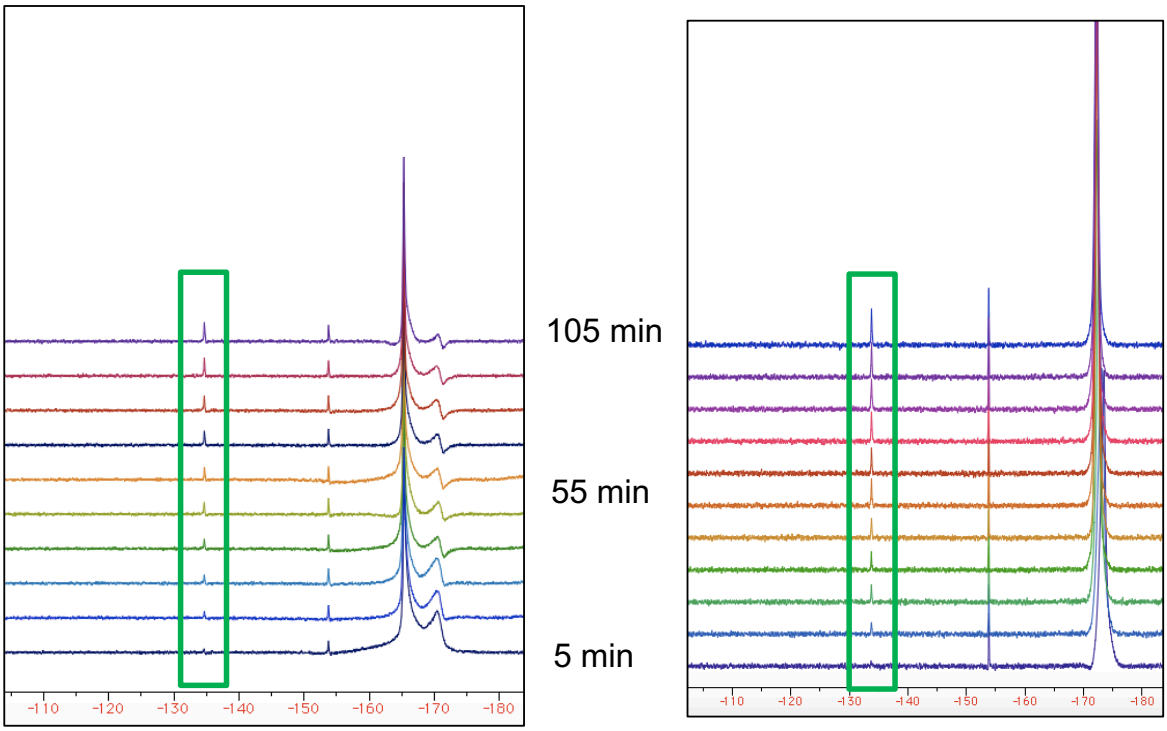

Figure 4.35:Comparision of catalysis of the fluorination of chloroacetic aicd in d4-methanol by Eu.p.DO3A (left) verses Eu.4.8 (right) (298 K, d_4-methanol, 500 MHz)

To explore if catalysis in water is possible using Eu.p.DO3A the fluorination of 2-bromopropinoic acid was first explored as shown in Figure 4.36.

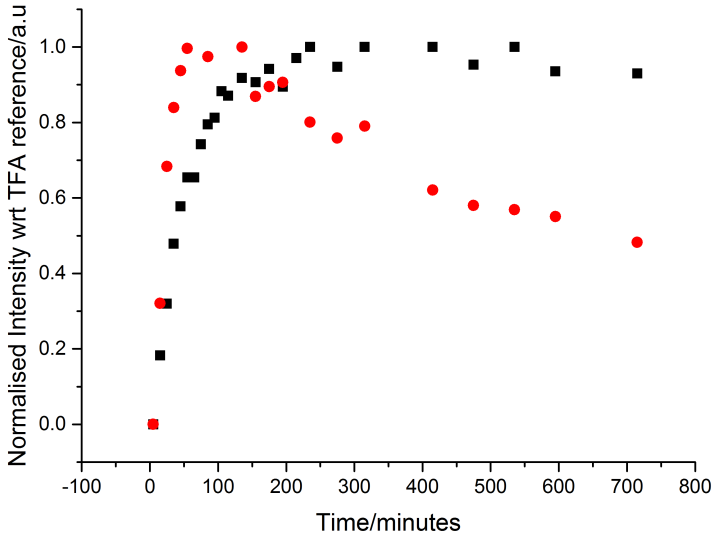

Figure 4.36: Changing integration of the ^{19}F NMR monitoring the formation of 2-fluoropropionic acid for control (black) and catalysed test with Eu.p.DO3A (red) measured over 13 h (298 K, D_2O, 500 MHz)

While there is an increased initial rate of the reaction for the catalysed verses control test, the rate of reaction decreases rather than plateauing as seen in the control.

As previously seen for the fluorination of 2-bromopropionic acid a second fluoride is observed in the ^{19}F NMR (Figure 4.37).

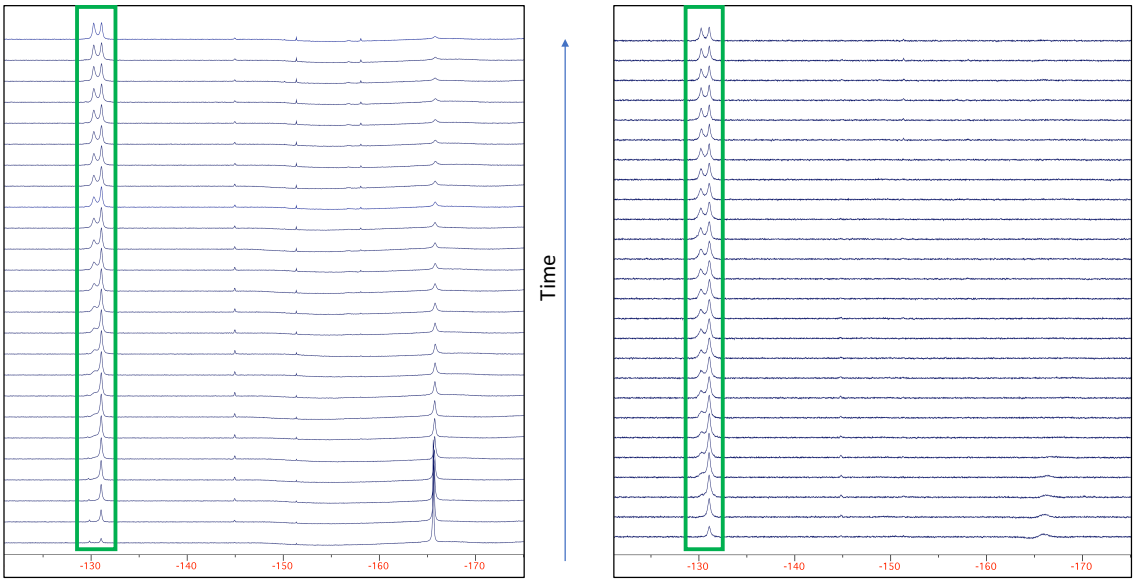

Figure 4.37: Comparison of ^{19}F NMR (298 K, D_2O, 500 MHz) for Left: Control 0.1 mol dm^{-3} 2-bromopropionic acid and 0.05 mol dm^{-3} TBAF.$3H_2O$. Right: Catalysed - 0.1 mol dm^{-3} 2-bromopropionic acid and 0.05 mol dm^{-3} TBAF.$3H_2O$ and 10% loading of Eu.p.DO3A over time

As previously discussed this is likely due to the formation of acrylic acid giving rise to both 2-fluoropropionic acid and 3-fluoropropionic acid. However, unlike the tests with Eu.4.9, the reaction in the presence of Eu.p.DO3A is enhanced and the free fluoride in solution rapidly lost as seen in Figure 4.37 (right), this then results in the decrease in overall integration of the product peak after around 2 hours (shown in Figure 4.36) due to competing side reaction - such as the polymerisation of acrylic acid - causing precipitation.

The fluorination of 3-bromopropinoic acid was also explored to see whether, like Eu.4.8 and Eu.4.9, the rate of reaction is affected by the increased chain length. Figure 4.38 shows the catalysed and un-catalysed rates of reaction for the fluorination of 3-bromopropinoic acid.

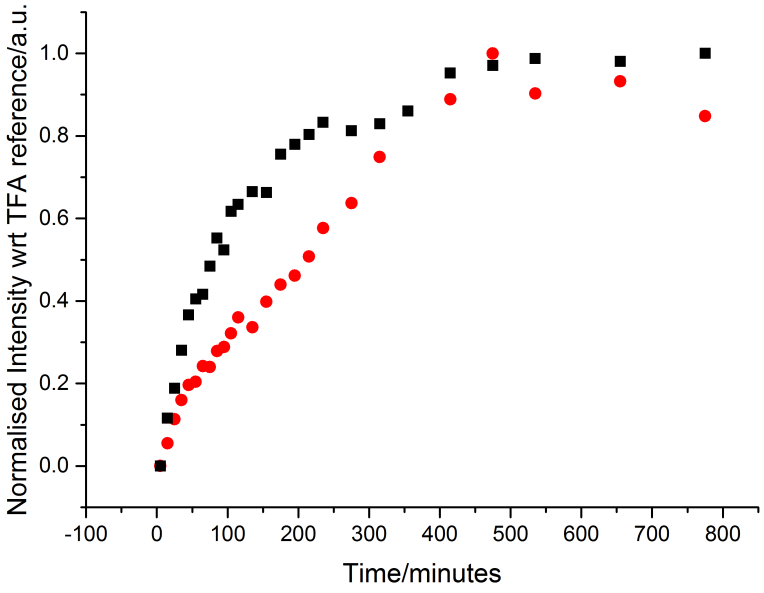

Figure 4.38: Changing integration of the ^{19}F NMR monitoring the formation of 3-fluoropropionic acid for control (black) and catalysed test with Eu.p.DO3A (red) measured over 13 h (298 K, D_2O, 500 MHz)

As shown, not only in the rate of reaction not increased by the presence of Eu.p.DO3A, there is a decrease in the rate of reaction compared to the control test. As for Eu.4.8 and

Eu.4.9 this may be due either to enhanced binding of the carboxylate and slower exchange of substrate, or as a consequence of ring size in controlling the rate of reaction.

4.4.5 Regioselectivity and Catalysis

One of the advantages of synthesising chiral lanthanides complexes such as Eu.4.8 and Eu.4.9 is that it may be possible to catalyse the fluorinations with the possibility of regioselectivity.

To explore this the substrate 2,3-dibromopropionic acid was chosen, the fluorination of this substrate has the potential to form a range products as outlined in Scheme 4.8

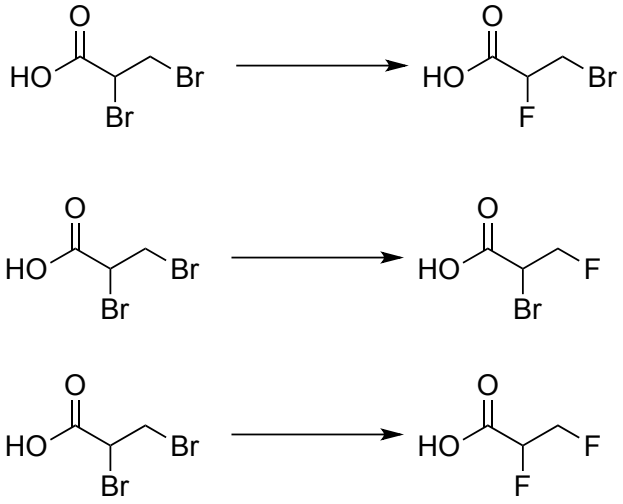

Scheme 4.8:Possible products from the fluorination of 2,3-bromopropionic acid

To explore if the use of these chiral catalyst Eu.4.8 can give regioselectivity compared to the un-catalysed reaction, the ^{19}F NMRs were monitored for the formation of any product peaks resulting from the fluorination of 2,3-dibromopropionic acid as shown in Figure 4.39.

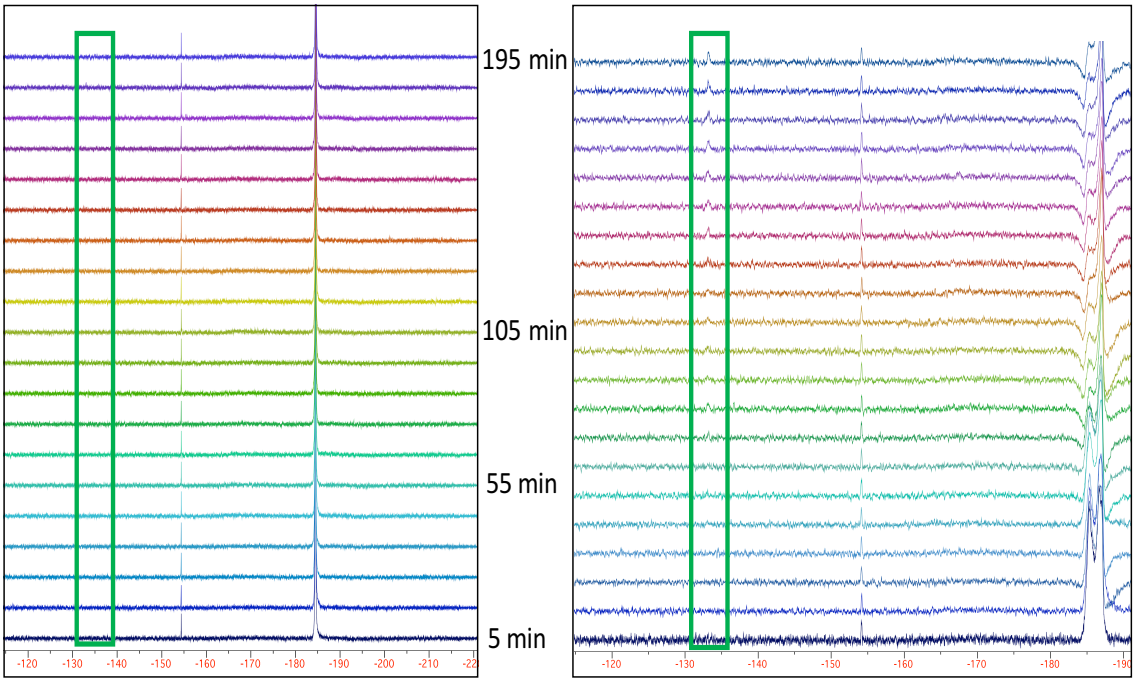

Figure 4.39: Comparison of ^{19}F NMR (298 K, D_2O, 500 MHz) for Left: Control - 0.1 mol dm^{-3} 2,3-bromopropionic acid and 0.05 mol dm^{-3} TBAF.$3H_2O$. Right: Catalysed - 0.1 mol dm^{-3} 2,3-bromopropionic acid, 0.05 mol dm^{-3} TBAF.$3H_2O$ and 10% loading of Eu.4.8 over time

While the control test shows no evidence of any product formation over 3 hours, the catalysed reaction does show conversion with the appearance of one peak. This indicates that there is only one product formed, mostly likely the due to the 2-fluoro-3-bromo-propinoic acid as the tests with 2-dibromopropionic acid and 3-dibromopropionic acid show that the rate of reaction for 2-dibromopropionic acid is faster than for 3-dibromopropionic acid.

Eu.4.9 was also explored to see if any catalysis (with or without regioselectivity and enantioselectivity) as shown in Figure 4.40.

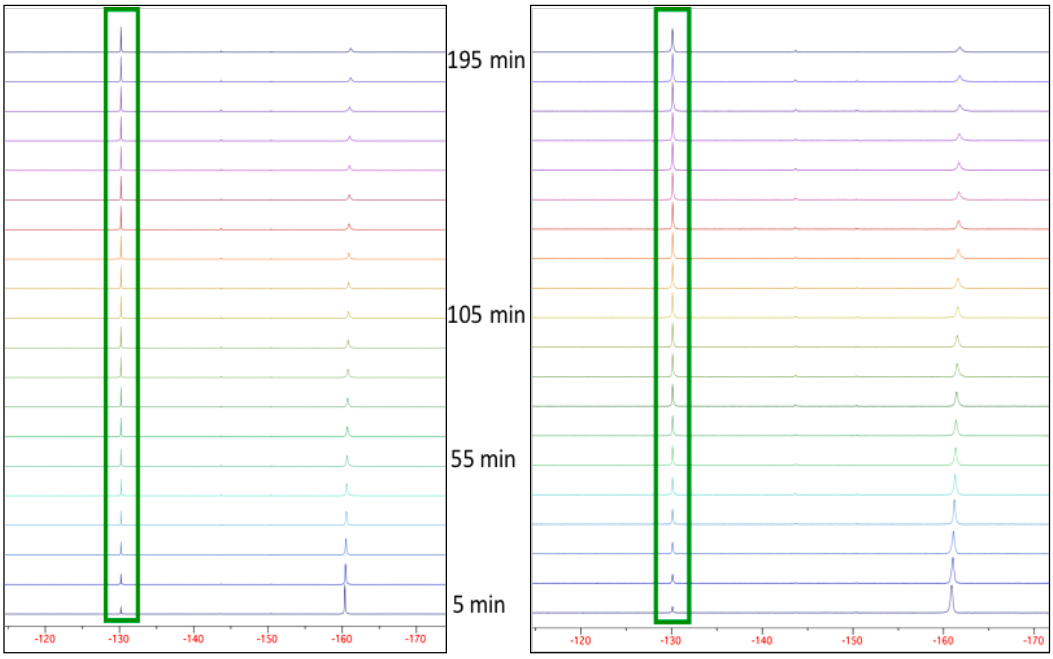

Figure 4.40: Comparison of ^{19}F NMR (298 K, D_2O, 500 MHz) for Left: Control 0.1 mol dm^{-3} 2,3-bromopropionic acid and 0.05 mol dm^{-3} TBAF.$3H_2O$. Right: Catalysed - 0.1 mol dm^{-3} 2,3-bromopropionic acid, 0.05 mol dm^{-3} TBAF.$3H_2O$ and 10% loading of Eu.4.9 over time

As shown for previous tests there is no catalysis in the presence of Eu.4.9. However, both the control and catalysed test both show the appearance of only one product peak, suggesting that as with Eu.4.8 one product is favoured, also likely to be the 2-fluoro-3-bromo-propinoic acid. These tests show that regioselective catalysis with Eu.4.8 is possible with evidence of only one fluorinated product in the ^{19}F NMR.

4.5 Conclusions

In this chapter I have shown the synthesis of two triamide complexes with pendant arms derived from N-acetylaspartate that vary in steric bulk and solubility. These complexes, along with Eu.p.DO3A, were used to explore fluoride binding, showing how their NMR spectra can be affected by changing the magnetic anisotropy of the system. Fluoride binding was also shown to affect the luminescence spectra for the three analogues with complex Eu.4.8 showing two binding events: an initial strongly bound equatorial fluoride, followed by the weak binding an axial fluoride. While complex Eu.4.9 showed a similar two step fluoride binding, it was preceded by the breakdown of large scale aggregation caused by self-assembly of the carboxylic acids on the N-acetylaspartate arms to nearby lanthanide complexes. Eu.p.DO3A also showed binding but only one binding event was observed due to the overall lower binding constants compared to the amide analogues resulting in the second weakly bound fluoride being in fast exchange.

Having assessed the fluoride binding of these systems, they were used to explore the unprecedented catalysis of series of α-halocarboxylic acids using a lanthanide bound in a chiral macrocycle. While Eu.4.9 showed no catalytic activity (due to the self-assembly causing large scale aggregation disrupting its ability to act as a catalyst), complexes Eu.4.8 and Eu.p.DO3A showed enhanced rate of reactions for several of these substrates, with Eu.p.DO3A able to enhance the rates of reaction in water. While these tests indicate these complexes have the potential to act as catalysts further work to measure and calculate turnover rates are needed to show the increased rates are not a stoichiometric enhancement but true catalysis.

While these tests act as a proof of concept for that the fluorination α-halocarboxylic acids can be successfully catalysed, the nature of these complexes means that they can be

modified to overcome solubility and self-assembly issues seen in this chapter. One such solution would be to attach the complexes to solid supports giving rise to heterogeneous catalysis.

4.6 References:

1. M. Woods, G. E. Kiefer, S. Bott, A. Castillo-Muzquiz, C. Eshelbrenner, L. Michaudet, K. McMillan, S. D. K. Mudigunda, D. Ogrin, G. Tircsó, S. Zhang, P. Zhao, and A. D. Sherry, *J. Am. Chem. Soc.*, 2004, **126**, 9248–56.
2. J.-C. G. Bünzli, *Chem. Rev.*, 2010, **110**, 2729–55.
3. D. Parker, R. S. Dickins, H. Puschmann, C. Crossland, and J. A. K. Howard, *Chem. Rev.*, 2002, **102**, 1977–2010.
4. O. A. Blackburn, A. M. Kenwright, P. D. Beer, and S. Faulkner, *Dalton Trans.*, 2015.
5. O. A. Blackburn, R. M. Edkins, S. Faulkner, A. M. Kenwright, D. Parker, N. J. Rogers, and S. Shuvaev, *Dalt. Trans.*, 2016, **45**.
6. O. A. Blackburn, N. F. Chilton, K. Keller, C. E. Tait, W. K. Myers, E. J. L. McInnes, A. M. Kenwright, P. D. Beer, C. R. Timmel, and S. Faulkner, *Angew. Chem. Int. Ed. Engl.*, 2015.
7. C. E. Housecroft and E. C. Constable, *Chemistry: An Introduction to Organic, Inorganic and Physical Chemistry*, Prentice Hall, 2010.
8. O. A. Blackburn, J. D. Routledge, L. B. Jennings, N. H. Rees, A. M. Kenwright, P. D. Beer, S. Faulkner, D. Parker, H. Puschmann, and S. Faulkner, *Dalt. Trans.*, 2016, **45**, 3070–3077.
9. O. A. Blackburn, A. M. Kenwright, A. R. Jupp, J. M. Goicoechea, P. D. Beer, and S. Faulkner, *Chem. - A Eur. J.*, 2016, **22**, 8929–8936.
10. A. Beeby, I. M. Clarkson, R. S. Dickins, S. Faulkner, D. Parker, L. Royle, A. S. de Sousa, J. A. G. Williams, and M. Woods, *J. Chem. Soc. Perkin Trans. 2*, 1999, 493–504.
11. O. Jacobson, D. O. Kiesewetter, and X. Chen, *Bioconjug. Chem.*, 2015, **26**, 1–18.
12. I. Ojima and 1945-, *Fluorine in medicinal chemistry and chemical biology*, Wiley-Blackwell, 2009.
13. S. Castellino and J. J. Sims, *Tetrahedron Lett.*, 1984, **25**, 4059–4062.
14. M. A. Giardello, V. P. Conticello, L. Brard, M. R. Gagne, and T. J. Marks, *J. Am. Chem. Soc.*, 1994, **116**, 10241–10254.
15. L. Sanzhong, Z. Baolian, X. Ming, A. JaÑczuk, X. Wenhua, C. Jinpei, and P. G. Wang, *Chinese Sci. Bull.*, 2001, **46**, 1673–1681.
16. T. Imamoto, T. Mita, and M. Yokoyama, *J. Org. Chem.*, 1987, **52**, 5695–5699.
17. J.-T. Hwang and C.-C. Liao, *Tetrahedron Lett.*, 1991, **32**, 6583–6586.
18. J. D. White and T. C. Somers, *J. Am. Chem. Soc.*, 1987, **109**, 4424–4426.
19. J. H. Walrod, D. A. Atwood, J. H. Walrod II, and D. A. Atwood, in *Encyclopedia of Inorganic and Bioinorganic Chemistry*, John Wiley & Sons, Ltd, Chichester, UK, 2012.
20. R. Osman, K. Namboodiri, H. Weinstein, J. R. Rabinowitz, H. Weinstein, and J. R. Rabinowitzs, *J. Am. Chem. Soc.*, 2002, **110**, 1701–1707.

5 Conclusions and future work

This thesis has explored the use of lanthanide complexes with heptadentate propargyl DO3A derivatives as building blocks in known and novel synthetises and their potential applications in anion binding, imaging and catalysis.

Firstly, propargylDO3A was used in click reactions with 2-azidopyridine to give complexes with multiple possible sites for protonation and coordination. Study of the pH dependence of the spectroscopic properties of these complexes, and of d-f hybrids derived from them, reveal a complex picture. These tests showed how the variation in ionic radius across the lanthanide series can affect whether the structure depends on pH and how the corresponding rhenium dyads can also result in quenching for the later lanthanides.

The potential use of strained dibenzocyclooctyne lanthanide complexes in bio-orthogonal click reactions in was also explored. While this work is still in the early stages, the results obtained show these structures are synthetically accessible. In the future, this work could be extended for uses in biologically relevant reactions and the possibility of varying the macrocycle to allow other metals such as Zr and Ga to be accommodated in a more appropriate binding pocket, allowing for imaging techniques such as PET to be used without recourse to new radioisotopes. Alternatively, the systems shown here have the potential to be used as theranostics (with 177-Lu), or as multimodal agents (using radioterbium isotopes).

The development of novel synthetic methods are a key step in creating new lanthanide based architectures which can be explored for potential applications. While key to the future progress of research, the development of new synthetic methods is not without challenges, as exemplified by the use of lanthanide complexes in gold catalysed coupling

explored in this thesis. Despite the challenges involved in this, it has been shown that this method can be used to create novel and interesting structures with high binding affinities for anions. Moreover, this technique also allows the synthesis of heterometallic complexes which show communication between the two lanthanide centres and can be modulated though the binding of a dianionic guest.

We have also explored how lanthanide complexes with heptadentate ligands bind to fluoride. We have established that there are two binding events by monitoring the changes in magnetic anisotropy and luminescent studies: initially formation of a strongly bound ternary complex involving equatorial fluoride binding is followed by weak binding of a second fluoride ion in the axial site on the lanthanide. It was then shown that the weakly bound axial fluoride can be displaced by competitive binding of a carboxylate, and that such displacement can be used to catalyse fluorination of α-halocarboxylic acids. Such catalysis is unprecedented and offers considerable scope for exploitation, though there are still unresolved issues surrounding self-assembly and water solubility of the complexes studied. It is proposed that further work could focus on the choice of pendant arms (for instance replacing aspartate residues with amines that would enhance solubility without leading to aggregation) or the use of solid-state supports to give heterogeneous catalysis, could be used to create effective catalysts that can be used in fluorination reactions which could be used in radiopharmaceutical and medical chemistry for ^{18}F labelling.

Throughout this thesis, we have also discussed the limitations of Horrocks equations, and have explored the challenges of accurately determining the value of q in lanthanide complexes. As we have discussed, in systems that show significant complexity the notion of q, as described by this equation, is often flawed. This is due in part to assumptions that the dominant quenching pathway is due to bound solvent molecules, but where this fails

to be the case, the calculated q values need to be treated with caution and taken in the context of the entire system. Furthermore, the role of quantum yield in weighting the observed lifetimes needs to be explored in detail.

6 Experimental Methods

6.1 General procedures

Commercially available solvents and reagents were used without further purification. Where anhydrous solvents used they were obtained by passing through a *MBraun MPSP-800 column* (degassed with nitrogen) and then used immediately. Water was deionised and microfiltered using a Milli-Q Millipore machine.

Silica TLC plates used were purchased from Merck (TLC Silica gel 60). Alumina TLC plates used were purchased from Sigma-Aldrich (aluminum oxide, pore size 60 Å, 254 nm indicator). Silica gel for column chromatography was purchased from Merck (Geduran, pore size 60 Å, 230 - 400 mesh, 40 - 63 μm) and neutral alumina was purchased from Sigma-Aldrich (aluminum oxide activated, neutral, Brockmann I, pore size 58 Å, 150 mesh); the neutral alumina was soaked in ethyl acetate before use.

Dialysis of lanthanide complexes was performed using a dialysis chamber purchased from Sigma Aldrich and using cellulose membrane with a 500 Da cut off. The complex was dissolved in deionised water, placed in the chamber with the appropriate membrane and the chamber was placed in a 5 L beaker filled with deionised water. Dialysis was effected through stirring for two days; the water being changed at least three times a day. Amberlite ion exchange resin® XAD16N 20-60 mesh was also used for the purification of lanthanide complexes where the complex was washed with water (minimum of 1 L) then the product recovered with 20 % acetonitrile.

NMR spectra were recorded at 298 K unless otherwise stated. NMR spectra were recorded at 298 K unless otherwise stated. 400 MHz ^{1}H NMR, 101 MHz ^{13}C NMR and 376 MHz ^{19}F NMR were recorded on a Bruker Avance III HD nanobay 400 MHz

spectrometer. 500 MHz ^{1}H NMR, 470 MHz ^{19}F NMR, DOSY spectra, COSY spectra, and NMR titrations were recorded on a Bruker Avance III 500MHz spectrometer NMR instruments. As is typical with such fluxional systems, ^{13}C-NMR spectra displayed very low signal to noise ratios and very broad resonances, making them unreliable and incomplete. The introduction of paramagnetic lanthanide centres only exacerbated the line broadening and took the recording of ^{13}C-spectra from exceedingly difficult to all but impossible. All coupling constants are quoted in Hz with all chemical shifts (δ) quoted in parts per million (ppm) and referenced to the residual solvent peak. Abbreviations when quoting NMR data are as follows: singlet (s), doublet (d), triplet (t), quartet (q), multiplet (m) and broad (br).

Mass spectra were obtained using either an Agilent Technology 1260 Infinity or a Waters LCT Premier XS. Accurate mass spectra were recorded to four decimal places using Bruker μTOF and Micromass GCT spectrometers and MALDI mass spectra were recorded on a Waters MALDI MicroMX.

UV-Visible spectroscopy was performed using a PG instruments T60u UV-Vis spectrophotometer. Solid state infra-red spectra were acquired using a Bio-Rad FTS 6000 Spectrometer.

Luminescence spectroscopy measurements were obtained using a HORIBA Jobin Yvon FluoroLog3 fluorimeter equipped with a Hamamatsu R928 detector and a double-grating emission monochromator; emission and excitation spectra were recorded at room temperature and in steady state mode unless otherwise stated. Emission lifetimes were obtained using the HORIBA Jobin Yvon FluoroLog3 fluorimeter system equipped with a Xenon flash lamp. Luminescence lifetimes were obtained by tail fit for Eu(III) and Tb(III) complexes using Fluoressence™ software. All lifetimes gave satisfactory fitting using a mono exponential decay function; attempted fitting to a double exponential decay

did not improve the fit unless otherwise stated. Near-infrared luminescence spectra from Yb(III) complexes were measured on the HORIBA Jobin Yvon FluoroLog3 fluorimeter system equipped with a Hamamatsu R5509-42 NIR PMT InGaAs detector cooled to -80 °C. Luminescence lifetimes of Yb(III) complexes were obtained by exciting the sample using a pulsed nitrogen laser (PTI-3301-337nm). Light emitted at right angles to the excitation beam was focused onto the slits of a monochromator (PTI120), which was used to select the appropriate Yb(III) emission wavelength (980 nm). The growth and decay of the luminescence at selected wavelengths was detected using a germanium photodiode (Edinburgh Instruments, EI-P) and recorded using a digital oscilloscope (Tektronix TDS220) before being transferred to the computer for analysis using Microsoft Excel. Luminescence lifetimes were obtained by iterative deconvolution of the detector response (obtained by using a scatter). pH values in water were measured using a Hanna Instruments pH210 Microprocessor pH Meter with a HI 1131B electrode.

6.2 Titration methodology

A non-dilution method was used for luminescence and NMR anion binding titrations. To ensure that the luminescence intensity was not altered by dilution, the titrant solutions were made using the complex stock solution as the solvent. The anion concentrations were typically more than one hundred times more concentrated than the lanthanide complex concentration. 1.5 mL of stock lanthanide solution was transferred to a quartz cuvette with a lid and then initial photophysical data was recorded. Successive emission spectra were recorded upon addition of known amounts of the titrant solution using an eppendorf pipette. In the case of a reverse titration the same no-dilution method as employed, where the complex solution was made using the anion stock solution as the solvent and with the complex concentration one hundred times more concentrated than the anion solution

6.3 Dynafit

Dynafit® was used to fit observed binding isotherms using procedures already developed in the group and discussed in detail in the literature.[1–3]

Example dynafit scripts

One binding event:

```
[task]
data = equil
task = fit
[mechanism]
Eu + F <==> EuF : K1 assoc
[constants]
K1 = 100??
[concentrations]
Eu= 1.87e-3
[responses]
[equil]
variable F
file ./pdo3a2.txt |response Eu = 1.4e11? , EuF = 1.4e9?
[output]
directory ./output/pDO3AJ2monoF
[end]
```

Two binding events:

```
[task]
data = equil
task = fit
[mechanism]
Eu + F <==> complex1 : K1 assoc
complex1 + F <==> comlpex2 : K2 assoc
[constants]
K1 = 1000??
K2 = 100??
[concentrations]
Eu= 1.14e-3
```

```
[responses]
[equil]
variable F
file ./252J1.txt |response Eu = 2.13e10 , complex1 = 1.10e8?
file ./252J2.txt |response Eu = 6.01e10 , complex1 = 1.67e8?
file ./252J4.txt |response Eu = 1.28e10 , complex1 = 4.58e7?
[output]
directory ./output/LM252
[end]
```

Reverse titration:

```
[task]
data = equil
task = fit
[mechanism]
Eu + acridone <==> complex1 : K1 assoc
[constants]
K1 = 1000??
[concentrations]
acridone= 5e-5
[responses]
[equil]
variable Eu
file ./acridone584603.txt | response complex1 = 9.35e10?
file ./acridone604635.txt | response complex1 = 1.36e10?
file ./acridone680710.txt | response complex1 = 5.71e10?
[output]
directory ./output/LM105acridone
[end]
```

6.4 Synthetic Methods

6.4.1 Click chemistry with DO3A complexes

2-azidopyridine 2.1[4]

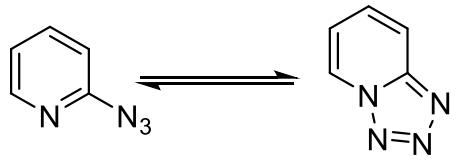

$TMSN_3$ was carefully added to a solution of 2-bromopyridine (0.48 ml, 5 mmol) and TBAF.xH_2O (1.31 g, 5 mmol). The solution was refluxed for 24 hours under N_2, resulting in an orange-red solution. Cooling to room temperature caused the solution to solidify and was dissolved in 2:98 methanol:dichloromethane (5 ml) then concentrated under reduced pressure. The residue was dissolved in ethyl acetate then washed with water and brine. The aqueous fractions were washed with ethyl acetate to recover crude product. The organic layers were combined dried ($MgSO_4$) and solvent removed under reduced pressure. The crude product was purified by column chromatography on silica with 2:98 MeOH:DCM to yield the product as a white solid (248 mg, 41 %).

^{1}H NMR (400 MHz, D_2O) δ_H/ppm 9.03 (dt, J = 7.0, 1.1 Hz, 1H), 8.10 (dt, J = 9.0, 1.1 Hz, 1H), 7.90 (ddd, J = 8.9, 6.8, 1.0 Hz, 1H), 7.46 (td, J = 6.9, 1.1 Hz, 1H). ^{13}C{^{1}H} (101 MHz; $CDCl_3$): δ_C /ppm 148.67, 131.99, 125.57, 116.71, 116.10. ESMS found *m/z* 242 for $[2M+2H]^+$.

tri-*tert*-butyl 2,2',2''-(1,4,7,10-tetraazacyclododecane-1,4,7-triyl)triacetate 2.2[5]

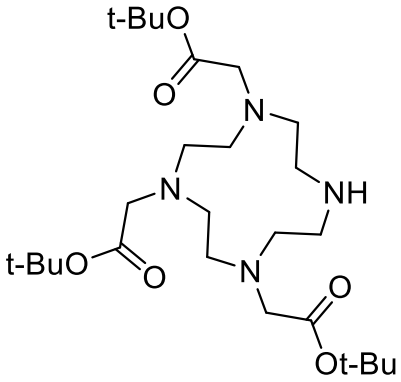

Cyclen (6.0 g, 34.8 mmol) was added to anhydrous acetonitrile (120 ml) and stirred until fully dissolved. $HNaCO_3$ (9.8 g, 116.7 mmol) was then added and stirred in an ice bath for 30 minutes. Tert-butyl bromoacetate (17.2 ml, 116.7 mmol) in anhydrous acetonitrile (80 ml) was added drop-wise over 30 minutes. The reaction stirred at room temperature for 48 hours under nitrogen. The inorganic solids were removed by filtration before the solvent removed under reduced pressure to give an off-white solid. Trituration with dichloromethane and hexane removed the excess tert-butyl bromoacetate starting material and recrystallized with toluene yielded the product as a white solid (9.09 g, 51 %).

^{1}H-NMR (400 MHz; $CDCl_3$): δ_H /ppm 10.04 (s, 1H), 3.39 (s, 4H), 3.31 (s, 2H), 3.12 (s, 4H), 2.94 (s, 12H), 1.48 (s, 27H). $^{13}C\{^{1}H\}$ (101 MHz, $CDCl_3$): δ_C /ppm 170.5, 169.6, 81.8, 81.7, 58.2, 51.3, 49.2, 47.5, 28.2, 28.2. ESMS found *m/z* 515 for $[M + H]^+$.

tri-*tert*-butyl 2,2',2''-(10-(prop-2-yn-1-yl)-1,4,7,10-tetraazacyclododecane-1,4,7-triyl)triacetate 2.3[6]

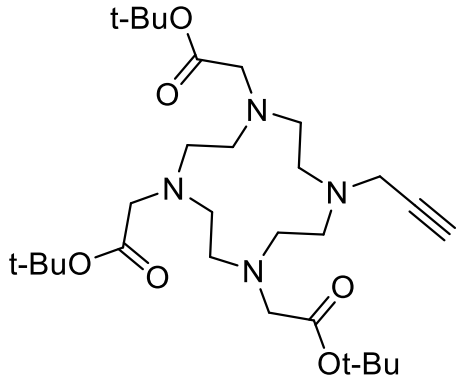

Compound **2.2** (6 g, 11.7 mmol) was dissolved in anhydrous acetonitrile (100 ml) before potassium carbonate (4.0 g, 29.2 mmol) was added and stirred for 20 minutes. In an ice bath propargyl bromide (1.0 ml, 11.7 mmol) was added drop-wise, then the reaction was stirred overnight at room temperature. The solution was filtered and the solvent removed under reduced pressure to give a pale oil, which was successively washed with toluene to give the title compound as a pale orange oil (3.1 g, 49 %).

^{1}H-NMR (400 MHz; $CDCl_3$): δ_H /ppm 3.36 (s, 2H), 3.22 (s, 6H), 2.76 (s, 12H), 2.62 (s, 4H), 2.07 (s, 1H), 1.38 (s, 27H). $^{13}C\{^{1}H\}$ (126 MHz; D2O): δ_C /ppm 170.60, 169.71, 81.93, 81.77, 58.30, 51.44, 49.29, 47.61, 28.32, 28.29. ESMS found *m/z* 553 for $[M + H]^+$.

2,2',2''-(10-(prop-2-yn-1-yl)-1,4,7,10-tetraazacyclododecane-1,4,7-triyl)triacetic acid 2.4[7]

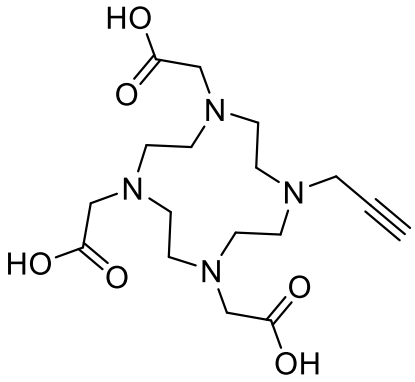

Compound **2.3** (0.7 g, 1.26 mmol) was dissolved in dichloromethane (8 ml) and TFA (8 ml) was added drop-wise, the solution was then stirred overnight at room temperature. The solvent was removed under reduced pressure and the residue was re-dissolved in the minimum amount of methanol and precipitated with diethyl ether. Trituration with diethyl ether produced the title compound as the bis-trifluoroacetate salt in a quantitative yield.

^{1}H-NMR (400 MHz; D_2O): δ_H /ppm 3.87-3.58 (m, 8H), 3.28 (m, 16H), 2.71 (s, 1H). $^{13}C\{^{1}H\}$ (126 MHz; D2O): δ_C /ppm 172.13, 162.77, 77.78, 66.00, 54.39, 49.71, 48.78, 43.60. ESMS found *m/z* 385 for $[M + H]^+$.

General synthesis of propargylDO3A lanthanide complexes

(Ln.p.DO3A) 2.5[7]

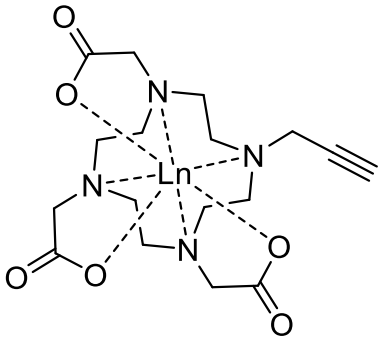

Compound **2.4** (1 equiv.) and lanthanide triflate (1.05 equiv.) in methanol (3 ml) were stirred for 30 minutes at 60 °C. The pH was adjusted to 4 by addition of aqueous NaOH, and the solution was stirred for 48 hours at 60 °C. The solvent was removed under reduced pressure and the resulting residue was dissolved in water the pH adjusted to 10 with aqueous NaOH to remove excess of lanthanide as its insoluble hydroxide. The resulting precipitate was centrifuged and the supernatant removed. The solvent was removed under reduced pressure and the product dissolved in the minimum amount of methanol and precipitated with diethyl ether. Further triturated with diethyl ether gave the desired product as a white solid.

Eu.2.5: Yield: 54 %. ^{1}H-NMR (400 MHz; D_2O) pD 10 δ_H /ppm 31.15, 22.81, 18.03, 13.62, 11.24, 10.09, -0.39, -0.83, -1.28, -3.93, -6.07, -6.73, -9.39, -11.25, -11.52, -12.32, -12.74, -14.65, -17.58, -20.09. Only resolved peaks outside 0-10 ppm region are reported. ESMS found *m/z* 557 for $[M+Na]^+$. Luminescence lifetime: H_2O: 0.49 ms, D_2O: 1.77 ms, q=1.5.

Gd.2.5: Yield: 58 %. ESMS found *m/z* 538 for $[M+H]^+$ and 561 for $[M+Na]^+$.

Tb.2.5: Yield: 53 %. ^{1}H-NMR (400 MHz; D_2O) pD 10 δ_H /ppm 462.42, 452.33, 315.87, 276.05, 104.08, 88.30, 82.77, 72.15, 60.06, 45.38, 12.04, -17.46, -39.12, -47.88, -49.33, -63.71, -70.23, -80.25, -86.14, -92.41, -111.76, -251.49, -268.36, -316.85, -407.08. Only resolved peaks outside 0-10 ppm region are reported. ESMS found *m/z* 563 for $[M+Na]^+$.

Yb.2.5: Yield: 67 %. ^{1}H-NMR (400 MHz; D_2O) pD 10 δ_H /ppm 134.73, 85.93, 62.80, 53.79, 39.64, 29.89, 24.51, 23.32, 20.18, 12.28, -4.93, -8.52, -10.95, -11.72, -17.75, -18.05, -20.01, -20.49, -30.15, -37.80, -45.74, -52.75, -56.42, -56.98, -82.61. Only resolved peaks outside 0-10 ppm region are reported. ESMS found *m/z* 577 for $[M+Na]^+$.

Lu.2.5: Yield: 60 %. ^{1}H-NMR (400 MHz; D_2O) pD 10 δ_H /ppm 3.99-3.81 (m, 2H), 3.74-3.40 (m, 6H), 3.28-2.74 (m, 16H), 2.30 (s, 1H). ESMS found *m/z* 579 for $[M+Na]^+$.

General synthesis of click complexes with lanthanide propargylDO3A complexes and 2-azidopyridine 2.6

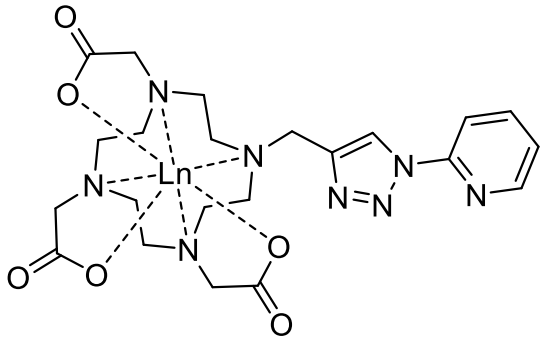

Complex **Ln.2.5** (1 equiv.), 2-azidopyridine (1.1 equiv.) and $(CuOTf)_2.C_6H_6$ (0.1 equiv.) were dissolved in methanol and stirred under N_2 at 75 °C for 24 hours. The solvent was removed under reduced pressure and the residue dissolved in water and extracted with diethyl ether. The aqueous layer was collected and the solvent removed under reduced pressure. The green residue was triturated with methanol and diethyl ether and filtered to yield the product as a light green powder. The product was purified further with Cuprisorb® stirring in water for several hours before being filtered and the solvent removed under reduced pressure to give a white solid. Salt was then removed by amberlite ion exchange column eluting with 20 % acetonitrile to isolate the product.

Eu.2.6: Yield: 19 %. ^{1}H-NMR (400 MHz; D_2O): δ_H /ppm 29.53, 26.49, 26.27, 25.54, 23.03, 14.88, 13.84, 12.11, 11.38, 10.17, -0.42, -1.11, -3.84, -5.13, -6.00, -6.56, -7.80, -8.49, -9.32, -10.42, -11.07, -11.46, -12.26, -12.78, -13.89, -14.57, -16.78, -17.52, -18.60, -19.41. Only resolved peaks outside 0-10 ppm region are reported. MALDI-MS (α-MeOH) found *m/z*: 654.03, calculated *m/z* 654.14 for $[C_{22}H_{29}O_6N_8Eu]$. UV-Vis (H_2O): λ_{max}/nm= 270.

Tb.2.6: Yield: 15 %. ^{1}H-NMR (400 MHz; D_2O): δ_H /ppm 162.10, 156.03, 102.83, 73.78, 49.74, 13.95, -0.43, -14.98, -18.81, -20.56, -22.29, -54.93, -62.04, -68.59, -71.45, -80.29, -85.81, -111.38, -139.61, -148.45, -292.62. Only resolved peaks outside 0-10 ppm region are reported. ESMS found *m/z* 683 for $[M+Na]^+$, HR-ESMS found *m/z* 683.1354, calculated *m/z* 683.13557 for $[C_{22}H_{29}O_6N_8TbNa]^+$. UV-Vis ($H_2O$): λ_{max}/nm= 270.

Gd.2.6: Yield: 17 %. MALDI-MS (α-MeOH) found *m/z*: 659.00, calculated *m/z* 659.14 for $[C_{22}H_{29}O_6N_8Gd]$. UV-Vis (H_2O): λ_{max}/nm= 270. $E_T \approx 25000$ cm^{-1}.

Yb.2.6: Yield: 16 %. ^{1}H-NMR (400 MHz; D_2O) pD 12: δ_H /ppm 115.81, 110.27, 88.97, 86.04, 80.81, 73.64, 62.94, 60.23, 53.62, 39.81, 29.89, 26.71, 24.22, 23.59, 12.26, 10.17, -0.18, -4.84, -6.98, -8.54, -11.11, -11.94, -16.71, -18.23, -19.31, -20.26, -30.24, -36.53, -50.29, -52.69, -55.71, -56.42, -59.92, -61.10, -65.32, -66.23, -68.60, -84.18, -106.61, -117.18. Only resolved peaks outside 0-10 ppm region are reported. ESMS found *m/z* 699 for $[M+Na]^+$, HRMS found *m/z* 699.15504, calculated *m/z* 699.15691 for $[C_{22}H_{29}O_6N_8YbNa]^+$. UV-Vis ($H_2O$): λ_{max}/nm= 270.

Lu.2.6: Yield: 11 %. ^{1}H-NMR (400 MHz; D_2O) pD 12: δ_H /ppm 8.59 (d, J = 5.2 Hz, 1H), 8.16 (t, J = 7.6 Hz, 1H), 8.06 (d, J = 7.5 Hz, 1H), 7.62 (t, J = 5.8 Hz, 1H), 4.41-1.57 (m, 25H). MALDI-MS (α-MeOH) found *m/z*: 675.77 calculated *m/z* 675.16 for $[C_{22}H_{28}O_6N_8Lu]^-$. UV-Vis (H_2O): λ_{max}/nm= 270.

General synthesis of d-f hybrids from lanthanide click complexes 2.7

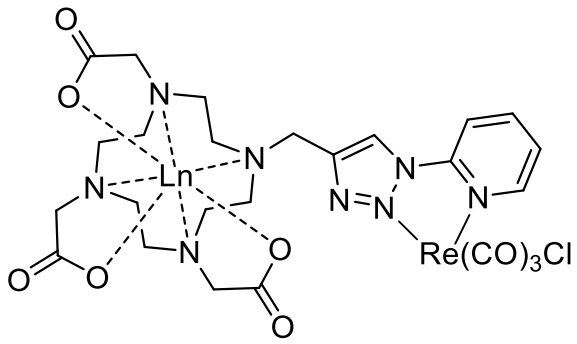

Complex **2.6** (1 equiv.) and $[Re(CO)_5Cl]$ (1.2 equiv.) in anhydrous THF were refluxed for 48 hours. The solvent was removed under reduced pressure and the residue dissolved in water and extracted with toluene. The solvent was removed under reduced pressure and the residue triturated with methanol and diethyl ether to afford the product as a solid precipitate.

EuRe.2.7: Yield: 26 % ^{1}H-NMR (400 MHz; D_2O): δ_H /ppm 29.52, 26.47, 26.27, 25.54, 23.05, 14.88, 13.80, 12.11, 11.39, 10.17, -0.42, -1.11, -3.84, -5.13, -6.00, -6.56, -7.80, -8.49, -9.32, -10.42, -11.09, -11.46, -12.26, -12.78, -13.89, -14.57, -16.78, -17.52, -18.60, -19.41. Only resolved peaks outside 0-10 ppm region are reported. IR-ATR $\nu_{C=O}$ /cm^{-1}: 2020, 1898. UV-Vis (H_2O): λ_{max}/nm= 260, 375.

GdRe.2.7: Yield: 37 %. IR-ATR $\nu_{C=O}$ /cm^{-1}: 2021, 1864. UV-Vis (H_2O): λ_{max}/nm= 260, 375. $E_T \approx 18000$ cm^{-1}.

TbRe.2.7: Yield: 34 % ^{1}H-NMR (400 MHz; D_2O): δ_H /ppm 162.11, 156.05, 102.83, 73.78, 49.76, 13.95, -0.45, -14.98, -18.81, -20.56, -22.29, -54.94, -62.04, -68.57, -71.45,

-80.29, -85.81, -111.38, -139.61, -148.45, -292.62. Only resolved peaks outside 0-10 ppm region are reported. IR-ATR $\nu_{C=O}$ /cm^{-1}: 2019, 1881. UV-Vis (H_2O): λ_{max}/nm= 260, 375.

YbRe.2.7: Yield: 29 % ^{1}H-NMR (400 MHz; D_2O) pD 12: δ_H /ppm 115.80, 110.27, 88.99, 86.04, 80.83, 73.64, 62.94, 60.23, 53.62, 39.81, 29.88, 26.71, 24.22, 23.59, 12.26, 10.17, -0.18, -4.85, -6.98, -8.54, -11.13, -11.94, -16.71, -18.23, -19.32, -20.25, -30.23, -36.53, -50.29, -52.68, -55.71, -56.42, -59.92, -61.11, -65.32, -66.23, -68.61, -84.18, -106.61, -117.18. Only resolved peaks outside 0-10 ppm region are reported. IR-ATR $\nu_{C=O}$ /cm^{-1}: 2018, 1899. UV-Vis (H_2O): λ_{max}/nm= 260, 375.

LuRe.2.7: Yield: 32 % ^{1}H-NMR (400 MHz; D_2O) pD 12: δ_H /ppm 8.58 (d, *J* = 5.2 Hz, 1H), 8.14(t, *J* = 7.6 Hz, 1H), 8.06 (d, *J* = 7.5 Hz, 1H), 7.62 (t, *J* = 5.8 Hz, 1H), 4.45-1.59 (m, 25H). IR-ATR $\nu_{C=O}$ /cm^{-1}: 2021, 1901. UV-Vis (H_2O): λ_{max}= 260, 375.

5*H*-dibenzo[*a*,*d*][7]annulen-5-one oxime 2.8[8]

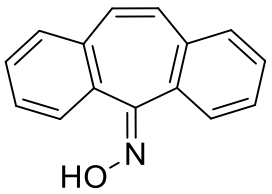

5-Dibenzosuberenone (25.0 g, 121 mmol), hydroxylamine hydrochloride (11.4 g, 164 mmol) and pyridine (70 ml) were refluxed at 125 °C for 20 hours. The solution was concentrated under reduced pressure and added to aqueous hydrochloric acid (5 % in 500 ml) and the mixture stirred for 20 minutes. The white precipitate was collected by

filtration and dried under vacuum to give crude dibenzosuberenone oxime (28.8 g). This crude product was used without further purification.

^{1}H-NMR (400 MHz; $CDCl_3$): δ_H /ppm 8.75 (br s, 1H), 7.71-7.64 (m, 1H), 7.63-7.56 (m, 1H), 7.47-7.34 (m, 6H), 6.92 (d, J = 3.1 Hz, 2H). ^{13}C{^{1}H} (101 MHz; $CDCl_3$): δ_C /ppm 156.45, 135.45, 134.58, 133.76, 130.84, 130.62, 130.57, 129.47, 129.21, 129.05, 128.95, 128.82, 127.85, 127.69. ESMS found *m/z* 222 for $[M+H]^+$.

(*Z*)-dibenzo[*b*,*f*]azocin-6(5*H*)-one 2.9[8]

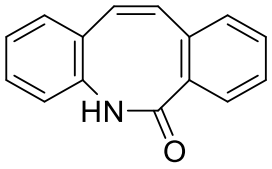

The crude dibenzosuberenone oxime **2.8** (8.0 g, 36 mmol) was added to polyphosphoric acid (125 ml) at 125 °C and heated at this temperature for 1 hour. The solution was poured into ice water (400 ml) and stirred for 30 minutes. The grey precipitate was collected by filtration and dried under vacuum (6.0 g, 75 %).

^{1}H-NMR (400 MHz; $CDCl_3$): δ_H /ppm 7.66 (s, 1H), 7.47 (dd, J = 7.6, 1.5 Hz, 1H), 7.30 (td, J = 7.5, 1.6 Hz, 1H), 7.25-7.11 (m, 5H), 7.06-7.04 (m, 1H), 6.96 (d, J = 11.7 Hz, 1H), 6.85 (d, J = 11.7 Hz, 1H). ^{13}C{^{1}H} (101 MHz; $CDCl_3$): δ_C /ppm 173.81, 135.42, 135.20, 134.84, 134.19, 133.14, 129.87, 129.71, 129.30, 128.42, 128.37, 128.18, 127.74, 127.14, 126.40. ESMS found *m/z* 222 for $[M+H]^+$ and 244 for $[M+Na]^+$.

(*Z*)-5,6-dihydrodibenzo[*b*,*f*]azocine 2.10[8]

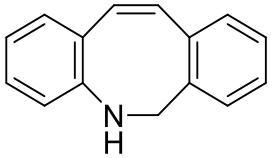

Dibenzo[b,f]azocin-6(5H)-one **2.9** (5.6 g, 25 mmol) was dissolved in anhydrous diethyl ether (130 ml) and LiAlH (2 g, 50 mmol) was added under N_2 and the solution refluxed under N_2 for 15 hours. The solution was quenched with iced water and the resulting green precipitate collected via filtration and dried. The precipitate was then washed with diethyl ether before the precipitate was dispersed in diethyl ether (100 ml) and stirred for 10 minutes before the solution was filtered. The filtrates were combined, dried ($MgSO_4$) and the solvent removed under reduced pressure giving the desired product as a yellow solid (3.7 g, 71 %).

^{1}H-NMR (400 MHz; CD_3CN): δ_H /ppm 7.29-7.19 (m, 3H), 7.16-7.14 (m, 1H), 6.90-6.82 (m, 2H), 6.57-6.49 (m, 2H), 6.46 (dd, J = 8.1, 1.0 Hz, 1H), 6.36 (d, J = 12.9 Hz, 1H), 4.99 (s, 1H), 4.51 (d, J = 7.3 Hz, 2H). $^{13}C\{^1H\}$ (101 MHz; $CDCl_3$): δ_C /ppm 147.23, 139.30, 18.24, 136.83, 132.83, 130.24, 128.96, 128.05, 127.71, 127.45, 127.44, 121.84, 118.03, 117.79, 49.64. ESMS found *m/z* 208 for $[M+H]^+$.

(Z)-2-chloro-1-(dibenzo[b,f]azocin-5(6H)-yl)ethan-1-one 2.11

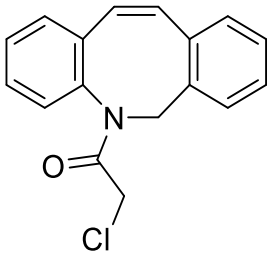

To 5,6-dihydrodibenzo[b,f]azocine **2.10** (1.5 g, 7.3 mmol) in dichloromethane (70 ml) $CsCO_3$ (5.6 g, 17.4 mmol) was added. At 0 °C chloroacetyl chloride (0.7 ml, 8.7 mmol) was added dropwise and the solution warmed to room temperature and stirred overnight. The solution was filtered and the filtrate washed with water (3 x 100 ml), the organics were dried ($MgSO_4$) and the solvent removed under reduced pressure (1.8 g, 91 %).

^{1}H-NMR (400 MHz; acetone-d6): δ_H /ppm 7.47-7.42 (m, 1H), 7.38-7.30 (m, 4H), 7.20-7.14 (m, 3H), 6.88 (d, J = 12.9 Hz, 1H), 6.76 (d, J = 12.9 Hz, 1H), 5.44 (d, J = 15.1 Hz, 1H), 4.33 (d, J = 15.1 Hz, 1H), 3.86 (d, J = 13.4 Hz, 1H), 3.74 (d, J = 13.4 Hz, 1H). ^{13}C{^{1}H} (101 MHz, $CDCl_3$) δ_C /ppm 165.51, 139.13, 136.18, 135.85, 133.46, 132.77, 131.46, 130.92, 130.20, 128.51, 128.42, 127.66, 127.26, 127.24, 127.11, 54.80, 42.13. HR-ESI-MS found *m/z* 306 for $[M+Na]^+$.

tri-*tert*-butyl 2,2',2''-(10-(2-(dibenzo[*b*,*f*]azocin-5(6*H*)-yl)-2-oxoethyl)-1,4,7,10-tetraazacyclododecane-1,4,7-triyl)(*Z*)-triacetate 2.12

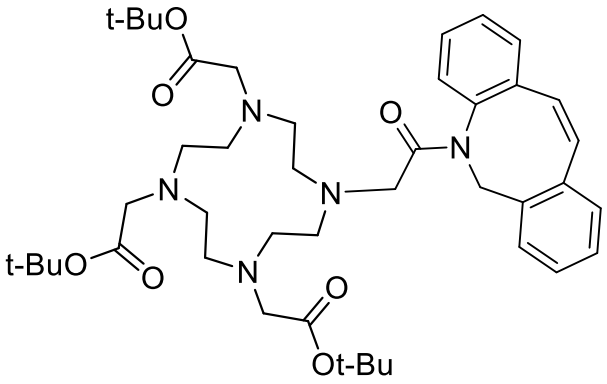

2-Chloro-1-(dibenzo[b,f]azocin-6(5H)-yl)ethan-1-one **2.11** (1.58 g, 5.6 mmol), **2.2** (1.9 g, 3.7 mmol) and potassium carbonate (4 g, 29 mmol) in acetonitrile (50 ml) were heated to reflux for 48 hours. The solvent was then removed under reduced pressure and the residue dissolved in dichloromethane. The solution was then filtered and the solvent removed under reduced pressure. (2.5 g, 93 %).

^{1}H NMR (400 MHz; $CDCl_3$); δ_H /ppm 7.19-6.99 (m, 8H), 6.74-6.64 (m, 1H), 6.54-6.46 (m, 1H), 5.21 (m, J = 10.9 Hz, 2H), 2.69 (m, 24H), 1.43-1.27 (m, 27H). ESMS found *m/z* 762 for $[M+H]^+$ and 784 for $[M+Na]^+$. HRMS found *m/z* 762.4795 calculated *m/z* 762.4800 for $[C_{43}H_{64}N_5O_7]^+$.

tri-*tert*-butyl 2,2',2''-(10-(2-(11,12-dibromo-11,12-dihydrodibenzo[*b*,*f*]azocin-5(6*H*)-yl)-2-oxoethyl)-1,4,7,10-tetraazacyclododecane-1,4,7-triyl)triacetate **2.13**

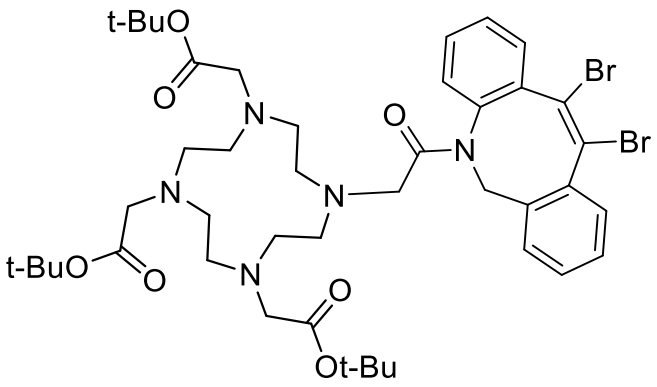

Compound **2.12** (1g, 1.31 mmol) and pyridinium tribromide (0.46 g, 1.44 mmol) were dissolved in dichloromethane (4 ml) and the solution stirred at room temperature overnight. The solution was diluted with dichloromethane, washed with 5 % aqueous hydrochloric acid (2 x 10 ml) and the organic layer dried over $MgSO_4$ and the solvent removed under reduced pressure. (164 mg, 14 %).

^{1}H-NMR (400 MHz; $CDCl_3$): δ_H/ppm 7.52-7.46 (m, 2H), 7.25-6.80 (m, 8H), 5.69 (m, 2H), 4.20-2.95 (m, 24H), 1.51 (m, 27H).

5-(11,12-Didehydrodibenzo[b,f]azocin-5(6H)-yl)-4-(2-Eu.DO3A)-acetaldehyde 2.16

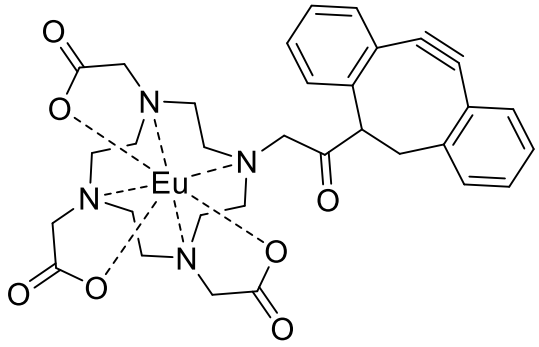

A solution of potassium tert-butoxide (121 mg, 1.08 mmol) in THF (4 ml) was added to compound **2.13** (397 mg, 0.43 mmol) in THF (2 ml) and the solution stirred at room temperature for 1 hour. The solution was diluted with ethyl acetate and was acidified with 5 % aqueous hydrochloric acid (3 x 20 ml) and brine (3 x 20 ml). The organics were collected are dried over Na_2SO_4, filtered and the solvent removed under reduced pressure and the crude product (**2.14**) was used without further purification. Crude **2.14** (200 mg, 0.2 mmol) was then dissolved in dichloromethane (3 ml) and TFA (3 ml) was slowly added to the solution and stirred at room temperature for 24 hours. The solvent was removed under reduced pressure and the residue triturated from methanol and diethyl ether to yield 2.15 as an orange-brown solid. Crude compound **2.15** (100 mg, 0.17 mmol) was then dissolved in methanol (2 ml) and stirred at 60 °C for 20 minutes, before europium triflate (110 mg, 0.18 mmol) was added and the solution stirred at 60 °C for 48 hours. The solvent was then removed under reduced pressure and the triturated with methanol and diethyl ether and the solid collected by filtration (115 mg, 47 %).

^{1}H NMR (400 MHz, d_4-methanol) δ_H/ppm 34.51, 32.66, 32.08, 31.69, 30.97, 10.90, -0.58, -1.69, -2.65, -3.46, -4.32, -4.94, -5.47, -7.67, -8.03, -8.65, -10.94, -13.00, -13.74, -14.29, -14.94, -15.21, -15.46, -15.82, -16.80, -17.98, -19.28. Only resolved peaks outside

0-10 ppm region are reported. MALDI-MS (α-MeOH) found *m/z*: 764.1112, calculated *m/z* 764.1562 for $[C_{31}H_{34}EuN_5O_7N_a]^+$. Luminescence lifetimes: MeOH: 0.89 ms, MeOD: 1.71 ms, q=1.

2-chloro-1-(11,12-dibromo-11,12-dihydrodibenzo [b,f]azocin-5(6H)-yl)ethan-1-one 2.17

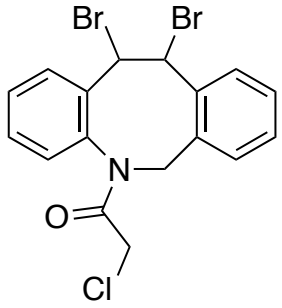

2-Chloro-1-(dibenzo[*b*,*f*]azocin-5(6*H*)-yl)ethan-1-one **2.11** (5.55 g, 19.56 mmol) was dissolved in dichloromethane (25 ml). Pyridinium tribromide (6.88 g, 21.51 mmol) was added and the reaction mixture stirred overnight at room temperature. The reaction was quenched with dichloromethane (50 ml), washed with 2 M hydrochloric acid (3 x 75 ml) and water (1 x 75 ml). The organic layer dried over $MgSO_4$ and the solvent removed under reduced pressure to yield 3.70 g crude product. 1.0 g of the crude product was then dissolved in ethyl acetate/dichloromethane 1:1 v/v and left to stand for 1 hour. The mixture was then filtered, and the product collected as an off-white solid (0.49 g, 21 %).

^{1}H-NMR (400 MHz, $CDCl_3$): δ_H /ppm 7.75 (d, *J* = 7.8 Hz, 1H), 7.32-7.05 (m, 6H), 6.93 (d, *J* = 7.3 Hz, 1H), 5.91-5.76 (m, 2H), 5.19 (d, *J* = 9.6 Hz, 1H), 4.28 (d, *J* = 14.7 Hz, 1H), 4.10 (d, *J* = 12.9 Hz, 1H), 3.90 (d, *J* = 12.9 Hz, 1H). ^{13}C{^{1}H} (126 MHz, $CDCl_3$): δ_C /ppm 166.83, 138.38, 137.10, 135.93, 132.17, 130.89, 130.84, 130.51, 130.30, 129.93,

129.35, 129.26, 128.84, 60.02, 55.42, 53.07, 43.05. ESMS found *m/z* 444 $[M+H]^+$. HRMS found *m/z* = 443.91813 calculated 443.91885 for $[C_{17}H_{15}Br_2ClNO]^+$.

5-(11,12-Didehydrodibenzo[b,f]azocin-5(6H)-yl)-4-(2-Chloro)-acetaldehyde 2.18

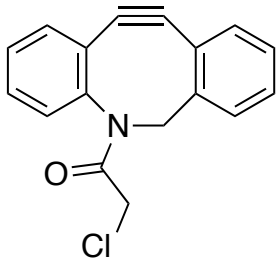

2-Chloro-1-(11,12-dibromo-11,12-dihydrodibenzo[*b*,*f*]azocin-5(6*H*)-yl)ethan-1-one **2.17** (200 mg, 0.45 mmol) was dissolved in anhydrous THF (2 ml). A 1 M solution of potassium tert-butoxide in THF (1.13 ml, 1.13 mmol) was added dropwise and the solution stirred at room temperature for 2 hours. A further portion of ^{t}BuOK solution (0.56 ml, 0.56 mmol) was then added dropwise and the mixture stirred for a further 2 hours. The reaction mixture was then diluted with ethyl acetate (10 ml), washed with hydrochloric acid (1 x 15 ml), deionised water (2 x 15 ml) and brine (1 x 15 ml) and dried over $MgSO_4$ and the solvent removed *in vacuo* to yield crude **2.18** as a red solid (122 mg, 96 %).

^{1}H-NMR (400 MHz, $CDCl_3$): δ 7.64 (d, J = 7.8 Hz, 1H), 7.59 (d, J = 8.1 Hz, 1H), 7.40 (d, J = 7.4 Hz, 1H), 7.36-7.27 (m, 2H), 7.24 (t, J = 7.4 Hz, 1H), 7.13 (t, J = 7.6 Hz, 1H), 7.03 (t, J = 7.6 Hz, 1H), 6.56 (s, 1H), 5.01 (s, 2H), 1.18 (s, 1H).

1-(1-benzyl-1,9-dihydro-8*H*-dibenzo[*b*,*f*][1,2,3]triazolo[4,5-*d*]azocin-8-yl)-2-(Eu.DO3A) -1-one 2.19

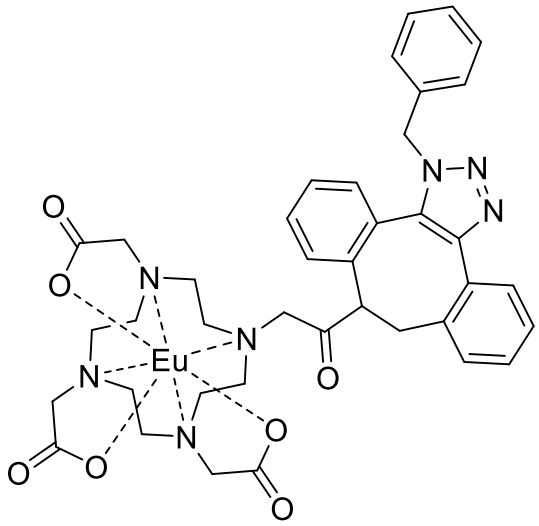

Complex **2.16** (95 mg, 0.13 mmol) was dissolved in methanol (2 ml) and benzyl azide added (0.021 ml, 1 eq.). The reaction mixture was stirred for 24 hours, before the solvent was removed *in vacuo* to yield the product as a red solid (70 mg, 62 %).

^{1}H NMR (400 MHz, d_4-methanol) δ_H /ppm 36.50, 35.04, 33.89, 33.48, 32.74, 32.19, 11.61, -2.68, -3.32, -3.65, -4.15, -4.56, -6.73, -7.19, -7.42, -8.00, -8.38, -10.37, -12.78, -15.36, -15.83, -16.09, -16.82, -17.15, -18.64, -19.26, -20.03. Only resolved peaks outside 0-10 ppm region are reported. Luminescence lifetimes: MeOH: 0.85 ms, MeOD: 1.76 ms, q=1.

6.4.2 Gold catalysed couplings with p.DO3A complexes

General synthesis of three component gold couplings with lanthanide propargylDO3A complexes, benzaldehyde and piperidine 3.1

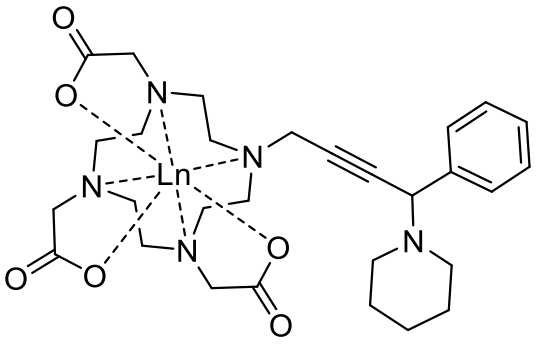

Ln.p.DO3A (2 equiv.) benzaldehyde (10 equiv.), piperidine (10 equiv.) and gold chloride trihydrate (1 equiv.) in water (3 ml) were heated to 40 °C for 20 hours. The solution was diluted with methanol and filtered. The solvent was removed under reduced pressure and the resulting residue triturated with methanol and diethyl ether. The yellow solid was washed further with diethyl ether and the crude solid purified by amberlite ion exchange column eluting with 20 % acetonitrile to isolate the product.

Lu.3.1: Yield: 45 %. ^{1}H-NMR (400 MHz; D_2O) δ_H /ppm 7.78 (m, 2 H), 7.42 (m, 3 H), 3.84-2.33 (m, 35 H).

Eu.3.1: Yield: 40 %. ^{1}H-NMR (400 MHz; D_2O) δ_H /ppm 39.30, 36.46, 31.45, 28.98, 25.85, 16.44, 13.06, -1.87, -2.70, -3.65, -4.44, -5.62, -7.59, -9.33, -9.62, -10.77, -12.08, -13.17, -17.23, -19.49, -21.85, -23.56, -32.86. Only resolved peaks outside 0-10 ppm region are reported.

General synthesis of three component gold couplings with lanthanide propargylDO3A complexes, 2-naphthaldehyde and piperidine 3.2

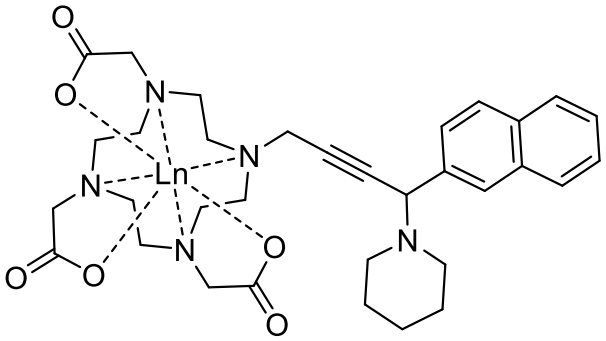

Ln.p.DO3A (2 equiv.) 2-naphthaldehyde (10 equiv.), piperidine (10 equiv.) and gold chloride trihydrate (1 equiv.) in water (3 ml) were heated to 40 °C for 20 hours. The solution was diluted with methanol and filtration. The solvent was removed under reduced pressure and the resulting residue triturated with methanol and diethyl ether. The yellow solid was washed further with diethyl ether and ethyl acetate to remove starting materials then the crude solid was purified by amberlite ion exchange column eluting with 20 % acetonitrile to isolate the product.

Lu.3.2: Yield: 35 %. ^{1}H-NMR (400 MHz; D_2O) δ_H /ppm 8.44-7.59 (m, 7 H), 3.94-1.07 (m, 35 H).

Eu.3.2: Yield: 31 %. ^{1}H-NMR (400 MHz, D_2O)) δ_H /ppm 44.70, 42.01, 38.63, 37.55, 34.67, 33.79, 32.91, 31.57, 24.53, 23.27, 22.22, 18.19, 17.96, 16.28, 15.82, 14.24, 13.49, 12.77, 10.13, -1.06, -2.85, -3.63, -4.92, -6.65, -7.97, -8.88, -9.18, -10.63, -11.40, -12.70, -13.43, -14.55, -15.69, -16.03, -16.92, -18.12, -18.60, -19.02, -20.20, -21.58, -22.94, -26.12, -39.24. Only resolved peaks outside 0-10 ppm region are reported.

prop-2-yn-1-ylcarbamic bromide 3.3[9]

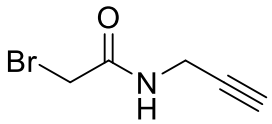

To a solution of propargylamine (2 ml, 31 mmol) in dichloromethane (100 ml) was added an aqueous NaOH (0.1 M) as a layer on top. Bromoacetyl bromide (8.6 ml, 99 mmol) was carefully added to the dichloromethane layer producing a white precipitate. The solution was stirred for 2.5 hours at room temperature producing a clear red-brown solution. The solution was diluted with water and dichloromethane and separated, the aqueous layer was washed with dichloromethane and the organics combined and washed with an aqueous Na_2CO_3 (50 mM). The organics were dried ($MgSO_4$) and the solvent removed under reduced pressure then placed in a vacuum desiccator overnight to yield the product as a tan solid (1.74 g, 32 %).

^{1}H-NMR (400 MHz; $CDCl_3$): δ_H /ppm 6.68 (s, 1H), 4.11 (dd, J = 5.3, 2.5 Hz, 2H), 3.92 (s, 2H), 2.30 (t, J = 2.5 Hz, 1H). $^{13}C\{^1H\}$ (101 MHz; $CDCl_3$): δ_C /ppm 165.55, 78.69, 72.24, 30.01, 28.71. ESMS found *m/z* 176 for $[M+H]^+$.

tri-*tert*-butyl 2,2',2''-(10-(2-oxo-2-(prop-2-yn-1-ylamino)ethyl)-1,4,7,10-tetraazacyclododecane-1,4,7-triyl)triacetate 3.4[9]

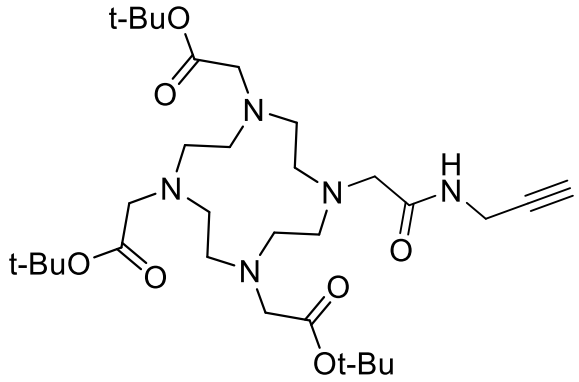

2-Bromo(propargyl) acetamide **3.3** (0.90 g, 5.11 mmol), **2.2** (2.2 g, 4.3 mmol) and potassium carbonate (4.7 g, 34 mmol) in acetonitrile (120 ml) were refluxed for 48 hours. The solvent was then removed under reduced pressure and the residue dissolved in dichloromethane. The solution was then filtered and the solvent removed under reduced pressure. (1.87 g, 71 %).

^{1}H-NMR (400 MHz; $CDCl_3$): δ_H /ppm 9.28 (br.s, 1H), 3.96-3.87 (m, 2H), 3.49-1.74 (m, 25 H), 1.37-1.35 (m, 27H). $^{13}C\{^{1}H\}$ (101 MHz; $CDCl_3$): δ_C /ppm 171.74, 171.70, 171.61, 81.75, 69.51, 57.76, 56.62, 56.35, 27.88, 27.79. ESMS found *m/z* 610 for $[M+H]^+$ and 632 for $[M+Na]^+$.

2,2',2''-(10-(2-oxo-2-(prop-2-yn-1-ylamino)ethyl)-1,4,7,10-tetraazacyclododecane-1,4,7-triyl)triacetic acid 3.5[10]

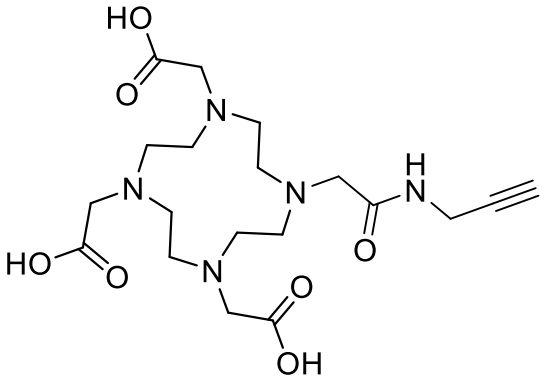

Compound **3.4** (1.87 g, 3.07 mmol) was dissolved in dichloromethane (20 ml) and TFA (20 ml) was added drop-wise, the solution was then stirred overnight at room temperature. The solvent was removed under reduced pressure and the residue was re-dissolved in the minimum amount of methanol and precipitated with diethyl ether. Trituration with diethyl ether produced the title compound as the bis-trifluoroacetate salt. (1.1 g, 81 %).

^{1}H-NMR (400 MHz; D_2O) δ_H /ppm 3.96 (s, 2H), 3.86 (s, 3H), 3.66 (s, 3H), 3.58 (m, 2H), 3.40 (br s, 8H), 3.15 (br s, 8H), 2.61 (s, 1H). ^{13}C{^{1}H} (126 MHz; D_2O): δ_C /ppm 165.95, 164.86, 82.16, 74.29, 57.92, 52.66, 50.99, 31.34. ESMS found *m/z* 441 for $[M+H]^+$ and 464 for $[M+Na]^+$.

General synthesis of lanthanide propargyl acetamideDO3A complexes

3.6

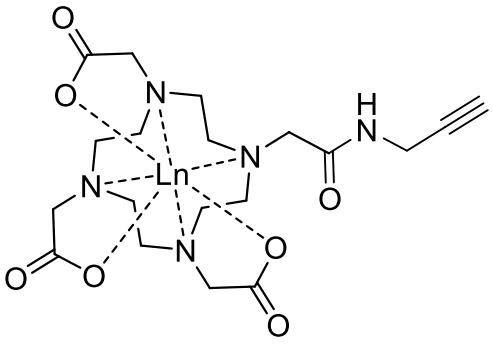

Compound **3.5** (1 equiv.) and lanthanide triflate (1.05 equiv.) in methanol (3 ml) were stirred for 30 minutes at 60 °C. The pH was adjusted to 4 by addition of aqueous NaOH. The solution was stirred for 48 hours at 60 °C. The solvent was removed under reduced pressure. The residue was dissolved in water the pH adjusted to 10 with aqueous NaOH to remove excess of lanthanide as its insoluble hydroxide. The resulting precipitate was centrifuged and the supernatant filtered. The solvent was removed under reduced pressure and the product dissolved in the minimum amount of methanol and precipitated with diethyl ether. Further trituration with diethyl ether gave the desired product as a white solid.

Lu.3.6: Yield: 61 %. ^{1}H-NMR (400 MHz; D_2O) δ_H /ppm 4.27 (m, 2H), 3.99 (m, 2H), 3.79 (m, 2H), 3.64-3.55 (m, 5H), 3.45-3.30 (m, 6H), 2.79 (m, 6H), 2.64-2.52 (m, 4H). ESMS found *m/z* 636 for $[M+Na]^+$.

Eu.3.6: Yield: 72 %. ^{1}H-NMR (400 MHz; D_2O) δ_H /ppm 33.11, 31.72, 30.78, 30.50, 12.91, 11.67, 10.91, -0.14, -0.28, -2.31, -3.29, -4.20, -5.55, -7.04, -7.62, -7.96, -10.89, -

11.56, -12.25, -14.31, -14.78, -15.58, -16.62. Only resolved peaks outside 0-10 ppm region are reported. ESMS found *m/z* 614 for $[M+Na]^+$.

Three component gold couplings with europium propargyl acetamideDO3A complexes, 2-naphthaldehyde an piperidine 3.7

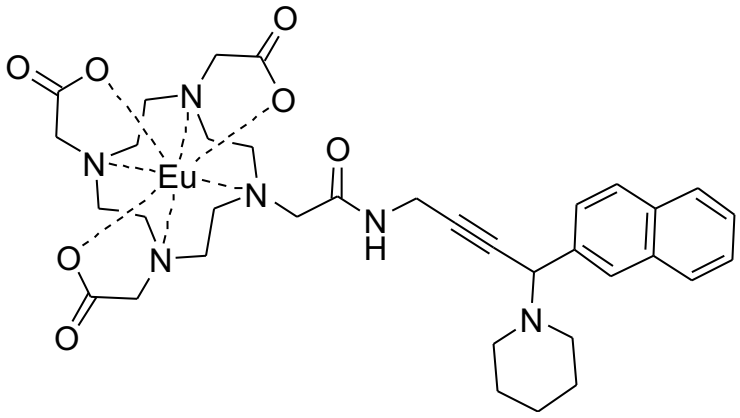

Eu.p.acetamide-DO3A (100 mg, 0.17 mmol) 2-naphthaldehyde (131 mg, 0.84 mmol), piperidine (84 μl, 0.84 mmol) and gold chloride trihydrate (32 mg, 0.08 mmol) in water (3 ml) were heated to 40 °C for 20 hours. The solution was diluted with methanol and filtration. The solvent was removed under reduced pressure and the resulting residue triturated with methanol and diethyl ether. The yellow solid was washed further with diethyl ether and ethyl acetate to remove starting materials then the crude solid was purified by amberlite ion exchange column eluting with 20 % acetonitrile to isolate the product. (75 mg, 54 %).

^{1}H NMR (400 MHz, D_2O) δ_H /ppm 33.69, 33.33, 32.88, 31.86, 30.77, 20.97, 20.85, 13.30, 12.21, 11.21, 0.00, -0.72, -1.29, -2.32, -2.97, -3.48, -4.58, -5.17, -5.73, -6.92, -7.39, -7.98, -8.32, -11.00, -11.33, -12.14, -12.97, -14.86, -15.19, -15.63, -16.41, -16.75. Only resolved peaks outside 0-10 ppm region are reported.

General synthesis of three component gold couplings with lanthanide propargylDO3A complexes, terephthalaldehyde and piperidine 3.8

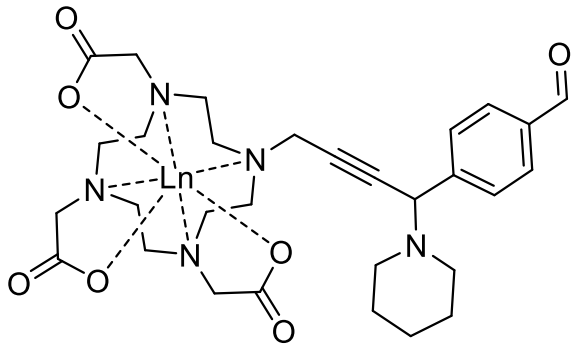

Ln.2.5 (2 equiv.) terephthaldehyde (10 equiv.), piperidine (10 euqiv.) and gold chloride trihydrate (1 equiv.) in water (3 ml) were heated to 40 °C for 20 hours. The solution was diluted with methanol and filtration. The solvent was removed under reduced pressure and the resulting residue triturated with methanol and diethyl ether. The yellow solid was washed further with diethyl ether and ethyl acetate to remove starting materials then the crude solid was purified by amberlite ion exchange column eluting with 20 % acetonitrile to isolate the product.

Lu.3.8: Yield: 30 %. ^{1}H NMR (400 MHz, D_2O) δ_H /ppm 9.93 (s, 1H), 8.15-7.20 (m, 4H), 4.02-1.91 (m, 35H).

Eu.3.8: Yield: 40 %. ^{1}H NMR (400 MHz, D_2O) δ_H /ppm 40.57, 36.99, 33.81, 29.21, 27.12, 23.04, 22.25, 15.45, 13.85, 11.40, 10.98, -1.17, -3.24, -3.87, -6.02, -6.64, -7.84, -8.80, -11.12, -12.25, -14.57, -17.09, -17.52, -20.07, -21.35, -23.11. Only resolved peaks outside 0-10 ppm region are reported.

General synthesis of bimetallic lanthanide complexes by three component gold coupling 3.9

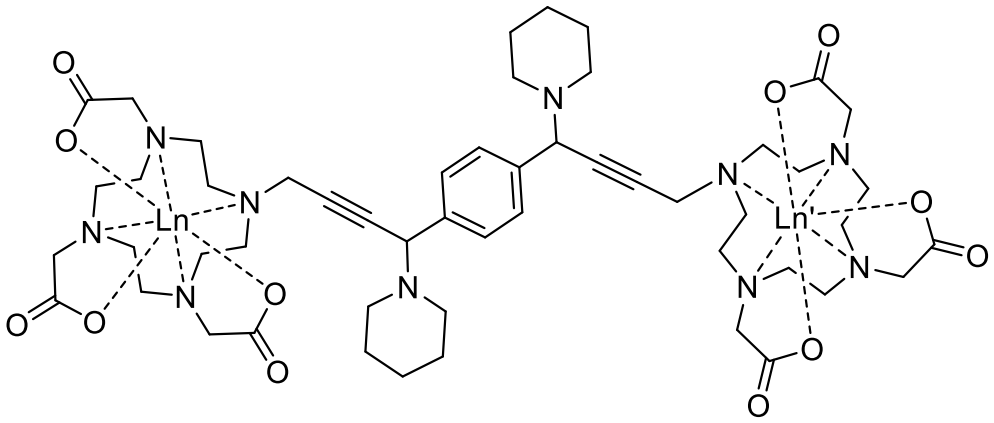

Complex **Ln.3.8** (5 equiv.), **Ln.2.5** (10 equiv.), piperidine (10 equiv.) and gold chloride trihydrate (1 equiv.) were stirred in water (3 ml) at 40 °C for 20 hours. The solution was diluted with methanol and filtration. The solvent was removed under reduced pressure and the resulting residue triturated with methanol and diethyl ether. The yellow solid was washed further with diethyl ether to remove excess piperdine then the crude solid was purified by amberlite ion exchange column eluting with 20 % acetonitrile to isolate the product.

LuLu'.3.9: Yield: 30 % ^{1}H NMR (400 MHz; $CDCl_3$); δ_H /ppm 7.65 (m, 4 H), 3.94-1.36 (m, 70 H).

EuTb.3.9: Yield: 38 % ^{1}H NMR (500 MHz, D_2O); δ_H /ppm 260.22, 220.01, 184.69, 136.64, 83.00, 71.11, 64.63, 61.76, 42.72, 40.30, 39.54, 35.95, 34.81, 33.79, 32.05, 31.15, 29.06, 25.25, 21.95, 21.22, 20.17, 15.52, 13.40, -1.10, -2.04, -4.42, -6.72, -8.12, -9.45, -11.47, -12.30, -12.68, -16.18, -49.49, -52.57, -67.52, -70.16, -71.72, -88.26, -95.76, -99.46, -106.77, -112.66, -125.06, -127.24, -142.01, -144.85, -197.31, -210.70, -230.79, -

248.22, -263.56, -398.87, -425.98, -464.21. Only resolved peaks outside 0-10 ppm region are reported. Luminescence lifetimes: Tb: MeOH: 1.79 ms, MeOD: 2.27 ms, q=1, Eu: MeOH: 0.93 ms, MeOD: 1.84 ms, q=1.

6.4.3 Rigid DO3AM derivatives

tri-*tert*-butyl 1,4,7,10-tetraazacyclododecane-1,4,7-tricarboxylate 4.1[11]

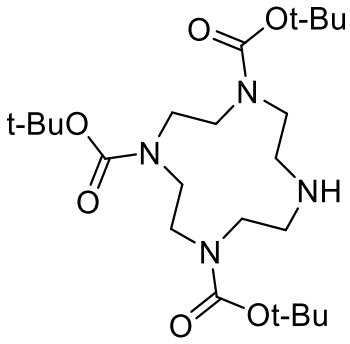

Cyclen (6 g, 35 mmol) and triethylamine (15 ml, 106 mmol) were dissolved in chloroform (170 ml) and stirred at 0 °C. To this solution di-*tert*-butyl dicarbonate (23 g, 106 mmol) in chloroform (130 ml) was added over 2 hours at 0 °C. The solution was allowed to warm to room temperature and stirred for 18 hours. The solution was washed with water and the organic layer dried ($MgSO_4$) and the solvent removed under reduced pressure yielding a yellow oil. The crude product was purified by column chromatography on silica eluting with diethyl ether. The product was isolated as a clear glassy solid (10.4 g, 63 %).

^{1}H NMR (400 MHz; $CDCl_3$); δ_H /ppm 3.61 (s, 4H), 3.28 (s, 8H), 2.84 (s, 4H), 1.45 (d, *J*= 7.8 Hz, 27H). $^{13}C\{^1H\}$ (126 MHz; $CDCl_3$): δ_C /ppm 155.23, 154.99, 78.89, 78.72, 50.72, 50.23, 49.14, 48.84, 48.84, 45.49, 44.52, 28.33, 28.13. ESMS found *m/z* 473 for $[M+H]^+$.

1-benzyl 10,4,7-tri-*tert*-butyl 1,4,7,10-tetraazacyclododecane-1,4,7,10-tetracarboxylate 4.2[11]

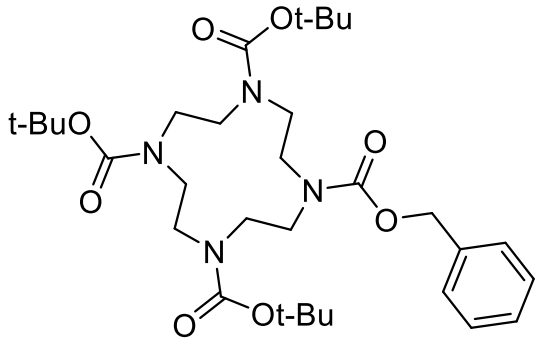

Compound **4.1** (9.0 g, 19 mmol) and triethylamine (3.2 ml, 23 mmol) were stirred in chloroform (150 ml) at 0 °C. Benzyl chloroformate (3.3 ml, 23 mmol) was added and the solution warmed to room temperature and stirred for 8 hours. The solution was then filtered and the solvent removed under reduced pressure to give a white residue. The crude product was purified by silica gel column chromatography (ethyl acetate: hexane, 30:70), giving the product as a glassy solid (9.28 g, 81 %).

^{1}H-NMR (400 MHz; $CDCl_3$): δ_H /ppm 7.36-7.29 (m, 5H), 5.11 (s, 2H), 3.47-3.25 (m, 16H), 1.46-1.41 (m, 27H). $^{13}C\{^{1}H\}$ (101 MHz; $CDCl_3$): δ_C /ppm 136.43, 128.50, 128.28, 128.13, 67.25, 60.40, 50.40, 28.51. ESMS found *m/z* 629 for $[M+Na]^+$.

benzyl 1,4,7,10-tetraazacyclododecane-1-carboxylate 4.3[11]

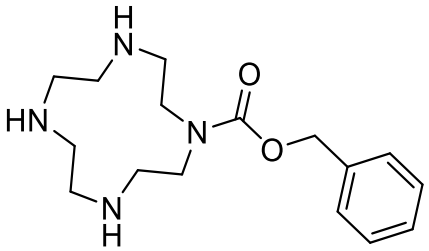

Compound **4.2** (6.5 g, 10.7 mmol) was dissolved in methanol (10 ml) and stirred at 0 °C. To this solution concentrated hydrochloric acid (9 ml) was added drop-wise. The solution was allowed to warm to room temperature then stirred for 8 hours. The solution was then concentrated at room temperature under reduced pressure to around 5 ml before the precipitates were removed by filtration and the crude product recrystallized from water and tetrahydrofuran to give the product as a crystalline solid. (4.1g, 91 %).

^{1}H-NMR (400 MHz; D_2O): δ_H /ppm 7.49-7.46 (m, 5H), 5.22 (s, 2H), 3.23-3.19 (m, 16H). $^{13}C\{^{1}H\}$ (101 MHz; $CDCl_3$): δ_C /ppm 157.37, 136.93, 128.60, 128.15, 128.12, 77.36, 49.66-46.17 (br). ESMS found *m/z* 307 for $[M+H]^+$.

di-*tert*-butyl (2-chloroacetyl)aspartate 4.4

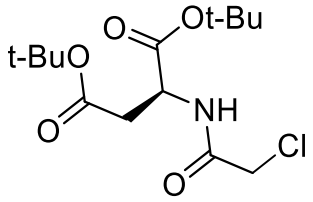

Di-*tert*-butyl ester L-aspartic acid (8 g, 28.5 mmol) and triethylamine (9.5 ml, 68.3 mmol) in dichloromethane (200 ml) were cooled to 0 °C. Chloroacetyl chloride (2.7 ml, 34.2 mmol) was added dropwise and the solution allowed to warm to room temperature and stirred overnight. The solution was washed with water (3 x 150 ml) and saturated solution of $HNaCO_3$ (3 x 150 ml). The organics were dried ($MgSO_4$) and the solvent removed

under reduced pressure. The crude product was purified by silica gel column chromatography (ethyl acetate: hexane, 1:2) yielding the desired product (8.1 g, 89 %).

^{1}H-NMR (400 MHz; $CDCl_3$): δ_H /ppm 7.53 (d, J = 8.1 Hz, 1H), 4.67 (dt, J = 8.3, 4.2 Hz, 1H), 4.07 (s, 2H), 2.92 (dd, J = 17.0, 4.3 Hz, 1H), 2.74 (dd, J = 17.0, 4.4 Hz, 1H), 1.46 (d, J = 6.9 Hz, 18H). ^{13}C{^{1}H} (101 MHz; $CDCl_3$): δ_C /ppm 169.79, 169.13, 165.76, 82.73, 81.90, 49.42, 42.50, 37.34, 28.09, 27.94. ESMS found *m/z* 344 for $[M+Na]^+$.

hexa-*tert*-butyl 2,2',2''-((2,2',2''-(10-((benzyloxy)carbonyl)-1,4,7,10-tetraazacyclododecane-1,4,7-triyl)tris(acetyl))tris(azanediyl))trisuccinate 4.5

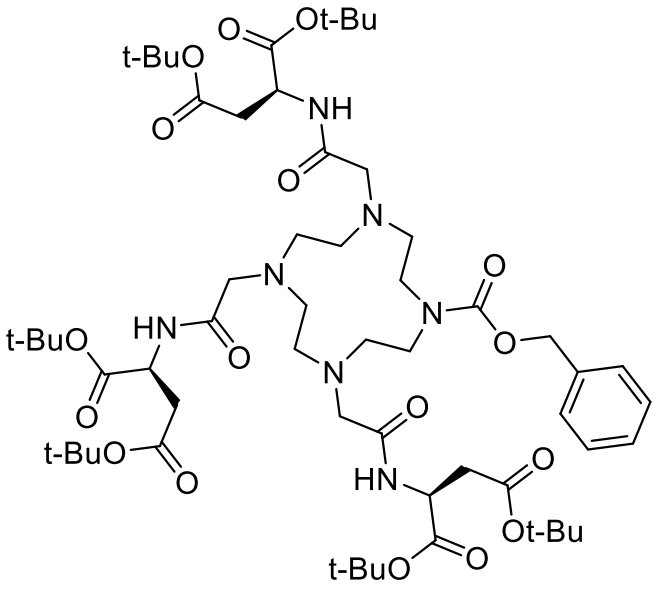

Compound **4.3** (0.71 g, 2.3 mmol) was dissolved in aqueous NaOH (20 ml) and extracted with chloroform (3 x 50 ml). The organic extracts were collected, dried ($MgSO_4$) and the solvent removed under reduced pressure. The residue was dissolved in acetonitrile (50 ml) and potassium carbonate (1.30 g, 9.4 mmol) added. The solution heated to 60 °C for 20 minutes before **4.4** (3.00 g, 9.4 mmol) was added and the solution heated to 70 °C for

48 hours. The solvent was then removed under reduced pressure and dissolved in water and extracted with dichloromethane. The organic extracts were collected dried ($MgSO_4$) and the solvent then removed under reduced pressure. The crude product was then purified first by silica gel column chromatography ($CHCl_3$: MeOH 98:2 to $CHCl_3$: MeOH 95:5), then by alumina gel column chromatography ($CHCl_3$: MeOH 96:4) to give the titled product (763 mg, 30 %).

^{1}H-NMR (400 MHz; $CDCl_3$): δ_H /ppm 7.71-7.67 (m, 2H), 7.35-7.34 (m, 3H), 5.11 (d, *J* = 3.1 Hz, 2H), 4.71-4.61 (m, 3H), 3.58-2.65 (m, 28H), 1.45 (d, *J* = 6.1 Hz, 54H). ESMS found *m/z* 1163 for $[M+H]^+$.

hexa-*tert*-butyl 2,2',2''-((2,2',2''-(1,4,7,10-tetraazacyclododecane-1,4,7-triyl)tris(acetyl))tris(azanediyl))trisuccinate 4.6

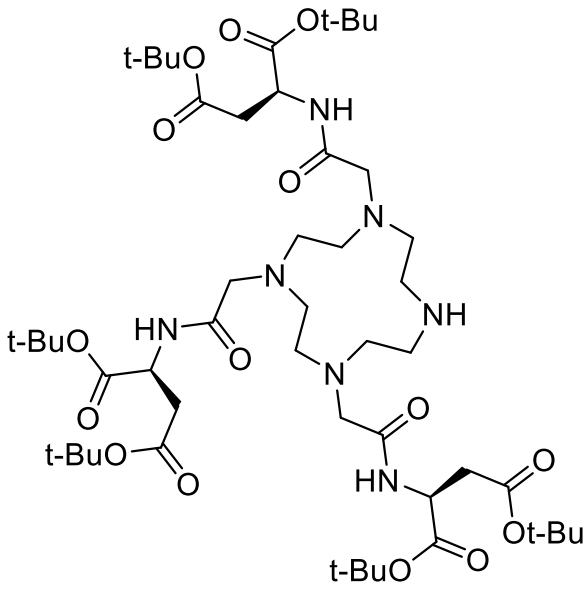

10 % Palladium on carbon (350 mg, 3.3 mmol) was covered in ethanol and compound **4.5** (763 mg, 0.66 mmol) in ethanol (10 ml) was added and the solution stirred under nitrogen. The flask was flushed with nitrogen before a hydrogen balloon was added. The reaction was stirred for 5 days under hydrogen. The solution was then filtered through

celite washing with dichloromethane. The resulting yellow solution was dried ($MgSO_4$) and the solvent was removed under reduced pressure to give the desired product as an off-white solid (517 mg, 76 %).

^{1}H-NMR (400 MHz; $CDCl_3$): δ_H /ppm 7.87-7.65 (m, 3H), 4.76-4.62 (m, 3H), 3.26-2.75 (m, 28H), 1.44 (q, J = 1.9 Hz, 54H). ESMS found *m/z* 1026 for $[M-H]^-$.

hexa-*tert*-butyl 2,2',2''-((2,2',2''-(10-(prop-2-yn-1-yl)-1,4,7,10-tetraazacyclododecane-1,4,7-triyl)tris(acetyl))tris(azanediyl))trisuccinate 4.7

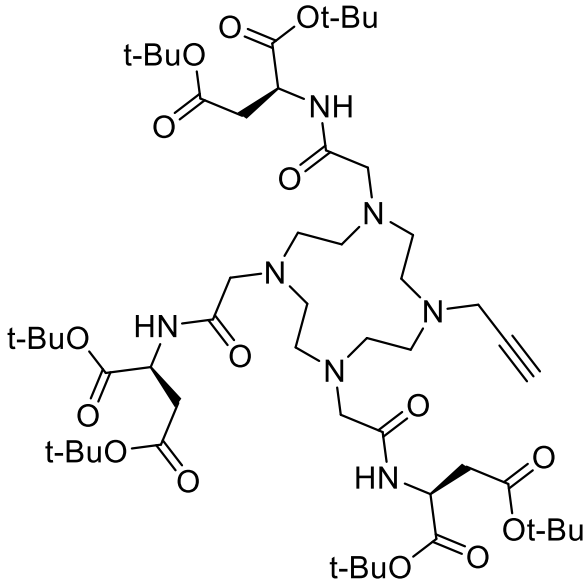

Compound **4.6** (165 mg, 0.16 mmol) in anhydrous acetonitrile (40 ml) and potassium carbonate (55 mg, 0.40 mmol) were stirred for 20 minutes. Propargyl bromide (14 µl, 0.16 mmol) was added dropwise at 0 °C and the solution heated to 50 °C for 48 hours. The solution was filtered and the solvent removed and the residue dissolved in toluene and washed with water. The organic layer was dried ($MgSO_4$) and the solvent removed under reduced pressure yielding the product **4.7** (99 mg, 62 %).

^{1}H-NMR (400 MHz; $CDCl_3$): δ_H /ppm 8.10-7.90 (m, 3H), 4.67-4.63 (m, 3H), 3.48-2.69 (m, 31H), 1.47-1.39 (m, 54H). ESMS found *m/z* 1066 for $[M+H]^+$.

Synthesis of europium propargyl hexa-*tert*-butyl triamide complex 4.8

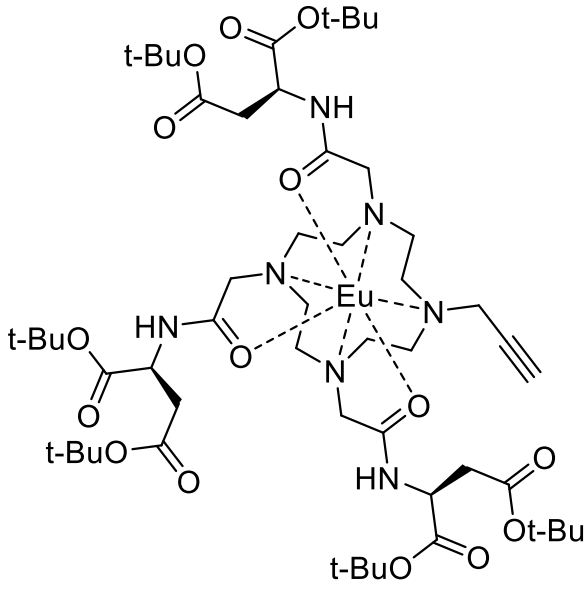

Compound **4.7** (218 mg, 0.20 mmol) was dissolved in methanol (5 ml) to which europium triflate (128 mg, 0.21 mmol) was added and the solution stirred at 60 °C for 48 hours. The solvent was then removed under reduced pressure and the yellow residue was washed with water and the yellow solid collected by filtration (115 mg, 47 %).

^{1}H-NMR (400 MHz; d_4-methanol): δ_H /ppm 25.72, 24.47, 22.61, 21.23, 20.92, 19.64, 18.81, 18.16, 17.81, 17.02, 16.64, 14.23, 13.12, 12.13, 10.82, -0.84, -1.39, -1.62, -2.25, -2.95, -4.04, -5.16, -5.67, -6.03, -6.40, -6.95, -7.28, -7.93, -8.73, -9.25, -10.15, -11.45, -11.98, -13.98, 14.84, 18.12, 18.41, -19.45. Only resolved peaks outside 0-10 ppm region are reported. MALDI-MS (α-MeOH) *m/z*: 1217.9264, calculated *m/z* for $[C_{53}H_{90}EuN_7O_{15}]^+$. Luminescence lifetimes: MeOH: 0.56 ms, MeOD: 1.19 ms, q=2.

Synthesis of europium propargyl hexa-acid triamide complex 4.9

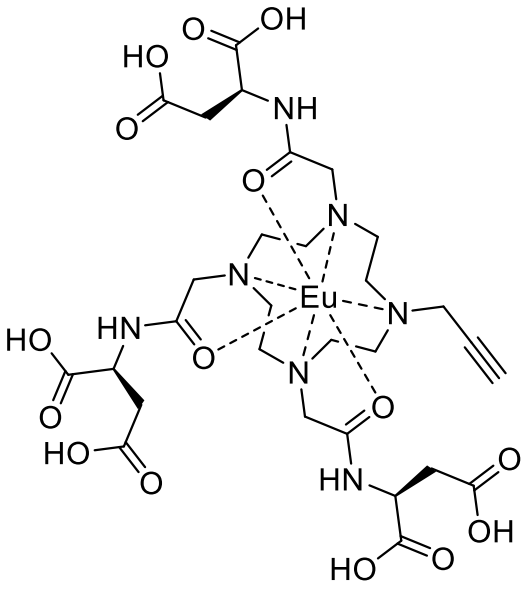

Complex **4.8** (180 mg, 0.14 mmol) was dissolved in dichloromethane (20 ml) and TFA (20 ml) was added drop-wise, the solution was then stirred overnight at room temperature. The solvent was removed under reduced pressure and the residue was re-dissolved in the minimum amount of methanol and precipitated with diethyl ether. The product was purified by amberlite ion exchange column eluting the product with 10 % acetonitrile (28 mg, 24 %).

^{1}H-NMR (400 MHz; D_2O): δ_H /ppm 27.70, 23.40, 22.60, 19.79, 19.21, 17.36, 14.57, 11.86, -1.11, -1.61, -2.13, -3.21, -4.74, -6.54, -6.93, -7.36, -8.56, -9.21, -10.78, -11.87, -12.20, -14.11, -14.67, -16.28, -17.20, -17.78, -19.32. Only resolved peaks outside 0-10 ppm region are reported. MALDI-MS (α-MeOH) *m/z*: 880.7623 calculated *m/z* for $[C_{29}H_{41}EuN_7O_{15}]^+$. Anal. Calcd for: $C_{29}H_{43}N_7O_{15}$ C, 39.51; H, 4.92; N, 11.12 Found: C, 39.57; H, 5.03; N, 10.96 %.

6.5 References

1. P. Kuzmič, *Anal. Biochem.*, 1996, **237**, 260–273.
2. J. A. Tilney, T. J. Sørensen, B. P. Burton-Pye, and S. Faulkner, *Dalt. Trans.*, 2011, **40**, 12063–12066.
3. M. Tropiano, O. A. Blackburn, J. A. Tilney, L. R. Hill, M. P. Placidi, R. J. Aarons, D. Sykes, M. W. Jones, A. M. Kenwright, J. S. Snaith, T. J. Sørensen, and S. Faulkner, *Chem. - A Eur. J.*, 2013, **19**, 16566–16571.
4. J. Laha and G. Cuny, *Synthesis (Stuttg).*, 2008, 4002–4006.
5. A. Dadabhoy, S. Faulkner, and P. G. Sammes, *J. Chem. Soc. Perkin Trans. 2*, 2002, 348–357.
6. M. Jauregui, W. S. Perry, C. Allain, L. R. Vidler, M. C. Willis, A. M. Kenwright, J. S. Snaith, G. J. Stasiuk, M. P. Lowe, and S. Faulkner, *Dalt. Trans.*, 2009, **33**, 6283.
7. M. Tropiano, N. L. Kilah, M. Morten, H. Rahman, J. J. Davis, P. D. Beer, and S. Faulkner, *J. Am. Chem. Soc.*, 2011, **133**, 11847–9.
8. A. Kuzmin, A. Poloukhtine, M. A. Wolfert, and V. V Popik, *Bioconjug. Chem.*, 2010, **21**, 2076–85.
9. D. E. Prasuhn, Jr., R. M. Yeh, A. Obenaus, M. Manchester, M. G. Finn, V. Ose, P. Pumpens, V. Ose, I. Gusars, and P. Pumpens, *Chem. Commun.*, 2007, **249**, 1269–1271.
10. R. F. H. Viguier and A. N. Hulme, *J. Am. Chem. Soc.*, 2006, **128**, 11370–1.
11. M. Woods, G. E. Kiefer, S. Bott, A. Castillo-Muzquiz, C. Eshelbrenner, L. Michaudet, K. McMillan, S. D. K. Mudigunda, D. Ogrin, G. Tircsó, S. Zhang, P. Zhao, and A. D. Sherry, *J. Am. Chem. Soc.*, 2004, **126**, 9248–56.